

SCIENTIFIC & TECHNICAL

REPORT
2018

IMPRINT

Full report title CSEM Scientific and Technical Report 2018

Editor and publisher CSEM SA
info@csem.ch
T +41 32 720 5111

Publication Frequency yearly
Media printed and electronic
Website www.csem.ch/str2018

Cover page design Contreforme
www.contreforme.ch

Printing Imprimerie Baillod SA, Bevaix (Switzerland)

PREFACE

Dear Reader,

From its founding to the present day, CSEM has been a cornerstone of technology development and transfer, both in precision microtechnologies (our DNA) and digitalization technologies. These intelligent technologies are the foundations on which smart systems are built, promising all industries new opportunities for economic growth.

To be digital is to think digital, to believe in innovation, and to believe in people. Together we can build tomorrow, starting today. We know that some economic players in Switzerland have taken the digital plunge. And we hope that their positive experience can be a source of inspiration for others who would like to but don't know how and where to start, encouraging them to join us. We look forward to guiding and supporting them on this journey.

While our close connections to industry help us anticipate the trends of tomorrow's markets, our tight links with researchers in Switzerland and abroad keep us up to date with cutting-edge academic research.

With more than 400 experts driven by a passion for science and innovation, we work day after day to expand our reach as a leading research and technology organization, transforming science into revolutionary technologies and promoting innovation in industry.

I hope you enjoy reading this report and that doing so gives you a real sense of how CSEM experts can, by applying their creativity and innovativeness, help industry and society to prepare for the future.

Mario El-Khoury

CEO, CSEM SA

CONTENTS

PREFACE

1 Optical Phase Retarder based on Plasmonic Nanostructures 40

MULTIDISCIPLINARY INTEGRATED PROJECTS—MIPS

DeepIoT—Embedded Deep Learning Algorithms for eHealth IoT	9	Freeform Micro-optics for Non-imaging Applications	41
FlexWave—Silicon Flexure Systems with Inkjet-printed Waveguides	10	HySurf—Microstructured Hybrid Surface with Improved Friction Properties	42
DISPOGEN—Oxygen Sensing at Home	11	Folded Micro-optical Connectivity Solution	43
LONGECG—Low-cost low-power Cooperative Sensors	12	Studying the Effect of Plasmonic Nanostructures to Enhance Solar Water Splitting	44
MIAM-3D—Metallic Inks Applied to Additively Manufactured 3D parts	13	Liquid Biopsy—A disposable Cartridge to Measure Proteins from Whole Blood	45
PocketDX—Compact Flow Cytometer for Industrial Water Quality Monitoring	14	First Microfluidic Valve with Integrated Mixer for In-line Sample Preparation	46
PROBIOTICS—a Pressure Monitoring Robust Unobtrusive Batteryless IoT Integrated Circuit & System	15	Calibration-free Liquid Dispensing of Microliter Volumes	47
Witness—an Autonomous Camera on a Sticker	16	AutoMiA—Automated Bovine Milk Analysis by Impedance Spectroscopy	48
3DprintedFluidics—Revolutionary Fluidic Components Enabled by Additive Manufacturing Technologies	17	Aptamer-based Electrochemical Detection of Aflatoxins on a Smartphone	49
HECTIC2—SiC-based MEMS Pressure Sensor Development	18	Low-cost Printed Electrochemical Urinalysis Sensors for Health, Fitness, and Nutrition	50
SILOSCAPE—Flexure-based Oscillators for Mechanical Watches	19	FluoSense—Highly Sensitive Fluorescence Detection with Silicon Photomultipliers	51
SmartShock—Mechanical Shock Resistance of Mesoscale Parts: Semi-automatic Design Testing and Adaptation	20	Stem Cell Organoid Culture Platform for Pharmaceutical and Industrial Applications	52
		Roll-to-roll Printed Wireless Sensors Platform on Low-cost and Flexible Substrates	53
		EchoPad—Flexible Pad-based Ultrasound System for Continuous Heart Monitoring	54

MICROSYSTEMS

21 PHOTOVOLTAICS & ENERGY MANAGEMENT 55

Neurons on 3D Microelectrode Arrays	24	Progress towards High-efficiency Perovskite/Silicon Tandem Devices	60
MEMS-based Gas Chronomatograph	25	Development of High Mobility TCOs for Heterojunction Solar Cells	61
Design and Fabrication of Microfluidic Systems for Two Phase Cooling	26	Multi-service Microgrid in an Industrial Environment	62
Adhesives for Solder Replacement	27	Data-driven Reinforcement Learning for Smart Controllers in Large Building Facilities	63
Packaging Design and Simulation for Space Applications	28	Model-based Online Estimation of the State of Charge in Lithium-ion Batteries	64
Semi-automated Diamond-based Thermo-compression Wire-bonder	29	Optimal Control Platform for Coupling Energy Vectors	65
Mechanical Strength of Precipitate Hardenable Al Alloys using ECAP	30	Performance of Home Energy Management Systems: Insights from the Prosumer-Lab	66
3D Printing of Sub-millimeter Sized Components	31		
Powder Features in SLM: How important is it?	32		
Selective Laser Melting of sub-200 µm Features of Components	33		

SURFACE ENGINEERING

35 SYSTEMS 67

ACEnano—A Tiered Approach for Nanomaterial Risk Assessment	37	Recurrent Neural Network (RNN) Based Temporal Classification of Land Usage Using Satellite Imagery	69
3D Printed Models to Understand Aerosol Evolution and Deposition in the Human Respiratory Tract	38	A Wireless Solar Powered Pressure Pad for Sail Performance Monitoring	70
Microstructures Stamped into Ti Dental Implants for Trademark Protection	39	Controlling the End-Effector Absolute Pose of a Large Hybrid Manufacturing Robot based on Real-time Laser Tracking Technology	71

3D Lightfield Imaging for 100% Inspection in MEMS and Microsystems Manufacturing	72	An Active Near-field Communication (NFC) System	104
Generic Condition-based Monitoring for CSEM VISARD Automation Platform	73	Miniature Acquisition, Processing and Wireless Communication System-on-Chip for Prosthetic Applications based on Electromyography (EMG)	105
RailCheck—Deep Learning for Railway Track Inspection	74	FastEye+, a High-speed Camera with Embedded Neural Networks for Smart Vision	106
Redesign, Manufacturing, and Testing of a Slip Ring Rotor for Space Applications based on Additive Manufacturing	75	Switched-capacitor Degeneration for PVT Robust and Power Efficient Biomedical AFEs	107
Flight Model Acceptance Test Campaign of Two Corner Cube Mechanisms for MTG	76	High-density Microelectrode Array with 4096 Full-duplex Channels	108
Close-Up Imager (CLUPI) for the EXOMARS Mission: Focus Mechanism Test Campaign	77	ANNEXES	109
RemoveDebris, in-orbit Experimentation of CSEM LiDAR Broadband Swept-Wavelength Infrared GaSb Laser for in-vivo Sensing Applications	78	Publications	109
High-power Femtosecond Laser System for High-throughput Manufacturing	79	Proceedings	112
oBPM™—Location Independent Continuous Optical Blood Pressure Monitoring	80	Conferences and Workshops	115
Pediatric Respiratory Rate Estimation through Deep Neural Networks	81	Research Projects	118
Chest-based PPG for Pulse Oximetry and Non-occlusive Blood Pressure Monitoring	82	Swiss Commission for Technology and Innovation	120
Wearable Vital Sign Monitoring System for Reinforced Speech Processing	83	European Commission Projects	123
Common-mode Rejection in the Measurement of Wearable ECG with Cooperative Sensors	84	European Space Agency, Swiss Space Office, and Swiss Space Center Projects	126
Enhanced Robotic Surgery with Multimodal Sensing	85	Industrial Property	127
Flexible, Hollow Organs with Inner Structures for Medical Validation and Training	86	Collaboration with Research Institutes and Universities	127
	87	Teaching	131
		Theses	132
		Commissions and Committees	133
		Prizes and Awards	136

ULTRA-LOW-POWER INTEGRATED SYSTEMS

89

Interoperability of ULP Wireless Sensor Networks	91
5G Technologies for IoT and Low-power Wireless Communications	92
Data Validation using Machine Learning	93
Remote Vital Signs Monitoring using a FMCW Radar and Machine Learning	94
A Power Optimized Hybrid TDMA-WiseMAC Switchable Protocol for Hand Prostheses	95
Comparison of 20 GHz Low-power Wide-range Oscillators in 28 nm CMOS	96
Link Budget, Power Trade-offs using Optimized Bluetooth 5 Transceiver IP	97
A Highly Efficient DC-DC Buck Converter for Load Currents from 1 μ A to 50 mA	98
Efficient Deep Learning Algorithm for Person Detection from Ceiling-mount Cameras	99
Intelligent Multispectral Imaging System for Detecting Human Skin	100
An Ultra-low-power High Dynamic Range Image Sensor	101
A Reticle-size X-ray Photon Counting Detector	102
A Super High-performance Ultra-low-power Temperature Compensated Real Time Clock	103

CSEM SA

CSEM is a private, non-profit research and technology organization (RTO) and a Swiss innovation accelerator—a catalyst for the transfer of technologies and know-how from fundamental research to industry. The organization is recognized as an innovation vector thanks to its provision of technology platforms that enable significant scientific and creative breakthroughs in today's world.

CSEM's research strategy is built around five main programs:

Microsystems—Dedicated to the development of complete and reliable microsystems solutions ranging from advanced manufacturing technologies, MEMS designs, and packaging concepts to more complex digital microfabrication technology—mainly based on 3D printing and additive manufacturing.

#additivemanufacturing #AM #mems #3Dprinting #design
#packaging #hermeticsealing #photonics

Surface Engineering—Research & development area focused on controlling surface structure and composition (both topographical and chemical) and on the optimization of (bio-) chemical, optical, and electrical properties, while developing related competitive manufacturing technologies suitable for industrial applications.

#functionalization #biosensing #biosurface #nanocoating
#printedelectronics #nanostructuring

Photovoltaics & Energy Management—Fostering innovation and accelerating the pace of technology transfer in the fields of photovoltaics and energy storage and systems—as well as in new market segments such as energy scavenging and the Internet of Things—are at the forefront of our R&D developments.

#smartgrid #storage #energydata #bipv #solarenergy #HJT
#perovskite #thinfilmpv #scavenging

Systems— Design, simulation, prototyping, and integration of micro- and nanotechnologies and advanced algorithms to create (sub-) systems for applications in scientific instrumentation, automation and robotic systems, and wearables and medical devices.

#medtech #automation #wearable #quantumtechnology
#time&frequency #simulation #macroMems #laser #robotics

Ultra-Low-Power Integrated Systems—Addresses the key challenges and the technologies required when building very-low-power (long autonomy), wirelessly interconnected, embedded smart systems or remote sensing nodes.

#smartdata #smartdust #zero-battery #IOT #edgecomputing
#wireless #machinelearning #AI #machinevision #datascience

MULTIDISCIPLINARY INTEGRATED PROJECTS—MIPS

Harry Heinzelmann

Multidisciplinary integrated projects (MIPs) form a horizontal program that mostly builds on technologies developed in the five topical research programs **Microsystems, Surface Engineering, Systems, Ultra-Low-Power Integrated Systems, and Photovoltaics & Energy Management**. The goal of the MIP program is to better exploit synergies, and to create solutions by combining several of CSEM's technologies.

Every year CSEM dedicates an important part of its resources to these highly interdisciplinary projects, targeting demonstrators with a high level of maturity (high technology readiness level (TRL)) for novel applications with high market potential in relatively short development times.

Besides typical MIPs, which last 1-2 years, Feasibility MIPs have been introduced, allowing the rapid exploration of new concepts. Another project type, Technology MIPs, addresses long-term co-developments with different technologies.

The MIP program is reevaluated annually, and consists of ongoing projects and new proposals in a healthy balance, making it possible to respond quickly to newly emerging market needs. In this way, CSEM's MIPs complement its five topical research programs in an ideal way. The MIP program enables CSEM to offer its industrial clients an even richer portfolio of technologies, beyond the possibilities of its thematic research programs alone.

An overview of 2018 MIPs follows; the projects are presented in more detail in the following pages.

Feasibility MIPs

DeepIoT—Embedded deep learning algorithms for eHealth IoT

The project DeepIoT brings the rapidly advancing technology of deep learning to the smart Internet of Things (IoT) technologies developed at CSEM. By combining our experience in the fields of IoT and artificial intelligence (AI), we built a deep-learning-algorithm-enabled, low-power wearable system that is more reliable and accurate than CSEM's current solutions.

Deep learning is a branch of machine learning based on a set of algorithms that model high-level abstractions in data. In the race to build AI-powered wearables, CSEM's health-related databases and associated medical know-how are an asset. DeepIoT's proof of concept is a deep learning algorithm to diagnose and analyze sleep patterns, with increased mean accuracy over existing solutions.

FlexWave—Silicon flexure systems with inkjet-printed waveguides

The project FlexWave aims at miniaturizing inkjet-printed waveguides for intensity-based optical sensing in mesoscale, flexure-based mechanical systems (MacroMEMS). Inkjet printing is a contactless process ideally suited for depositing onto fragile parts ("additive manufacturing"), thus allowing the integration of optical sensors with high sensitivity and resolution while being insensitive to surrounding electrical fields.

The project assesses the suitability of intensity based optical sensing and the transfer of optical signals over flexures in opto-mechanical devices. The proposed development could allow fast,

low-cost force and displacement sensing in small spatial confinements, such as in microassembly applications.

Classical MIPs

DISPOGEN—Oxygen sensing at home

Molecular oxygen is one of the most monitored parameters in environmental research, biotechnology, medical and biological research, the life sciences, and pharmaceutical manufacturing. In line with the trend of "sensors everywhere", DISPOGEN's objective is to develop a contactless oxygen sensing solution for smartphones. This system is based on disposable optical sensors developed at CSEM, offering outstanding performance in humid and liquid environments.

The final demonstrator includes disposable sensors, a smartphone add-on reader, and a mobile application, all of which can be tested by our industrial partners. This technology offers interesting solutions for both industrial and domestic applications.

LONGECG—Low-cost, low-power cooperative sensors

Cooperative sensors for physiological parameters are based on active dry electrodes characterized by simplified and safe cabling, but currently with the main drawback of requiring one battery per sensor. Moreover, they are quite large, and solutions for better ergonomics and usability are needed.

The goal of the project LONGECG is to make a demonstrator of a medical multi-lead ECG Holter with a new kind of cooperative sensor that will exhibit low-power consumption, and be low-cost, defibrillator-proof, and centrally powered. The development includes a new approach of flatter cooperative sensors with a centralized battery, under the medical device development standards of ISO 13485.

MIAM-3D—Metallic inks applied to additively manufactured 3D parts

MIAM-3D aims at developing a process to apply metallic inks (e.g., Ag ink) onto 3D surfaces and inside thin channels, both manufactured from high performance polymer structural substrates processed by additive manufacturing. Such a process will respond to Industry 4.0's demand for manufacturing complex shapes such as functional electrodes on 3D parts for space, medical, automotive, and aviation applications.

The proposed solution is based on an inkjet-printed seed layer and metal plating onto 3D structures, such as for slip ring assemblies (SRA). The concept could significantly simplify current manufacturing processes.

PocketDX—Compact flow cytometer for industrial water quality monitoring

The project aims at developing a miniaturized flow cytometer (low footprint and weight) to be used for environmental, food, and life-science applications. The targeted portable device consists of a sample preparation module (featuring a microfluidic mixer and an incubation chamber for staining the targeted cells or organisms), a fluid actuation module (managing reagents, cleaning liquids, and waste), a multi-wavelength optical readout module (based on optical scattering and fluorescence), and data processing algorithms.

The miniaturized cytometer will allow us to detect and quantify biological targets while reducing the consumption of reagents and decreasing the measurement time from typically three days to 15 minutes for typical tests in the field of on-site water monitoring. Other promising applications exist, potentially in food quality monitoring and point-of-care diagnostics.

PROBIOTICS—Pressure monitoring robust unobtrusive batteryless IoT integrated circuit & system

The booming IoT market is suffering from power and size bottlenecks that currently prevent ubiquitous wireless sensor node (WSN) deployment. The project PROBIOTICS addresses these problems by realizing the first robust, extremely miniaturized, pin-sized, energy autonomous IoT node combining energy harvesting, storage and management, sensing (e.g., pressure, temperature), on-chip digital signal processing, and wireless data transfer.

The technological approach is to integrate, in a few cubic millimeters, three main hardware components: a system-on-a-chip (SoC) integrated circuit, an ultra-compact MEMS pressure sensor, and a surface-mount device PV-cell—all combined in a representative WSN able to transmit data to a cell phone despite its extreme miniaturization and scarce energy resources. The outcome is an easily customizable, energy autonomous IoT sensor node platform.

Witness—Autonomous camera on a sticker

Witness is an autonomous image recording device integrated onto a palm-size flexible sticker. This device can be considered as a disposable watcher dedicated to monitoring. It records pictures of the faced scene (room, warehouse, exteriors) at regular intervals, when activity is detected, and stores them in a local flash memory for off-line use. The purpose of the device is to provide a very cheap and easy to deploy surveillance system based on the “what happened?” concept.

The project is highly multidisciplinary and combines high-efficiency flexible PV cells, ultra-thin optics, ultra-low-power image capture, algorithms to process the captured data, and an efficient integration of all these components into a working device.

Technology MIPs

3DprintedFluidics—Revolutionary fluidic components enabled by additive manufacturing technologies

Recently available multi-material 3D printers (for piezo-ceramics, polymers, metal inks) offer new opportunities in manufacturing. In the project 3DprintedFluidics, active fluidic components and systems are addressed with the goal of increasing functionalities while reducing footprint size and assembly cost.

The ultimate goal is to build a smart pump with integrated flow control for dispensing liquids with microliter accuracy. In a first phase, individual components, such as pumps, valves, flow sensors, and light barrier channels, were designed and produced. Target markets are laboratory automation, point-of-care diagnostics, and drug delivery.

HECTIC2—SiC-based MEMS pressure sensor development

This project deals with the development of packaging solutions for harsh environments. In our approach, silicon carbide (SiC) serves as a base material and atomic layer deposition deposited aluminum oxide (Al_2O_3) acts as a conformal, protective, insulating coating.

During the previous year main technology blocks have been developed, including the deep etching of SiC, high-temperature compatible Ohmic contacts, Pt-based wire bonding, and SiC–SiC bonding. This year's goal was to improve critical steps and stabilize the fabrication process, and to demonstrate package hermeticity at high temperatures. First prototype SiC-based MEMS pressure sensors were realized. Target applications are the monitoring of turbomachinery, gas turbines, and reaction engines.

SIOSCAPE—Flexure-based oscillators for mechanical watches

Over the past ten years, the precise mechanical structuration of silicon, on scales from micrometers (MEMS) up to centimeters (MacroMEMS), has allowed the development of innovative watch mechanisms. The project SIOSCAPE has the objective to design, produce, and characterize silicon-based oscillators and escapements in order to lower the technological risks prior to proposing the technology for industrialization by the Swiss watch industry. The experience gained from previous developments is a very sound basis for this project.

A novel oscillator was designed and fabricated, and showed improved performance compared to its predecessors. Further, a novel anti-shock concept for flexure-based watch oscillators was developed.

SmartShock—Mechanical shock resistance of mesoscale parts: Semi-automatic design testing and adaptation

This project aims at the development of a unique semi-automatic system for the analysis of mechanical deformation and stress in high-speed impacts such as mechanical shocks. Such a system would make it possible to go beyond today's quasi-manual analysis of slow-motion videos and would allow for the design optimization of mesoscale structures in precision mechanical parts, such as Si-based watch movements or MEMS steering mechanisms.

The envisaged system will allow us to perform quantitative data analysis of slow-motion videos acquired by a specially designed high-speed camera synchronized with the existing mechanical shock-testing setup. Frame-by-frame image analysis will extract quantitative deformation data regarding the investigated mesoscale parts and the corresponding mechanical stress will be calculated and compared to theoretical simulations.

DeepIoT—Embedded Deep Learning Algorithms for eHealth IoT

E. Türetken, J. Van Zaen, R. Delgado-Gonzalo

CSEM is bringing the rapidly-advancing technology of deep learning to the world of the Internet of Things (IoT). Building on its experience in the fields of healthcare, IoT, and artificial intelligence (AI), CSEM is developing deep learning algorithms to diagnose and analyze sleep patterns. The algorithms are designed to be reliable for consumer healthcare applications and to be integrated into low-power wearables with limited computational resources.

Deep learning is a branch of machine learning based on artificial neural networks that hierarchically model high-level abstractions in data. Thanks to the recent availability of large-scale labeled datasets and powerful hardware to process them, the field has enjoyed great success in many fields including computer vision, natural language processing and speech analysis. The technology is likely to be disruptive in many application domains and expected to render conventional machine learning techniques obsolete. Consequently, the technology is increasingly being adopted in the rapidly-growing wearables and IoT markets within the framework of wellness and healthcare Industry 4.0.

The estimated amount of health and fitness trackers worldwide in 2015 was around 25 million units^[1], and the number of manufacturers in the wearables market is growing fast. According to CCS Insight, the wearable market (e.g., smart watches, fitness bands, etc.) is expected to grow in value from just over \$10 billion in 2017 to almost \$17 billion by 2021.

In this race of building AI-powered wearables, the know-how of CSEM represents a competitive advantage with respect to other industrial players thanks to its long-term experience on low-power embedded systems and healthcare-related data analytics applications. CSEM is actively involved in several industrial projects regarding health tracking that would benefit from the deep learning technology. Examples of current customers comprise manufacturers of wrist devices, armpods, connected running shoes, and smart textiles, with whom data-driven health tracker systems have been developed.

As a proof of concept (PoC), CSEM developed several deep learning architectures for sleep staging and evaluated two embedded implementations with different levels of spatiotemporal abstraction:

- Multi-Layer Recurrent Neural Networks (ML-RNNs): RNNs are powerful architectures designed to model long-term temporal relations in the data. They have been shown to work very well in natural language processing applications.
- Convolutional Neural Networks (CNNs): CNNs are neural networks that can hierarchically capture local patterns with increasing semantic complexity in spatiotemporal data.

The data for the PoC is taken from the PhysioNet/Computing in Cardiology Challenge 2018^[2]. The dataset is contributed by the Massachusetts General Hospital and includes 1985 subjects which were monitored at a sleep laboratory for the diagnosis of sleep disorders. However, ground truth sleep stage annotations are publicly released only for 994 subjects, which is what we used for the PoC.

The dataset is split into training and test subsets with 90% of subjects used for training and the rest for testing. The input to the

algorithms is a short temporal sequence (5 minutes) of heart-rate variability (HRV) values and a binary value that denotes whether the subject moved. Both inputs are derived using efficient algorithms from raw sensor readings. The output is a three-class vector that signify the likelihood of a subject's sleep stage: WAKE, REM and NREM.

The deep learning algorithms are compared against a hand-designed baseline algorithm, which is based on the analysis of the HRV spectrogram and motion sequences (Table 1). Both, the CNN and ML-RNN architectures employ fully connected and normalization layers, and the latter is based on an efficient version of LSTM networks with forget gates.

Table 1: Performance comparison of the developed algorithms.

	Mean Classification Accuracy	No of Parameters
Baseline	47%	N/A
ML-RNN	68%	1.2 M
CNN	76%	107 K

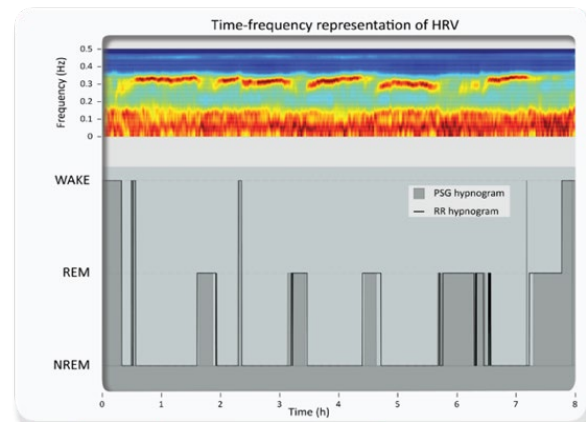


Figure 1: Sleep staging result for a healthy patient. The dark gray bands are hand-labeled by physicians and the solid black line is automatically computed by the analysis of HRV.

The RNN-based network brings about 20% improvement in mean accuracy over the baseline method and the CNN about 30%. Higher accuracy obtained by the CNN network suggests that high frequency patterns in the data, which RNNs are ineffective at modeling, is informative for the sleep staging task.

Both architectures are small in size and require limited computational resources to run. Future work includes optimizing them and embedding them on a resource-limited processor such as nRF52 SoC from Nordic Semiconductors in one of our low-power wearable systems.

[1] <http://www.statista.com/statistics/413265/health-and-fitness-tracker-worldwide-unit-sales-region/>

[2] <https://www.physionet.org/challenge/2018/>

FlexWave—Silicon Flexure Systems with Inkjet-printed Waveguides

J. Kruis, J. Disser, F. Lütolf, S. Droz

Optical waveguide structures have been tested on silicon flexures. Prior art focused on inkjet-printed waveguide structures on rigid substrates. This work deals with the challenges associated with printing waveguides on flexures. Preliminary results show successful realization of small waveguides on flexures and no significant mechanical issues with a large number of cycles. By the end of the project the optical performance over cycles will be validated and if proven successful, a gripper structure with integrated sensors will be realized. This gripper illustrates a whole range of new integrated sensor opportunities and opto-mechanical structures on precision flexure systems for applications in watch-making, micro-assembly etc.

There is a major global trend towards additive manufacturing like 3D printing as it allows unprecedented customization of functional pieces. Inkjet printing is a mature, contactless process within additive manufacturing, which offers a comparably high throughput while still being suitable for a variety of materials and substrates (especially curved or fragile parts). Previously CSEM has shown its capability of using inkjet printing for creating optical waveguides with losses of $0.61 \pm 0.26 \text{ dB/cm}$ ^[1].

The integration of optical sensors into (micro-) mechanical systems has also received a lot of attention recently, as they can achieve high resolutions, are insensitive to surrounding electrical fields and can operate under strong spatial confinement. CSEM silicon flexure systems have been used for the creation of MEMS, micro-components for mechanical watches, micro-assembly, miniature robots and beam steering^[2]. Within these contexts, integrating photonics and optics for the purpose of sensing adds a significant value. An example of a system that can benefit of integrated sensors is the gripper shown in Figure 1.

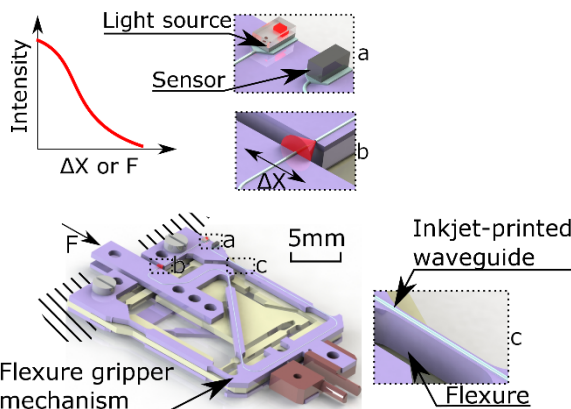


Figure 1: Combining flexure mechanisms, e.g., a flexure gripper mechanism, together with inkjet-printed wave guides for intensity based sensing of displacement (ΔX) or force (ΔF).

Investigating whether waveguide structures operate properly on silicon flexure systems addresses two challenges: the limited surface area for depositing the waveguide and the required performance over a large number of cycles.

The first challenge comes from the fact that the flexure systems are very small: Typically, flexures are around 50 microns wide

and narrow rigid bodies require radii of curvature of 300 microns for connecting the waveguides on the individual flexures.

In the context of this project, a process has been developed for printing waveguides with widths in the order of 50 μm and alignment precisions in the μm range. The process was optimized to yield waveguides with a width corresponding to the size of a single droplet ($\approx 40 \mu\text{m}$) with sufficiently small radii of curvature (300 μm , potentially lower values could be reached).

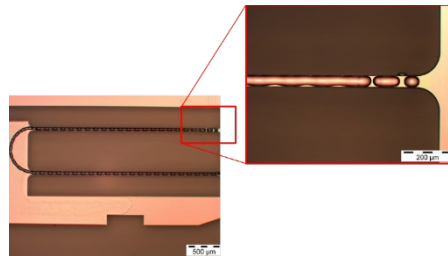


Figure 2: Waveguide printed on top of narrow 50 micron Si beams.

The second challenge is the optical and mechanical performance over large numbers of cycles. The number of cycles required is application dependent but the more the better. A typical range of interest is $1\text{e}3$ to $1\text{e}7$ cycles. A custom fatigue setup was created to evaluate optical and mechanical fatigue.

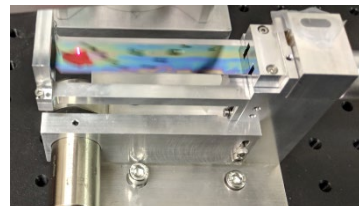


Figure 3: A custom designed opto-mechanical fatigue measurement setup with a silicon flexure moved for $1\text{e}7$ cycles.

The preliminary results on mechanical fatigue look promising, as no significant mechanical damages have been observed during first tests with up to $1\text{e}7$ cycles. The optical fatigue is currently being evaluated. If successful, the optical structures will be printed on top of the gripper illustrated in Figure 1 and assembled as a demonstrator for the technology.

The project has been supported in the frame of the MIP initiative and CSEM thanks the SERI (State Secretariat for Education, Research and Innovation) for their funding and support.

[1] P. M. Theiler, F. Lütolf, R. Ferrini, "Non-contact printing of optical waveguides using capillary bridges", Opt. Express 26, 11934-11939 (2018).

[2] J. Kruis, F. Barrot, L. Giriens, D. Bayat, R. Fournier, S. Henein, S. Jeanneret, "Design and fabrication of a novel centimeter scale three dimensional silicon tip, tilt and piston mirror mechanism," in EUSPEN 2013, Berlin, 2013.

DISPOGEN—Oxygen Sensing at Home

S. Heub, R. Ischer, R. Smajda, R. Pugin, J. Bennès, O. Chételat, M. Correvon, M. Despont, G. Weder

Oxygen is one of the most often monitored parameters in research and industry. In the recent years, CSEM has developed a contactless optical sensing technology for oxygen monitoring in many applications such as respiration, 3D cell culture systems, beverage process control and water quality. CSEM is pushing the technology further with the release of cost-effective disposable oxygen sensors with a smartphone readout.

Molecular oxygen is needed for aerobic life and, therefore, is one of the most monitored parameters in biotechnology, food production, industrial safety and pharmaceutical bioprocessing. In parallel, the demand for non-invasive, automated and wireless monitoring systems is growing to ensure product safety, quality and regulatory compliance.

Over the past years, CSEM has developed a new range of optical oxygen sensing systems including an objective-like reader for cell culture^[1] and a fiber-based reader for incubators^[2]. The sensors have shown advantages compared to current commercial solutions in particular in the reliability and robustness of the sensing layer. They are also more cost-effective. Wireless monitoring with standalone reader and mobile display is still an unreacheted market.

The project DISPOGEN builds on the expertise of CSEM in microelectronics, optics, and nanotechnology. The goal is to provide an innovative oxygen sensing solution, so called “O2@home”, for domestic, technical and industrial applications (Figure 1). Oxygen concentration and sensor ID can be measured non-invasively through any transparent packaging or container.



Figure 1: DISPOGEN's concept: a contactless and wireless system for oxygen sensing.

CSEM oxygen sensor (patented technology) consists of a luminescent-reactive dye embedded in a hierarchical porous matrix. The production is compatible with industrial manufacturing processes. In addition, a matrix barcode can be printed for sensor identification and database (Figure 2).

These oxygen sensors are disposable and coupled with a portable reading device paired with a smartphone (Figure 3). This reader provides its light source (LED) and its detector (photodiode) and all the optoelectronic components for oxygen measurement. The system uses the camera of the smartphone

to identify the matrix barcodes. Live oxygen readout and sensor ID are sent to the user's smartphone via Bluetooth and displayed on the screen via an Android application. The data are saved and stored in a distant database.



Figure 2: Disposable oxygen sensor (1 x 2 cm) with a printed matrix barcode using a biocompatible ink.

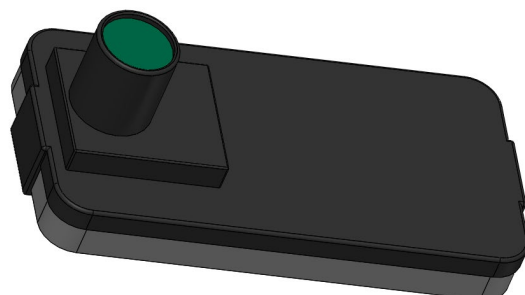


Figure 3: The reading device is developed as an accessory for a 5.2" smartphone with an Android OS. It includes low consumption electronics, battery, proximity sensor, a photodiode, and Bluetooth communication.

The DISPOGEN oxygen sensing solution fulfills all requirements for high precision, reliable, non-invasive, and wireless oxygen sensing. In this context, oxygen control can be used to assess e.g., microbial activity, quality of modified atmosphere to slow down the growth of aerobic microorganisms, dissolved oxygen in fishkeeping or prevent oxidation reactions. Besides, it enables applications requiring associated database management. This system also fits with the connected devices for home applications. It could be used to alert for oxygen depletion in a working room or in a private aquarium.

This project was executed in the frame of CSEM's MIP program, and CSEM would like to thank the Swiss Confederation and the Canton of Neuchâtel for their financial support.

[1] G. Weder, R. Ischer, M. Favre, R. Smajda, P. Albert, M. Liley, “DEMOX—a Miniature Non-invasive Optical Oxygen Sensor”, CSEM Scientific and Technical Report (2015) 47.

[2] S. Heub, M. Jungo, R. Ischer, G. Weder, A. Grivel, R. Smajda, X. Bulliard, R. Pugin, M. Despont, “Non-invasive Measurement of Oxygen and Carbon Dioxide in Microscope Biochamber”, CSEM Scientific and Technical Report (2017) 71.

LONGECG—Low-cost low-power Cooperative Sensors

A. Fivaz, O. Chételat, M. Crettaz, J. Wacker, J.-A. Porchet, K. Badami, M. Rapin

A new architecture of cooperative sensors especially suited for their integration in clothes for the long-term measurement of multi-lead ECG is in development. All sensors are connected to the same wire used as potential reference, synchronization, and remote powering. The sensors are essentially a low-power ASIC that ensures low-cost, highest miniaturization, and high quality ECG signals with dry electrodes.

Medical diagnostics based on classical measurements such as ECG (electrocardiograph) are usually performed in clinical settings by means of numerous adhesive gel electrodes, all linked to a recorder by cumbersome cables. However, disease symptoms do not appear on demand and so patients can benefit from daily long-term monitoring which is only possible with wearable devices. Existing portable solutions (so-called Holter) are bulky with loose cables and hence not wearable in a modern sense (not integrated), as shown on the left of Figure 1.

CSEM proposed the concept of *Cooperative Sensor* to address the integration of dry electrodes in garments while keeping the highest signal quality. In the context of ECG, cooperative sensors are active electrodes (i.e., with in-situ amplification) *connected in parallel* to a bus in contrast to the classical approach that uses electrodes which are usually passive, rarely active, and always connected with shielded or multi-wire cables in a *star arrangement* to a central unit. Therefore, one of the major advantage of CSEM's cooperative sensors is a drastic reduction of connecting complexity, which is particularly advantageous for systems with many electrodes in a wearable form factor.

However, so far, cooperative sensors required to be powered by their own power supply, which limits the integration and made battery management difficult. In the so-called LongECG development, we focus on a variant of cooperative sensors that allows them to be centrally powered via the single wire to which all sensors are connected. The same wire is therefore used as reference potential for the ECG measurement, for synchronization, and for powering. The return of the powering current is achieved via the body. In order to comply with the medical standards that drastically limit leakage currents (i.e., currents flowing across the body) to a very low level, the sensors must be ultra-low-power. This feature is of course also beneficial for autonomy, thus enabling continuous multi-lead ECG recordings of 20 or more days. In order to make the sensors as small and flat as possible, all sensor electronics is integrated in an ASIC (Application Specific Integrated Circuit).

The recorder shown in Figure 2 is also connected to the wire linking the sensors. It includes a rechargeable battery and memory for 20 days of autonomy. When disconnected from the garment, the recorder can be connected to a computer for data download and battery recharging via a USB link.

Special attention has been paid to the ergonomics and usability in the early phase of the project. Several doctors were consulted to define the medical needs. Moreover, mockups of textiles and sensors have been designed and prototyped. A particularly interesting design (patent pending), shown on the right of Figure 1, features sensors that can be freely positioned by

doctor by clipping them in a similar way as buttons in one of the numerous holes offered by a textile mesh. In Figure 1 (right), two blue sensors with a diamond shape are visible. We designed the electronics so that up to 10 sensors can be inserted. The mesh is conductive on its outer surface and is therefore the connecting wire required for this new architecture of cooperative sensors. This design illustrates well the advantage of the approach, since free positioning would be virtually impossible for any architecture with more requiring connecting constraints (e.g., a shielded cable per electrode in the classical approach). The recorder is not visible in Figure 1, but is placed on the side.



Figure 1: Classical solution (called Holter) to measure medical multi-lead ECG (left) and wearable solution with dry-electrode cooperative (right) showing a mock-up of the targeted wearable (button sensor inserted in an electrically conductive mesh allowing free positioning of sensors).



Figure 2: Recorder with USB connector for connection to garment as well as download and recharging with a computer.

This activity follows a set of achievements progressively obtained at CSEM thanks to a close collaboration between the MedTech (medical technology) and Systems-on-Chip (SoC) research activities where several variants of CSEM patented cooperative sensors have been demonstrated and tested against medical standards. The presented architecture focuses on ECG, but other signals can as well be measured. Cooperative sensors are in particular well suited for a new generation of wearables that will allow multi-signal measurement from a large number of spots spread over the body paving the way to wearable imaging technology^[1].

[1] M. Rapin et al., "Wearable Sensors for Frequency-Multiplexed EIT and Multilead ECG Data Acquisition," IEEE Transactions on Biomedical Engineering, July 2018.

MIAM-3D—Metallic Inks Applied to Additively Manufactured 3D parts

H. Sudan, L. Kiener, N. Marjanovic, J. Schleuniger, A. Mustaccio, N. Glaser, A. Lücke, S. Liberatoscioli*

MIAM-3D aims at developing a process to apply printed and plated metallic inks on 3D surfaces and inside thin channels, both built from structural polymer substrates processed by additive manufacturing (AM). The association of AM to manufacture complex shapes, ink printing and plating shows an interesting potential to bring electronics functionalities to a wide range of products. In particular, the metallization of inner channels is a pre-requisite to route electric power or signals inside the structure of a part and therefore to enable the supply of integrated components such as sensors or active elements for heating, cooling, magnetic fields generation, etc. To define target specifications, the project considered an industrial use case from RUAG Slip Rings SA (RSSR), namely the re-design of a Slip Ring Assembly (SRA). To date, MIAM-3D showed the feasibility of the base bricks, namely the deposition and plating of inks on tilted and curved surfaces, as well as inside channels.

The Additive Manufacturing of polymer materials enables a wide range of applications in the field of functionalized parts. During the last twenty years, huge development efforts were dedicated to those technologies, leading to multiple proof of concepts. Fused Deposition Modeling (FDM) techniques allow producing multi-material parts, thanks to the extrusion of melted thermoplastic filaments through multiple nozzles. By using filaments charged with conductive material, mechanical parts including basic electrical functions can be produced. The main drawbacks of FDM are that the parts show anisotropic mechanical properties and poor surface resolution. Furthermore, the thermosetting polymers charged with conductive particles show limited electrical conductivity. An alternative to FDM is Material Jetting 3D Printing which uses printheads to dispense droplets of photosensitive materials that solidify under ultraviolet. Thanks to multiple printheads, multi-material parts including conductive materials can be produced but their electric conductivity and overall durability are poor. Finally, the use of raw metallic inks processed with inkjet or Aerosol jet printing shows moderate conductivity and is limited to 2D or 2.5D surface applications.

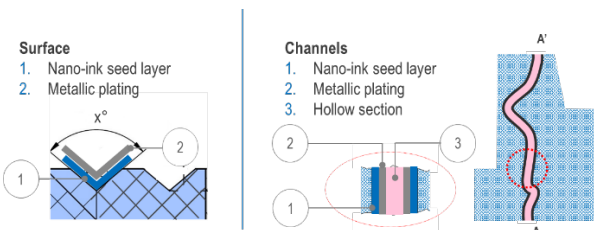


Figure 1: Cross sections of the geometries to be functionalized and illustration of the plated seed-layer. The outer surface has the shape of a V-groove roaming the perimeter of a cylinder. The channel is inside the structure.

To overcome those drawbacks, MIAM-3D proposes to use standard AM processes to manufacture complex shapes and to print metallic inks which will be used as a seed layer for a subsequent metallic plating process. The plated inks will therefore offer the conductivity of the bulk material, a strategic asset when electrical power is to be transmitted. Moreover, the durability of metallic plating layers is well proven. Provided an upgrade of the inkjet setup, inks can be printed on surfaces including 3D topologies. The inks can also be injected to coat hollow channels running inside the structure of the part (see Figure 1). Subsequent plating of the channels will allow achieving high electrical conductivity. As shown on Figure 1 and Figure 2,

the Slip Ring Assembly (SRA) use-case of RSSR gathers both requirements: conductive layers on curved and tilted surface, as well as inside channels in order to route the signals from one location to another.

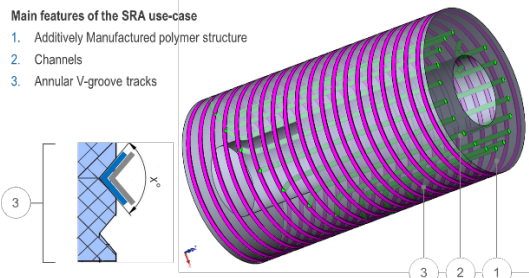


Figure 2: Pre-design of the SRA use-case with its main features.

Current status

The critical geometries shown in Figure 2 were successfully achieved thanks to DLP 3D printing of a ceramic-polymer composite (see Figure 3). Some fine tuning of the geometries is ongoing to improve the shape of the V-grooves. Silver nanoparticles ink was successfully printed to representative V-groove samples and finally plated with copper. The electrical resistance of the plating is in the range of 1Ω and the adhesion was validated by means of tape lift testing. The conductive channels were successfully achieved on representative samples by means of an electro-less plating of nickel. The current line resistance is in the range of 1Ω . For both tracks and channels, the electrical properties will be further improved since the plating parameters are not yet optimized. The project is currently continuing with the plating and testing of the prototypes illustrated by Figure 3.

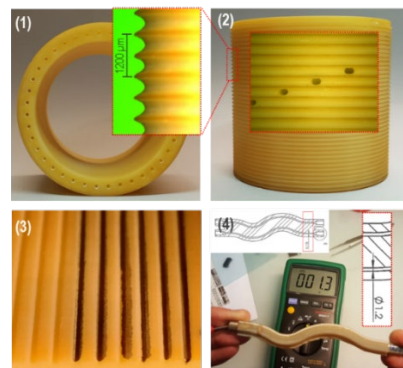


Figure 3: (1) & (2) 3D printed SRA prototype, (3) V-grooves plated ink layers, (4) channel test sample electrical resistance measurement.

* RUAG Slip Rings SA (RSSR)

PocketDX—Compact Flow Cytometer for Industrial Water Quality Monitoring

Z. Halvorsen, V. Revol, S. F. Graf, N. Schmid, H. F. Knapp, P. Cristofolini

Monitoring the quality of water is a constant concern for public health and particularly for the water treatment industry. By law water quality has to be guaranteed until the entry of buildings. Therefore, there is a growing demand for rapid and reliable instruments for in-line monitoring the microbiological quality of drinking water at low costs per data point. We demonstrate here an automated and compact sample preparation module with zero dead volume. A ten-fold reduction of the dye consumption for lower manufacturing costs could be achieved thanks to a novel microfluidic rotary valve concept.

Fluorescent staining coupled with flow cytometry (FCM) is used for quantification and characterization of bacteria in both natural and engineered environmental water sample^[1]. This method allows precise and rapid detection of the total microbial cell count of a water sample. Water samples are incubated and stained with an asymmetrical cyanine dye (SYBR® Green I) that binds to nucleic acids and results in the formation of a DNA-dye complex that emits green and red light when excited by a 488-nm blue laser^[2]. The ratio of the green to red fluorescence levels is used to differentiate bacteria with high and low nucleic acid content (HNA and LNA).

Most commercially available flow cytometers are full-sized laboratory bench-top instruments, which are too sensitive and bulky to be operated in water distribution facilities. In addition, sample preparation is usually conducted manually by a trained laboratory expert using costly proprietary dye solution. Consequently, there is a great potential in developing in-line flow cytometers that adopt miniaturization and automation of the fluidic sample preparation.

A novel sample preparation module combining fluid distribution and mixing in one microfluidic device has been developed for automated operation with lower reagent consumption and waste generation per measurement, reduced manufacturing costs, lower power consumption and lower weight. This, in turn enables the rapid, precise and fully automated analysis of bacteria quantity in water at relatively low costs. Further details can be found in another report^[3].

The sample preparation was validated using a commercial optical readout module which was calibrated with calibration beads before running the experiment. Using the automated sample preparation module, 90 µL of water sample containing known concentrations of e-coli bacteria were stained with a fluorescent stain (SYBR Green I). Samples were pre-warmed to 37°C ($\pm 2^\circ\text{C}$) followed by staining for 13 minutes with 10 µL of SYBR® Green I (sigma-Aldrich, Switzerland) at a concentration of 1x (which is a 10,000x final dilution of DMSO stock solution). The prepared solution was then directed to the capillary inside the optical read-out module at a constant flow rate of 20 µL/min. SYBR® Green I solution fluorescence was visualized using a two-dimensional FL1 (emission filter 533/30) vs FL2 (emission filter 715 LP) log-scale density plot.

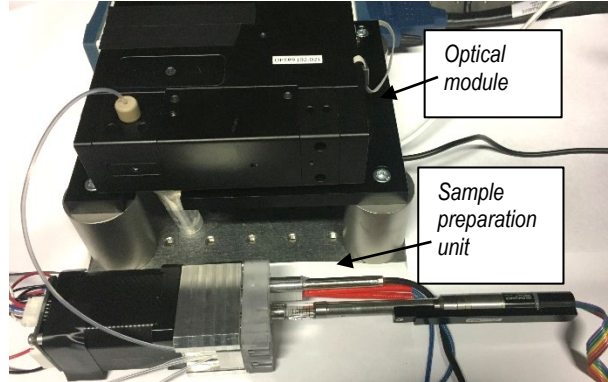


Figure 1: Configuration of miniaturized flow cytometer consisting of a fluidic sample preparation unit, a multi-wavelength optical readout module (scattering and fluorescence) and real-time data processing algorithm.

The results of the measurement with an e-coli concentrations of 10^5 and 10^6 CFU/ml are shown in Figure 2. The results confirm the correct functioning of the sample preparation module. Further quantitative investigation are on-going.

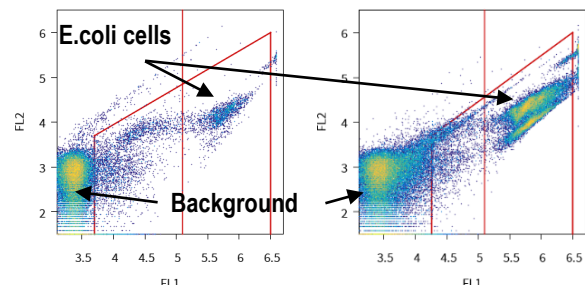


Figure 2: Flow cytometric analysis of a water sample contaminated with *E. coli* cells (10^5 and 10^6 CFU/ml).

In order to further reduce the cost of this FCM platform, a novel optical readout module is under development. Silicon photomultipliers will be used instead of the traditionally expensive photomultiplier tubes. Furthermore the fluorescent filters will be replaced by a diffractive optical system. Both factors will lead to an overall reduction of the manufacturing and assembly costs.

This work was supported by the Swiss Confederation and MCCS (Micro Center Central Switzerland).

[1] F. Hammes and T. Egli, 'Cytometric methods for measuring bacteria in water: Advantages, pitfalls and applications', Analytical and Bioanalytical Chemistry. 2010.

[2] SLMB, 2012. Determining the Total Cell Count and Ratios of High and Low Nucleic Acid Content Cells in Freshwater Using Flow Cytometry. Analysis Method 333.1, the Swiss Food

Book.(Schweizerisches Lebensmittelbuch). Federal Office of Public Health, Switzerland.

[3] Z. Halvorsen, N. Schmid, V. Revol, S. F. Graf, H. F. Knapp, "First microfluidic valve with integrated mixer for in-line sample preparation", CSEM Scientific and Technical Report (2018) 46.

PROBIOTICS —a Pressure Monitoring Robust Unobtrusive Batteryless IoT Integrated Circuit & System

D. Ruffieux, P.-A. Beuchat, A. Bischof, R. Catteneoz, J. Deng, C. Denizot, D. Dominé, S. Emery, M. Fretz, R. Godinho Caseiro, J. Kilchoer, V. Kopta, Y. Liechti, T. Mavrogordatos, C. Monneron, T. C. Müller, J.-L. Nagel, T. Overtstolz, F. X. Pengg, E. Perez, P. Persechini, M. Pons Solé, N. Reamy, C. A. Salazar Gutierrez, N. Scolari, D. Severac, D. Sigg, A. Vouilloz, L. Zahnd, Y. Zha

PROBIOTICS aims at realizing the first robust, extremely miniaturized, pin-sized, energy autonomous Internet-of-Things node combining energy harvesting, storage and management, sensing (e.g., pressure, temperature), on-chip digital signal processing and wireless data transfer. It addresses the booming IoT market by leveraging CSEM multidisciplinary skills to solve both the power and size bottlenecks currently preventing ubiquitous WSN deployment.

The Internet-of-things (IoT) holds the promises to connect wirelessly almost any sensor node (WSN) to the cloud accelerating the digitalization of our society. Wide and ubiquitous deployment is however currently facing a critical bottleneck. How to energize the foreseen billions of nodes in a maintenance-free way? IoT market penetration is hindered by the reliance on technologies that fuel the smartphone revolution: These off-the-shelf parts (COTS), targeting high performances, high complexity applications, are too energy-greedy to ensure the kind of autonomy requested by the envisioned tiny nodes. In order to overcome this challenge, the missing components required to build an extremely low power, unobtrusive, energy autonomous WSN capable of interacting with the mobile infrastructure via the Bluetooth Low Energy standard are being developed.

As a representative sensing element, an SOI-based, ultra-compact, piezo-resistive, chip scale packaged pressure sensor is being designed. Through-silicon via are used to connect the top sensing face of the device to the electrical pads on the bottom, easing assembly. It is associated to a system-on-chip (SoC) integrated circuit that is capable of acquiring and processing locally the signal in order to reduce the payload to be transmitted wirelessly, since each byte is associated to a high energy penalty. Such an energy-efficient computing scheme performed at the edge, coupled with a smarter data management approach yields tremendous power savings despite the added complexity.

This approach makes possible for the SoC to harvest its own energy from a miniature PV-cell, provided an efficient Power Management Unit (PMU) is used to optimize the energy distribution, usage and storage. Precise time and frequency references are obtained with two crystal oscillators (XO) running at 32 kHz for timekeeping and scheduling and 48 MHz for ADC/radio operation. Complementing the two XOs, a programmable on-chip ring oscillator whose frequency can be locked to one of the references is used to clock the sub/near threshold microcontroller (MCU) operated at 0.5 V at various speeds from a few kHz up to 20 MHz, for maximum flexibility.

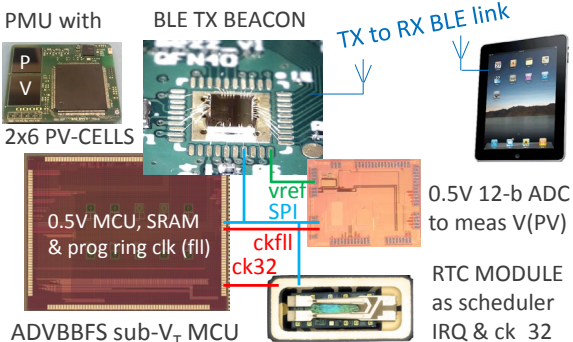


Figure 1: Preliminary WSN demonstrator made with test-chips.

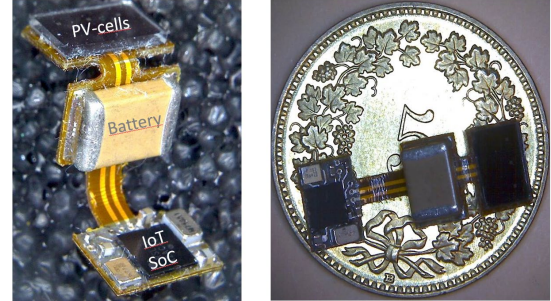


Figure 2: Photographs of the energy autonomous miniature IoT WSN.

Running the MCU at 0.5 V rather than 1 V trades maximum speed off for a large quadratic power gain (4x) but also amplifies the sensitivity to PVT variations. Unchecked, the latter, yields to a frequency variations of 100x. However, it can be mostly eliminated ($\pm 10\%$ residue) thanks to a simple patent-pending current servo loop that adjusts individually the substrate voltage of N and PMOS transistors. Most of the speed penalty can be cancelled without any additional circuitry by forward-biasing the MOS transistors, at the expense of an increased leakage. With bulk voltages spanning -1 V (REV) to 0.6 V (FWD) referred to the N & PMOS supply rails, PVT compensation and 100x frequency scaling is obtained when using MIE Fujitsu 55 nm DDC CMOS technology. The robust control scheme allows to dynamically and adaptively scale the MCU performances and its associated system clock at run time, guaranteeing minimum energy dissipation over a wide range of frequencies. With this approach, a record low dynamic power of 3 μ W/MHz was measured for the 32 b-MCU. The combined 0.9/0.5 V 1 Msps 12-b ADC digitizing the sensor data makes use of the same principle, consuming merely 20 μ A. Compared to the 6 mW, 1-2 Mbps BLE TRX running at 0.95 V, it allows data acquisition and computing operation with 1 pW/bit and 0.1 pW/bit respectively, or between 3 and 4 orders of magnitudes less than communication.

Figure 1 shows the intermediate WSN demonstrator that was built with the three MCU, ADC and BLE test-chips and a COTS RTC. As a simple PMU replacement, two homemade 1.5 cm² six-segments, SMT compatible PV-cells, delivering 30 μ W at 500 lux, are used to supply -1 V, 0.5 V, 1 V and 3 V. Capacitors absorb peak currents such as when the ADC measures the PV-cells voltages and as BLE beacons encoding that information are transmitted to a tablet. The MCU operates at various speed and in retention to optimize the overall consumption at runtime.

As an outlook, Figure 2 shows the miniature WSN implemented with a COTS IoT SoC incorporating CSEM BLE IP. After folding, the WSN, supplied by a 100 μ Ah 1.5 V SMT battery recharged by a 3-segments miniature PV-cell delivering 3 μ W at 500 lux, is about the size of the inner digit of Swiss 5 cts coin!

Witness—an Autonomous Camera on a Sticker

S. Blanc, M. Crettaz, E. Favre, M. Fretz, C. Gimkiewicz, R. Krähenbühl, P.-F. Rüedi, E. Türetken, P. Nussbaum

Witness is an autonomous ultra-low power image recording device integrated on a flexible palm sized sticker. Powered only by solar energy, it records still pictures of the environment based on a motion detection algorithm and stores them in a local memory for off-line use. The device is primarily dedicated to surveillance applications, where a surveillance perimeter is created by placing units on walls and ceilings. Due to its autonomy and generic processing capabilities, CSEM expects the Witness platform to find numerous other uses far beyond this scope.

The Witness project has succeeded in this multi-disciplinary challenge by resolving five key technical challenges.

A highly efficient, flexible and adhesive PV Cell

A flexible disc-shaped Photovoltaic (PV) cell with an adhesive surface was designed and tested. A first prototype of 80 x 80 mm and 0.2 mm thickness has been produced and mechanically tested for bending stress. The power delivered is 2.55 mW @1 kLux.



Figure 1: Front side view of the PV cell with the magnetic dock (left) cell flexibility (middle) and camera docked on PV (right).

A patented system for magnetic attachment (dock) of the camera button has been designed and integrated into the PV cell (gold plated disc) while preserving the cell flexibility. It opens the possibility to attach buttons with other functionalities than a camera, as well as mounting the active side of the PV front or back (for mounting on a wall or a window).

Ultra-thin, wide angle optics

An ultra-thin optic with a 120 ° field-of-view has been designed to meet the requirements of the application. The patented approach is based on a macro-lens array (2 x 2) with a lens shift compensating for the small fill factor (20%) of the imager. The lens also compensates the illumination homogeneity with a central obscuration.

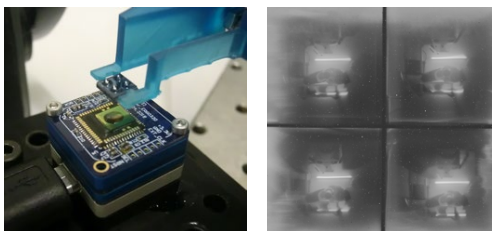


Figure 2: Lens array prototype during assembly on CMOS imager (left) and resulting 4 pictures (right).

The milling process of the diamond-turned prototype didn't reach expectations in terms of sub-pixel alignment of lenses. An alternative approach providing accurate lens alignment consists of wafer-level optics and this is compatible with existing micro-optical fabrication techniques at CSEM.

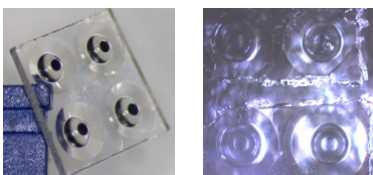


Figure 3: Original lens (left), replicated version (right).

The aspherical shape of the lens requires a diamond-turned mold for the prototype. The measured profile demonstrated the expected shape replication. However, demolding results in a lens sag of 300 µm and as such the manufacture still requires improvement.

Ultra-low power image capture ASIC

An ultra-low power (sub-mW) and high dynamic range (120 dB) QVGA sensor has been developed and tested. The innovation lies in a novel and patented pixel architecture based on the integration time to saturation scheme.

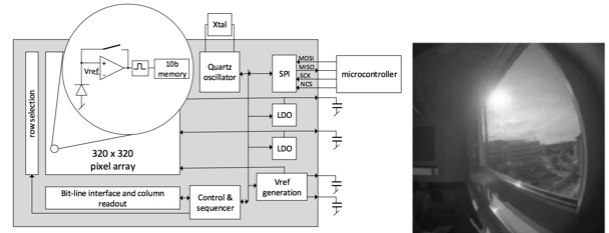


Figure 4: Chip architecture (left) and resulting image (right).

Algorithms to target power efficiency and flexibility

The algorithms dedicated to motion detection, image compression, and storage in local memory are developed and optimized on a Nordic (nRF52) platform for flexibility and power efficiency. The complete system, achieves less than 1 mW consumption on average.

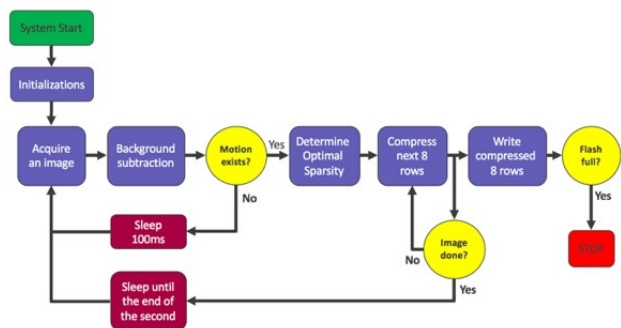


Figure 5: Functional architecture of the software system.

Efficient System Integration

This functioning data logger "Witness" integrates the whole camera functionality into a button of 30 mm diameter and 4 mm thickness. Careful selection of the commercial components (processor, memory, power management unit) ensured reaching the stringent power consumption requirements.

3DprintedFluidics—Revolutionary Fluidic Components Enabled by Additive Manufacturing Technologies

S. F. Graf, J. Kaufmann, S. Berchtold, T. Volden, N. Schmid, O. Chandran, S. Lani, J. Schleuniger, F. Lütolf, V. Revol, H. F. Knapp

Additive manufacturing offers new freedom to conventional manufacturing. While some industries have fully adopted additive manufacturing, this potential is currently not fully used for creating innovative designs of fluidic components and systems. We focused on the design of fluidic components which can be used as building blocks for new applications. By combining state of the art printing technologies as Fused Deposition Modeling (FDM), Stereo Lithography Apparatus (SLA), inkjet and screen printing, crucial components such as valves (passive and active) and pumps (mechanically or magnetically actuated) have been developed and integrated with sensors to monitor pressure and measure light scattering. These components can also be combined into compact, integrated systems.

3D printing is getting more and more popular. Even the sharp calculating automotive industry prints an increasing number of parts instead of using conventional manufacturing methods. Emerging multi-material 3D-printers (piezo-ceramics, polymers, metal inks) together with hybrid assembly are opening new opportunities for functional components. In this project, new design approaches for active fluidic components were investigated. The ultimate goal is to be able to realize complex fluidic functions in customized chips including actuators, chambers, manifolds and sensors.

In the first year, innovative designs were explored for individual components: pumps, valves, light barriers, pressure sensor and connectors.

3D printed pumps & valves

On-chip pumps and valves in microfluidic chips are often realized using flexible PDMS structures, which are actuated pneumatically^[1]. A drawback is the required pneumatic connection which is cumbersome to connect and prone to leakages. For these reasons, alternatives using mechanical actuation as well as magnetic actuation were selected. One pump design is illustrated in Figure 1. It was printed in a SLA process and works with a pump chamber and co-printed check valves. Another example of a printed Tesla valve is shown in Figure 1.



Figure 1: Pump with integrated check valves for mechanical actuation (left); Printed Tesla valve (right).

For the magnetic actuation, a pump chamber was FDM printed, then closed-off with a PDMS-membrane in a dispensing and curing process. Finally a magnet was assembled by hybrid bonding for a completely contact-free actuation. In a next step, the magnet will be replaced by printed magnetic particles to minimize assembly steps.

Integrated pressure sensor

Printed pressure sensors would enable to functionalize fluidic components such as manifolds in order to monitor and control the flow. A capacitive pressure sensor was realized on a SLA printed substrate. Metallic electrodes were inkjet printed together

with a water soluble sacrificial layer onto the substrate. A cross-section in Figure 2 shows the fluidic channel with the underlying electrodes. The measured capacity is thus directly related to the pressure. Current effort is put into thinning the pressure sensor membrane as well as increasing sensitivity by bringing the electrodes closer together.

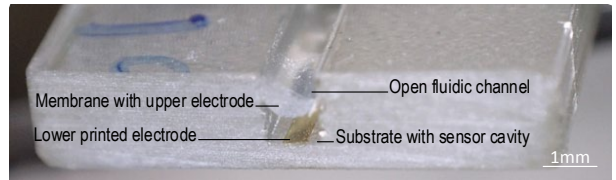


Figure 2: Cross section of a printed pressure sensor flush with the fluidic channel. Covertape to close-off channel not shown.

Light barriers

Light barriers are often used in fluidic chips to detect bubbles or particles in the flow. As shown in Figure 3, a light barrier was realized by inkjet printing a waveguide into a SLA realized substrate. Passing particles or air bubbles result in a change of the measured intensity. This information can be used to trigger an event (e.g., valve opening) in the corresponding operating system.

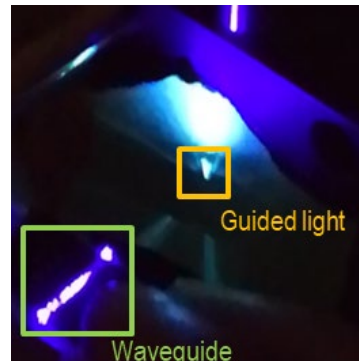


Figure 3: Light barrier printed across a channel to detect air bubbles or particles in the fluid.

In a next step, the developed fluidic components will be characterized in detail and integrated into an organ-on-a-chip platform.

This work was supported by the Swiss Confederation and MCCS (Micro Center Central Switzerland). CSEM thanks them for their support.

[1] M. Unger, H. P Chou, A. Scherer, S. Quake, "Monolithic microfabricated valves and pumps by multilayer soft lithography, Science, 288 (2000) 113.

HECTIC2—SiC-based MEMS Pressure Sensor Development

G. Spinola Durante, R. Jose James, M. Fretz, S. Ischer, A. Hoogerwerf, M. Despont, O. Dubochet, M.-A. Dubois, S. Mohrdiek

Silicon carbide (SiC) is a highly corrosion and temperature resistant material, which makes it the material of choice for many harsh environments sensor applications. Its chemical inertness makes it also biocompatible^[1]. The high temperature resistance makes it useful for developing MEMS suited for monitoring of gas turbines, jet engines, oil and gas wells, and space rockets^[2]. CSEM is developing the key front-end and back-end fabrication processes of SiC-based MEMS sensors in order to fabricate fully functional pressure sensors with operating temperature in air up to +600°C^[3].

Piezoresistive pressure sensors are formed of a cavity covered by a compliant membrane in which piezo-resistors have been defined. Silicon piezoresistive pressure sensors have been around since the 1960s. The use of SiC as a pressure sensor material has many advantages, due to its high temperature and chemical resistivity. However, the realization of such a pressure sensor requires the mastering of several technologies. An important one is the hermetic bonding of the SiC sensor to the back-plate to form a reference cavity.

The hermetic SiC to SiC bonding has been performed with a CSEM proprietary low-temperature laser bonding technology that has been developed in previous projects. The testing of the hermetic seal has been performed on sets of two back-plates bonded together with a laser (Fig. 1a). The seal is first tested for liquid-tightness by verifying the absence of dye penetration in the cavity (Figure 1a). A subsequent Helium leak test is carried out with an Inficon ULFab100 machine to verify the tightness of the seal.

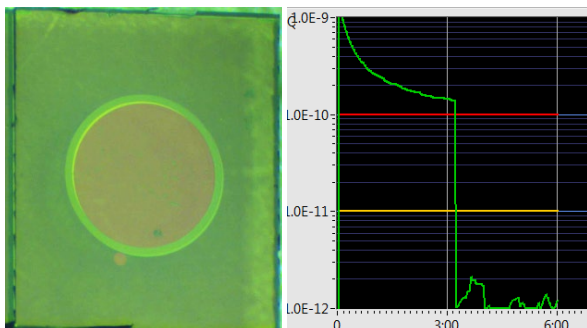


Figure 1: (a) Two lids sealed with laser and immersed in dye-penetrant liquid. In red, the wet (hermetic) area; (b) Helium leak-test profile after 10h in air at 600°C.

The yield of the hermetic laser bonding of the two lids together is very high, with a 100% pass for dye-penetration after 1 week testing. Samples of these chips were Helium leak-tested before and after 10 h at 600°C in air (Figure 1b). 100% of the sampled chips were still hermetically sealed. After testing 500 h at 600°C in air, 60% of the chips were still hermetic, indicating a degradation trend^[4].

Though a few samples already have shown some potential, the technology still requires to be improved to show its full potential and reliability for operation up to 600°C in air. Investigations are now ongoing at CSEM to further optimize the technology and bring it to a high TRL to ensure fast and rapid time to market for CSEM customers and project partners.

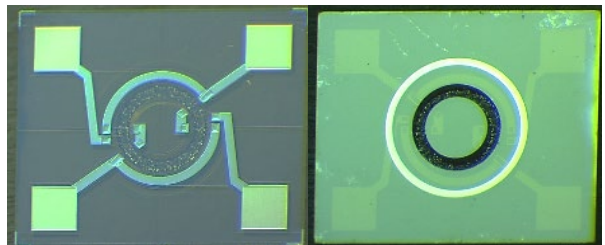


Figure 2: SiC-based MEMS pressure chip prototype realized.

The key processes are expected to become combined in one SiC-based MEMS fabrication technology aiming firstly at making a pressure sensor, starting from the current layout configuration (Figure 2) and secondly a temperature sensor out of the same bonding scheme, by exploiting the piezo-resistive temperature dependence.

It can be expected that a broad portfolio of harsh environments sensors can be addressed by CSEM with this technology, such as gas sensors, force sensors, and accelerometers.

These promising technology bricks and the related MEMS designs will be addressing a highly dynamic and emerging field and market of sensor components for harsh environments. Key enabling aspects are chemical resistance, intrinsic shock resistance due to doped piezo-resistance, and high-temperature stability due to process design choices.

In collaboration with customers, CSEM will be able to customize the above explored SiC-based MEMS technologies: developed products can therefore be tailored to various needs to match operation in harsh environments.

This work was supported by the Swiss Confederation and MCCS (Micro Center Central Switzerland).

[1] S.E. Saddow, "Silicon Carbide Biotechnology", Elsevier, 2016.
[2] M. B. J. Wijesundara, R. G. Azevedo, "Silicon Carbide Microsystems for Harsh Environments", Springer, pp. 1-26, 2011.
[3] G. Spinola Durante, et al., "HECTIC - Harsh Environment Ceramic Technology Involving Silicon Carbide", CSEM Scientific and Technical Report (2017) 17.

[4] G. Spinola Durante, P.-A. Clerc, M. Fretz, A. Hoogerwerf, R. Jose James, M. Despont, O. Dubochet, M.-A. Dubois, S. Mohrdiek, "Packaging technologies for harsh environments based on silicon-carbide (SiC) substrates", Proceedings of IMAPS MiNaPAD Event, Grenoble (France), May 2018.

SILOSCAPE—Flexure-based Oscillators for Mechanical Watches

F. Barrot, F. Cosandier, G. Musy, L. Giriens, S. Droz, Y. Petremand

For the past ten years, CSEM has demonstrated that, using micro-manufacturing techniques inherited from the microelectronics industry, it is possible to batch process with a micrometric precision, centimeter scale silicon parts featuring fine mechanical functions. High precision mechanical watch parts can particularly benefit from this approach. CSEM, combining its expertise in the domains of precision mechanisms and micro-manufacturing techniques, is a pioneer and aims at becoming the Swiss Competence Center for the design, manufacturing, assembly, and characterization of hybrid silicon based innovative watch micro-mechanisms.

Silicon is characterized by an ideal elastic behavior, a high fracture strength and a low density. It is amagnetic and corrosion free; using microfabrication techniques inherited from the microelectronic industry, it can be batch processed in 2.5D with a micrometric precision for the production of large quantities of centimeter scale mechanical parts comprising fine mechanical functions such as flexure blades. Silicon has opened up new opportunities for the design and production of novel and innovative watch mechanisms.



Figure 1: Overview of flexure based mechanical oscillators invented, designed and produced at CSEM over the past ten years.

CSEM was a precursor in this field [1], paving the way for a new trend that is now followed by several key players in the Swiss watch industry. The oscillator, together with the escapement, is one of the most delicate and high added-value parts of a mechanical watch. For the past ten years, CSEM has proposed several original designs of mechanical watch oscillators [2,3] while, at the same time, carrying on its pioneering work by pushing back the frontiers of silicon micromechanical structuring and improving its mastering of the production of such delicate parts [4]. The CR4 is the last watch mechanical oscillator designed and produced by CSEM (Figure 1).

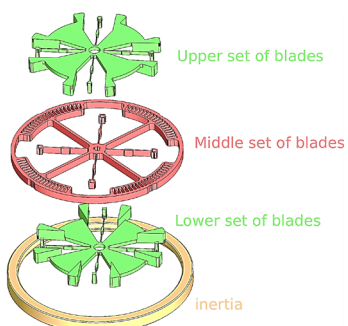


Figure 2: The CR4 mechanical oscillator – exploded view.

Like the Butterfly and Wittrick oscillators (Figure 1), the CR4 is guided by a set of flexure blades combining the restoring function of a hair spring together with the guiding function of a pivot. The CR4 is made of the stacked assembly of three silicon slabs comprising 2 pairs of blades, featuring a total 3x4 blades dispatched on three levels (Figure 2). Characterized by a better isochronism than its predecessors, the CR4 features a low displacement of its center of rotation alike the Wittrick, and is also characterized by a high quality factor.

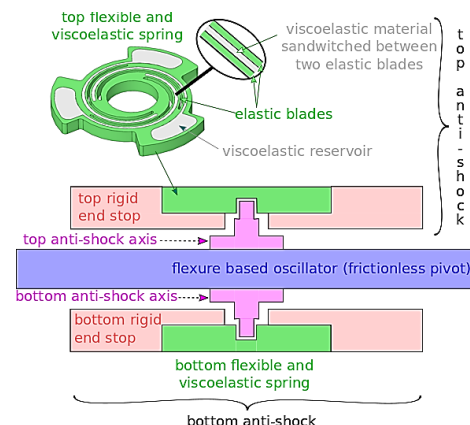


Figure 3: Anti-shock for flexure based mechanical watch oscillators.

Oscillators guided by flexures are characterized by the absence of friction; to protect them from shocks, a classical anti-shock implementation is not appropriate due to the constant friction exhibited by classical anti-shocks and the absence of physical pivot axis in flexure based oscillators. Therefore, CSEM imagined a novel anti-shock concept targeted for flexure based watch oscillators [5] which consists in assembling a top and a bottom axes to the oscillator at the location of the virtual pivot (Figure 3). These axes only come into contact with the fixed parts of the anti-shock when subjected to shocks above a given amplitude (typically > 60-100G). Two stages of protection are activated depending on the amplitude of the shock. For casual shocks on the wrist, the anti-shock axes will come into contact with viscoelastic springs that will dissipate the energy of the shock by shearing of a viscoelastic material so as to avoid consecutive rebounds that would cause unwanted energy losses; for accidental shocks the larger diameters of the anti-shock axes can also come in contact with rigid end stops.

[1] A. Perret, "Le silicium comme matériau dans la fabrication de pièces mécaniques", SSC, 2001.

[2] F. Barrot, et al., "Hybridization of Silicon Micro-components", CSEM Scientific and Technical Report (2014) 13.

[3] F. Barrot, et al., "Un nouveau régulateur mécanique pour une réserve de marche exceptionnelle", SSC, 2014.

[4] S. Jeanneret, et al., "Procédés de micro-fabrication avec application horlogère, développements récents", SSC, 2008.

[5] S. Droz, et al., "shock-absorber device, in particular for a micromechanical clockwork component", US 2016/0291548 A1.

SmartShock—Mechanical Shock Resistance of Mesoscale Parts: Semi-automatic Design Testing and Adaptation

I. Marozau, S. Widmer, P. Jokic, B. Schaffer, P. A. E. Schmid, O. Sereda, M. Dadras

Miniaturization of high-precision silicon-based mechanical parts of MEMS components and devices impose increasing requirements for their reliability, and particularly for their resistance to mechanical impacts. This becomes especially important for novel application markets such as watch industry, where mesoscale Si-based mechanical parts become promising candidates to replace classical metal-based designs. The present approach to assess the mechanical shock resistance of mesoscale parts relies on qualitative analysis of slow-motion shock test videos. Within the current project we develop a unique semi-automatic system for the analysis of mechanical deformation and stress in precision mechanical parts at mesoscale level during high speed impacts, such as mechanical shocks. The system allows to overcome the main drawbacks of the present approach.

The project aims to develop a novel semi-automatic system for the analysis of mechanical deformation and stress in precision mechanical parts at mesoscale level during high speed impacts, such as mechanical shock. This allows the determination of weak points and enable optimization of the design for the structures containing mesoscale precision parts. The main areas of application of such a system is the watch industry, especially for designs where Si parts with high mechanical performances are used, as well as MEMS-based micromechanical systems. For these technologies, the evaluation of mechanical shock resistance of tiny Si parts and determination of the design weaknesses is an important issue.

The state of the art approach consists of “manual” analysis of slow-motion videos acquired with a high-speed camera. Its main drawback is related to inconsistency of the analysis due to the rather qualitative and non-quantitative approach. The proposed approach allows to overcome this limitation by implementing a semi-automated system that performs quantitative data analysis of slow-motion videos. The developed system consists of a specially-designed high-speed camera, synchronized with the existing mechanical shock testing setup (Figure 1). Acquired high-speed videos are analyzed frame-by-frame using a developed post-processing data analysis software that extracts quantitative measurements of deformations on the targeted mesoscale parts. Mechanical stress is calculated from these measurements as a function of time and mechanical acceleration up to the failure of the part. The data is then compared to the theoretical simulations.

The proposed system consists of 4 integrated components:

1) Mechanical shock testing setup that allows conducting mechanical shock test of macro- and mesoscale Si-based parts. The test parameters, such as shock acceleration and shock pulse duration are controlled and logged in-situ using a reference accelerometer.

2) FastEye high-speed camera (Figure 2) developed at CSEM that features a 1 MP image sensor which can acquire full resolution images at frame rates of up to 2 kfps. By combining high signal-to-noise ratios and global shutter pixels, the sensor captures high quality, smear-free images.



Figure 2. FastEye high-speed camera.

3) Frame-by-frame video analysis module. The module is a part of the CSEM VISARD (Vision Automation Robotics Designer) platform that is used to control the camera, to acquire and log the image data, and to perform the data analysis using a dedicated algorithm.

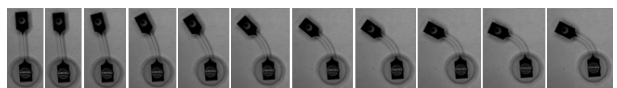


Figure 3. Deformation of a Si-part during the shock test at $\sim 200g$. Each next image is taken with a delay of 0.67 ms after the previous one (1500 fps). The total part length is 12 mm. The central beam width is 10 μm .

4) Tunable simulation module, which is applied for theoretical simulation of the behavior of the selected mesoscale parts subjected to mechanical shock. This information is used to support the experimental data and to provide suggestions on possible improvement of the mechanical resistance of the evaluated parts.

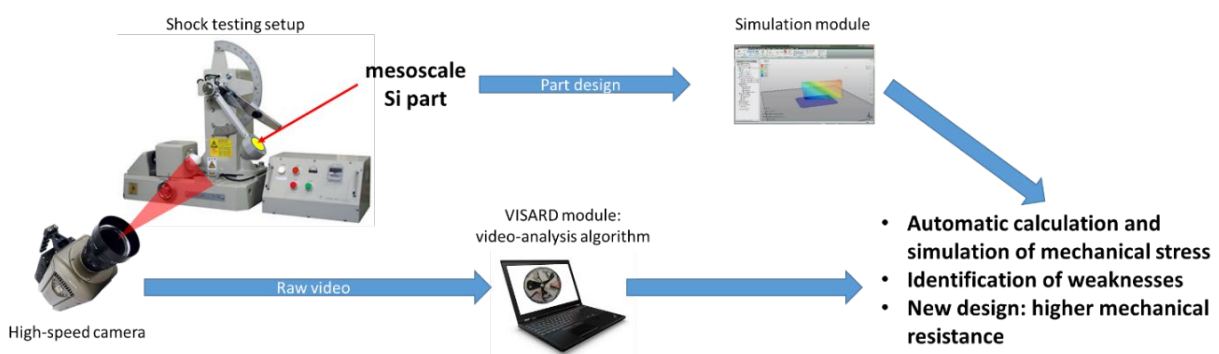


Figure 1: Schematic representation of the proposed system.

MICROSYSTEMS

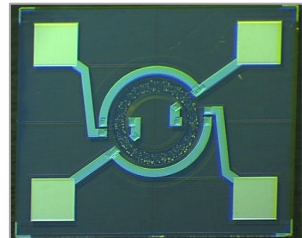
Michel Despont

The use of microsystem technology continues to grow, fueled by the need for ever smaller, lower power, smart devices. Integration of different technologies and miniaturization are at the heart of CSEM and its **Microsystems** program aims to bring innovation through the development of new micro-manufacturing technologies, the use of MEMS technology, and the introduction of advanced packaging concepts.

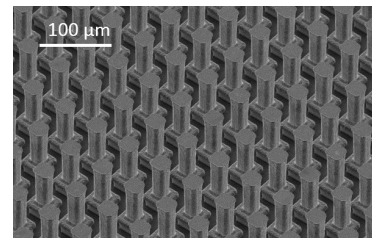
The microsystems market, according to various studies, enjoys a healthy 13–14 percent CAGR and is approaching a market size of 15 billions US dollars. Microsystems are used almost everywhere, in devices that sense and monitor our environment and influence our daily lives. For example, today's cars can make use of dozens of integrated sensors and actuators for monitoring and controlling engine functions as well as for safety, navigation, and passenger comfort. Similar trends can be seen in portable devices, such as smart phones, with a dozen sensors incorporated into the most recent models. Moreover, global technology trends such as the Internet of Things (IoT), the Smart City, Industry 4.0, or personalized medicine require the massive use of connected sensors and promise large new markets for ultra-miniaturized microsystems for applications in fields such as building automation, healthcare and the life sciences, consumer and home automation, transportation, industrial and environmental monitoring, security, and retail and logistics. All of these applications are looking for autonomous, low-power, small-form-factor, and low-cost sensor and actuator devices.

A large part of the microsystems market is taken by large companies such as ST Microelectronics, Bosch, or Texas Instruments, which target mainly the consumer and automotive markets and make significant efforts in process standardization in order to cope with the permanent cost pressure of such applications. Beyond these mass markets, a large proportion of sensors and actuators are fabricated in moderate volumes for specialty but high-added-value markets. The fabrication of these moderate volumes of microsystem devices requires customization, and necessitates significant know-how from multiple disciplines, including fabrication technology, packaging, material science, and reliability. Hence, although the fabless model may be gaining some momentum, providers of MEMS-based microsystems are mostly relying on the Integrated Device Manufacturing (IDM) model, and use their own, dedicated, manufacturing facilities.

Swiss industry, and in particular its SMEs, has recognized the potential of developing specialty microsystem-based products as a strong differentiator and is present in many niche markets, successfully competing on a global level. For SMEs in particular, it is crucial to fill the pipeline of innovation from fundamental research to the industrialization of new technologies in order to be able to continue to offer innovative products. CSEM has a track record in bringing microsystems technologies to market, and is uniquely positioned to be an essential partner in bringing ideas to market for many Swiss high-tech SMEs active in the domain of highly miniaturized microsystems. Moreover, CSEM is looking at cross-disciplinary solutions—benefiting from nanotechnology, bioscience, and material science—in order to deliver innovations in MEMS and enable new microsystems.



SiC pressure sensor for high-temperature environments.

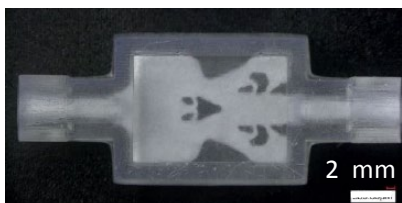


*CMOS-based multi-electrode array with 3D electrodes, targeting intra-tissue measurement of *in vitro* 3D neuronal models.*

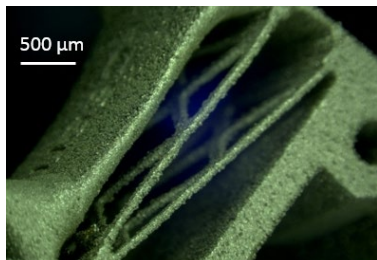
MEMS play a major role in the **Microsystems** program, and this role will be supported by increased efforts to develop advanced manufacturing and integration technologies. In particular, the recent advances in digital manufacturing open up new opportunities to create and optimize MEMS devices and microsystems. CSEM strongly believes that “traditional” MEMS technologies will be augmented by these new manufacturing technologies to provide new functionalities and deliver the versatility required for fast market introduction.

Packaging, meanwhile, no longer serves mainly as a “device protection” and increasingly integrates added functionalities. These include an interface to the outside world (optical paths, electrical leads, actuators ...), environmental compatibility (biocompatibility, withstanding high temperatures, etc.) or built-in sensors or quality monitoring features (antennas, pressure sensitive surfaces, etc.). This makes the border between the package and the device fuzzier. Hence, it is essential to elaborate a common strategy with regard to developing—under one roof—the new processes, new devices, and new packaging that will enable the creation of novel microsystems. With its **Microsystems** program, CSEM aims to create an environment that is adapted to the new challenges of microsystems and that benefits Swiss industry.

Looking back over recent years, the **Microsystems** program has seen significant progress related to the development of micro-components for mechanical watches and integrated optoelectronic devices. Although these topics are of great importance to Swiss industry, the technology spectrum being developed within the program must address a broader range of applications. The program has therefore, over the last few years, incorporated several new initiatives in order to diversify into new application fields, including instrumentation, aerospace and medical devices, all of which are important markets for Swiss industry.



3-D printed check microvalve.



Details of a 3D micromechanism based on compliant structures with <100 μm min. feature size made on steel alloy with SLM technology.

At CSEM, the microsystems strategy is oriented along several lines of action, encompassing design, microfabrication, and packaging technologies. They are:

- 1) Innovation for mechanical watches, at the crossover point of high-performance materials, advanced manufacturing, and innovative designs.
- 2) Excel in microsystem technology for harsh environments, for a broad range of applications ranging from medical to aerospace.
- 3) Develop key technologies in the field of infrared sensing and imaging.
- 4) Enhance the technology portfolio in optical MEMS and optoelectronic device assembly.
- 5) Life-interacting microsystems for applications in medtech and engineered environments for biological models.

Long-term objectives

The global objective of the **Microsystems** program is to establish MEMS device advanced micro-manufacturing and packaging technologies for CSEM's partners and to offer to Swiss and international industries a full product-development platform from the feasibility demonstration of new device ideas to industrialized, qualified fabrication processes including the production of MEMS in small volumes. Therefore, the activities of this program are aimed at continuing to excel and to build up new competences in microsystems technology—in particular for application fields such as watch technologies, scientific instrumentation, optoelectronics, and medical device technology—with a strong focus on packaging, reliability, and cost reduction for demanding applications.

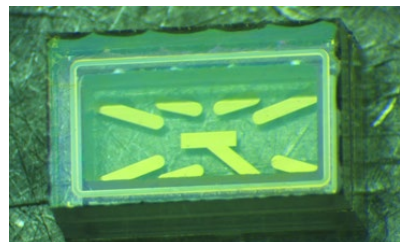
The **Microsystems** program strategy has been organized into three activities—namely, (1) *MEMS Devices*, (2) *Functional Packaging*, and (3) *Advanced Micro-Manufacturing*.

The *MEMS Devices* activity deals with the development and industrialization of specific MEMS in a wide spectrum of applications. The global objective of this activity is to maintain a state-of-the-art platform capable of developing and fabricating reliable MEMS products, from prototypes to small volume production or for technology transfer. This platform, at the service of Swiss SMEs and industries, consists of a fully equipped MEMS

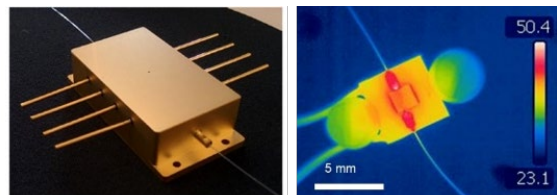
fabrication clean room, a reliability laboratory, and an R&D infrastructure focusing on the pursuit of advanced and novel MEMS-based devices. Today, development is underway in the fields of watches and timekeeping, instrumentation and aerospace, and health, biotech, and lifestyle. These are domains in which Swiss industry is highly successful at a global level and which have a large impact on the Swiss economy.

For industrial applications, reliability is of the utmost importance and CSEM's reliability and microstructure characterization capabilities are a powerful tool for supporting process development aiming at eliminating defect- and stress-generated failure modes and performance limitations. The continuous improvement and systematic documentation of development and production process flows within ISO-9001 ensures the successful exploitation of the technology platforms developed. This enables a systematic approach to MEMS development, from feasibility demonstration, via prototyping, to industrialization.

The *Functional Packaging* activity focuses on (i) the development of new integration platforms for CSEM's customers, and (ii) the realization of new products based on these platforms. The chosen approach allows CSEM to serve a large number of customers in different application fields and markets. The activity's primary objectives are the integration of active MEMS dies, sensors, and actuators into prototype systems and products for different applications and markets. The activity addresses today's global packaging challenges in the fields of sensor platforms for medical and environmental monitoring, the integration of measurement solutions for harsh environments, and optoelectronics. The integration of microsystems continues to be a key element of many future high-technology application areas. Hybrid integration technologies—from embedded silicon in polymer to M(O)EMS—find broad uses in markets such as health care and energy. Combined with hermetic sealing and embedded self-testing, they open up additional applications for sensors in harsh environments, such as in the medical field. In addition, miniaturization in optoelectronics continues to be an innovation driver, from devices to architecture.



Robust and hermetic enclosure for a miniaturized optical transceiver for space applications.



Fiber-coupled, packaged waveguides with effective heat dissipation.

The goal of the *Advanced Micro-Manufacturing* activity is to answer the need of the Swiss industry to fabricate small-dimension components (typically $<1\text{ cm}^3$) that can take advantage of a 3D aspect and that would not be achievable using existing technology such as clean room microfabrication (MEMS and CMOS). The envisaged solution is to develop a new combination of manufacturing technologies to improve the performance of microsystems. The core technology is based on additive manufacturing (AM), a worldwide “big trend” linked to digitalization, IoT, and Industry 4.0. This technology brings with it more flexibility and can increase the complexity of systems. However, it is still lacking user confidence, and still needs to be developed in order to achieve the small dimensions and structure quality required for its use in microsystems. The combination of its skill sets in materials, microfabrication, surface engineering, and characterization is allowing CSEM to tackle the challenge of combining different technologies and to make these new manufacturing technologies available to Swiss industry. Hence, CSEM’s attention is focused on two points: (1) the process optimization of 3D printing technology for the fabrication of small structures made of functional materials, and (2) the heterogeneous integration of 3D printing technologies with other microfabrication technologies (in particular with MEMS).

Needless to say, the **Microsystems** program will continue to work closely with the other CSEM programs (Surface Engineering, Ultra-Low-Power Microelectronics, Systems, and Photovoltaics & Energy Management) to create unique solutions for our industries. One of the major USPs of CSEM, we will continue to cultivate this multidisciplinary approach to answer the needs of our customers.

Highlights

The comprehension of fundamental neurobiological mechanisms is of great importance to our understanding of how the brain functions and of the causes of neuronal disorders in diseases such as epilepsy or Alzheimer’s. In terms of research in this field, in vitro neuronal network models are becoming more and more widely used for biological and neuroscientific investigations, not only into the neurobiological mechanisms of neural communications and dynamics but also into the effects of pharmacological compounds on neural networks. Within an InnoSuisse project, Swiss start-up 3Brain has teamed up with CSEM to develop its next generation in vitro brain-on-a-chip device and model for drug discovery and neurotoxicological assays. A key innovation has been the post-CMOS fabrication of 3D microneedles, forming a 3D in vitro sensor able to penetrate brain tissue, thus specifically targeting the intra-tissue measurement of structured 3D in vitro models.

For micromechanisms, such as those used in mechanical watches, understanding materials’ strength and resistance to fatigue is of the utmost importance. The typical size of these mechanisms’ mechanical structure ranges from tens of micrometers to few millimeters, which—in terms of material behavior—is at the intersection of the microscopic and the macroscopic and is defined as the “mesoscale” world. As the physical models used for microscopic (atomistic) and for macroscopic (bulk) scales are fundamentally different, there is a need for a model at the mesoscale that bridges these two worlds, with the specificity to take into account the probability of a defect at a position exposed to a given strain. Moreover, for this scale, the quality of the surface—which is very much influenced by the

manufacturing methods used (additive manufacturing, deep reactive ion etching, micromolding...)—has a major influence because the defect density at the surface is large compared to bulk and because, often, surfaces are exposed to strain concentration. Hence, for mesoscale, sizes and structuration methods matter when it comes to understanding device failures. CSEM has developed such models and has built the testing infrastructure necessary for the high-throughput, precise characterization of material strengths at the mesoscale for typical structures and manufacturing processes used to fabricate micromechanisms. Thanks to this work, we are able to set precise design rules for the conception of micromechanisms.

A good way to innovate is to combine advanced technologies to create unique functionalities and performance. In this respect, within an InnoSuisse project, we have used 3D microprinting to integrate a polymer-based shock-stopper/absorber onto a MEMS micromirror used for laser steering applications. The geometrical freedom and materials use made possible by 3D printing and the technology developed by CSEM enable us to perform high-accuracy registered printing on delicate and structured substrates (such as on a MEMS micromirror), bringing with it a new way to innovate in microsystems technology. Thanks to the integration of such a printed structure on the micromirror, the device’s resistance to shock has been improved by more than four times, reaching almost 1,000 G of shock resistance.

Neurons on 3D Microelectrode Arrays

J. Kernen, C. Martin-Olmos, O. Dubochet, F. Cardot, M. Despont, G. Weder

In vitro microelectrode array technology is a tool of choice for sensing electrical signals from neurons. In collaboration with 3Brain AG, CSEM is developing 3D microelectrode arrays for three-dimensional neuronal cell culture systems towards brain-on-a-chip. In contrast to conventional models, 3D neuronal models have a greater predictive power in drug screening for brain diseases.

Neurodegenerative disorders, such as Alzheimer's or Parkinson's diseases, affect millions of people around the world. Neuronal *in vitro* models on the electric activity is of particular interest to look at deleterious or protective roles of molecules on specific cell types, as well as drug screening. Microelectrode arrays have evolved into a widely used and effective technology to study neural networks and visualize signal propagations occurring between thousands cells^[1].

Generally, three-dimensional cell culture systems have gained increasing interest in drug discovery and tissue engineering due to their evident advantages in providing more physiologically relevant information and more predictive data for *in vivo* tests.

CSEM is moving from conventional 2D by innovative 3D microelectrode arrays towards three-dimensional neuronal cell culture systems, to bridge the gap between *in vitro* and *in vivo* drug screening, and possibly decrease the use of animals.

The 3D microelectrode is composed of a probe over a pedestal. The schematic fabrication process is shown in Figure 1. A photoresist mold (3) is created on an integrated circuit chip (1), featuring openings (4) over the electrical contacts (2) for individual electrode addressing. The openings (4) are filled by using pure gold electroplating, and the photoresist is stripped, leading to the formation of the gold pedestals (5). A thick photoresist mold (6) is created over the chip, featuring openings (7) over the pedestals (5). The openings (7) are filled by using pure gold electroplating, and the photoresist is stripped, leading to the formation of the gold probes (8) connected to the pedestals (5).

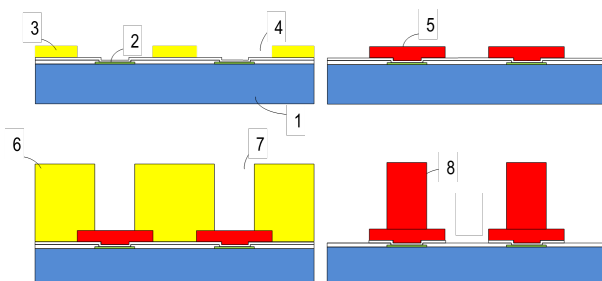


Figure 1: Schematic of 3D microelectrode array microfabrication.

The active surface of the biochips is functionalized for cell attachment. The culture of neuronal cells is particularly challenging since mature neurons do not undergo cell division. One way to overcome this is to differentiate pluripotent cells, such as embryonic stem cells or induced pluripotent stem cells, into neurons. Human neural precursors were seeded on the biochips and maintained for several weeks at 37°C. The electrical information of neurons acquired from each 3D microelectrode will be then converted into a color-coded video to

observe the spatial distribution and the propagation of electrical wave signals. Prior to record neuronal network activity, e.g., in the presence of drugs, first neuronal cultures were performed with dissociated cultures (instead of neurospheroids or mini-brains) in order to optimize cell attachment, cell differentiation and imaging (Figure 2).

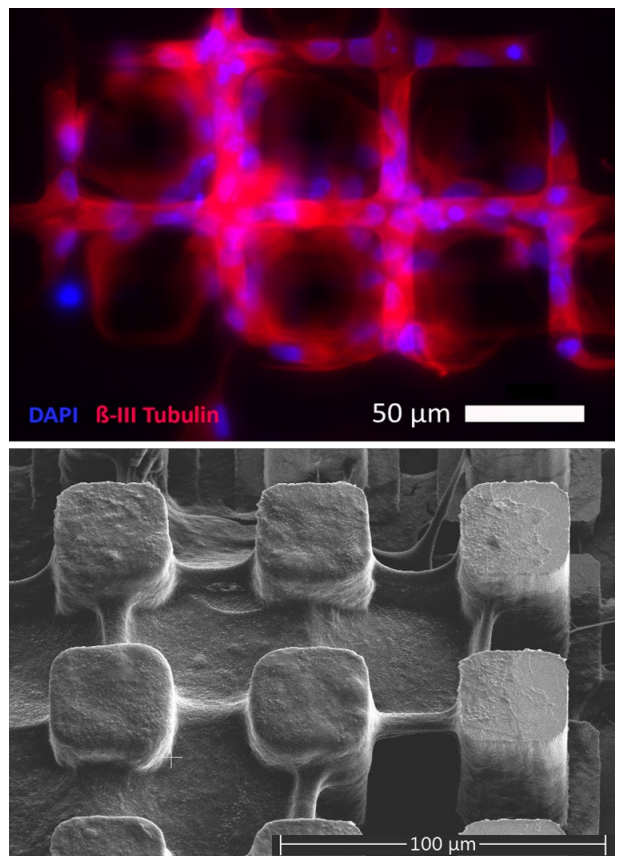


Figure 2: Immunofluorescence staining (top) and scanning electron microscopy (bottom) showing human neurons (β -III Tubulin positive) grown on 3D electrodes for 12 days.

Typical neuronal network activity was first measured on 2D microelectrode arrays where each pixel represents one electrode that records electrical signals. The combination of 3D electrodes with CMOS technology for electrophysiology imaging is underway.

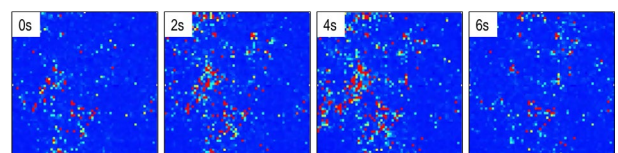


Figure 3: High-resolution electrical read-outs on 2D microelectrode arrays showing changes in spiking activity after 2, 4 and 6 seconds.

[1] 3Brain AG, 8820 Wädenswil, Switzerland

MEMS-based Gas Chronomatograph

A. Hoogerwerf

MEMS-based gas chromatographs allow, through their small size, gas analyses to be carried out using a much reduced consumption of carrier gases and power. This opens the way to truly portable gas analysis systems. At CSEM, we have fabricated all the key components of a MEMS gas chromatograph: pre-concentrators, columns, and thermal conductivity detectors (TCDs).

Gas chromatographs (GCs) are the golden standard of chemical analysis. GCs are typical benchtop instruments, weighing tens of kilos and requiring a large tank of carrier gas, such as helium. MEMS-based GCs promise a significant reduction in the volume of the GC components, which in turn leads to a reduced gas and power consumption. The main three components are the pre-concentrator, the column, and the detector.

The pre-concentrator consists of a volume of absorbent material that accumulates absorbed air-borne chemicals over time. The pre-concentrator is then rapidly heated to desorb all chemicals in a sudden burst for their analysis. A picture of the MEMS pre-concentrator fabricated at CSEM is shown in Figure 1. The white material in the pre-concentrator is the Tenax® absorbent material.

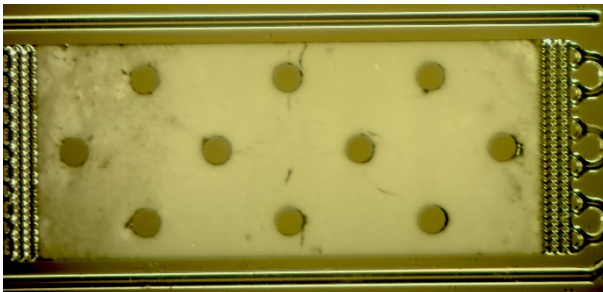


Figure 1: A Tenax® filled-pre-concentrator. The minor "cracks" observed are resulting from the drying of the absorbent.

The column separates the incoming gases, resulting in different gases eluting from the column at different times. The column is typically a long tube (up to 30 m) that is coated on the inside with a stationary phase. The gases passing through the column interact with the stationary phase, delaying their passage. Different gases experience different interactions and, thus, different delays. It is the difference in delays that gives the column its ability to separate the gases. The column tubes are normally rolled up into loops and are placed in a forced-convection oven for their temperature control.

MEMS-based columns are formed of serpentine channels, etched into silicon that are subsequently covered by bonding the silicon wafer to a glass one using anodic bonding. This technology makes that MEMS columns typically have a rectangular cross-section, as opposed to conventional columns that have a circular one. Hence, although a microfabricated column has some advantages in terms of integration in the GC as well as integration of sensors (TCDs), square cross-section creates a difficulty with the deposition of a stationary phase of uniform thickness on the inside walls of the column. The thickness of the stationary phase affects the time the gases are retained and, thus, the separation quality of the columns. Its uniformity is therefore of paramount importance for the separation characteristics of the column. However, most deposition techniques will result in an accumulation of the stationary phase in the corners of the column cross-section, resulting in a very poor separation. CSEM uses a molecular vapor deposition (MVD) technique that deposits a stationary

phase at the rate of one molecule per cycle. As a result, very uniform depositions of the stationary phase could be obtained, independent of the shape of the column.

The verification of the presence of the stationary phase throughout the column presents a major challenge. The presence was first verified in very short (25 cm) columns. These columns have a fluidic resistance low enough to allow the forcing of a liquid through it. The observation of the contact angle of water throughout the short column showed a clear difference between coated and uncoated columns. This confirmed the presence of the stationary phase through these short columns.

A more direct observation of a 20 nm alumina stationary phase was also obtained. For this observation, a coated column was cut throughout its length and placed sideways on a support wafer. The sliver of column was then directionally etched. This removed approximately 8 μm of silicon from the column cross-section. The glass and the alumina were not etched, because of the selectivity of the etching. The resulting cross-section is shown in Figure 2. The remainder of the now free-standing alumina coating is clearly visible.

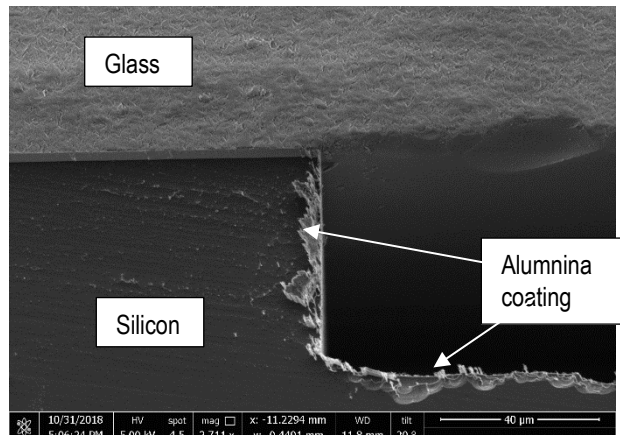


Figure 2: Etched cross-section of a coated column.

The fabrication technology of the TCDs uses a free-standing platinum resistor sandwiched between two LPCVD silicon nitride layers. The resistors are under-etched in a KOH solution, resulting in free-standing resistor bridges. The platinum resistor material allows for a straightforward temperature measurement by the TCDs. The LPCVD nitride allows the resistances to be heated up to 800°C without any detrimental effect.

Design and Fabrication of Microfluidic Systems for Two Phase Cooling

T. Frei, A. Hoogerwerf, A. Mapelli*, D. Alvarez Feito, M. Despont, V. Gass**

Micro oscillating heat pipes are among the most promising two-phase cooling system of microsystems when a rigorous thermal management is required. Rectangular microchannels with dual hydraulic diameter were engraved in silicon and borosilicate glass was used to close the meandering microchannels. The design is tailored to obtain orientation independent micro cooling systems.

Thermal management is required wherever heat is generated or temperature needs to be carefully controlled. Microchannels cooling represents the state-of-the-art cooling technology in applications ranging from monolithic silicon detectors to high-performance computer^[1, 2]. Two-phase microfluidic cooling systems have the advantages of a superior temperature uniformity and minimal load driven temperature variation than the single phase counterparts, in addition to being able to be directly integrated at chip level. Among the different types of micro heat pipes, micro oscillating heat pipes (μ OHPs)^[3, 4] have been identified as the most promising technology to offer two-phase cooling in different studied scenarios for applications ranging from single chip cooling in a high-energy physics experiment to multiple chips cooling in microgravity. A μ OHP consists of a meandering of channels partially charged with a fluid. The fluid motion is the results of the phase change of the fluid: the motion of liquid and vapour plugs is generated by the expansion and contraction of vapour volume.

The project aims to develop micro oscillating heat pipes for high-energy physics experiments and space applications. The first step consists in increasing the understanding of the behavior of μ OHP at all orientation in order to refine the design. Additionally, the development of a novel sealing and packaging solution to encapsulate the fluid inside the microchannels while keeping the thickness of the μ OHPs as low as possible is required.

The μ OHPs are characterized by excellent thermal performance and simple design with a wickless structure. The fact that they are micro-fabricated permits to reach thicknesses under the millimeter. The design of this μ OHP relies on dual-diameter microchannels to increase the capillary pressure of the working fluid. Thus, also increasing the maximum effective thermal conductivity and extending the range of orientation angle where the μ OHP is working. Thermal performance of μ OHPs using single diameter design degrades progressively when the orientation angle increases. However, dual-diameter μ OHPs are orientation-independent if the capillary pressure is higher than the pressure drop^[5]. The first design includes rectangular microchannels with a width of 400 μ m and 225 μ m over 400 μ m of depth. The interconnected microchannels are etched in silicon wafers. A borosilicate glass wafer is bonded on top forming a meandering closed loop. It enables visual observation of the flow inside the device when in operation. In addition, an Invar

connector is thermocompressed on the glass using a gold-gold bond to connect the filling system.

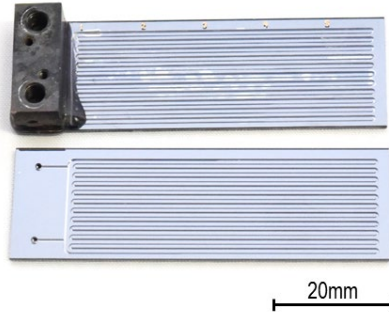


Figure 1. Two micro oscillating heat pipes side-by-side.

A comparison of theoretical thermal performance of several fluids is done by comparing the maximal capillary pressure drove by the dual-diameter design with the frictional pressure drop encountered during the fluid motion in the form of a figure of merit (M_{OHP}). The heat required to start the oscillation of the fluids and the heat corresponding to the evaporation of all the trapped fluid serves as additional comparison elements.

Numerical calculation of the Figure of Merit in function of the charging ratio for several fluids

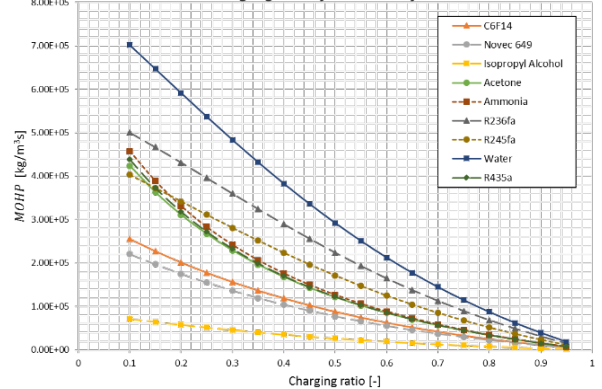


Figure 2. Plots of the figure of merit M_{OHP} in function of the filling ratio of the heat pipe.

Among the fluids compared, R236fa, R245fa and Acetone are potential working fluids for the demonstration of the proof of principle with good theoretical thermal performance and showing start-up at low power input.

- CERN, 1211 Genève, CH
- Swiss Space Center, EPFL, 1015 Lausanne, CH
- [1] A. Mapelli, *et al.*, "The NA62 GTK, From silicon microchannel cooling plates to tracking detectors", PoS(Vertex 2017) 021.
- [2] B. Agostini, *et al.*, "State of the Art of High Heat Flux Cooling Technologies", Heat Transfer Engineering, 2007.

- [3] T. P. Cotter, "Principles and prospects for micro heat pipes", 5th International Heat Pipe Conference, 1984.
- [4] L. L. Vasiliev, "Micro and miniature heat pipes - electronic component coolers", 2008.
- [5] G. H. Kwon, S. J. Kim, "Experimental investigation on the thermal performance of a micro pulsating heat pipe with a dual-diameter channel", Int. J. Heat Mass Transfer, 2015.

Adhesives for Solder Replacement

M. Fretz

There may be situations where conventional solders are not compatible with the bond requirements. Electrically conductive adhesives (ECA) are an interesting alternative. If used well, they can be more than just a quick fix. CSEM investigated several ECAs and compared their performance when exposed to hot moisture and temperature cycling with solder wires typical for SMD bonding.

Classical SMD bonding on PCBs involves either tinned HAL surfaces (hot air leveling) or a gold finish on a solderable nickel layer. Components are usually robust enough to withstand typical solder temperatures around 300 °C. Lead-containing and lead-free solders (for RoHS compliance) are well established and perform satisfactorily under these circumstances. However, novel applications often involve hybrid technologies and temperature sensitive parts such as pressure sensors or other MEMS components. ECAs can be a viable solution when following problems are encountered.

- Temperature sensitive components such as pressure sensors or bio-chips
- Non-solderable surfaces, (e.g., aluminum) on MEMS chips or thin gold layers on oxidized underlying layers
- Flux residues or their washing off could destroy delicate components (again, think MEMS-based pressure sensors)
- Gold scavenging of tin based solders is the cause for the formation of brittle intermetallic Au-Sn phases.

ECAs address all the above issues as they neither require very high curing temperatures (as low as 80 °C), nor subsequent washing steps or have compatibility issues of the surface metal with regard to the formation of intermetallic phases. They are well-established in many applications featuring noble metal surfaces (Figure 1). They provide a strong mechanical bond with excellent chemical resistance against acids and solvents and good long-term performance. Yet it is generally believed that they do not provide a sufficiently good electrical connection on oxidizing metals such as tin because ECAs lack the flux to break an initial oxide layer.

We tested the long-term performance of several ECAs on tin surfaces and compared them with a conventional solder wire for SMD bonding. The results are contrasted with results for the control group including the same adhesives and solder wire on gold surfaces. Following accelerated life tests were carried out on a 0 Ω SMD resistor:

- Exposure to 85°C and 85% RH (so-called 85/85 test)
- Temperature cycles between -55°C and 85°C, according to MIL-STD 883K, method 1010.9, test condition A.

These SMD resistors are well bonded to custom-designed PCBs with connection pads arranged in a four-point configuration. Hence, measured DC resistance values exclude metal lines on the PCB and cables. Deterioration of the PCB is therefore not impacting the measurement.

Unsurprisingly, all tested adhesives showed initial electrical resistance values below 20 mΩ, comparable or even slightly lower than measured values for the solder. Long-term performances in above mentioned accelerated life tests revealed clear differences between the adhesives. Adhesive A in Figure 2 remains competitive with solder, whereas adhesive B showed a dramatic increase in electrical resistance.

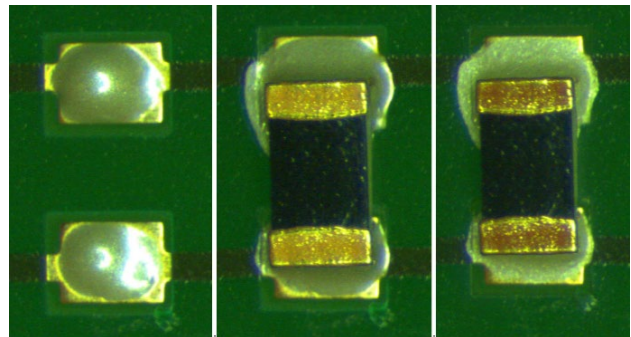


Figure 1: ECA bonding of a SMD resistor on a PCB with a typical gold finish surface. After dispensing; middle: SMD placed (left); adhesive cured (right).

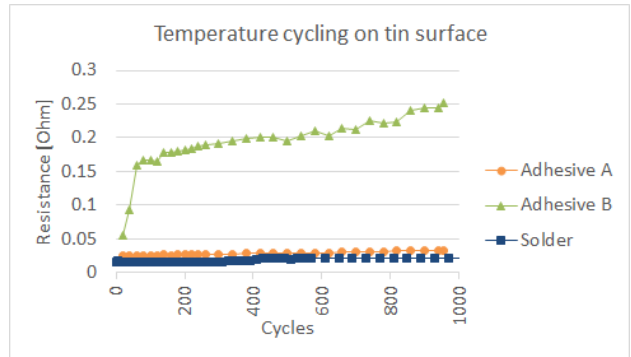


Figure 2: Electrical resistance comparison between two ECAs and a conventional solder wire of a 0 Ω SMD resistor.

The results on tinned HAL surfaces are mixed: 'Standard' ECAs for noble surfaces fail to produce a reliably low initial resistance. However, a further tested ECA, specifically advertised for tin surfaces, shows acceptable initial resistance values in the range of solders on tin.

This adhesive was further subject to above specified accelerated life tests. It survives 1'000 temperature cycles without discernible degradation in electrical resistance, but it fails when exposed to an 85/85 environment.

Concluding, in harsh environments ECAs may replace solder if combined with gold-finish surfaces. On tin surfaces such as HAL, acceptable results can only be achieved with the right choice of adhesive in non-harsh environments. Particularly the combination of moisture and heat cause the ECAs to fail rapidly on tin surfaces.

This work was partly supported by the Swiss Confederation and M CCS (Micro Center Central Switzerland). CSEM thanks them for their support.

Packaging Design and Simulation for Space Applications

G. Spinola Durante, V. Revol, R. Jose James, K. Krasnopski

In the framework of an ESA funded project (Hopwell) aiming at developing miniature hermetic optoelectronic packages, CSEM has devised an integrated methodology to design packages for functionality. The methodology consists at first in defining a parametric (Solidworks) CAD model for the packages. Optical simulations are then performed on a simplified model and the optical simulation results, including tolerancing, are taken into account into the parametric CAD model. It is then directly imported into a FEM simulation tool (COMSOL) and solved to validate the coupled thermo-mechanical performances and ensure long-term functionality of the design by minimizing mechanical stress, while operating in the environment.

Four different miniaturized optoelectronic package designs were developed within an ESA funded project. In Figure 1 is represented schematically the integrated design flow approach.

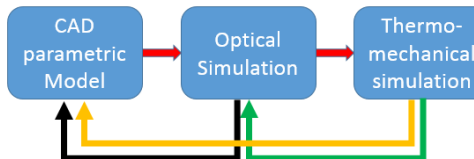


Figure 1: Optical micro-packages design flow.

The design concepts have been discussed and agreed with ESA, according to CSEM previous experience in the field of laser-based hermetic sealing of transparent substrate^[1,2,3]. A first design includes the VCSEL type laser array without any collimating lens. The second design includes the VCSEL array with a collimating multi-lens array. In two more designs a focusing multi-lens array is included (see Figure 2).

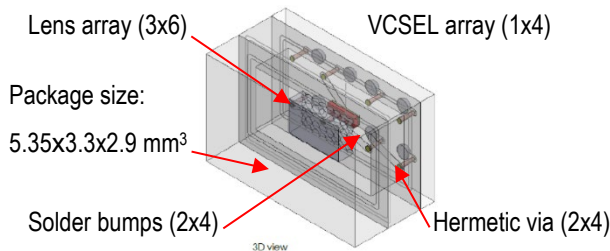


Figure 2: Parametric CAD Model including focusing lens (Solidworks).

All of the designs require to be analyzed at first with a ray-tracing software to assess if the performance is within the limits of the optical requirements. A simplified model is set up and solved with the optical design software tool ZEMAX. The designs include the mechanical dimensioning and tolerancing of all components and subcomponents. In particular, the effect of geometrical tolerances on the optical performance is considered in Figure 3.

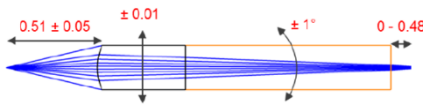


Figure 3: Optical tolerance simulation results (ZEMAX).

^[1] R. Jose James, et al., "Low Temperature Hermetic Sealing of Sapphire Substrates", CSEM Scientific and Technical Report (2014) 41.

^[2] S. Berchtold, et al., "Low-temperature Laser-assisted Sealing of Glass Lid on Silicon", CSEM Scientific and Technical Report (2016) 31.

All of the designs have to be optimized during optical simulation by means of a goal function. Then the CAD models are consistently updated and imported into the COMSOL program for simulation of thermo-mechanical stress (Figure 4).

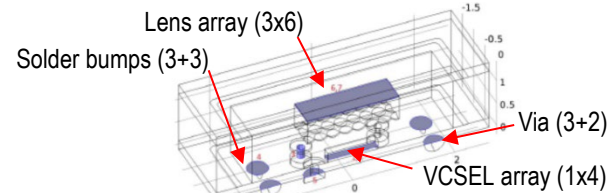


Figure 4: FEM model imported and cut to half-symmetric (COMSOL).

Figure 4 shows highlighted in blue the areas where stress is averaged out for easier comparison. The purpose is to ensure low levels of stress during laser die-attach and/or adhesive bonding of the VCSEL, and adhesive via-filling. Thermo-mechanical stress analysis can also be used to check stress levels assuming different materials and ambient temperature, according to the extremes defined in the thermo-cycling requirements (Figure 5).

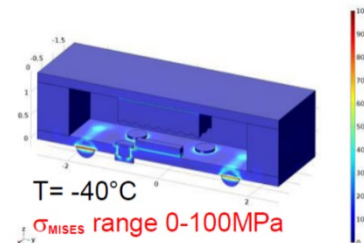


Figure 5: Example of Von Mises stress-plot for comparative analysis of adhesive choices at -40°C during thermo-cycling test.

The last step of the package design requires careful choice of metallization and its layout design. The packaging design phase is usually concluded with the description of the assembly process flow.

In conclusion the comparison of different design approaches is therefore much simplified and supported by an integrated design flow, to find the most promising package designs in accordance with stringent reliability requirements as present in a space environment. This research activity has received funding from the European Space Agency.

^[3] M. Fretz, et al., "ACTION – Hermetic Packages and Flexible Substrates for Implants", CSEM Scientific and Technical Report (2016) 33.

Semi-automated Diamond-based Thermo-compression Wire-bonder

G. Spinola Durante, K. Krasnopolski, M. Fretz, R. Jose James

A new custom-made equipment is shown to perform diamond-based thermo-compression wire-bonding. The main advantage over conventional ultrasonic wire-bonding is the possibility to use thicker wires of up to 0.4 mm and wire materials with low diffusion coefficients like platinum and other materials more suitable for harsh environment conditions, including high temperature in air [1]. A semi-automated setup has been devised with motors on all axis to enable accurate alignment in the range of a few microns. Some typical shear test values are shown to prove that the method yields good performance for bonding of 25/250 μm platinum wires. A few application cases are also sketched in the conclusions in order to hint at its industrial potential.

In the microelectronic industry the ultrasonic wirebonding technology has been extensively used with aluminum wires, being cheap and providing reliable interconnects for IC packaging and suited for large volume manufacturing. Nowadays copper wires are also used due to their high thermal conductivity, mostly in the area of high-power applications (microprocessors, high power chips and modules ...). Another related technology is based on ultrasonic bonding of gold wires and is suited for brittle substrates and dies. It has a very high current capability and is therefore much used for packaging of semiconductor lasers and other optoelectronic components.

To enable a wider range of materials, another approach is to perform thermo-compression bonding of wires. This allows for use of a broader selection of metals, including those with lower diffusion coefficients like platinum. The advantage over gold is not to have limitations due to high diffusion coefficients and thus less likelihood of intermetallic formation over time. The temperatures and pressures required to perform this bonding step are typically up to 600°C and up to 300 MPa. A system with a diamond head (Figure 1a) achieves both levels of pressure and temperature in air, without being subjected to degradation by itself.

CSEM uses a commercially available diamond-tip thermo-compression head and has built an equipment around with motorized stages to achieve a motion repeatability of a few microns. This enables an accurate alignment of the wire onto the pad. A tension force is applied to the wire to avoid misplacement during the thermo-compression process by using pulleys as can be observed in Figure 1a.

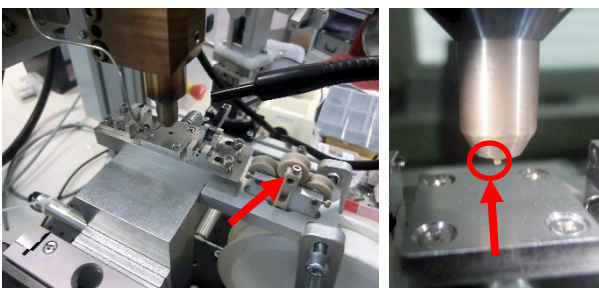


Figure 1: (a) Motorized OEM equipment; (b) Close-up on diamond tip.

Figure 1b is a close up of the diamond tip to emphasize the fact that the diamond is not completely flat, but rather has a cutting edge on its side. This edge feature on the diamond will indent the

wire during the thermo-compression bonding to induce a locally well-defined weakness outside the bond where the wire will break upon pulling it (Figure 2a).

The motorized stage in the setup also enables a rotation of 180° to perform a second thermo-compression bond on the wire, and pre-cutting the wire in the correct direction to leave the bonded wire on the substrate (Figure 2b).

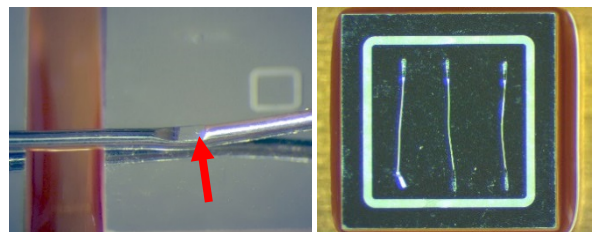


Figure 2: (a) Diamond-head imprint on a 250 μm thick platinum wire; (b) 25 μm wires platinum wires bonded on a chip.

The bond test results with platinum wire of 25 μm diameter have shown good pull-test values around 6-8 g. The thicker wires of 250 μm diameter have been shear tested and yielded values around 1.5 kg. Another interesting aspect of this method is the possibility to thermo-compression bond thick wires even along all directions on curved surfaces. This cannot be achieved with standard ultrasonic bonding, because it requires a constant pressure and friction together with the planarity of the substrate.

The main application case for this technology is to interconnect sensors specifically for high temperature operations. Another interesting application will be to interconnect high power chips and high power modules working in harsh environments, and thus requiring chemically stable (non-oxidizing) inter-connections. Other interesting applications are in the area of bio-sensor interconnections, where selected wire materials are required from the point of view of functionality and non-toxicity. Special attention is also given to electric motor interconnections where high reliability is in demand. Thermo-compression has been proven to have advantages over conventional soldering due to limited or no intermetallic formation.

This equipment enables CSEM to offer its customers a new process suited for the highly dynamic and innovative field of sensor components bonding for harsh environments.

This work was partly supported by the Swiss Confederation and MCCS (Micro Center Central Switzerland).

[1] G. Spinola Durante, et al., "HECTIC – Harsh Environment Ceramic Technology Involving Silicon Carbide", CSEM Scientific and Technical Report (2017) 17.

Mechanical Strength of Precipitate Hardenable Al Alloys using ECAP

V. Pejchal, M. André*, R. Müller*, M. Dadras

Equal Channel Angular Pressing or in short ECAP is a process of severe plastic deformation that consists of extrusion of a circular or square cross-section sample around a corner of a channel. This extrusion technique results in microstructure refinement and thus strengthening of the material without reduction of the cross-sectional area of the sample. In 2018 CSEM worked in partnership with HEIG-VD to investigate the effect and potential benefits of this technique on aluminum alloys that contain significant amount of precipitates.

Microstructure refinement is one of the most efficient ways of strengthening aluminum alloys. Effect of ECAP on microstructure, hardness and especially refinement of precipitates in aluminum alloys was investigated. Three different alloys were studied using 50 mm long, 10 x 10 mm cross-section samples. The investigated aluminum alloys were (i) AlMg_3 , (ii) AlCu_6PbBi and (iii) AlAg (50:50w%). The alloy AlMg_3 was used to first set-up the ECAP process, perform repeatability assessment and determine the optimal extrusion strategies for multi-pass process (with or without rotation between each pass). The second investigated alloy belongs into the 2000 series alloys with Al_2Cu precipitates and the third investigated alloy contains Ag_2Al precipitates promising microstructural evolution lead to significant strengthening of the alloy^[1].

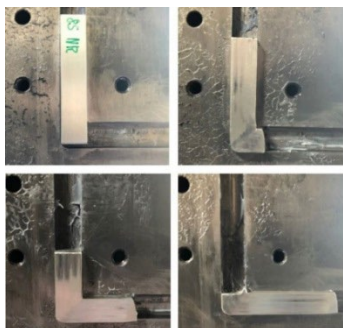


Figure 1: Images showing four stages during the ECAP process from the beginning until the end of the sample extrusion.

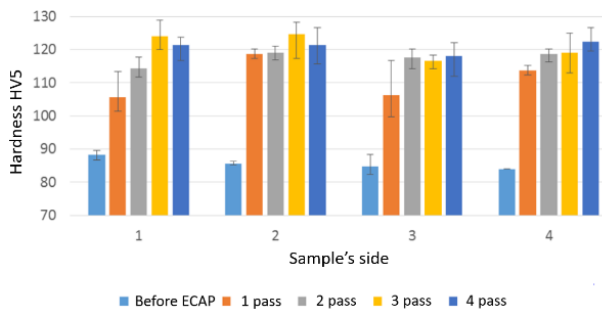


Figure 2: Evolution of hardness along four sides of AlMg_3 following four ECAP passes. After each pass the sample was rotated 90°.

Following the initial feasibility study on alloy AlMg_3 during which the process protocol was established, more detailed investigation of the influence of the ECAP process on hardness of the AlMg_3 alloy was performed. It has been shown that hardness of this alloy increases approximately 30-40% before it reaches its plateau after already two ECAP passes. Thus the hardness before ECAP around 85 HV5 increased up to 120 HV5.

- HEIG-VD

Three different strategies during the multi-pass ECAP extrusion were investigated (i) no sample rotation between each pass, (ii) 180° rotation, and (iii) 90° rotation. It has been observed that if the sample was rotated 90° before each subsequent pass the resulting hardness was comparable on each of the sides of its square cross-section. On the other hand, if the sample is not rotated or the rotation between each ECAP cycle is 180° the difference in hardness between lateral and horizontal sides on the order of 10%.

Experiments on AlCu_6PbBi showed no significant difference in evolution of size and shape of precipitates as the investigated alloy was already extruded from production. It has been observed that Al_2Cu precipitates show signs of brittle fracture.

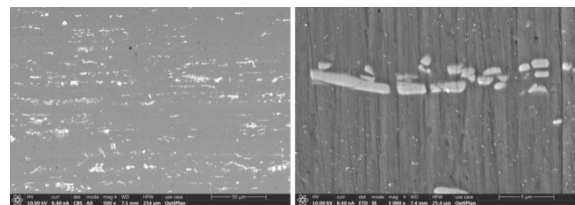


Figure 3: SEM micrographs reveal the Al_2Cu precipitates in AlCu_6PbBi after one ECAP pass. Al_2Cu particles exhibit brittle fracture.

Solution treated or aged treated Al-Ag alloys showed high strengthening during deformation. The deformation was concentrated on the shear bands and highly deformed sheared areas were observed (Figure 4). Additionally, the deformation of these precipitates suggest significant plastic deformation which is in contrast with brittle failure of Al_2Cu precipitates in AlCu_6PbBi alloy.

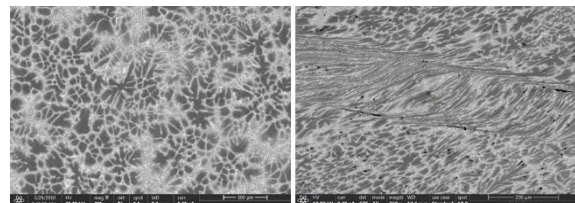


Figure 4: Micrographs of Al-Ag (50:50w%) sample before (left) and after (right) ECAP. Although the sample broke into several pieces signs of severe plastic deformation and refinement of Ag_2Al precipitates is evident.

Two main conclusions could be drawn from the present investigation; (i) Al_2Cu precipitates exhibit brittle behavior and ECAP process does not provide significant refinement of these precipitates and (ii) Ag_2Al precipitates show significant plastic deformation and refinement after ECAP.

[1] Y. Z. Tian, et al., "Microstructures, strengthening mechanisms and fracture behavior of Cu–Ag alloys processed by high-pressure torsion". Acta Mat., vol. 60, pp. 269-281, 2012.

3D Printing of Sub-millimeter Sized Components

S. Lani, N. Hendricks, O. Chandran

Since several years, CSEM is focusing on the integration of 3D printing technologies to manufacture precise components by using high throughput technologies. One of them is stereolithography, relying on UV hardening of a liquid photopolymer. Structures down to 75 μm has been previously fabricated. Within this project, we are developing a new UV stereolithography system with the capability to manufacture structures down to 15 μm . Preliminary tests have so far demonstrated capability to manufacture structures down to 40 μm and channel sizes of 50 x 75 μm without fine tuning of the process parameters.

From prototyping to small series production, UV stereolithography (SLA) is the most interesting 3D printing technology in terms of spatial resolution and throughput. Commercial systems have a resolution limited to the pixel size (for DLP® based system, typically in the range of 25 to 50 μm) or the laser spot size of the projection unit (typically ~150 μm). Typical minimum objects size with such system is in the range of 75-200 μm .

Since several years CSEM is using SLA for prototyping and small series production either for making a mono-material 3D components or by combining it with others technologies like MEMS microfabrication. The R&D focus has always been toward precision manufacturing. Thus, CSEM has developed its own "microSLA" system, taking inspiration from what has been developed by Gong, et al.

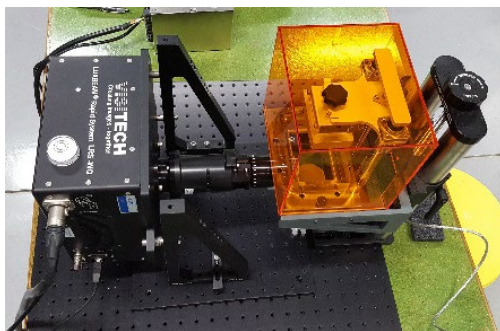


Figure 1: MicroSLA system developed at CSEM.

The developed system is relying on a high resolution DLP® based projection unit from Visitech® with a pixel size of 7.5 μm , a pixel array of 2500 x 1600 mirrors corresponding to an image size of 19.35 x 12.10 mm^2 and a LED UV source at 385 nm, that is connected to a modified Solus SLA printer from Reify3D®, already in use at CSEM. The assembled system is presented in Figure 1. The projector parameters, particularly the LED power is controlled by a SPI interface and the pattern is controlled by using Solus Contour® software from Reify3D®. Layer thicknesses used are of 10 μm and 25 μm .

As a comparison with printer with larger pixel, a first resin was evaluated: Flexlite resin from Tethon®: This material presents several advantages like high transparency giving easy control of the printing result and high flexibility leading to low residual stress structures. It has shown high potential for the realization of 3D molds for electroplating but with previous systems, with larger pixel, it has been difficult to achieve embedded channels smaller than 400 μm . With this new setup, the channel size has been decreased 125 μm and was used to fabricate molds on conductive substrates. The molds successfully passed the plating and grinding steps and was removed mechanically thanks to its high flexibility.

To evaluate the achievable resolution, a second resin was evaluated: PEGDA based resin with photoinitiator matching the projection unit wavelength. This material has been developed by BYU^[1] to manufacture high resolution microfluidic components. Similar patterns used with the Flexlite resin have been evaluated with features down to 0.1 mm sizes as well as a design to evaluate minimum channel size (50 x 75 mm^2).

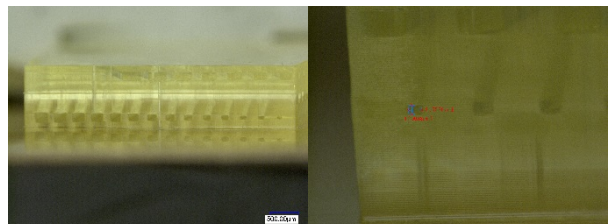


Figure 2: Channel size evaluation test vehicle (left); smallest channel fabricated (right).

Even though, an increase of resolution by a factor 3 to 4 has been demonstrated for channel sizes compared to previously used system at CSEM with a pixel size of 52 μm we are expecting a similar in structure size reduction (around a factor 2 so far) with further improvement of the process or the optical setup. Targeted geometries are line widths of 15 μm and channel sizes of 30 μm both with a minimum aspect ratio of 10. Applications will be within microfluidics (from simple to complex components, channels on substrates), precise mechanical parts (that can be further improved with a coating), or complex opto-mechanical packages. Improvement of the material composition will also be pursued to obtain more durable/reliable materials as well as properties matching the application such as a black resin for optical applications.

[1] C. I. Rogers, K. Qaderi, A. T. Woolley, G. P. Nordin, Biomicrofluidics, 2015, 9, 1–9.

Powder Features in SLM: How important is it?

S. Zabihzadeh, F. Cheriegie, S. Lani, O. Chandran, O. Sereda

This project highlights the importance of the powder quality on the properties of the fabricated parts by SLM. The influence of SLM process, such as heat and power on the recycled powders is discussed as well.

The ability to fabricate metallic parts with a complex geometry, high structural integrity and lighter weight at low cost and high speed makes the Selective Laser Melting (SLM) an attractive 3D printing technique in both academic and industrial domains^[1]. In SLM, the metallic parts are produced directly by selectively melting and fusion of the powder^[1]. Quality of the powder play an important role in the microstructure, density, surface finish and thermomechanical properties of the fabricated parts, thus influence the targeted functionality of the built part^[2]. The well-equipped characterization laboratory of CSEM established a characterization protocol for verification of the quality of SLM powders. Figure 1 displays a schema of most significant powder parameters for SLM. Analyzing the chemical composition of the initial powder provides information about the chemical composition of the fabricated sample. While knowledge about the crystalline phase and microstructure of the initial powder helps in better understanding the phase transformation and microstructure of the produced sample. Particle size is the key factor in determination of printed layer thickness and plays a major role in the surface roughness of the printed specimen. A decrease in the surface roughness by reducing the particle size has been reported in literature^[2]. The size distribution and morphology of the particles influence their agglomeration and compactness and as a consequence changes the density of the fabricated sample. Flowability and cohesive index^[3] of the powders are two other key parameter as they have an impact on the uniformity of the deposited layer consequently the sample density. So far, several metallic powders such as stainless steel, Ti-powder, Ti6Al4V, Ni-based powders have been spotlighted. One of the main focus of this project is reflected in the influence of the particle size and particle size distribution on the density and surface roughness of the fabricated part.

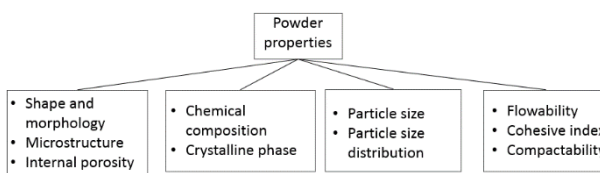


Figure 1: most significant powder parameters for SLM process.

One of the advantages of Additive Manufacturing techniques, is its high sustainability in term of raw material consumption. In SLM, to make this advantage the most profitable it is necessary of recycling the un-welded powders (powders out of localized

^[1] C. Y. Yap, et al., "Review of selective laser melting: Materials and applications," *Appl. Phys. Rev.*, vol. 2, no. 4, p. 041101, 2015.

^[2] A. T. Sutton, et al., "Powder characterisation techniques and effects of powder characteristics on part properties in powder-bed fusion processes," *Virtual Phys. Prototyp.*, vol. 12, no. 1, pp. 3–29, jan. 2017.

melting area) and re-use them for fabrication of new parts. Hence another objective of this study is to investigate the impact of the recycling on the powder properties and subsequently, the properties of the fabricated parts. The high temperature and high power laser inside the SLM chamber can affect the powders and change their properties. Figure 2 displays a representative SEM micrograph of 316L powders a) from a new batch and b) after three times recycling. A circular shaped morphology is observed for most of the particles. However, on the external surface of few recycled particles, black color zones are detected. Based on the results of EDX analysis, these zones are identified as heat affected zones or oxide islands^[4] and are rich in Si, Mn and O. These observations emphasize the important aspect of a regular quality control of the powders used in SLM. The impact of such morphology changes on the properties of the printed samples is under investigation. So far, the specimens fabricated with the three times cycled powders (Figure 2b) showed similarities in terms of density and hardness to the specimens printed using the new powders.

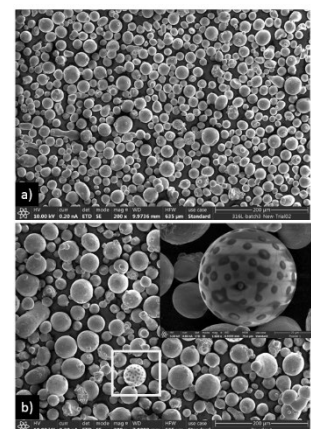


Figure 2: Representative SEM micrographs from 316L powders. (a) New batch; (b) Three times cycled batch. The insert shows a magnified example of a particle with heat affected zones.

The properties of the SLM fabricated parts are directly related to the properties of the employed powders. Particle size, size distribution and particle morphology are the main parameters in controlling the density and surface roughness of the produced parts. Powder properties such as the internal friction, compactness and flowability are directly linked to the particle size and morphology as well^[2].

^[3] A. B. Spierings, et al., "Powder flowability characterisation methodology for powder-bed-based metal additive manufacturing," *Prog. Addit. Manuf.*, vol. 1, no. 1, pp. 9–20, 2016.

^[4] C. S. Kriewall, et al., "Investigation of Heat-affected 304 L Ss Powder and Its Effect on Built Parts in Selective Laser Melting," 2016.

Selective Laser Melting of sub-200 µm Features of Components

O. Chandran, S. Lani, F. Cheriege, K. Vaideeswaran, S. Zabihzadeh, V. Pejchal, H. Saudan, L. Kiener, O. Sereda

Among the variety of technologies available to additively manufacture metallic parts, Selective Laser Melting (SLM) is the most extensively explored^[1]. A growing number of industries (aerospace, medical, energy, transportation...) work towards integrating such technology in their production portfolio through the purchase of "turnkey systems". Such systems, oriented towards the production of large parts, are not able to print fine features (<200 µm), this challenge was tackled this year by CSEM in order to 3D print high quality, sub-200µm components using 316L stainless steel. This challenge was addressed by a thorough optimization of printing parameters to achieving high-quality parts and post-processing solutions for surface roughness reduction.

The Selective Laser Melting relies on the interaction between a laser and a powder bed^[2]. Such interactions mainly depend on the laser characteristics (spot size and power) and the printing parameters used (scanning speed, hatch spacing, scanning strategy). Taking into account the above-mentioned aspects, a first evaluation of laser powers and scanning speeds fitting the requirement of fine features was realized on a Trumpf TruPrint 1000 SLM machine for 3D printing of metal components. The quality of the printed parts was assessed in terms of dimensions, microstructure, density and mechanical properties.

Once an optimized process window defined, an XRD investigation showed presence of austenite phase with a part density higher than 99% (when compared to theoretical density). Further mechanical analysis revealed a Yield strength of 510 MPa, Ultimate Tensile Strength of 615 MPa, and Elongation of 54%, which are in agreement with already published works for SLM processed 316L^[3]. The minimum feature size for SLM process usually lies around 150 µm^[4], the CSEM optimized process window allows for the printing of features as thin as 60 µm with a part overall surface roughness in the 6-8 µm range (Ra).

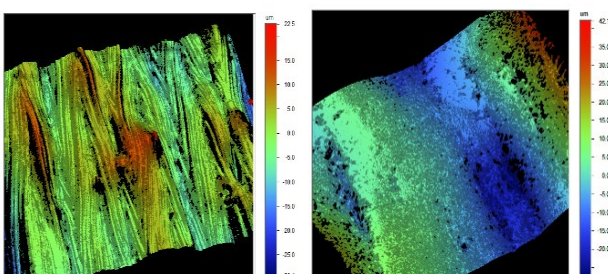


Figure 1: Surface roughness of a SLM 3-D printed part before post-processing (left) and after post-processing (right), measured using an optical interferometer, window size (500 x 500 µm).

The second step of the work focused on post-processing techniques for surface roughness reduction. The range of roughness previously mentioned, though very typical for SLM

printed part^[5], can be improved using grinding based post-processing techniques targeting removal of partially melted or partially sintered powder particles at the surface of printed parts. Once applied to 3D-printed parts, such technics diminished the measured roughness from ~5-6 µm to ~1-2 µm (Ra) (Figure 1).

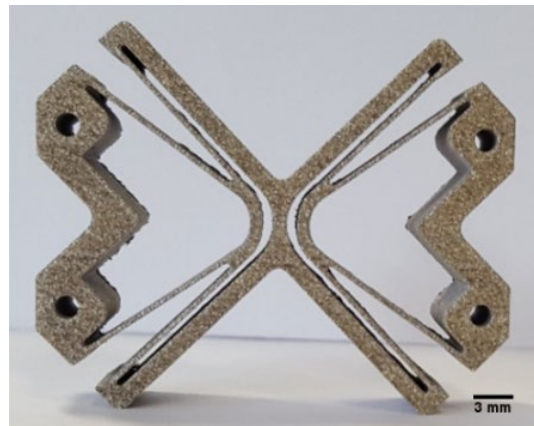


Figure 2: Flextec, a CSEM developed and printed part composed of fine features for space applications.

The successful 3D-printing of high quality sub-200 µm features using 316L relied on the combination of a finely tuned process window and an appropriate post-processing. The "know-how" developed in this study was leveraged for the printing of CSEM Flextec, parts partially composed of fine blades making it challenging to print.

In conclusion, the process parameters window defined, allowed for the printing of part features as thin as 60 µm printed with high part density and high mechanical properties. The overall surface roughness of SLM printed parts could be diminished from ~5-6 µm to ~1-2 µm (Ra) using grinding based post-processing technics, with research continuing toward reaching a surface roughness lower than 0.1 µm (Ra). The approach and work here reported is currently being extended to other SLM processable alloys (17-4 PH, Al, Ti and Ni alloys).

- [1] Roland Berger, Additive manufacturing: A game changer for the manufacturing industry ? (2013).
- [2] L. Yang, "Design for Additive Manufacturing. In: Additive Manufacturing of Metals: The Technology", Materials, Design and Production. (Springer, Cham, 2017).
- [3] C. Qiu, M. Al. Kindi, A.S. Aladawi, I. Al. Hatmi, "A comprehensive study on microstructure and tensile behaviour of a selectively laser melted stainless steel". Sci. Rep. 1–16 (2018). doi:10.1038/s41598-018-26136-7.

- [4] SLM Solutions. Selective Laser Melting Machine SLM®125 / Technical Specifications. Available at: <https://slm-solutions.com/products/machines/selective-laser-melting-machine-slmr125>. (Accessed: 7th September 2018).
- [5] Y. Kaynak, O. Kitay, "Porosity, Surface Quality, Microhardness and Microstructure of Selective Laser Melted 316L Stainless Steel Resulting from Finish Machining", (2018). doi:10.3390/jmmp2020036

SURFACE ENGINEERING

Helmut F. Knapp

The smaller components get, the more important their surfaces become. Miniaturization allows us to fabricate components whose properties increasingly depend on their surfaces: the topographical and chemical properties determine effects such as surface adhesion, wettability and friction, optical reflectivity and color, electrical conductivity, and (bio-) chemical affinity. The determination, understanding, and controlled modification of surface topography and chemistry are therefore of high importance for the development of small components and devices, and the ability to fabricate engineered surfaces at large scales and a competitive cost is a key competence in supporting industrial applications.

The **Surface Engineering** program addresses some of the most important areas for controlling surface structure and composition (both topographical and chemical) and developing related competitive manufacturing technologies suitable for industrial applications. In addition to elaborating scientific knowledge of the design and understanding of functional surfaces and developing related up-scalable manufacturing methods, the Surface Engineering program also develops higher level integration pathways that enable CSEM to develop devices in which surface properties are a critical factor. Solutions can be offered to industry at all levels of this value chain.

Within the program, the development and fabrication of nano-structured surfaces and nanoporous films with added functionality is addressed, as is the design and realization of nano-optical components based on nano-engineered surfaces. Furthermore, biochemical functionalized surfaces are developed for use in (affinity) sensors and as cell- and tissue-support substrates, including microfluidics and sample handling instrumentation. Finally, a flexible and broad material and process technology base is established for the printing of components and hybrid systems for the fast and low-cost employment of flexible devices.

Long-term objectives

The global long-term objectives of the **Surface Engineering** program are twofold.

First, the program aims at strengthening those areas where CSEM's offering is unique and valuable for Swiss industry. These positions include the development of surfaces and functional coatings with properties that are optimized for specific applications, along with the appropriate up-scalable production methods, highly specialized components and instrumentation for handling and sensing cells and other biological matter, and printing technologies for electrical and optical components on flexible substrates.

Second, it is of the utmost importance that given the ongoing trend of miniaturization, state-of-the-art understanding of surfaces and technologies to optimize their properties is available at CSEM. Surfaces are key to the improved performance of components and systems and thus also affect all other technology programs of CSEM.

The **Surface Engineering** program is based on three activities:

The activity *Nano Surface Engineering* addresses micro/nano-manufacturing technologies for the cost-effective production of nano-structured surfaces and functional nanocoatings with unique properties, as well as the engineering and production of micro-/nano-photonics components. While the first two topics remain focused on origination and up-scalable replication methods as well as sol-gel materials with controlled porosity and surface functionalization, the last topic includes methods for the small-scale production of optical components by printing and additive manufacturing, including the emerging field of free-form optics.

The activity *Bio Surface Engineering* deals with interfaces and instrumentation for handling and measuring biological entities. In bio-interfaces, surface functionalization and structuring are optimized for their application in cell supports and other cell-handling components. In bio-sensors, sensors are developed for biochemical sensing by electrochemical and optical methods for applications in *in vitro* and *in vivo* diagnostics and environmental sensing. Finally, bio-instrumentation is being developed for the handling, treatment, and analysis of biological samples, ranging from molecules to small model organisms.

The activity *Printable Electronics* addresses the development of materials and processes for the functional printing of layers and structures onto 2D and 3D substrates in order to generate functional components and to combine such printed components with conventional surface-mounted components into fully functional hybrid systems. A particular emphasis is put on flexible substrates and potentially large-scale printing processes including sheet-to-sheet and roll-to-roll printing.

These three activities have strong mutual synergies, for example in the development of printed electrochemical sensors that are specifically functionalized for applications in environmental or biochemical sensing, for the development of cell culture supports with optimized surface topography and chemistry and integrated electrochemical sensors for monitoring, or for plasmonic sensing for high-sensitivity, label-free analytics.

Beyond that, the work carried out in the **Surface Engineering** program is a critical enabler for a number of projects in other research programs, examples being surface treatment for hermetic sealing solutions in functional packaging, the design of novel optical filters and masks that can be directly designed onto vision sensors, and surface roughness optimization in intermediate adsorption layers for increased conversion efficiencies in amorphous silicon PV cells.

Highlights

Some of the work from this last reporting period is shown on the following pages. It includes micro/nano-structuring of surfaces to optimize their wear/friction behavior, to emboss security features into implants, or to create plasmonic structures for enhanced water splitting or optical functionality. First results with free-form micro-optics and optical interconnects are also reported.

Printed sensors achievements are given for roll-to-roll printed wireless sensors (Figure 1), flexible ultrasound transducer arrays, and electrochemical pH sensors.

Concerning biological applications, components and systems are described for handling biological entities (stem cell organoids, monolayers, neuronal cultures) or handling samples and analyzing biochemical species in urine, blood, water, or milk. Viscosity-independent controlled dispensing of liquids is one such development (Figure 2).

Several of the technologies from the **Surface Engineering** program have either sparked interest from or have found their way into industry through CSEM partners. This is particularly true for the *Nano* and *Bio Surface Engineering* activities. Nevertheless, the youngest activity, *Printable Electronics*, is picking up as well.

Recent examples from the three activities include:

- Steel tools containing optical security features, which can be used for embossing these features into titanium dental implants, for the company Thommen Medical (Figure 3).
- High wear-resistance/low-friction hybrid surfaces combining nitrocarburized surfaces with dry lubricants, for the company Gerster.
- Automated production line for a stem cell organoid culture platform based on hydrogel microwell arrays, for the company SUN Bioscience (Figure 4).
- Disposable electrochemical sensors, screen printed at high throughput, for applications in urine analysis, food analysis, or pH monitoring of cutting fluid.
- Flexible, printed ultrasound transducer arrays for continuous cardiovascular function monitoring.
- Automated system for the classification and sorting of fertilized zebrafish eggs based on deep learning algorithms, for the Helmholtz Zentrum für Umweltforschung.

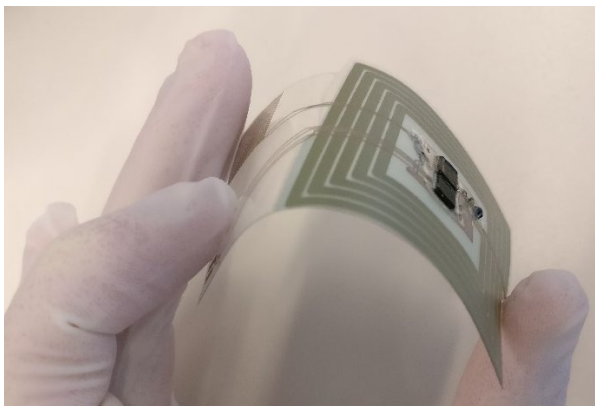


Figure 1: pH and force sensors, in combination with an antenna, printed onto a flexible substrate to make wireless, stand-alone sensors.



Figure 2: Demonstrator for calibration-free liquid dispensing based on CSEM's proprietary controlled pressure dispensing technology.

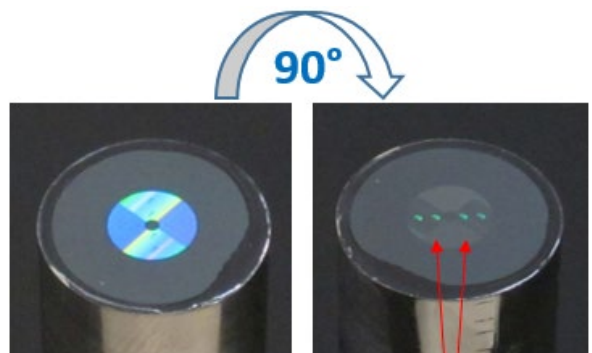


Figure 3: Steel stamping tool for embossing security features onto titanium implants. The arrows point to ™ logos.



Figure 4: Microstructured stamps for casting hydrogel microwell arrays.

ACEnano—A Tiered Approach for Nanomaterial Risk Assessment

L. Burr, D. Schmid, S. Generelli, S. Cattaneo

With increasing usage of nanomaterials, risk assessment is crucial to create new adequate regulations. In the frame of the European ACEnano project, CSEM is developing innovative characterization techniques to describe nanoparticles, their properties and their toxicity. In particular, CSEM focuses on three key properties of nanomaterials, namely their surface hydrophobicity, solubility and reactivity.

Used for centuries, ultrafine particles have been employed and studied extensively in the past few decades. In particular, particles with dimensions below 100 nm, also known as nanoparticles, have attracted attention due to their appealing new properties. In use for a wide range of application, from drugs to batteries, these particles are not yet fully understood and the notion of them being harmful to the human body as well as for the environment rises among the scientific community and the population. Currently, no regulation exists for nanomaterials due to the absence of reproducible and standardized detection and characterization techniques. In the frame of the European ACEnano project, CSEM is developing innovative characterization techniques to classify nanoparticles, their properties and their toxicity.

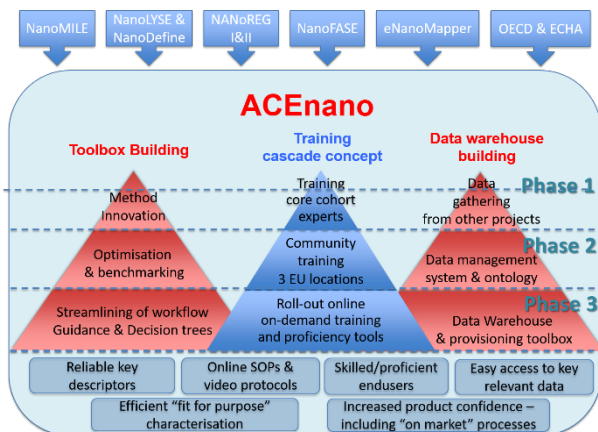


Figure 1: ACEnano will create a “conceptual toolbox” including a tiered approach to cost efficient nanomaterials analysis that will facilitate decision-making in choice of techniques and SOPs, linked to a characterization ontology framework for grouping and risk assessment.

Among the key properties of nanomaterials are surface hydrophobicity, particle solubility and particle reactivity, for which there is a substantial lack of techniques for reproducible assessment.

Hydrophobicity is the property of repelling water rather than absorbing or dissolving in it and is an important characteristic in nanotechnology for evaluation of risk (interaction of nanomaterials with biological media) but also for improvement of nano-drugs. CSEM is developing new methods for hydrophobicity assessment of nanomaterials based on hydrophobic interaction chromatography (HIC) with elution investigation in hydrophobic columns and on 2D surface analysis

[1] J. Adrian, S. Pasche, J. Diserens, S. Sánchez-Baeza, H. Gao, M. Marco, G. Voirin, "Waveguide interrogated optical immunosensor (WIOS) for detection of sulfonamide antibiotics in milk, Biosens. Bioelectron. 2009, 24, 3340-3346.

with CSEM's waveguide interrogated optical sensor (WIOS) instrument^[1].

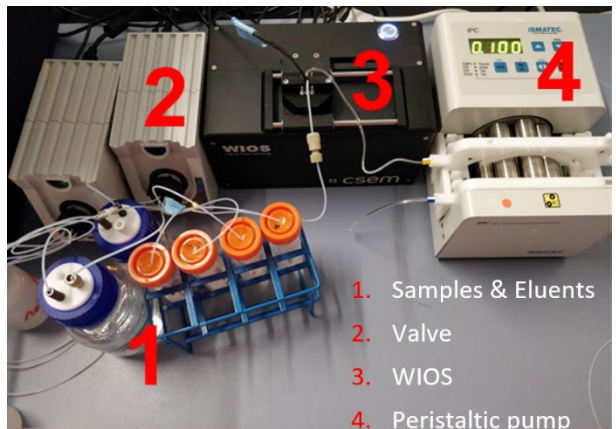


Figure 2: Test-setup for nanomaterial hydrophobicity assessment based on CSEM's WIOS instrument.

Solubility is another important parameter influencing the way in which nanomaterials interact with the environment. The focus in ACEnano lies on interaction with biological media and CSEM is developing a microfluidic sample preparation system allowing to automatically mix and incubate up to 24 samples in a standard-size well plate for hours up to several days and for consecutive analysis by single-particle inductively coupled plasma mass spectrometry (SP-ICP-MS).

Reactivity describes yet another essential property of nanomaterials. The focus in ACEnano lies on catalytic reactivity and its colorimetric detection^[2]. In collaboration with RIKILT, CSEM is developing a standalone optofluidic monitoring system that allows for manual or robotic pipetting of samples for up to 24 parallel assays in a standard-size well plate, automated mixing, incubation and parallel absorbance readout.

First tests carried out with reference nanoparticles with the methods described above gave promising results. In the following months, the tests will be further developed and tested with a panel of nanomaterials defined by the consortium, to assess their suitability for routine nanoparticle characterization.

The ACEnano project is a collaboration between 28 European, Chinese and Korean consortium partners (www.acenano-project.eu) and received funding from the European Union's Horizon 2020 research and innovation program under grant agreement No. 720952. CSEM thanks them for their support.

[2] C. Corredor, M. Borysiak, J. Wolfer, P. Westerhoff, J. Posner, "Colorimetric detection of catalytic reactivity of nanoparticles in complex matrices", Environ. Sci. Technol. 2015, 49, 3611-3618.

3D Printed Models to Understand Aerosol Evolution and Deposition in the Human Respiratory Tract

G. Andreatta, B. Dunan, R. Smajda, O. Chandran, N. Blondiaux, S. Lani, M. Palmieri, M. Asgari•, F. Lucci•*, S. Majeed•, J. Bialek•, S. Steiner•, S. Frentzel•, J. Hoeng•, J.-P. Schaller•, A.K. Kuczaj••

From air pollutants to pharmaceutical aerosols, many inhalable aerosols contain volatile compounds. The constant interaction of such volatile species between liquid and vapor phases leads to aerosol evolution, which can subsequently affect the aerosol deposition in the human respiratory tract. CSEM and Philip Morris International R&D have jointly designed and developed *in vitro* model lung casts using 3D printing methods with controlled temperature in order to evaluate the influence of the aerosol growth in biologically relevant conditions on its final deposition on the surface.

In recent years, a pool of scientific studies have been devoted to understanding the mechanisms involved in respiratory drug delivery and quantifying the received material doses^[1]. This has led to the development of relevant dosimetry tools, including *in vitro* human lung casts. In spite of the progress made in the current exposure systems and human lung models, there are still large gaps remaining to be filled with adequately developed tools. For example, complexities of the anatomical structure and physiological operating conditions of the human respiratory tract are not fully represented in existing models^[2,3].

Our aim was to obtain a model cast representative of the physiology of a lung, including its physical characteristics, a controlled temperature (T) of 37°C, and a humidity rate above 85%. Additive manufacturing technologies were chosen to respond to this challenge. 3D printing allows for the reproduction of scanned lungs in plastic material as well as the addition of a complex network regulating the temperature and rate of humidity around the lung cast.

The first design was a simplified model aimed to be tested for experimental correlations with computational simulations of aerosol evolution and deposition. The design included junctions and external channels for temperature and humidity control. Stereo-lithography was selected due to its high resolution, and the polymeric material was chosen in order to obtain a suitable thermal conductivity, high resistance to T , and a low roughness of the surface. Figure 1 shows the resulting cast.

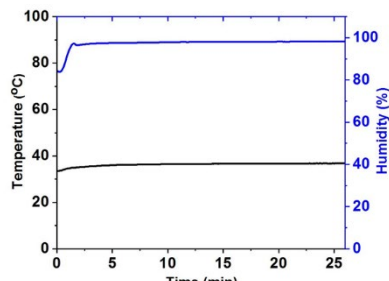


Figure 1: Printed bent pipe as a simplified model toward cast (left). The developed cast enables us to regulate the temperature and humidity rate of the flow to desired values (right).

- PMI R&D, Philip Morris Products S.A., Quai Jeanrenaud 5, 2000 Neuchâtel, Switzerland.
- Faculty EEMCS, Multiscale Modelling and Simulation, University of Twente, P.O. Box 217, 7500 AE Enschede, The Netherlands.
- [1] J. Heyder "Deposition of inhaled particles in the human respiratory tract and consequences for regional targeting in respiratory drug delivery", Proc. Am. Thorac. Soc. 1(4), 2004, p. 315.

Following this proof of concept, a geometrically realistic cast of the human upper respiratory tract was developed and constructed. The process is shown in Figure 2.

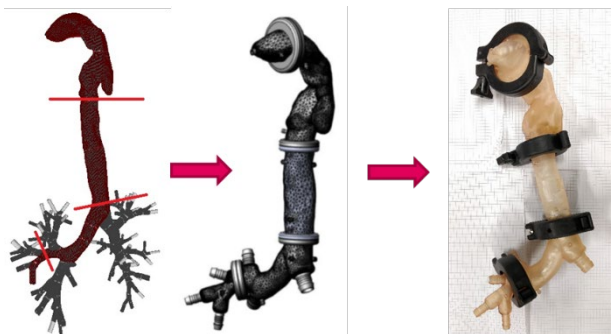


Figure 2: From left to right: scanned lung representation with chosen representative path; CAD drawing of the lung cast with junctions and external channels for T control; the final prototype.

The functionality and the control of the temperature in the cast were then tested while flowing air at a relevant flow rate. The shell temperature is homogenous, and the inside temperature reaches 37°C (Figure 3).

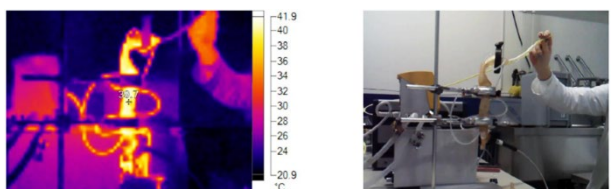


Figure 3: Thermal image (left) and visible light image (right) of a lung cast connected to a water bath at 46°C and with air flow of 2.5 l/min at 60% humidity. The cast shows a homogeneous shell temperature with an internal temperature of 37°C.

The developed cast is based on a realistic respiratory tract model and has the feature to control the airflow temperature. Current efforts are dedicated to experimental and computational assessment of deposition for various types of aerosols and conditions.

- [2] S. Majeed, S. Frentzel, S. Wagner, D. Kuehn, P. Leroy, P. A. Guy, A. Knorr, J. Hoeng, M. C. Peitsch, "Characterization of the Vitarcell® 24/48 *in vitro* aerosol exposure system using mainstream cigarette smoke", Chem. Cent. J. 8(12), 2014, p. 62.
- [3] Y. Zhang, W. H. Finlay, "Experimental measurements of particle deposition in three proximal lung bifurcation models with an idealized mouth-throat", J. Aerosol Med. 18(4) 2005 p.460.

Microstructures Stamped into Ti Dental Implants for Trademark Protection

R. Krähenbühl, D. Kallweit, C. Schneider, M. Schnieper

To distinguish the high-quality products made in Switzerland and prevent them from being counterfeit, we investigated, developed and realized submicron-structuring technologies directly embossed into dental titanium based devices (implants and abutments) of Thommen Medical. To develop such nanostructured identification, we elaborated the design and submicron-structuring of the stamping tool with holograms and diffractive optical elements (DOE's). Furthermore, using these tools we developed an embossing process which transfers these micro-structures directly into dental titanium devices using pure physical structuring of the surface. As a result, we were able to successfully emboss different types of dental implants and abutments, as well as to proof a serviceability of the tool over 5000 stamping cycles.

In order to safeguard the genuineness of the high quality Swiss MedTec products of Thommen Medical™ and to allow their quality assurance and traceability, in this project we developed, together with FHNW, an embossing process of sophisticated sub-micron features, like holograms and Diffractive Optical Elements (DOE), into dental devices based of titanium material. In particular, several nano-structures were integrated into one layout (see Figure 1), having different security features (the TM logos as grating structures in orthogonal direction, the Swiss Handcraft as a micro image, and two zebra like structures forming the DOE's (TM logo as a binary and Thommen Medical as a four level structure, inverse on stamp to be true on device).



Figure 1: One of the final stamps (upper part) showing the different security features such as periodic gratings in different direction (90-degree switching effect, lower left), as well as DOE's projecting the inverse TM and Thommen logos onto a wall (lower right).

To be capable to stamp nanostructures into dental implants made of titanium alloys, high resistant stamping tools made from steel with a hardness of up to 67 HRc were realized. To find the optimal morphological and thermo-mechanical embossing parameters, different shapes of steel stamps, as well as various grating structures having different periods and depths were realized, characterized and tested. As a result, it turned out, that the diameter of the stamp should be preferentially bigger than the embossing area on the dental abutments/implants, to prevent an over-pressing effect. Furthermore, the optimal stamp-grating period laid at 1.8 µm with a depth in the range of 250-400 nm.

Extensive stamping trials have been carried out on different positions of the dental devices using a Zwick/Roell Z100 tension

test machine. The optimal compressive pressure laid between 0.45-0.99 kN/mm², depending on the exact shape of the dental abutment/implant. The best results were achieved when stamping on the flat surface of the dental devices (see Figure 2 on the left). As most influencing embossing parameters, process temperature, load and surface roughness of stamping area have been identified. A lower surface roughness of the stamping area and higher process temperatures ease the stamping process.

A durability test of the stamp was carried out using a ring stamp on a servo-hydraulic testing machine (hydropulser) to run thousands of stamping cycles together with a Katana robotic arm, which simultaneously moved the Titanium plates, preventing that the same spot is embossed twice. The cycling tests revealed a serviceability of up to 5'000 stamping trials (see Figure 2 on the right). Wear of the stamp surface was pronounced on one side, indicating a light slope of the stamp surface. Still the holographic effect was nicely visible on the stamp, but it started to get more difficult to be recognized on the imprinted Ti devices.

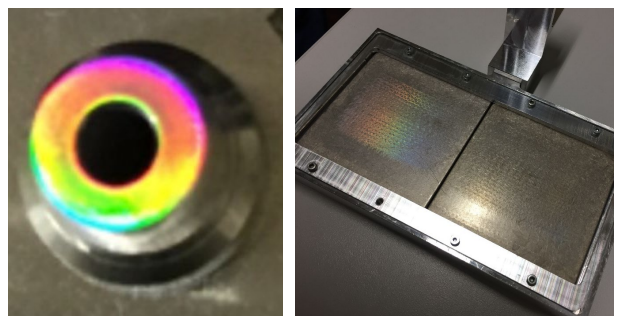


Figure 2: Final imprinted devices (left) and titanium plate (right) after 5000 stamping cycles.

The technical outcome of the project was very satisfying in terms of transferring the holographic grid onto a dental product and creating holographic patterns, as well as DOE's. They were even leading to two patent applications protecting the here developed fabrication method. In future, main focus will be to promote this innovation to bigger size implants and other devices of the medical market (e.g., Trauma or Orthopedic applications).

The authors would like to thank Innosuisse (CTI) for their financial support (Project No 8679.2 PFIW-IW).

Optical Phase Retarder based on Plasmonic Nanostructures

B. Gallinet, L. Driencourt, F. Lütolf, R. Ferrini, D. Kazazis[•], Y. Ekinci^{••}, F. Federspiel^{••}, R. Frantz^{••}

Plasmonic nanostructures with a strong and spectrally narrow birefringence have been developed. Strong color effects depending on the polarization have been observed, which could have applications in optoelectronic devices such as displays or imagers, as well as in optical security.

Surface plasmon resonances in metallic nanostructures enable the confinement and manipulation of the electromagnetic field well below the diffraction limit, thus opening new paradigms for optical devices. In addition, subwavelength resonators are able to act on the phase of the light, making them essential building blocks for metasurfaces. This project aims to the development of a colored optical retarder and its integration in optoelectronic devices. This is achieved by design and fabrication of plasmonic nanostructures showing a strong and spectrally narrow birefringent effect that yields a color effect which can be actively controlled by e.g., liquid crystals.

The basic working principle is shown in Figure 1a. A plasmonic phase retarder is placed between a first polarizer with a fixed orientation and a tunable analyzing polarizer^[1].

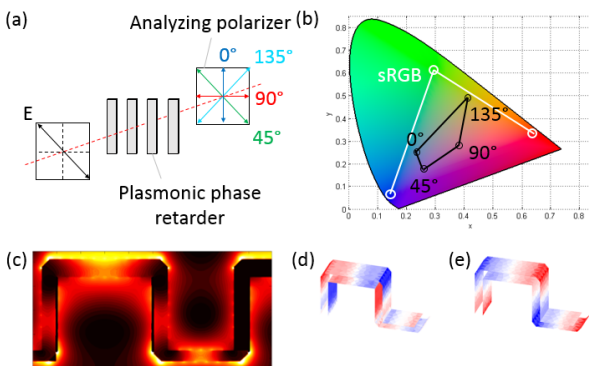


Figure 1: (a) Plasmonic phase retarder placed between a fixed polarizer and a tunable analyzing polarizer; (b) Designed colors in CIE space obtained as a function of the orientation of the analyzing polarizer; (c) Electric field intensity at plasmonic resonance; (d-e) Surface charge distribution (d) below and (e) above resonance. Red: positive. Blue: negative.

In a metallic nanostructure, the birefringence is determined by plasmonic and non-resonant contributions (i.e., effective refractive index). Numerical calculations have been performed to gain a deep insight into the near and far-field optical properties, which is necessary to design and optimize the combination of these contributions. The presented silver nanostructure has a deep-subwavelength periodicity (220 nm and below) in order to avoid diffraction effects. Constraints from the fabrication process have been included through the analysis of scanning electron microscopy measurements in order to provide a realistic design. The polarization-dependent transmission amplitude and phase have been calculated and used to obtain the transmission for different angles of the analyzing polarizer (Figure 1b). Sharp

interference effects occur for crossed polarizations (45° and 135°), yielding strong purple and yellow colors.

A plasmonic phase retarder has been fabricated by UV-nanoimprint of a grating master and evaporation of a silver thin film, followed by encapsulation. The polarization-dependent transmittance is shown in Figure 5a, with a plasmon resonance at 480 nm for the TM polarization.

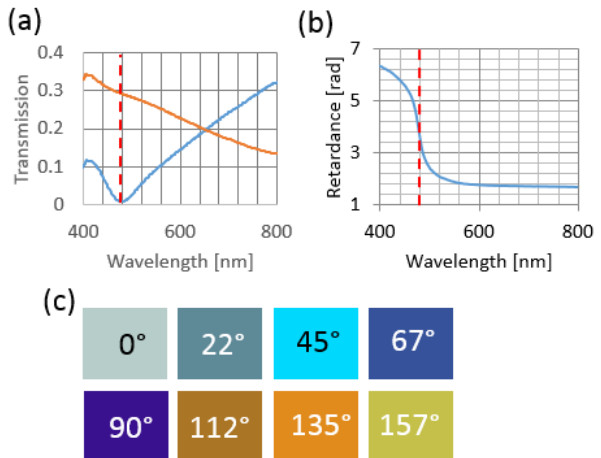


Figure 2: (a) Transmission for TM (orange) and TE (blue) polarization of a fabricated plasmonic phase retarder. (b) Ellipsometric measurement of the retardance, showing a strong phase variation around the plasmonic resonance. (c) Measured colors under rotation of the analyzing polarizer.

Ellipsometry measurements have been performed to assess the phase retardation between the transmitted TM and TE fields (Figure 2b). A strong phase variation is observed at the plasmon resonance, in perfect agreement with simulations. This phase behavior for a thickness below 100 nm cannot be obtained from nanostructured phase retarders. A variety of colors, from blue to purple, orange and yellow are generated from the structure (Figure 2c) in agreement with the theoretical predictions.

In summary, plasmonic phase retarders with spectrally narrow phase variations have been fabricated using a nanoimprint process, and their ability to control the optical phase beyond standard birefringent materials demonstrated. Further developments in the project include phase retarders with high color saturation and their combination with active liquid crystal layers.

This work was supported by the Nano-Argovia program (Swiss Nanoscience Institute, University of Basel).

• Paul Scherrer Institut, PSI
•• Rolic Technologies Ltd.

[1] L. Dümpelmann, et al., "Four-fold color filter based on plasmonic phase retarder", ACS Phot. 3, 190 (2015).

Freeform Micro-optics for Non-imaging Applications

O. Fernández, P. Leroux, T. Aderneuer, A. Lücke, R. Ferrini

Freeform (micro-)optics is considered as a game changer in the field of optical design as it offers many advantages compared to its symmetric counterparts, especially for complex illuminations tasks. However because of their complex surface profiles, both the design and the characterization of such innovative (micro-)structures is considerably challenging. Here we report on the development of in-house algorithms for the optical design, simulation and characterization of freeform lenses and microlens arrays for complex prescribed irradiance problems.

Freeform lenses

The goal of non-imaging optics is to transfer radiation from an extended source to a target to achieve a specific spatial and/or angular distribution of radiation on the target,^[1] a problem often referred as *lens design for a prescribed irradiance*.

Non-symmetrical light distributions are often needed in applications such as lighting (human centric, street, road, rack, office lighting, etc.), optical imaging & sensing, and image projection. However, unless special optical configurations are adopted, the performance of optical systems degrade when the symmetry is broken.^[2] These cases demand indeed freeform components, defined as *those components whose shape is fully determined by the optical functionality and which are not limited by symmetry constraints*.

At CSEM we have developed design and simulation tools for freeform lenses for prescribed irradiance problems based on the Ray-Mapping approach and Monte Carlo ray-tracing respectively.

A two level (i.e., light/dark) light distribution is defined (Figure 1; left) and the lens is calculated according to the predefined characteristics of both the source and the target. The resulting irradiance distribution is then simulated using CSEM ray tracing algorithm (Figure 1; right).



Figure 1: Target (left) and achieved (right) irradiance distributions.

Freeform microlens arrays, FMLA

The concept of freeform optics can be extended to the micro-optics domain in general and thin-film optics in particular by designing freeform microlens arrays, FMLA.

The advantages of FMLA include thin form-factor, low-weight, large-area and cost effective production. As a flip size, FMLA are more challenging to characterize since, contrary to the standard spherical microlenses, their shapes are controlled by many more parameters or even by non-parametric expressions.

On the other hand, the empirical characterization of fabricated FMLA in the laboratory is usually extremely challenging due to alignment errors, lack of precise light sources and/or detectors for each application.

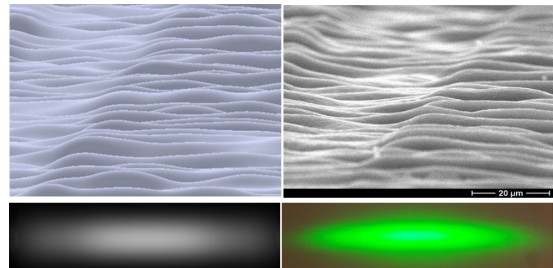


Figure 2: (Left) Constructed ray-traceable FMLA (top) and simulated irradiance distribution (bottom). (Right) SEM picture of the real FMLA (top) and experimentally determined irradiance distribution. Under collimated incoming beam.

To overcome this limitation, CSEM has developed a semi-empirical characterization method. The surface topology of the FMLA is experimentally determined using for example surface profilometry. The resulting point cloud is transformed into a ray-traceable CAD solid compatible with ray-tracing simulation. Finally, the optical performance of the CAD solid is simulated under precise conditions (alignment, source emission profile, detector size, etc.).

An example of the developed method is presented in Figure 2, which shows the very good agreement between the experimental results from the real FMLA and the simulation of the built ray-traceable FMLA.

Further work

Future activities will focus specifically on the development of freeform micro-optics, which finds application in several fields such as solid-state lighting (incl. professional, automotive, and human-centric lighting), day lighting, photovoltaics, security, anti-counterfeiting, branding, optical sensing, imaging, and displays (incl. augmented and virtual reality).

CSEM is currently working towards extending the design algorithms to gray-level irradiance distributions and incorporating the fabrication constraints at the FMLA design stage, as well as developing the origination and replication processes for fabrication of FMLAs on large surfaces.

[1] R. Wu, H. Hua, Optics Express 24(2) pp.1017-1030 (2016).

[2] K. Fuerschbach, *Freeform, φ -Polynomial Optical Surfaces: Optical Design, Fabrication and Assembly*, PhD Thesis University of Rochester, Rochester, New York (2014), p. 6.

HySurf—Microstructured Hybrid Surface with Improved Friction Properties

K. Vaideeswaran, J. Gobet, S. Biselli, V. Courbat, P. Margraf*, O. Sereda

Nitrocarburisation is a surface hardening technique usually applied to improve the wear resistance of steel surfaces. On the other hand, dry lubricants are utilised to lower the coefficient of friction (COF). Currently, the lifetime of steel components, in many applications using either of these techniques individually, are faced with the limitations of the two techniques: high COF for nitrocarburised surfaces and low wear resistance of dry lubricant coatings. Thus, the current study involves the creation of a hybrid surface using the impregnation of a dry lubricant on to a nitrocarburised surface. The mechanical strength and hardness of Gerster SA's nitrocarburised surfaces accompanied by the impregnation of the porous outermost layer with a solid lubricant creates a "hybrid surface" possessing both outstanding wear resistance and a low COF, with a high adherence to substrate.

The nitrocarburising (NC) process parameters (atmosphere, temperature, dwelling time) were optimised by Gerster SA, leader in steel surface treatment in Switzerland, to obtain samples that have a distinct porous surface structure (in terms of size, shape and density) as observed by metallographic and microscopic investigations. The porosity thus obtained is suitable for the impregnation of a dry lubricant. CSEM implemented its know-how in surface engineering and lubrication jointly with Gerster to define and test dry lubricants suitable for such surfaces. Analyses were conducted with multiple commercial lubricants (containing lubricating particles e.g., Polytetrafluoroethylene (PTFE) and MoS₂ in thermoplastic or thermosetting polymer matrix) and upcoming lubricants (e.g., parylene, sol-gel based polysilazanes and thermally diffused zinc) were analysed. The goal was to obtain a void-free interface with the NC surface (hybrid surface). In parallel, metallic samples without nitrocarburisation were coated with the same dry lubricant as a reference (henceforth called non-NC). The tribological analyses were conducted against a quenched steel ball on all surfaces with and without lubrication were also conducted in parallel.

Without any lubricant, the NC surface showed a wear rate 5 times lower than the non-NC surface, although the COF remains >0.6. The best lubricant among the tested ones for both surfaces (NC and non-NC) was found to be a commercial lubricant containing PTFE particles in a thermoplastic polymer matrix with the following remarkable properties:

- Cost effective application by dip coating, results in a suitable thin (<2 µm) impregnating layer (see Figure 1).
- In the presence of a thin film of dry lubricant (<2 µm) and under the application of high loads (~800 MPa, applied force= 0.5 N), the hybrid NC surface retained a CoF <0.2 for over 400 m of sliding (see Figure 2). On the other hand, the COF for the lubricated non-NC increased from ~0.1 to > 0.3 within 120 m.
- Meanwhile, while the steel ball sliding against the lubricated non-NC surface showed heavy wear, the corresponding ball sliding against the hybrid NC surface showed very limited wear.
- Electron microscopy of the sliding tracks in the hybrid NC-surface shows the presence of the NC nodules as well as the lubricant, whereas no traces of the lubricant were found in the sliding track on the non-NC surface.

In this manner, the clear advantage of combining nitrocarburisation with the impregnation of a dry lubricant towards forming a hybrid surface has been demonstrated.

* Gerster SA, Güterstrasse 3, CH-4622 Egerkingen, Switzerland

We thank the CTI for the financial support for this project, undertaken with the CTI project number 18611.1 PFEN-NM.

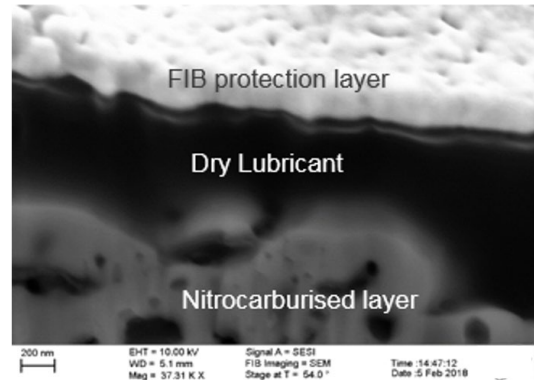


Figure 1: Focused Ion Beam (FIB) section showing the continuous interface between the lubricant and the nitrocarburised layer.

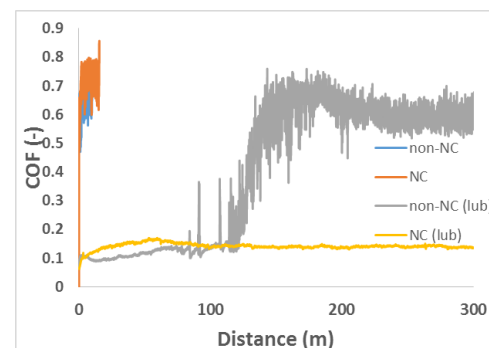


Figure 2: COF evolution (applied force = 0.5 N) on non-impregnated NC and non-impregnated non-NC, as well as impregnated NC steel (hybrid surface) compared to impregnated non-NC (reference surface), showing the advantage of the hybrid surface.

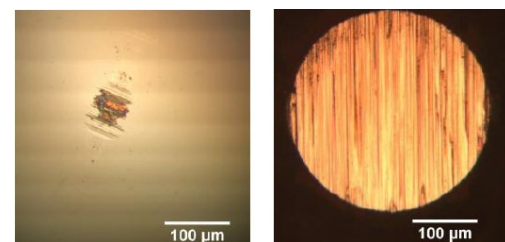


Figure 3: Optical microscope images of the 2 mm diameter steel counter body (load 0.5 N) after 400 m of sliding on the hybrid surface (NC, left) versus the lubricated reference surface (non-NC, right). The hybrid surface reduces drastically the wear of the steel counterpart.

Folded Micro-optical Connectivity Solution

A. Luu-Dinh, R. Krähenbühl, C. Schneider, F. Zanella, R. Ferrini

Current optical connectivity solutions use optical fibers as transmission media for long and medium distance communication. In short range data communication, the electrical interconnects are being replaced with optical ones for optical transceivers for data-and telecom. However, up to now, most of the available solutions are based on straight optical connectivity. In this project, CSEM demonstrated the feasibility of micro-optical elements capable to deflect the light by 90 degrees. The origination and replication of such micro-structures rely on wafer-scale fabrication processes, which enable a cost effective technology platform for mass volume production.

Current optical connectivity devices are mainly based on straight solutions for light coupling. However, with the transition of optics closer to the device (e.g., for connected devices) and even to monolithic chip integration, space is becoming more and more limited. In particular, datacom applications require interconnections to active optical devices (e.g., lasers, LEDs and detectors), to waveguides in electro optical boards, and to waveguides in photonic integrated circuits (PIC), where it is essential to have a compact folded optical connection (preferably at 90 degrees).

In this project, two reflective solutions were evaluated, i.e: a 45-degree mirror and a quarter ball lens (Q-Lens), both exploiting total internal reflection (TIR). For the low-cost manufacturing of these micro-optical elements, UV polymer replication was chosen. Additional alignment walls were implemented in the layout design in order to enable passive optical fiber alignment (Figure 1).

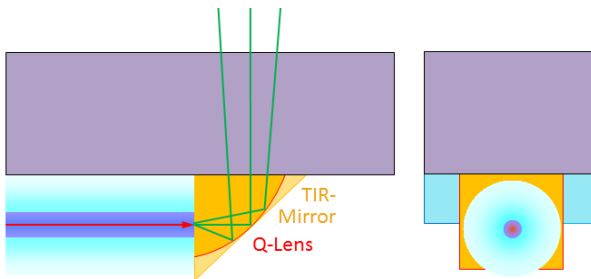


Figure 1: Schematic of Q-lens and micro-prism directly replicated on a wafer (a) Side view of the optical configuration. (b) Coaxial view of the glass fiber hold by the alignment walls.

The geometry of the micro-optical structures was designed targeting the application both to multimode fibers (MMFs, operating at 850 nm with a core size of 50 μm and a numerical aperture NA = 0.20) and to single mode fibers (SMFs, operating at 1300nm with a core size of 9 μm and a numerical aperture NA = 0.13).

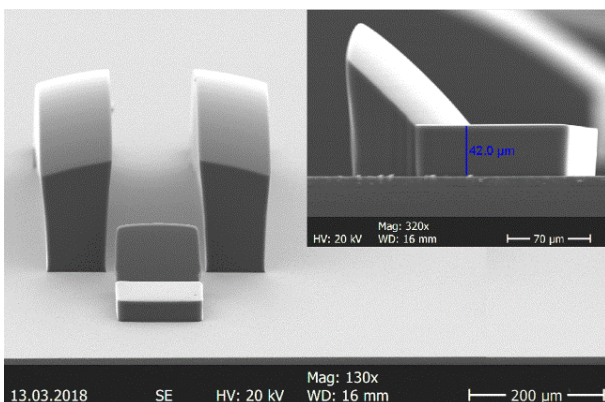


Figure 2: Scanning Electron Microscope (SEM) image of a Q-lens on wafer with alignment walls.

The fabrication of the masters for the 45-degree mirrors and the Q-Lenses was realized with direct laser writing plus chemical post polishing and photolithography plus resist reflow processing, respectively. Note that the definitive Q-lens shape together with the alignment walls is obtained by UV-molding with the photomask defining the final shape on the wafer (Figure 2).

In order to compare the performance of the Q-Lenses with respect to the 45-degree mirrors, optical losses were measured with a Kingfisher multi-fiber (E9 & G50) and multi wavelength (850, 1310 & 1550 nm) light source and an InGaAs (918D-IGOD3R) detector from Newport (Figure 3). To check the quality of the end facets, the horizontal (x-axis) beam profile was measured using a 200 micron detector fiber at different positions along the beam propagation axis

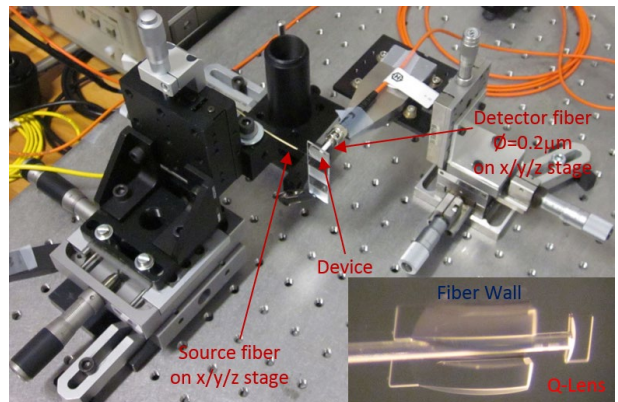


Figure 3: Optical characterization setup to measure beam profile at different propagation distances.

The measurement (Figure 4) show that the Q-lenses provide the best optical performances with negligible losses with respect to commercial single micro-prisms (i.e. $\approx +0.5$ dB).

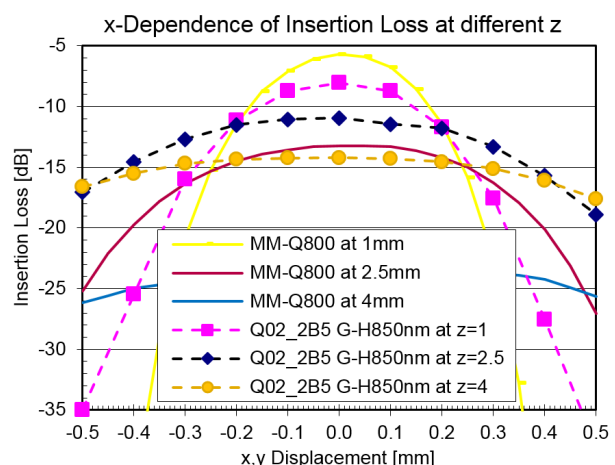


Figure 4: Optical measurements of beam profile at different propagation distances.

This project was funded by the Commission for Technology and Innovation (CTI) under grant No 27659.1 PFNM-NM.

Studying the Effect of Plasmonic Nanostructures to Enhance Solar Water Splitting

L. Driencourt, B. Gallinet, A. Luu-Dinh, C. E. Housecroft •, S. Fricke, E. C. Constable •

An approach to increase the quantity of hydrogen gas produced by solar water splitting is presented here, towards clean dihydrogen production. In particular, the enhancement of light absorption in a semiconductor electrode from plasmonic nanostructures has been studied theoretically. The best result was obtained when a high density of silver nanoparticles is used. A hybrid hematite/silver nanoparticles electrode was finally fabricated.

Hydrogen gas can be converted to electricity with a fuel cell. However, industrial dihydrogen is currently mainly produced in a non-sustainable way, by using natural gas. Water splitting using sunlight is a promising technique for clean dihydrogen production. Different approaches are studied, for instance using a photovoltaic cell as a power source for water electrolysis^[1]. In this project, a metal oxide semiconductor electrode is immersed in an aqueous electrolyte and used both as a light harvester and a catalyst. Confinement of the electromagnetic field by plasmonic nanostructures is studied for increasing the quantity of light absorbed in the electrode.

An idealized design of such hybrid structure is shown in Figure 1a. Hematite ($\alpha\text{-Fe}_2\text{O}_3$) is chosen as metal oxide material, because its small bandgap (2 eV) offers interesting possibilities for plasmonic enhancement through near-field effect. This geometry was simulated with surface integral equation (SIE)^[2] for different sets of the plasmonic metal in order to study and optimize the absorption of light in the hematite part of the geometry.

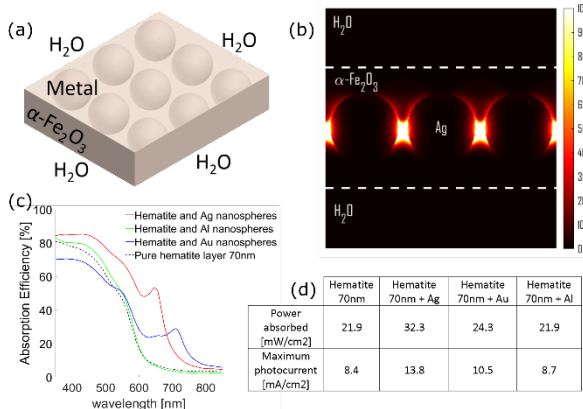


Figure 1: (a) Simulated geometry consisting in an infinite layer of hematite containing metallic nanoparticles periodically distributed. (b) Electric field intensity in a cross section at the plasmon resonance wavelength of the silver nanospheres. (c) Absorbed electric field in the hematite part of the geometry for different metals. (d) Integrated values under solar light (AM1.5G). The maximum photocurrents were calculated from the absorption efficiency spectra by assuming an internal quantum efficiency of 1.

The electric field intensity in a cross section is shown in Figure 1b for silver nanospheres. A field intensity enhancement of about 100 times is reached. The computed light absorption spectra in hematite (Figure 1c) and the integrated values under solar light expressed as an absorbed power density and a photocurrent

• University of Basel, Department of Chemistry

^[1] Schüttauf, J.-W., et al., J. Electrochem. Soc. 163 (2016).

(Figure 1d) show that the highest increase is obtained when silver nanoparticles are used. However, gold is chemically inert and therefore easier to use experimentally.

On the basis of these insights, a hybrid structure with hematite as semiconductor and silver nanoparticles is fabricated and optically characterized. A commercial Ag ink (60-80 nm nanoparticles) is spin coated on fluorine-doped tin oxide (FTO) coated glass (Figure 2a). An electrochemical deposition from an iron precursor in aqueous solution is then performed on top of the nanoparticles^[3]. Hematite is finally produced by annealing the sample in air at 550°C. The fabricated layer shows a high porosity and surface area (Fig. 2b).

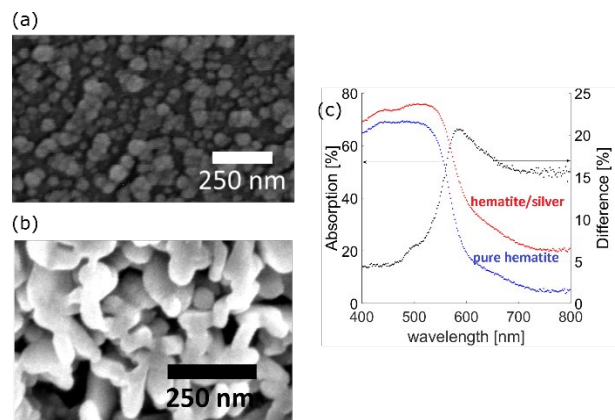


Figure 2: (a) SEM picture showing silver nanoparticles coated on a glass substrate. (b) SEM picture of the hematite layer made with electrodeposition. (c) Absorbance of the hybrid structure hematite/silver compared to pure hematite.

The light absorption in the hybrid structure is increased compared to a pure hematite sample (Figure 2c). In particular the silver nanoparticles show a plasmon resonance centered at 585 nm.

In summary, design rules for increasing the absorption of light in a metal oxide electrode with plasmonic nanoparticles have been established with numerical simulations. Silver was found as the best plasmonic material and the fabrication of hybrid hematite/silver nanoparticles samples was demonstrated. Further developments in the project include performance assessment for H₂ production and development of cost effective methods for producing efficient electrodes for water splitting.

This work was supported by the Swiss Nanoscience Institute PhD School (University of Basel).

^[2] B. Gallinet, et al., J. Opt. Soc. Am. A. 27 (2010).

^[3] P. S. Shinde, et al., J. Phys. Chem. C 119 (2015).

Liquid Biopsy—A disposable Cartridge to Measure Proteins from Whole Blood

S. F. Graf, S. Berchtold, T. Volden, N. Schmid, V. Revol, H. F. Knapp

Cancer is one of the leading causes of death in the European Union [1]. The highest chance for a cure lies in an early detection and immediate treatment. Within the European Project BioCDx [2], a companion diagnostics device is developed for cancer diagnostics and therapy monitoring. For this purpose, a generic liquid biopsy cartridge has been developed to receive a whole blood sample from a finger prick. On the cartridge the whole blood is automatically processed to plasma which is then analyzed for certain breast cancer markers using an immuno-assay on a bio-optical chip. Smooth bidirectional flow as well as on-cartridge liquids are key factors for a successful diagnosis. Integrated flow front sensors allow to closely monitor the process on the cartridge.

There is an ever increasing need for minimal invasive methods to detect and monitor cancer since early treatment has been proven to strongly increase chances of remission. One liquid biopsy method relies on the specific detection of target proteins expressed by cancer tumors.

For such applications we have developed a generic fluidic cartridge for point-of-care (PoC) devices with the following properties:

- Sterile loading port
- On-cartridge plasma extraction
- Metering loop
- Bubble removal using flow front sensors
- Remotely activated on-cartridge valves
- Smooth, controllable and bi-directional multi-liquid flow
- On-cartridge pre-loaded liquid reservoirs
- No contamination risk due to liquid stop valves (no contact possible between blood and instrument)
- Thermal management of bio-sensor

For the project BIOCDx, this cartridge (see Figure 1) has been adapted to uptake a whole blood sample smaller than 100 µl. The bio-functionalized hybrid optical chip provided by Lionix International BV was packaged onto the microfluidic platform. This chip has integrated optical wave guides forming an asymmetric Mach-Zehnder Interferometer (aMZI). As shown in preliminary tests, a smooth and repeatable flow is required to obtain reproducible measurements on this type of sensor. Via an immuno-assay a phase shift of the optical signal is generated and measured. In a first application, antibodies to detect markers for breast and prostate cancer will be spotted onto the bio-optical chip by laser induced forward transfer (LIFT).

With the help of rapid prototyping, such as micro milling, the ideal geometry was initially determined and is now being transferred to an injection molded cartridge. Special features include the exact on-cartridge metering of 15 µl plasma and the compact on-cartridge valves which allow to move the fluids over the sensor or bypass it.

The interfacing instrument for this project is developed by LRE Medical and shown in Figure 2. Three syringe drivers and a valve actuator together with a spring contact connector were integrated on a bread board. With the dedicated electronic board, and the graphical user interface, the operator can precisely monitor and control the flow down to 4 µl/min.

For a successful measurement, no air bubbles are allowed to pass the sensor when the measurement has started. For this purpose we developed a compact flow front sensor: This sensor monitors a channel and reports if liquid, air or an air bubble is present. In the unlikely event of an air bubble, it would be bypassed from the sensor.

The functionality of cartridge and instrument have been demonstrated and in the upcoming months will be used in a small clinical study to detect certain breast cancer markers to proof its potential as a companion diagnostic tool.

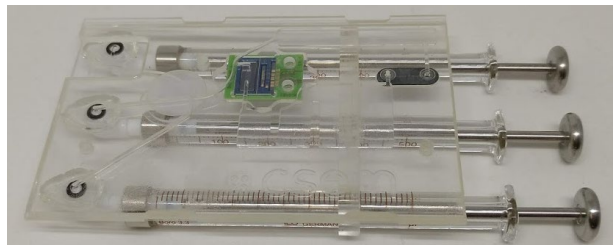


Figure 1: BIOCDx cartridge with preloaded buffers, integrated sample preparation, sensor chip and on-cartridge valves.

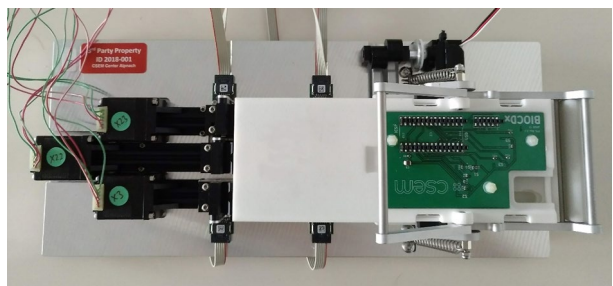


Figure 2: Bread board system developed by LRE medical to operate the cartridge.

This work was supported by the Swiss federation, MCCS Micro Center Central Switzerland, and the European Commission (H2020-732309 BIOCDx). CSEM thanks them for their support.

[1] World Health Organization, "Leading causes of death in Europe: fact sheet".

[2] BioCDx consortium, project ID 732309, "A miniature Bio-photonics Companion Diagnostics platform for reliable cancer diagnosis and treatment monitoring", <http://biocdx.eu/>

First Microfluidic Valve with Integrated Mixer for In-line Sample Preparation

Z. Halvorsen, N. Schmid, V. Revol, S. F. Graf, H. F. Knapp

A microfluidic distribution valve with integrated mixer has been developed for small volume sample preparation. This valve allows for fully automated sample preparation processes with high chemical compatibility and a ten-fold reduction of the reagent consumption compared to existing solutions. It enables the rise of in-line analytical methods requiring a labelling process such as flow cytometry, mass spectroscopy, miniaturized assays for biochemical reactions and cell based assays.

Key facts

- In-line automated sample preparation module based on patented microfluidic valve with integrated mixer
- Zero dead volume enabling a 10-fold decrease in reagent consumption for labelling water samples in flow cytometry
- Compact and cost-efficient design
- Scalable to other sample preparation procedures

Flow Cytometry (FC) has established itself as one of the most powerful analytical technologies for making controlled high throughput, multi-parameter measurements on large numbers of cells and bacteria. While FC are mostly used in laboratory settings today, there is a strong need to enable in-line FC for water, food or generally process monitoring. This demands for full automated operation but also for decreasing waste and reagents consumption.

While the readout and data analysis are already automated and optimized in state-of-the-art devices, the automation of sample preparation remains a challenge. It is currently labor-intensive and can be affected by a host of potentially confounding variables.

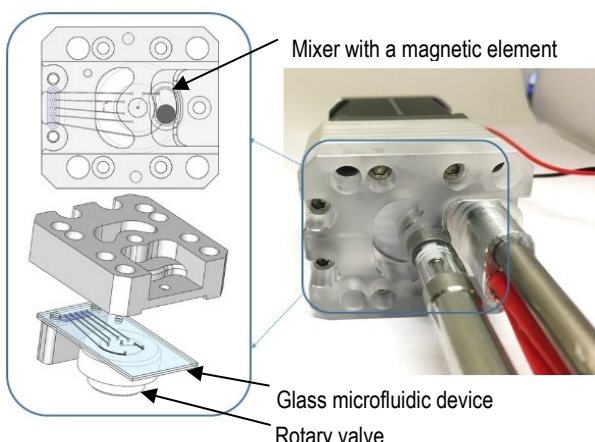


Figure 1: Microfluidic rotary valve integrated magnetic mixer.

The novel patent pending^[1] sample preparation platform presented in Figure 1 and 2 is capable of filtering, dosing, mixing, incubating and cleaning. A miniaturized bidirectional syringe pump is used to load reagents (in this case: water sample, fluorescent dye, cleaning and rinsing solution) into a microfluidic device which is placed directly onto a rotary distribution valve.

[1] Patent application: EP18188767.0

[2] Z. Halvorsen, V. Revol, S. F. Graf, N. Schmid, H. F. Knapp, P. Cristofolini, "PocketDX—Compact flow cytometer for industrial

The glass-based microfluidic device contains several micro-channels which lead to the individual reagents, an optical detector, and a mixing reservoir. The mixing reservoir contains a magnetically actuated mixing element.

The rotary distribution valve is used to selectively connect the different reagents as well as to actuate the mixing element. Thus, active mixing is realized which has the advantages of achieving 100% mixing efficiency even with a very high volume ratio between the reagent and the sample in a very short time scale.

The entire sample preparation platform has a minimized dead volume to avoid cross-contamination and to reduce the amounts of sample, reagent, and cleaning agents needed to conduct a measurement. It provides fast and safe switching between different fluidic reservoirs. The compact and fully enclosed design of the module overcomes issues with biohazard containment risk by opening and manually preparing flow cytometry samples.

Furthermore, combining the fluid distribution and mixing in one microfluidic device leads to less reagent consumption and waste generation per measurement, reduced manufacturing costs, lower power consumption and lower weight.

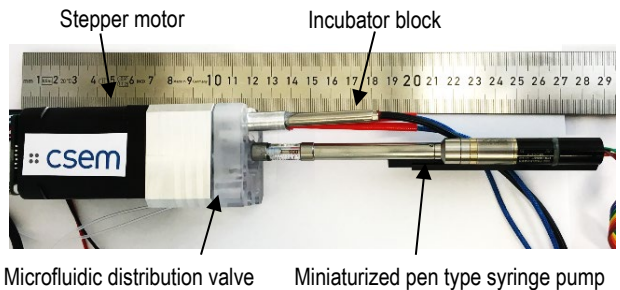


Figure 2: Miniaturized fluidic sample preparation unit (side view) consisting of a bidirectional syringe pump, a glass based microfluidic device, a rotary valve driven by a stepper motor with an integrated active magnetic mixer and a heating element as part of the incubator block.

The presented sample preparation platform was connected to an industrial flow cytometer to monitor the quality of drinking water as demonstrated in another report^[2]. The invention can also be easily extended for the use in other applications of automated sample preparation to e.g., monitor pathogens in food product.

This work was supported by the Swiss Confederation and MCCS (Micro Center Central Switzerland).

"water quality monitoring", CSEM Scientific and Technical Report (2018) 14.

Calibration-free Liquid Dispensing of Microliter Volumes

J. Goldowsky, J. Kaufmann, N. Schmid, V. Revol

Microliter and sub-microliter dispensing of liquids is used in a broad range of applications, such as bio-printing, bio-analytics (e.g., immunoassays) or production technologies (e.g., glue dispensing). In many cases the used liquids are expensive or the exact amount of liquid dispensed has to be known to be able to perform the appropriate sequences reliably. Monitoring the dispensing cycle from within a gas phase in communication with the dispensing reservoir yields in the benefit that such systems are calibration free and do not depend on the liquid dispensed. While such measurement techniques have already been proven for larger volumes (ml to ~100 µl), the current work focuses on small volumes (micro and sub-microliter), where measurement accuracies of 2 to 5% can be achieved.

Key facts

- Calibration-free pneumatic dispensing in the range of 0.1 to 100 µl with CV between 2 and 5%
- Dispensed volume is monitored and logged
- Measurement is independent of the liquid properties
- Driving pressure between 1 and 10 bar
- Technology scalable to lower or higher volumes

CSEM has developed process control solutions by observing the properties and behavior of a gas in fluid communication with the liquid to be dispensed^[1]. Such indirect measurement methods are beneficial since the measurement is independent from the liquids properties.

Based on the "pressure-based flow system approach"^[1] an improved measurement system has been developed. The system is based on monitoring the states of the gas within the cartridge during (1) inflow of the gas into the system to create an overpressure for dispensing and (2) dispensing. While during the inflow of gas into the cartridge (1) knowledge can be gained about its fill level, a pressure monitoring during the dispensing (2) is used to calculate the dispensed amount. For details on the physical principles refer to the previous work^[1].



Figure 1: Demonstrator of the calibration-free dispensing head.

The newly designed system (Figure 1) is able to measure pressure changes of fractions of a Pascal within the liquid gas phase during dispensing. Additionally the measurement method for calculating the overall gas volume within the cartridge has

been significantly improved by adding a flow sensor into the streamline between pressure reservoir and cartridge. This leads to more precise calculations of the fill level of the cartridge and thereby to more precise results during dispensing cycles. The system can be used with pressures up to 10 bar.

As the timing of the various valves and the synchronized read-out of the pressure sensors is critical for robust operation, the process control is done by an AM335x ARM Cortex-A8 processor including two independent programmable real-time units (PRUs). The PRUs enable low-latency switching of outputs (such as valve control lines) and the outsourcing of sensor data read operations. During time critical processes, the main processor takes care of less critical communication and calculation procedures while the PRUs control the timing and sensor reading.

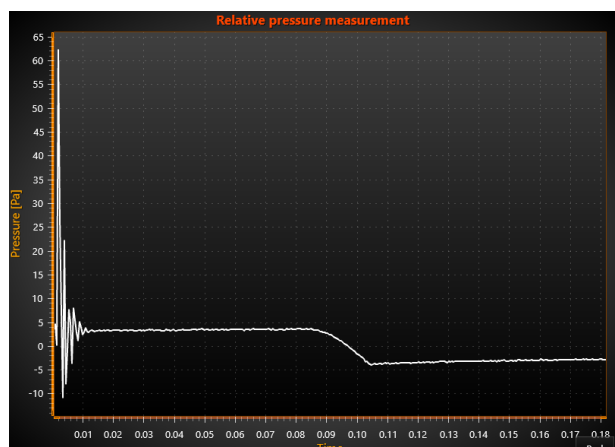


Figure 2 Typical relative pressure measurement output during a dispense cycle (here 133 nl) resulting in a pressure drop of 8 Pa.

Figure 2 shows a typical measurement output for a droplet of approx. 133 nl from a cartridge holding 3 ml of ethylene glycol. Ongoing work is the fundamental characterization of the systems performance in terms of accuracy, repeatability and limitations of dispensing and gas volumes.

Metering solutions, such as this one, are the basis of SmartLab applications with automatic logging of experiment data^[2]. CSEM thanks the Swiss federation and MCCS Micro Center Central Switzerland for supporting this work.

[1] S. F. Graf, et al., "Compact, Pressure-based Flow System for Sequential Actuation of Fluids with Integrated Flow Monitoring", CSEM Scientific & Technical Report (2014), 114.

[2] T. Volden, et al., "Portable Systems for Metered Dispensing of Aggressive Liquids", SLAS Technology 2018, Vol. 23(5), 470-475.

AutoMiA—Automated Bovine Milk Analysis by Impedance Spectroscopy

C. Beyer, J. Sun, M. Höchemer, R. Limacher

Early screening of somatic cell count (SCC) in incoming raw milk samples loads, i.e., before pooling, is necessary for avoiding waste of large amounts of milk. A simple, portable and automated milk analysis tool is needed that can efficiently determine SCC in the presence of fat particles. In collaboration with an industrial and academic partner, CSEM aims at the elaboration of high level signal processing and auto-clustering algorithms that will allow automated discrimination and quantification of different cell populations for use with impedance flow cytometers.

The quality of bovine raw milk depends, among other factors, on the concentration of somatic cells. A high somatic cell count (SCC > 100 cells / μl) indicates a potential infection of the cow udder (mastitis) and decreases the quality of dairy products like cheese. Presently, analyses of the somatic cell load in raw milk are performed manually (by classical microscopy) at laboratories of large dairy facilities or fully automated at centralized analytical service laboratories. A measurement system, based on impedance flow cytometry in a microfluidic channel, can potentially count and analyses SCC in a much simpler and less expensive way.

In the framework of an InnoSuisse project, CSEM develops in collaboration with a local SME and the University of applied Sciences Lucerne novel algorithm for determination of SCC in the range of 10 to 2000 cells per microliter. The final algorithm shall reliably discriminate somatic cells from the other particles without the assistance and support of application experts. The project partners strive to accomplish unprecedented precision with a relative standard error of mean (rSEM) of less than 8% compared to SCC measurement of SuisseLab AG Zollikofen.

Bovine raw milk is a complex matrix composed in its decreasing majority by weight of water (87.1%), fat droplets / globules (2.2%–5.5%), lactose (4.6%), proteins (3.3%) and somatic cells (<0.1%), which include mostly white blood cells (75%) and epithelial cells (25%). Raw milk contains roughly 25000 particles/ μl with a diameter larger than 0.5 μm , mostly fat globules of different sizes. During inflammation (mastitis) the somatic cell concentration increase from roughly 50 to 1000 or 2000 cells / μl while the concentration of fat globules decreases.

Somatic cells and fat globules are present in all different kind of shapes and their maximum size range from 5 to 12 μm and 0.5 to 10 μm , respectively^[1]. Both constituents consists of a plasma membrane and cytoplasm, but, instead of cell organelles the fat globules contain a triglyceride core in either solid or liquid form.

The approach of resistance-based single cell flow cytometry represents a well-established method for counting and sizing any kind of cells and particles. Extending it to a spectroscopic and impedimetric single particle analysis allow for label-free cell characterisation applications, for which advanced and powerful fluorescence activated cell sorting devices (FACS) provided the gold standard. The heart of this technology termed impedance flow cytometer consists of a microfluidic chip supplied with microelectrodes (Figure 1). Particles passing the electrodes

change the bulk impedance of the suspension between the electrodes. Applying a constant high frequency potential across the electrodes allows to continuously monitor this change by measuring the differential current between them. Enumeration and size, as well as information about the physiological conditions of the analysed cells are gathered from the processed impedance signals^[2].

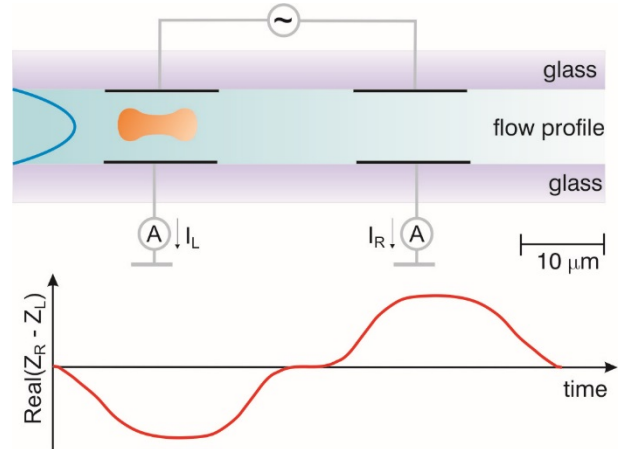


Figure 1: Measurement setup for impedance flow cytometry based on differential impedance spectroscopy - Figure from Beyer^[3].

The major challenge of the project is the automated differentiation of somatic cells from fat globules with a typical ratio of 1:500. Since both constituents are similar in terms of size and structure including encapsulation by plasma membrane, novel characteristics, i.e., features of impedance signal, for each particle have to be found to discriminate them. In order to accomplish high detection accuracy, multiple approaches are pursued. Among others, the potential of wavelet based event detection is investigated to improve the precision in cell counting. In addition, machine learning algorithms are utilised to extract a set of signal features, which will serve as a solid base for novel cluster algorithms.

The developed algorithm shall be easily integrated in FPGA platforms for real-time analysis and shall be robust against confounding factors, like signal drifts. Final tests at customer sites will be conducted to demonstrate the accuracy and robustness of algorithm.

This project is supported by InnoSuisse grant 25714.1 PFNM-NM.

^[1] Lopez, et. al. (2011), "Milk fat globules enveloped by their biological membrane", Current Opinion in Colloid & Interface Science 16:391.

^[2] Spencer, et. al. (2011), "Positional dependence of particles in microfluidic impedance cytometry", Lab on a Chip 11.7: 1234-1239.

^[3] Beyer (2013), "Investigation of Potential Interactions of Electromagnetic Fields with Proteins and Cells", ETH Diss No: 21405.

Aptamer-based Electrochemical Detection of Aflatoxins on a Smartphone

S. Jafari, D. Migliorelli, S. Generelli, S. J. Sturla •

Aflatoxins are natural contaminants present in food and feed products. These carcinogenic toxins are stable and heterogeneous compounds which, when present, cannot be eliminated completely. Therefore, they should be managed by strict food safety testing. The current testing processes have many limitations such as being time consuming, expensive and in need of specialized personnel, therefore unable to prevent fraud and to assure consumer safety completely. As an innovative solution, the present project proposes the development of a new generation of smartphone-based food analyzers, which provide simple, rapid, on site food safety testing for aflatoxins. This project is part of Marie Curie EU Horizon 2020 FoodSmartphone project (Grant Agreement N. 720325. foodsmartphone.eu).

Aflatoxins are natural contaminants produced by certain fungi (mainly *Aspergillus flavus* and *Aspergillus parasiticus*) which grow in warm and humid regions. They can contaminate a wide range of food and feed products on the farm, at harvest or during storage. These carcinogenic toxins are a heterogeneous and very stable group of compounds. Therefore, they should be managed by strict food safety testing. Because of their known carcinogenicity, many countries, including EU set strict limitations on the maximum level of aflatoxins in food and feed products.

The development of a new generation of smartphone-based food analyzers, which provide simple, rapid, on site food safety testing for aflatoxins and other contaminants, will be a powerful tool for ensuring food traceability and safety. This device should provide sensitive, selective and cost-effective detection of food contaminants. It should be user friendly, so to be used by non-experts such as farmers, truck drivers and consumers.

The smartphone-based bioanalytical device is an ideal choice for the proposed food analyzer. Smartphones are widely accessible and they have built-in parts such as a processor, camera, flashlight, battery that can be repurposed for electronic integration of the food analyzer. The wireless real-time data transfer and the time and GPS coordinates would help inspectors map the spread of food contaminants. Most importantly, they can be used by non-experts consumers.

In this study, we developed an aptamer-based biosensor for electrochemical detection of aflatoxin B1 in cereals. To do this, an aptamer probe has been used as a novel biorecognition element which binds to the target analyte with high selectivity and specificity. The aptamer probe is immobilized on the electrode surface and labelled with a redox indicator (methylene blue) to generate a redox signal, which is measured by the electrochemical technique square wave voltammetry. The specific binding of the aptamer to the target analyte involves a conformational change in the aptamer structure, which moves the methylene blue in closer proximity to the electrode and facilitates the electron transfer, resulting in the signal enhancement (Figure 1).



Figure 1: The aptamer-based biosensor working principle, the conformational change of the aptamer after binding with aflatoxin brings the methylene blue near the surface of the electrode, increasing the current signal.

The sensor was used for detection of aflatoxin B1 from 5 to 20 ng/mL in buffer and the increase in the signal (Figure 2) was correlated with an increase of aflatoxin B1 concentration. In order to apply this system for the screening of aflatoxins (types B1 and M1) in real samples, automated microfluidic sample preparation strategies will be investigated and the miniaturization of the final prototype will be taken into consideration. The integration of the aptasensor into a smartphone will be accomplished either by USB connector or Bluetooth and a user friendly software will be designed in order to convert the quantitative numerical result in a semi-quantitative output (green = good sample, yellow = warning, need for further tests, red = contamination detected) indication of the sample contamination level.

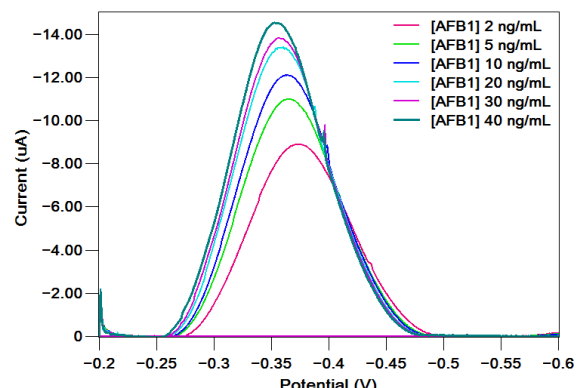


Figure 2: The square wave voltammetric curves of the aptamer-methylene blue probe in binding buffer in absence and presence of aflatoxin B1 at different concentrations.

• Laboratory of Toxicology, Department of Health Science and Technology, ETH Zurich, Switzerland

Low-cost Printed Electrochemical Urinalysis Sensors for Health, Fitness, and Nutrition

D. Schmid, K. Petropoulos, S. Generelli, D. Migliorelli

CSEM has developed low-cost disposable sensors for urinalysis. We demonstrated successful measurements of glucose, pH, sodium, and magnesium levels in urine using custom printed electrochemical sensors, covering the concentration ranges of interest. The sensors give a quantitative indication on the markers and sense ions – information that commercial colorimetric sticks do not offer. Future applications of such sensors include personal monitoring for health, fitness or nutrition.

Personal monitoring of physical and physiological parameters (acceleration, position, heart rate, blood oxygenation) has become commonplace these days. People are monitoring their performance in sports, their sleep, stress, and activity in general. These parameters carry a lot of information on our health and wellbeing, however they do not have direct indication on biochemical processes and analyte concentrations that govern correct functioning of our body. These insights traditionally had to be gathered by invasive monitoring, mainly in blood.

However, this information might be partly collected noninvasively from other body fluids. CSEM has shown in the past monitoring in sweat [1] and saliva [2]. Sweat analyte monitoring is not yet clinically proven and sampling is not always possible (the person has to sweat). Saliva probing might be unpleasant, monitoring is less well documented and analyte concentrations are significantly lower. Urine on the other side also allows for noninvasive daily monitoring and is well accepted and analyte concentrations relevance is clinically proven. Standard urinalysis with colorimetric test strips for example can semi-quantitatively detect a wide range of disorders. Some of the drawbacks of these kits are related to limited sensitivity and failure to monitor crucial parameters (such as dissolved ions) and frequently false positive results [3].

Based on its electrochemical sensor platform [4], CSEM has developed low-cost disposable sensors that can be applied directly in urine. Current sensor functionalizations allow direct multiplex monitoring of pH, Na⁺, Mg²⁺ and glucose in a single analysis (Figure 1).

pH	Na ⁺	Mg ²⁺	Glucose
Full 4.5-8	Normal <10 mM	Low 1-3 mM	Normal <1.4 mM
Normal 5.5-6.5	High >30 mM	High 3-8 mM	Diabetes >3 mM

Figure 1: Parameter range of interest in urine, which can be fully covered by CSEM's electrochemical sensors.

All the above mentioned markers are very important physiological parameters. pH is an acknowledged factor for nutrition and indicator for kidney diseases, Na⁺ reflects daily salt uptake and report risk for hypertension, Mg²⁺ can indicate gastrointestinal losses and glucose can announce kidney diseases as well as diabetes. Additionally, specific sensors for further ions and clinically relevant biomarkers could be developed if needed.

[1] M. Viviani, T. Parkel, R. Junuzovic, D. Migliorelli, F. Pereira, S. Generelli, "Wearable sensors for ion monitoring", CSEM Scientific and Technical Report (2016), 45.

[2] S. Generelli, D. Migliorelli, H. Chai-Gao, S. Paoletti, T. Broger, "Rapid and cost-effective detection of tuberculosis (TB)", CSEM Scientific and Technical Report (2016), 46.

It could be shown with real urine samples that for the tested parameters pH, Na⁺, Mg²⁺ and glucose, the full range of interest can be covered. Figure 2 highlights CSEM's pH sensor robustness when brought into direct contact with untreated urine samples.

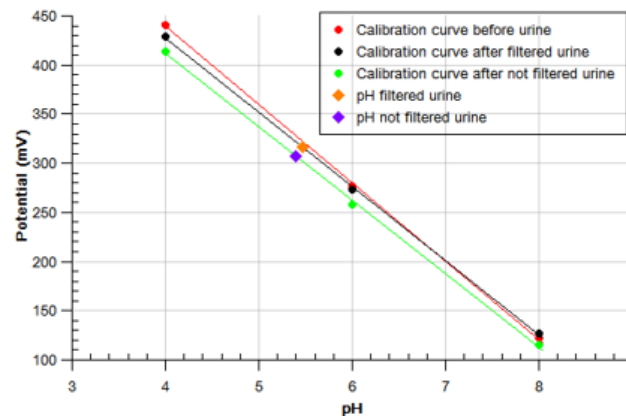


Figure 2: pH calibration curves and measurements in filtered and unfiltered urine.

Key opportunities for urinalysis sensors are wellbeing, fitness, nutrition, in particular salt uptake or disease monitoring. Target population groups include hobby and professional athletes, the elderly or the chronically ill. The simple and unobtrusive urine monitoring prototype available at his day can be integrated in toilets or used in standalone portable solutions. The integration of these novel measurements with the state-of-the-art fitness trackers or other wearable health devices will bring an added value in the management of well-being in everyday life (Figure 3).

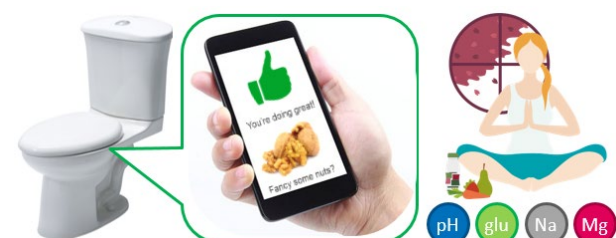


Figure 3: Electrochemical urine sensors could be used for personal nutrition monitoring and help improve health and wellbeing.

[3] T. H. Han, "Urinalysis: The usefulness and limitations of urine dipstick testing", Child Kidney Dis. 17 (2013) 42.

[4] <https://www.csem.ch/Biosurface>

FluoSense—Highly Sensitive Fluorescence Detection with Silicon Photomultipliers

L. Hofer, C. Hofer, G. Orawez, P. Cristofolini, S. Cattaneo

A prototype sensor based on silicon photomultipliers was developed and tested for high-sensitivity fluorescence intensity and lifetime measurements. The sensor allows compact, light and mechanically robust detection modules, which are suitable for point-of-care fluorescence applications.

Silicon photomultipliers (SiPM) are solid-state single-photon devices built from an avalanche photodiode (APD) matrix on a common silicon substrate. This novel device combines the advantages of conventional silicon APDs, namely small size, low-voltage operation, and robustness, with those of PMTs, namely high gain, sensitivity and stability. The small dimensions of SiPM permit compact, light and mechanically robust detector modules, which are very attractive for portable applications.

The goal of the FluoSense project was to build and characterize a compact prototype sensor for low level luminescence detection using SiPM, and to test various detection modes. The main objective was the detection of ultra-low luminescence intensities down to the photon counting level. A second objective was to investigate the suitability of SiPMs for single-point time-resolved luminescence measurements (e.g., fluorescence lifetime measurements) at low intensities.

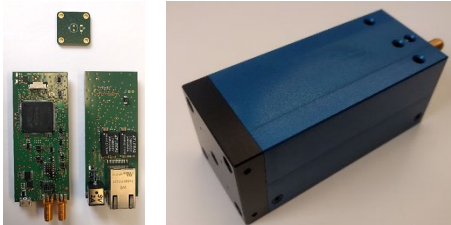


Figure 1: PCBs modules (left); Assembled SiPM detector prototype with housing (right).

Figure 1 shows the realized SiPM prototype sensor. The sensor incorporates three PCB boards: a sensor board carrying the SiPM, a main board with a digital part for acquisition and algorithmic (uC and FPGA) and an analogue part for signal conditioning, and a power supply and interface board including USB communication to an external PC.

The sensor supports three detection modes:

- Analog integration (integrator + uC): The full pulse charge at SiPM output is measured by integrating over the pulse area → Analog fluorescence intensity measurement
- Pulse counter (FPGA): Counts the number and the height of SiPM pulses → Digital fluorescence intensity measurement
- Time-to-digital converter (FPGA): Time-correlated pulse and pulse height counting → Fluorescence lifetime measurement

To characterize the sensor, fluorescence intensity and fluorescence lifetime measurements were performed using fluorescein sodium salt dissolved in water. For the intensity measurements, a CW diode laser at 450 nm (Osram PL450B) was used. Serial dilution showed a linear response over approximately four orders of magnitude from tens of micromolar down to nanomolar fluorophore concentrations. The lower detection limit is given by the dark count rate of the SiPM, while the upper limit is due to the saturation of SiPM pixels. One should point out that the fluorescence intensity measurements were carried out in a rather rudimentary optical setup. An optimized

setup with an increased collection efficiency would allow reducing the limit of detection even further.

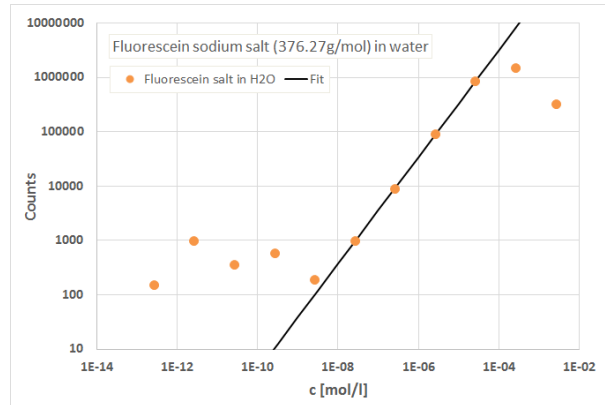


Figure 2: Fluorescence intensity measurements with diluted solutions of fluorescein sodium salts, showing an LOD in the nanomolar range.

Fluorescence lifetime measurements were carried out with a pulsed laser diode (Horiba PicoBrite PB-450L, 451 nm, 30 nm FWHM, 0.8-1.4 ns FWHM) on fluorescein sodium salt solutions at various concentrations. Accurate lifetime values could be extracted for concentrations down to the nanomolar range, yielding values in agreement with those expected from the literature.

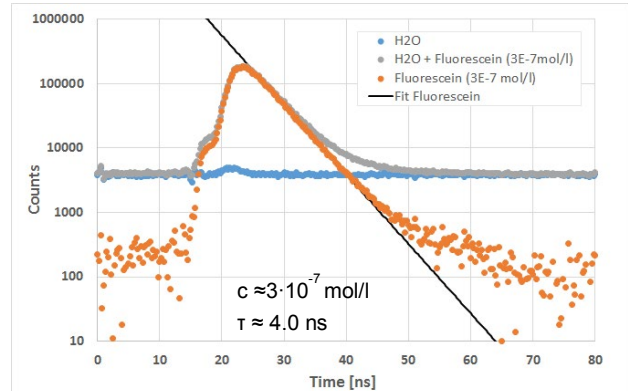


Figure 3: Fluorescence lifetime measurements with diluted solutions of fluorescein sodium salts.

As a next step, the SiPM detector prototype will be further optimized and tested with commercial fluorescence and chemiluminescence diagnostics kits, in order to test the different detection modes and fine-tune the measurement parameters. The final goal is a complete reader incorporating all necessary components in a compact and cost effective package, optimized for point-of-care or environmental applications.

Stem Cell Organoid Culture Platform for Pharmaceutical and Industrial Applications

S. Heub, R. Ischer, M. Jungo, M. Despont, G. Weder

In collaboration with SUN bioscience, CSEM developed an automated production line to manufacture the Gri3D™ platform for standardizing organoids at large scale. Organoids can be grown from the stem cells of each patient and open the door to personalized medicine.

Model systems drive modern biological and biomedical research. In vitro 3D tissue cultures are emerging as the tool of choice for personalized drug testing and regenerative medicine. When grown in the right 3D environment, stem cells self-organize into organoids that mimic real organs both in cell composition, genetic makeup and architecture.

Until now, however, the field has been struggling with the reproducibility of organoid cultures at large scale.

CSEM was approached by SUN bioscience to industrialize the production of their organoid screening platform, Gri3D™, which allows to generate thousands of uniform organoids at once^[1].

Gri3D™ combines 3D cell aggregation with the versatility of synthetic biocompatible hydrogels for long-term culture on a single platform. The fabrication process includes the replication of microstructures from a polymer-based master in hydrogels that are crosslinked from a mixture of reactive precursors. The microstructured stamps exhibit ultra-dense microwell patterns with diameters ranging from 0.1 to 3 millimeter (Figure 1).



Figure 1: Microstructured stamps for casting hydrogel microwell arrays.

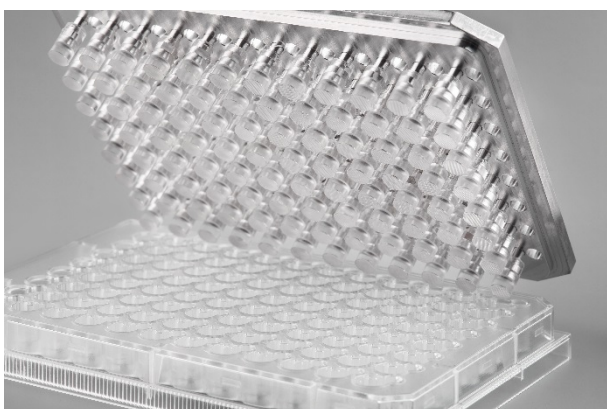


Figure 2: Assembled casting head for hydrogel microstructuring in a 96-multiwell Gri3D™ platform.

The stamps are assembled onto casting heads for either 24- or 96-multiwell Gri3D™ platforms (Figure 2). Several different microwell arrays can be mounted on the same casting head for customizable patterns within one Gri3D™ plate. Prior to automated replication, a liquid handling robot is used to mix and dispense the hydrogels. A major challenge is the absence of air bubbles that is verified by a specific algorithm for quality control. The development of this automated Gri3D™ manufacturing line, allows high production volumes at high plate-to-plate reproducibility, a prerequisite to enter the life science market. Gri3D™ can now become a standard for organoid applications with numerous advantages:

- Complete 3D culture in a single focal plane
- Thousands of uniform organoids at once
- Suitable for long-term culture of sensitive cells
- Only one platform for the entire organoid protocol

Retinal, liver, cerebral, pancreatic and many other organoids types have already been successfully grown on Gri3D™. For example, intestinal organoids are used to model cholera infections. The rapid fluid loss from the intestine due to the cholera toxin, leading to severe dehydration, can be modeled on intestinal organoid cultures. They show a rapid swelling due to hypersecretion of electrolytes and water to the central lumen.

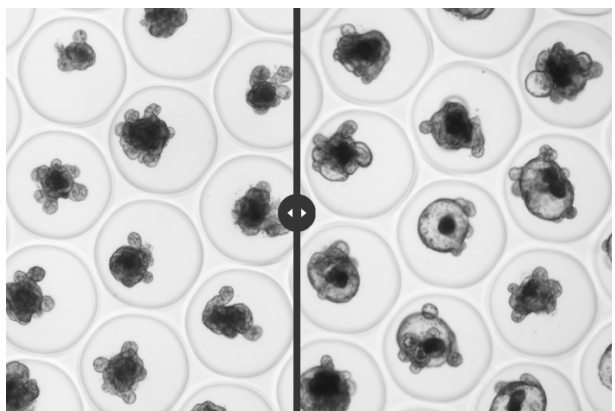


Figure 3: Intestinal organoids on Gri3D™ modeling cholera infectious disease before (left) and after (right) exposure to cholera toxin.

The technology in combination with patient-derived organoid assays offers many applications and results in more accurate predictions of drug responses. For pharmaceutical companies, personalized testing can be performed to preselect patient populations where accurate biomarkers are lacking, for individual patients, their medications can be pre-selected based on efficacy measured on their own organoids.

[1] This work was supported, in part, by the Commission for Technology and Innovation (CTI).

Roll-to-roll Printed Wireless Sensors Platform on Low-cost and Flexible Substrates

J. Disser, N. Glaser, C. Hennemann, F. Geister, A. Mustaccio, J. Ackle

The requests for smart labels for life style, food monitoring or fast first on-site checks rise. To cover future market demands of such products, additional developments are needed to produce the smart labels cost effectively and in high volumes to be used as disposables. We demonstrated that truly low cost sensors can be produced on one foil, including the signal transmission circuit. Combining CSEM's printed sensors and RFID technology with the roll-to-roll equipment of Swiss partners, we fabricated a sensor demonstrator showcasing the opportunities of printed electronics.

One of the major drawbacks for smart labels is the expensive production of flexible circuits and non-established production processes to integrate printed sensors. Printed electronics not only provides low-cost sensors, the technology can also be used to print the circuit-board on flexible foils. We already demonstrated that roll-to-roll screen printing can be used as a low-cost and high-volume production technology for the fabrication of flexible circuits. In addition, the same printing technology can also be used to print sensor electrodes (e.g., for pH and enzymatic sensors, or sensors for humidity, or force sensing). The combination with SMD components leads to a wireless sensing platform and a working device fully equipped with all the electronics to control the sensor and to communicate with a smartphone. This hybrid integration of the printed circuit with the SMD assembly on low temperature substrates (e.g. low cost PET) is what is missing in the industry.

The key components of our sensing platform include a printed antenna, printed force and pH sensors and the SMD components integrated on the flexible substrate.

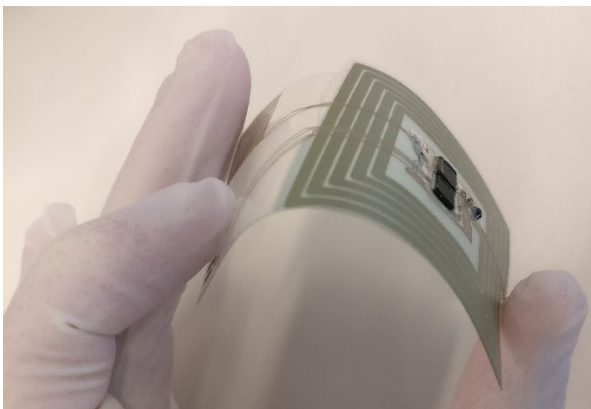


Figure 1: Stand-alone printed wireless platform on flexible substrate.

We have developed design rules to realize a printed circuit that matches the antenna performance as simulated with standard tools for PCB design. Highly conductive inks were screen printed to yield an antenna with an inductance between $1.4 \mu\text{H} - 1.8 \mu\text{H}$ and a low resistance (less than 10 Ohm) in order to establish a proper RFID connection. A solder-free process was used to mount the SMD's on the circuit. The lab generation of the system is shown in the Figure 1.

The second stage of development involved the transition from our sheet based lab printing process to a high throughput industrial roll-to-roll printing machine. Together with Gallus Ferdinand Rüesch AG we developed the design rules to reach even superior print results on the industrial machine than in the lab (Figure 2). The printing speed can go up to 10m/min, allowing the fabrication of an average of 14'000 platforms per day.

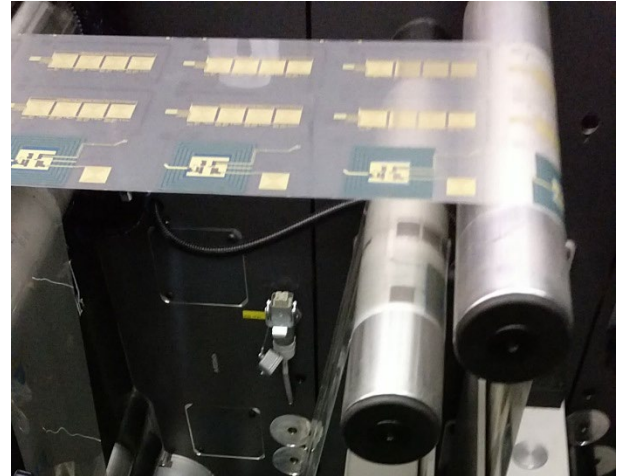


Figure 2: Gallus Ferdinand Rüesch AG production line in St-Gallen while roll-to-roll printing.

An Android application has been developed during this project to read the signals from the platform through the RFID connection. The tablet displays the force applied on the sensors and the pH (Figure 3). The powering and the readout of the sensor signals are provided by the tablet through the antenna.

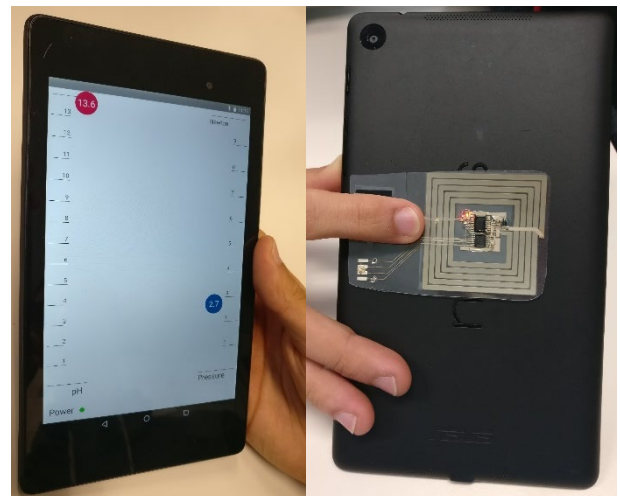


Figure 3: Tablet displaying pH and force measurement (left), platform interfaced with the tablet (right).

In total, four layers have been roll-to-roll printed on a thin and flexible substrate, the SMD components assembled and the platform interfaced with a tablet. Several technological steps and design rules have been successfully transferred to industrial manufacturing.

EchoPad—Flexible Pad-based Ultrasound System for Continuous Heart Monitoring

N. Marjanović, F. Zanella, J. Disser, O. Fernandez, A. Mustaccio, M. Chrappa, M. Schnieper, A. Mozorov •, P. Hunziker ••

In the EchoPad project, a consortium comprising of CSEM, a research-oriented healthcare provider (University Hospital Basel, UHB) and a spinoff-company of the University of Basel specialized in embedded high-performance medical monitoring (HighDim GmbH, Riehen BS) joined forces to tackle an unsolved problem in clinical medicine, namely continuous monitoring based on ultrasound imaging technology. The project delivered proof of concept of a flexible ultrasound transducer, suited signal processing pipelines and image processing algorithms.

Flexible transducer arrays are desirable because they can be wrapped around objects or curved body surfaces hence increasing the angular coverage relative to rigid transducers, such as those used in handheld medical probes. The larger aperture and conformal nature of flexible transducers may improve the detection of objects that are outside of the direct sight lines of rigid transducers by collecting additional acoustic information. The flexibility of the transducers is particularly important in the future era of personalized healthcare, where availability of shape-conformable and wearable devices for monitoring and diagnostics is essential.

The main motivation for the EchoPad project is to develop and provide an ultrasound imaging system for single-patient continuous monitoring of the cardiovascular function (e.g., during surgery or in intensive care units) featuring a user-friendly low-cost/disposable polymer based ultrasound transducer fixed to the patient chest.

The key components include: *i*) a flexible ultrasound transducer based on polymer piezoelectric material, *ii*) the required electronic front end and signal processing chain, and *iii*) reconstruction algorithms suited to the flexible transducer.

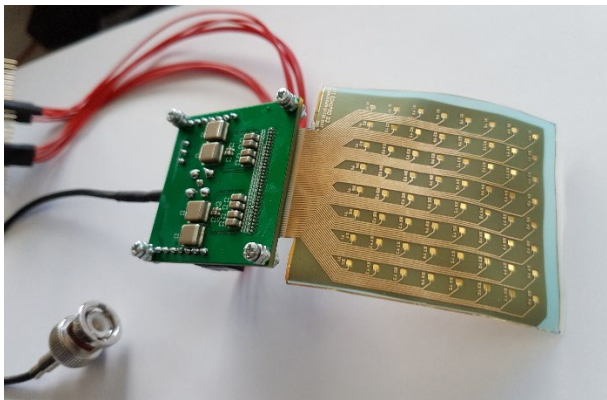


Figure 1: Flexible 8x8 transducer array (EchoPad) fabricated by CSEM connected to the interface PCBs provided by HighDim GmbH.

For this purpose different formulations/grades of PVDF-TrFe piezopolymers have been tested. The fabricated flexible 8x8 transducer array – EchoPad shown in Figure 1 – has been electro-acoustically characterized in water, using a dedicated setup developed by CSEM in collaboration with HighDim. HighDim designed the PCBs and software interfacing the computer and ultrasound wave generator (Lecoeur Electronique US-Wave) to the EchoPad allowing switching individual channels of the 8x8 array (Figure 2). The EchoPad is powered by two Keithley source-measurement units at ± 70 V. A microphone amplifier is used to enhance the recorded signal.

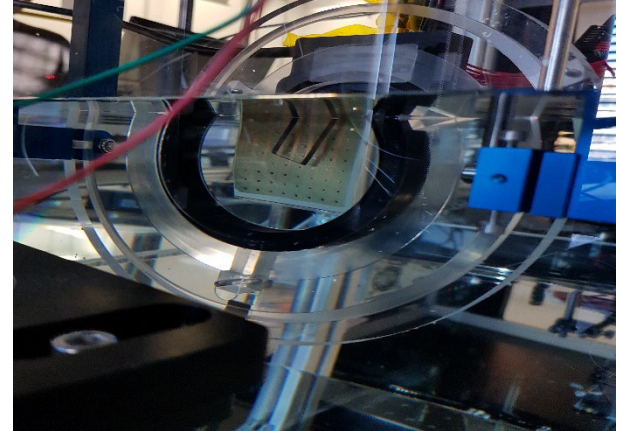


Figure 2: EchoPad in front of the microphone at CSEM's electro-acoustic setup.

The EchoPad is operating in the frequency range from 5 to 10 MHz. Various series of signals have been used to test the device and record the echoed signal by means of an oscilloscope (Figure 3).

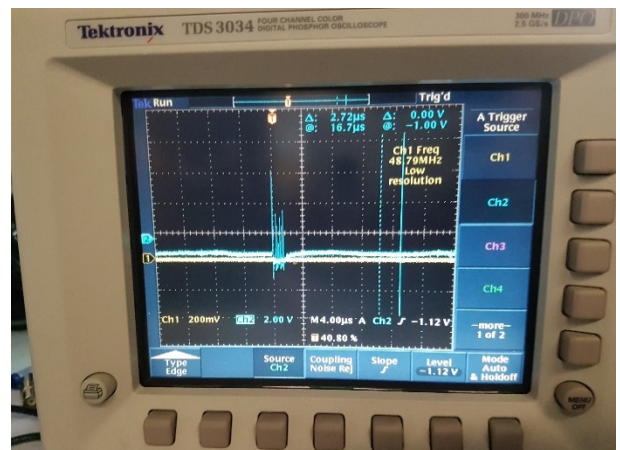


Figure 3: EchoPad emitted signal at 5 MHz captured by oscilloscope.

A 64 (8x8) active channels transducer array emitting ultrasound signals in the range of 5 – 10 MHz on a flexible substrate has been successfully demonstrated, requiring a powering at ± 70 V.

Mathematics of coherent image formation were studied by UHB. Several software simulation variants modelling the image formation process in coherent imaging were developed, adapted to the topological features of several image acquisition setups.

The authors would like to thank Innosuisse (CTI) for their financial support (Project No. 25374.1 PFNM-NM).

• HighDim GmbH, Riehen, Switzerland

•• University Hospital Basel, Switzerland

PHOTOVOLTAICS & ENERGY MANAGEMENT

Christophe Ballif

2018 has been marked by contrasting news related to the energy field, to CO₂ emission, and to solar. Let's start with the difficult ones:

- The latest IPCC report was released and contained clear statements and a global warning about the need to act quickly on global warming and CO₂ emissions. Even though it is still technically possible to mitigate temperature rise to 1.5–2°C, it is becoming apparent that a huge overshoot on CO₂ concentration will take place and that massive adaptation, at high costs, will be required.
- There is further accumulated evidence of the already strong impacts of global warming on agriculture and migration, leading—for example—to wars and to punctual natural disasters.
- There is still only weak or “alibi” action from many, if not most, governments on these topics, reflecting the votes and preoccupations of citizens who are focusing mostly on immigration issues and/or direct and short-term economic considerations.
- The extended but mostly discrete influence of cash-rich fossile fuel lobbies (including distribution companies), which have a strong influence on policies and high-profile politicians. This is accompanied by an attempt to discredit climate science, leading to phenomena such as people suffering repeated hurricanes, but not thinking once critically about the possible cause for the increased average storm energy.
- The fact that the renewable energy industry did not have enough time and profit margins to become as powerful in lobbying politics, even though it increased volumes and performance remarkably.

Amid this news, there are still some reasons for hope:

- As illustrated in Figure 1, for the first time, in 2016, more peak capacity of renewable electricity was installed compared to fossile fuel power plant capacity.
- The expression of some strong positive intentions or bills (e.g., generating 100 percent clean electricity in California), or a switch to full electrical or CO₂-free mobility announced in various European countries.
- The fact that PV continues on its road of price decline. As illustrated in Figure 1b, even in Germany the auction prices for solar electricity are below those of any other conventional energy (down to 3.8 €cts/kWh for the lowest-cost bids, with an average at 4.6 €cts/kWh in June 2018). Large PV power plants are now definitely cheaper than any other electricity source, including new fossil fuel and nuclear power plants.
- And, in more and more places, there is a continuous mobilization of people and communities to address the questions, to propose solutions, and even sometimes to take goverments to court.

To tackle global warming seriously, by 2050 PV should be a (if not the) major contributor to electricity and energy production. What will that take? Assuming world electricity consumption of 40,000 TWh by 2050 (vs ~22,000 TWh in 2017, and assuming

there will be both an increase in people and a shift to electricity), a total of 25 to 30 TW of PV panels would need to be installed—that is, around 1 TW per year. This has to be compared to 97 GW of PV panels produced in 2017, indicating that a massive worldwide upscaling of solar energy needs to take place, by a factor of 10 in the next decade.

If a massive increase in renewables does not take place, jointly with a reduction of all CO₂, sources and an efficient use of energy, a full reshaping of the environment, agriculture, and cities, with hundreds of millions of displaced people threatened by heat and food or water shortages is likely.

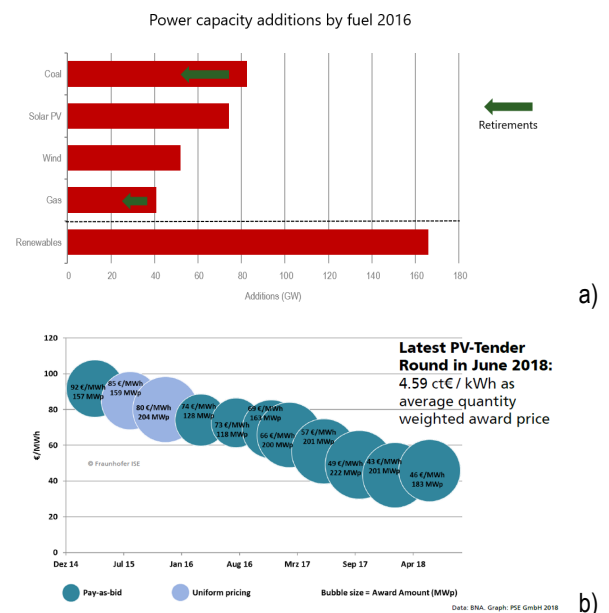


Figure 1: (a) Annual PV installation by region until 2016 (Source, IEA); (b) PV electricity price for tender in Germany from 2014 to 2018 (Data: BNA; graph: PSE GmbH).

Noticeably, a combination of photovoltaics (complemented of course by other renewables including hydro, wind, biomass, and geothermal energy, as well as some remnants of the ancient electricity system) and electric mobility, power-to-gas, ground heat storage, pumped hydro, and ice storage for getting air conditioning system to run at night can be seen as a clear possible way to move cost-effectively to a new energy system. In this context, we can possibly consider an intermediate scenario (between full action as required and doing nothing), still meaning a double-digit growth of the PV market and a full transformation of the energy system.

With respect to solar energy, a further driving force will be given by a reduction of the levelized cost of electricity, which can be achieved most easily by a module efficiency increase, by module cost reduction, and by increasing modules' and components' lifetimes. By reducing the balance of system costs per watt, module efficiency remains a key leverage. Average c-Si module efficiency (around 17.4 percent in 2017) has gained around 0.35 percent per year in the last ten years. Hence, to find a place in the market in 2025 at the multi-GW level, a technology must typically be able to deliver more than 21 percent efficient modules at 20–22 cts/W. Essentially, the further decrease in solar

electricity costs will give even more financial means to manage solar electricity, favoring its penetration. This is even more true for Switzerland, where space constraints should also favor high-efficiency technologies for a large proportion of installations.

Improvement in PV technology continues to open other amazing opportunities and niche markets. These include the field of “active” building—where PV plays an architectural role (Figure 5)—solar mobility with boats, cars, or planes, and energy scavenging for the Internet of Things (IoT). All these topics also contribute to sensitizing people to the possibilities offered by photovoltaics.

With its dense network of established companies, its start-ups, its network of universities and higher education institutions that receive topical public funding, and its popular vote supporting a new energy strategy, Switzerland has excellent cards at hand, as it can develop, test, and implement some of the solutions worked out in the energy field and in energy systems at a pre-market entry level. It is especially well positioned, with several high-tech companies and many companies active in the field of building integrated photovoltaics (BIPV), as well as with a solid grid structure that allows for the testing of many advanced systems and control solutions.

This can happen even though in the field of photovoltaic cells a large part of production has shifted to Asia. The remaining European production companies need to refocus on niche products, or on advanced PV technologies. “Made in China 2025” and some of the unfair trade practices of China have also put many leading European equipment builders in a difficult position. At this stage though, Swiss exported equipment/solutions and know-how continue to play an important role. In addition, European companies continue to invest (e.g., Enel/3Sun and Ecosolifier, all investing in heterojunction technology), as does the Russian company Hevel (producing at >160 MW heterojunctions level based on Swiss technology developments) but at a lower volume level. Noteworthy worldwide interest in silicon heterojunction is now on the map with recent announcement of 600 MW fabs based on technologies developed or supported by CSEM and EPFL. There is also an interest in technologies for other types of passivating contacts (made at higher temperature compared to heterojunction) that can allow an extension of the learning curve of standard (up from PERC solar cells, which are now starting to dominate the market).

Long-term objectives

In this context, the **Photovoltaics & Energy Management** (PV&E) program continues to develop innovative process technologies, device concepts, and new high-tech solutions to better serve the Swiss and global renewable energy industry. More generally, the **PV&E** program targets the following objectives:

- To provide cutting-edge innovation in the field of photovoltaic devices, realizing the best devices with a high potential for industrialization, from advanced crystalline silicon to multi-junction solar cells.
- To design and develop highly reliable modules, for the power market, for the transportation sector, or with the highest potential for adoption by the public in the built environment.
- To support the development of next-generation equipment and metrology systems, all along the value chain of photovoltaics, creating a sustainable cleantech value for existing and future CSEM customers.
- To provide new solutions for specialized devices, coatings, or materials with higher added value, and for PV components with enhanced functionalities.
- To bring solutions to the energy/electricity management field as we transition toward a society essentially powered by renewables, in which energy efficiency and management will be realized through intelligent hardware, algorithms, and data analytics.

These solutions are brought to the market either by supporting companies or through the creation of start-ups. To meet these challenging objectives and to support the transition to an energy system in which solar will play an essential role, CSEM and its **PV&E** team collaborate particularly closely with the EPFL PV-Lab in Neuchâtel, with Swiss universities and ETH entities (EMPA, EPFL), as well as with universities of applied sciences—in particular SUPSI (accreditation, power plants) and BFH (the BFH-CSEM energy storage center). CSEM also collaborates with multiple international organizations or agencies, for example in the framework of European or bilateral projects.

In 2018, CSEM was able to further develop its activities related to the program PV & Energy Management. Following the 2017 merging of teams working on energy management within CSEM, the **PV&E** program has now three solid activities. At the end 2018, around 60 persons (FTE) are involved in the program. This includes an increase in solar cell and energy systems activities and a phasing out of activities related to organic PV.

The program is summarized in Figure 2 with its subdivisions by activity. The bottom part of this figure illustrates the technology infrastructure platforms available. This corresponds to hardware facilities platforms, which are complemented by additional software/hardware in laboratories (e.g., simulation platforms for electrical grids, for plasma modelling, micro-grid hardware...).

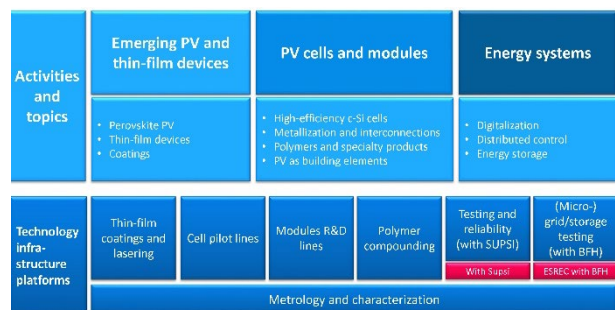


Figure 2: Schematics of the activities in the **Photovoltaics and Energy management** program. Top part: activities. Bottom part: technology infrastructure platforms.

Emerging and thin-film PV activity

In this activity, CSEM provides the industry with a high level of expertise regarding customized PV cells for product integration. It also makes available its know-how in coatings for optoelectronics applications to address various industrial challenges (e.g., layers for various sensors, DLC layers for power electronic applications, decorative coatings). The multidisciplinary team applies laser patterning, thin-film deposition, and printing and etching methods to design and produce cells that meet the most challenging demands, thanks

to top-level facilities and latest-generation equipment. Our applications are demonstrated, for instance, in the field of energy harvesting, for different products and processes ranging from watches to smart farming. The activity runs in synergy with other CSEM programs, for example combining energy-harvesting solutions with ultra-low-power designs to make IoT devices and various wearables fully autonomous.

At the same time, CSEM is preparing the future of PV, with new materials and cell architectures from the forefront of academic research (e.g., passivating contacts for crystalline solar cells). In particular, CSEM is exploring more efficient and potentially lower cost solar cells in collaboration with world-leading institutes and universities. This includes in particular multiple junction devices based on perovskite semiconductor absorber.

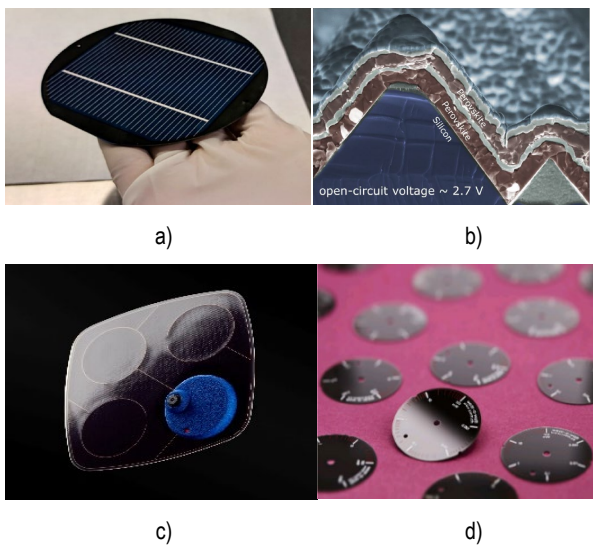


Figure 3: a) First large-area perovskite–silicon tandem cell with screen-printed contacts. b) First demonstration of triple junction PK/PK/Si with quasi-conformal coating on the solar cell pyramids. c) Flexible, customized thin-film silicon solar cells, allowing the powering of a low-energy-consumption camera. d) Example of series of small solar dials with a thin-film silicon absorber.

These two parts of the activity tackle challenges according to the following topics —

Thin-film devices:

- Technology and pilot-series production of customized thin-film silicon solar cells acting as energy scavengers
- Development of flexible solar cells (based on thin-film silicon technologies)
- Integration of PV cells into final products (thin-film, III–V)
- Development of complete energy harvesting systems
- Benchmarking of cell technologies for various applications

Emerging PV:

- Materials and interface development with vacuum and non-vacuum techniques for perovskite and related temporal stability properties
- High-efficiency perovskite solar cells, with a focus on perovskite as a component for multi-junction cells

Coatings and patterning:

- Layers and processes for passivating contacts (Si-based; combined with oxides, nitrides, or transparent conductive oxides)

- State-of-the-art transparent conductive coatings and electrodes for smart sensing and detectors
- Light management and microstructured substrates, films, and foils
- Materials and processes for optoelectronics (LED, OLED, TFT, sensors, smart windows, PV)
- Multifunctional coatings and layers for decorative, lubricating, and/or electronic applications
- Lasering and printing processes

Some of the highlights for the past year are shown in Fig.3. They include the realization of solar cells as SMD-ready components, the collection of real-life energy scavenging data with 43 solar watches (with cells on wristbands and dials), the design of processes allowing, for the first time, >25% certified tandem perovskite–Si devices, large area screen-printed tandem PK cells with 22.6%, the first demonstration of a triple-junction based on a perovskite/perovskite/silicon configuration and the introduction of more reliable perovskite devices that can now be screen printed.

PV Cells and Modules activity

In this activity, CSEM develops and matures materials, processes, and technologies for the cost-effective manufacturing of reliable and high-efficiency PV cells and modules, as well as for an optimum integration of PV products into dedicated applications (building integration, mobility, and energy harvesting).

In solar cell technology, the global goal is to allow an extension of the learning curve of crystalline silicon (95 percent of the PV market). This can be done by considering improved crystalline silicon solar cells (mostly with higher voltage thanks to contacts that also passivate the surface). Two further extension options involve either changing the device architecture and going to so-called back-contact solar cells (IBC cells) or implementing another junction on top of silicon (tandem perovskite–Silicium), as illustrated in Figure 4. Thanks to its unique, flexible, high-end R&D platforms, CSEM masters high-performance silicon solar cell manufacturing over the full processing chain from wafer texturing to reliability testing, delivering high cell efficiency and maximum module outdoor performance at controlled costs, with a focus on large area passivation technologies. CSEM demonstrates key expertise and a high efficiency track record in the fabrication of crystalline silicon heterojunction solar cells, back-contacted heterojunction solar cells, high-temperature passivating contacts, and technology blocks for advanced PERX concepts, as well as next generation multi-junction devices: perovskite/silicon.

CSEM also masters the materials, processes, and technologies necessary for metallization, cell interconnection, and module integration to achieve maximum module performance, reduced PV electricity costs, and long module lifetimes. CSEM has complete expertise in fine-line printing by screen, stencil, and inkjet printing, as well as full process flow for the copper plating of heterojunction solar cells. CSEM further develops advanced interconnection technologies, such as multi-wire and shingling technologies. CSEM possesses a (unique for such an institute) flexible R&D polymer platform, and masters customized polymer compounding, extrusion, and process, for long-term reliability, as well as for specialty polymer design and manufacturing.

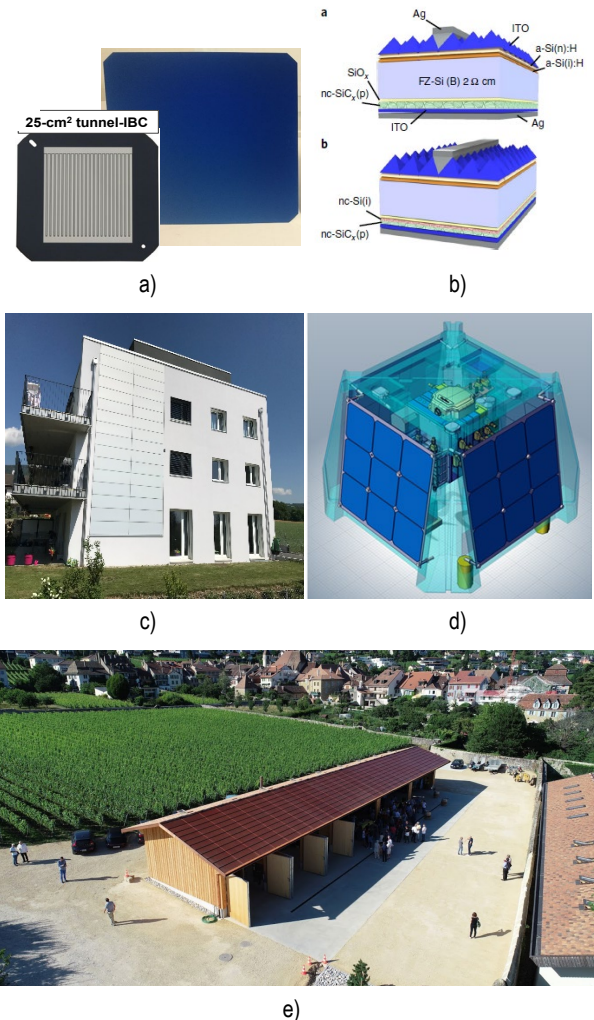


Figure 4: a) 25 cm², 24.8% IBC solar cells. b) Toward an extension of PERC with fired rear-side contacts (A. Ingenito, *Nature*, 2018). c) First white PV façade in Boudry, Switzerland. d) Design of stratospheric modules including novel CSEM packaging formulations. e) Terra-cotta solar architecture on the “Caves du Château d’Auvernier” (project NECAN, supported by the State of Neuchâtel with CSEM and Issol).

In addition, the speed and scale at which PV products are being deployed are accompanied by a broadening of the integration of PV devices and elements. In the targeted applications, PV products must meet performance and reliability requirements; but they must also deliver the required aesthetics, color, shape, weight, and system specificities. CSEM masters PV product integration, with significant expertise in innovative solutions for BIPV applications, with various solutions for modifying the color and esthetical aspects of modules. In addition, customized PV solutions are developed for specific applications for mobility, from the stratosphere to land and sea.

For all these activities, CSEM develops extensive know-how and high-end equipment and processes for cell and module metrology and dedicated characterizations, which can be developed for or transferred to its industrial partners.

Some of the 2018 highlights include (see also Figure 4) the realization of certified >24.0% screen-printed silicon heterojunction cells (European record), 24.8% back-contacted cells (25 cm², screen printing), the realization of numerous record values for p-type and cast-mono heterojunction, one industrial partner (Meyer Burger) making a world record 341W 60-cell modules, based on heterojunction and new generation multi-wire

contacts co-developed with CSEM, the introduction—together with EPFL—of a new type of passivating contact—which is activated by firing (A. Ingenito et al., *Nature Energy*, 2018), the development of a novel approach for colored PV modules, the first realization of a white PV facade (Solaxess), the extension of the colorization capabilities of PV (several new terra-cotta projects), and the development of a new generation of stratospheric solar modules that will equip high-altitude balloons. For 2019, there will be a refocus on the most industry-relevant approaches, in particular with respect to solar cells made with high-temperature passivating contacts.

Energy Systems activity

In the ongoing energy transition, the size and number of active energy resources is exploding and energy vectors will be more and more interconnected, creating a complex system of systems. The *Energy Systems* activity is at the intersection of power and energy, control, and data science. The objective of this multidisciplinary activity is to create tools to operate new energy systems with limited observability and to increase visibility with regard to the state of their components. The activity is structured around three topics. Within the energy data topic, we apply artificial intelligence techniques to generate value from energy data. This includes, for instance, forecasting energy production and consumption on multiple time scales and tracking individual appliances from aggregate power measurements. In topic of electricity storage, we develop characterization methods and dynamic models to predict the performance of storage devices in complex operating conditions. With these models, we can also optimize the design and control of storage systems. Finally, in the decentralized control topic, we develop multi-level control from, for example, the device level to grid-interactive functions. Typical solutions allow, for instance, an increase in local consumption of renewable energy, in system flexibility, and in power quality. We focus on single- or multi-vector microgrids operating at scales ranging from single buildings to cities. With our thermal-control technologies, the energy consumption of existing buildings can be reduced while maintaining or improving user comfort.

These topics address the following global challenges:

- Giving new tools to system operators to monitor and control grids with more and more active elements
- Making buildings and grids more energy efficient and more flexible through advanced control
- Optimizing the way batteries are designed and operated in renewable energy systems

Our technologies will find their way into all three parts of the physical energy system:

- Generation—mainly solar PV but also wind power and possibly other clean technologies
- Networks and interfaces—electricity networks, electricity storage, power-to-gas, power-to-heat, thermal networks, and heating and cooling storage
- Consumption—households, commercial, industry, and (more marginally) transportation

Applications of CSEM technologies have already been demonstrated on inverters, in direct current (DC) microgrids, and in energy management systems for residential and commercial buildings. We work with component vendors, system integrators, and utilities to turn these technologies into successful products.

Some of the 2018 highlights, partly illustrated in Figure 5, include smart data treatment from over 50,000 PV power plants allowing, among other elements, the detection of incorrect configuration of size or location, or higher or lower system performance; the validation of our model-based state-of-charge estimation for storage with a new algorithm delivering error levels below 3 percent; and experimental work leading to the filing of two patents for the control of microgrids and energy management in buildings.

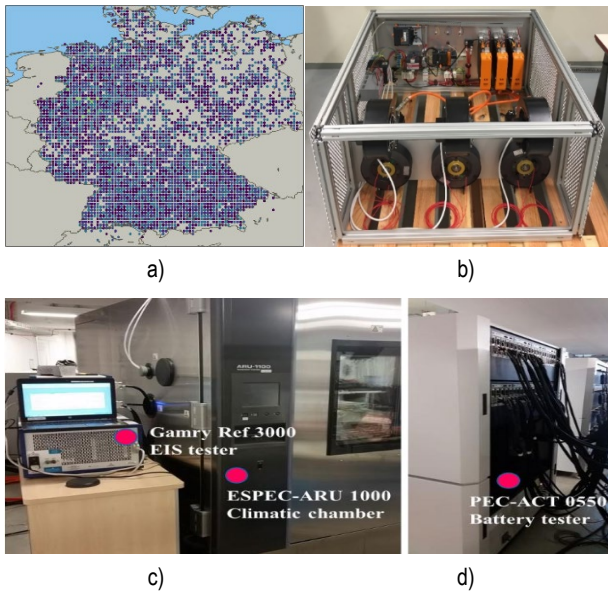


Figure 5: a) Mapping and smart analysis of 50,000 PV systems. b) Variable speed drives to be implemented at the Neuchâtel sewage treatment station with DC micro-grid grid control. c) Hardware at the BFH-CSEM energy storage research center, used for the validation of the new state-of-charge model.

Progress towards High-efficiency Perovskite/Silicon Tandem Devices

A. Walter, S. J. Moon, B. A. Kamino, A. Paracchino, J. Diaz Leon, S. Nicolay

In the framework of the European Horizon 2020 project CHEOPS (low-Cost and Highly Efficient phOtoVoltaic Perovskite Solar cells) and the Swiss SNF BRIDGE Program, CSEM has been working towards the realization of high efficiency perovskite/silicon tandem cells, with a focus on the use of inorganic hole and electron collection layers. With devices exceeding 25%, and most processes compatible with production technologies, CSEM places itself at the forefront of research in that promising and highly competitive development area.

On top of the promise of high efficiency (as high as 23.7% for single junction devices^[1]) at reduced costs, perovskite-based devices have gained a lot of traction to be used in a multi-junction configuration. There, the high-bandgap perovskite (PK) absorber is stacked on top of a lower bandgap absorber (e.g., c-Si, CIGS or a low bandgap PK). By minimizing photo-generated carrier thermalization losses, multi-junction devices allow to overcome the theoretical Auger efficiency limit of single junction Si based devices. This is of particular interest in an industrial landscape where c-Si PV manufacturers are beginning to look towards future technologies to continue to push their efficiencies even higher and to further lower system costs. CHEOPS and the BRIDGE Power project aims at tackling the difficult task of developing 2-terminal PK/Si tandem cells approaching the symbolic limit of 30% efficiency.

To that end, CSEM developed the different building blocks required for efficient tandem devices. In a first part, CSEM was charged with optimizing the single junction PK solar cells, as well as upscaling its deposition and processing to large area minimodules with record efficiencies^[2]. This included the development of charge transport layers (CTLs) by industry relevant techniques. Specifically CSEM designed NiOx layers by low-temperature sputtering deposition as a hole transport material, as well as low-temperature ALD SnO₂ as an electron transport layer. The latter can be deposited without damaging the underlying sensitive PK and makes it possible to sputter the front TCO without suffering from sputter damage. Moreover this achieved the desired goal of having fully inorganic CTLs, which is a condition for an improved thermal and air stability of the device.

Implementing these developments on a silicon heterojunction bottom cell with a polished front led to a best result of 24% using a standard ITO front contact. In addition, CSEM developed a more transparent IWO contact by low-power RF sputtering. This let more light pass into the bottom cell, allowing for higher current. Moreover, the low-power RF sputtering limit the sputter damage, leading to higher Voc. All in all, an efficiency of 25.4% (Figure 1) was achieved, surpassing the highest published PK/Si tandem efficiency to date. It is noteworthy that said published efficiency is also the result of a collaboration between EPFL PV- Lab and

CSEM that led to the highest published and certified efficiency (25.2%) using a textured Si subcell for improved optical properties^[3].

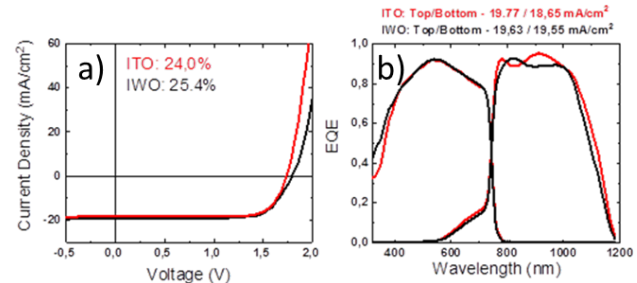


Figure 1: a) IV curve of hero cells comparing the difference between standard ITO and an optimized IWO on small area cells (1.43cm^2) b) Comparison of EQE of devices upon improving the top TCO transparency. Note that this is the highest reported photocurrent values for flat perovskite-silicon tandems.

Building on the know-how in terms of both high efficiency tandem design and upscaling, CSEM was then able to produce record efficiency large area (57.4 cm^2) tandem of 22.6% (Figure 2). Such demonstrator cell features industrial front metallization schemes. This was made possible thanks to CSEM's expertise in low-temperature silver paste screen printing.

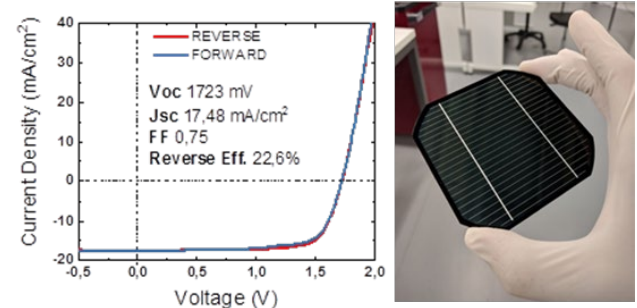


Figure 2: IV curve of large area demonstrator tandem with screen-printed metallization at an aperture area of 57.4 . Right: Photograph of large area demonstrator cell.

These recent developments position CSEM as a frontrunner in the PK/Si tandem research community, attracting the attention of traditional PV manufacturers.

[1] NREL, "NREL Efficiency Chart," 14 December 2018. [Online]. Available: <https://www.nrel.gov/pv/assets/pdfs/pv-efficiency-chart.20181214.pdf>. [Accessed 17 December 2018].

[2] A. Walter, S.-J. Moon, B. A. Kamino, L. Lofgren, D. Sacchetto, F. Matteocci, B. Taheri, J. Bailat, A. Di Carlo, C. Ballif, S. Nicolay, "Closing the cell-to-module efficiency gap: A fully laser scribed perovskite minimodule with 16% steady-state aperture area

efficiency", IEEE Journal of Photovoltaics, vol. 8, no. 1, pp. 151-155, Jan. 2018.

[3] B. A. Kamino, B. Paviet-Salomon, S.-J. Moon, N. Badel, J. Levrat, G. Christmann, A. Walter, A. Faes, L. Ding, J. J. Diaz Leon, A. Paracchino, M. Despeisse, C. Ballif, S. Nicolay, "Low Temperature Screen-Print Metallization for the Scale Up of 2-Terminal Perovskite-Silicon Tandems ", submitted, 2018.

Development of High Mobility TCOs for Heterojunction Solar Cells

L. Ding, J. Diaz Leon, G. Christmann, S. Nicolay

In the framework of the European Horizon 2020 AMPERE project (Automated photovoltaic cell and Module industrial Production to regain and secure European Renewable Energy market), CSEM develops transparent conductive oxide films with a twofold goal: improve the solar cell efficiency by improving the TCO's electron mobility and reduce the cost of manufacturing of the solar cell by developing non-indium-based TCO.

Silicon heterojunction technology (HJT) solar cells hold the power conversion efficiency record (>25%), 1-2% higher than conventional silicon technologies^[1]. It has shown a large potential to address the challenges of efficiency, cost, reliability and durability of photovoltaic cells and modules production. The AMPERE project^[2] focuses on the industrialization and automation of demonstrated innovative technologies to manufacture HJT solar cells and bi-facial modules in Europe. CSEM is notably working on fulfilling the goals of improving cell performance by developing high-mobility TCOs and reducing cell production cost by developing cheaper TCOs. High mobility TCOs are typically hydrogenated impurity-doped indium oxide based. Their high electron mobility enables high conductivity for low carrier concentration, hence low parasitic absorption and high photocurrent in cells; cheaper TCO are typically based on the earth-abundant tin or zinc oxides. The main candidate materials evaluated in AMPERE are high-mobility tungsten-doped indium oxide (IWO) and In-free aluminum-doped zinc oxide (AZO). Both materials are obtained at CSEM by RF-sputtering in a research-scale tool from planar targets. At this stage in the project material quality is investigated and optimized with respect to the performance obtained when integrated in project partner CEA-INES pilot-line rear emitter mono-facial cells. Figure 1 shows that the cells with AZO exhibit identical performances than the ones with CSEM indium tin oxide (ITO) reference process.

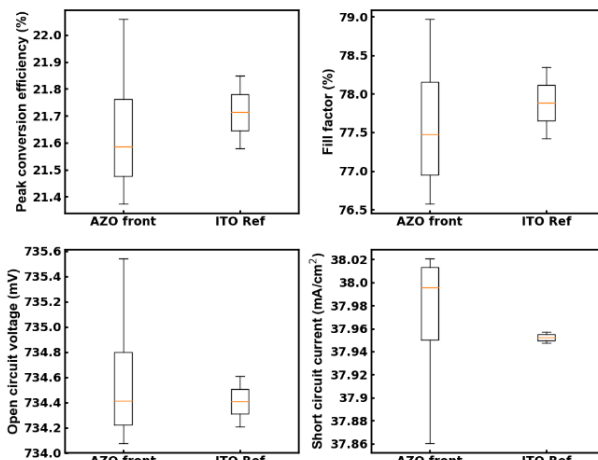


Figure 1: Light IV measurements of HJT cells having an AZO front electrode and comparison with ITO CSEM reference process.

[1] NREL, "NREL Efficiency Chart," 7 July 2018. [Online]. Available: <https://www.nrel.gov/pv/assets/pdfs/pv-efficiencies-07-17-2018.pdf>

This confirms the high potential of AZO as indium-free alternative to ITO.

IWO is processed at CSEM using solely residual water present in the chamber as a sufficient source for H incorporation and high mobility. IWO was tested as front and back electrode in solar cell precursors fabricated at CEA-INES, and compared to CSEM ITO reference process. Figure 2 shows that IWO front electrode leads to a very significant current gain of 0.4 mA/cm², while back IWO on the other hand leads to a more modest gain of 0.1 mA/cm². Altogether a full IWO cell leads to a total current gain of 0.5-0.6 mA/cm².

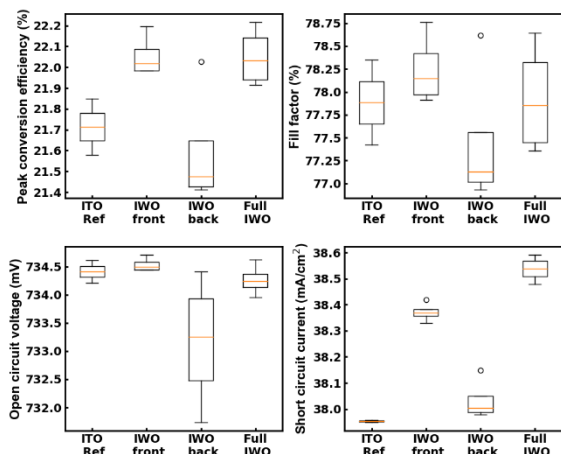


Figure 2: Light IV measurements of cells having an IWO front electrode, an IWO back electrode, and both, and comparison with CSEM ITO reference process.

Overall the best device with IWO front leads to an efficiency gain of 0.3-0.4% compared to full ITO. These results highlight the great potential of IWO as high mobility high transparency TCO for use in heterojunction solar cells.

The project continues with further optimization of the TCO processes for pilot-line HJT cell precursors; later TCOs' reliability will be investigated and deposition process itself will be optimized.

[2] www.ampere-h2020.eu

Multi-service Microgrid in an Industrial Environment

N. Koch, P.-J. Alet, A. Hutter

This report presents a lean control architecture for microgrids, with an implementation in direct current (DC) microgrids. The purpose of this architecture is to combine local objectives (e.g., self-consumption of locally-produced energy) with system-level objectives (e.g., mitigation of power fluctuations). This patent-pending solution has applications in industrial environments with local power production and DC loads with high peak power and regeneration capability.

With the cost of photovoltaic power generation below socket parity in many places, end-users have a clear financial interest in self-consuming the power they produce. On the other hand, recognition that infrastructure costs are mainly driven by peak power, rather than energy, is leading to an increasing fraction of retail electricity prices being based on peak power. This evolution presents a challenge for end-users with highly variable power profiles. Microgrids, especially with battery storage, are a promising way to manage the complexity of power networks with an increasing number of distributed, variable renewable energy sources (VRES)^[1]. Through the DCSMART project, CSEM has developed a control architecture for microgrids to benefit both end-users and system operations.

System architecture

The architecture of the DCSMART microgrid is shown on Figure 1. It is composed of a bidirectional grid-tied inverter, controllable and non-controllable loads, a photovoltaic installation and an energy storage system for energy and power buffering. The DC architecture eliminates conversion steps and eliminates synchronisation and balancing requirements associated with AC microgrids.

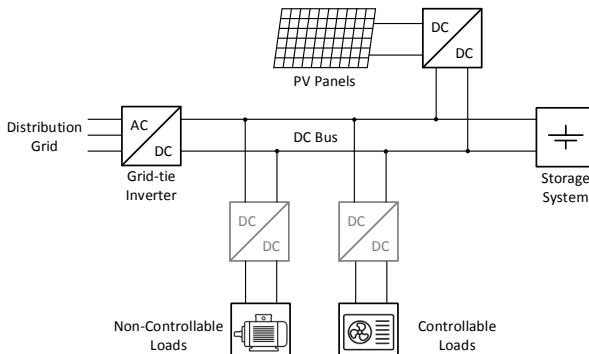


Figure 1: Electrical architecture of the microgrid.

Control strategy

The purpose of the developed strategy is to control the charging/discharging of the storage system in order to achieve local and system-level objectives, namely:

- Increasing self-consumption → reduction of energy cost for prosumers
- Performing peak-shaving on the power exchanges with the grid → reduction in capacity charge for prosumers, reduction in peak load for DSO

- Performing ramp-rate control of the grid power → reduction in rapid fluctuations for DSO

A given fraction of the storage system capacity is allocated to each objective, virtually splitting the overall storage capacity^[2]. This distribution can be freely adapted, thus the relative weight given to each service is flexible.

The implementation of the control strategy is split in three different levels (Figure 2): the physical system, the first control level characterized by fast and simple controllers, and the supervision level where more advanced and slower control techniques are used.

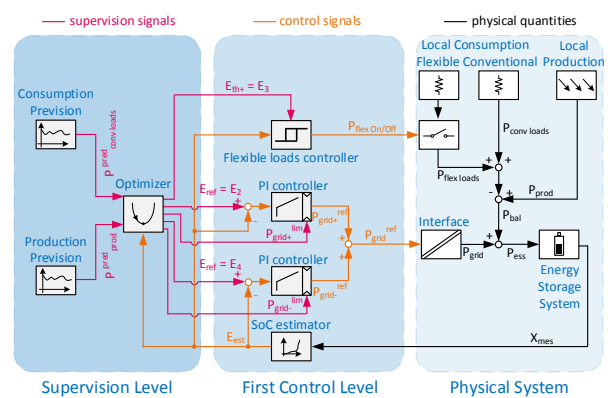


Figure 2: Detailed implementation of the control strategy.

Economic benefit

The economic assessment of the developed solution demonstrated the benefit of its multi-service approach. When electricity prices have a large power-related fraction, savings of 16% compared to a basic control strategy can be achieved thanks to its peak-shaving capability.

Moreover, this solution makes profitable the use of a storage system sooner and in a greater extent than with a classic strategy when taking into account its leveled cost of storage (LCOS). Indeed, the system is profitable for an LCOS 0.10 CHF/kWh higher than with the classic strategy.

The DCSMART project has received funding in the framework of the joint programming initiative ERA-Net Smart Grids Plus, with support from the European Union's Horizon 2020 research and innovation programme under grant agreement No 646039.

[1] N. Hatziargyriou, H. Asano, R. Iravani, C. Marnay, "Microgrids," IEEE Power and Energy Magazine 5(4), 78–94 (2007) [doi:10.1109/MPAE.2007.376583].

[2] N. Koch, C. Rod, C. Ballif, P.-J. Alet, "Robust control strategy for the energy storage system of a multiservice DC microgrid," presented at CIRED Workshop, 7 June 2018, Ljubljana, Slovenia.

Data-driven Reinforcement Learning for Smart Controllers in Large Building Facilities

B. Schubnel, R. Carillo, A. Hutter, P.-J. Alet

Today, buildings consume almost half of the primary energy in Switzerland, 30% of which is used for heating, air conditioning and domestic hot water^[1]. Making smart controllers that optimize energy consumption and comfort is part of the way to reduce this primary energy consumption. Within the European project THERMOSS, CSEM is building the next generation of industrial smart building controllers using a combination of simulation, reduced modelling and reinforcement learning techniques.

CSEM has a longstanding experience in designing smart controllers for building automation, in particular using model predictive control (MPC). Within the THERMOSS project, we used the recent advances in deep learning to simulate and design a smart controller for a large office building.

This building, located on the EPFL campus, has 100 rooms of various sizes and orientations, a centralized and fluid-based heating/cooling unit, and two centralized ventilation units that each provide air supply to half of the rooms. In each room valves control the supply of heating/cooling fluid, and blinds can reduce solar gain. The diversity in room configuration (types of valves, number of blinds per rooms, variable or constant air supply) makes the modelling and controlling problem particularly cumbersome. Creating with existing tools (e.g., EnergyPlus) a realistic simulation of the whole building dynamics would require a lot of efforts. On the other hand, it is not possible to try new control strategies directly on the building site so creating a realistic model is a necessity.

With an objective to build smart controllers that are sufficiently general and robust to be embedded in industrial applications, we have investigated the following approach to modelling the building.

First we have constructed a simple simulation of the building using the DIMOSIM suite developed by CSTB, a partner in the THERMOSS project. In line with our replicability objective, we tried and minimized the hand-crafted feature work. In particular, we did not try to fine-tune building parameters, shapes and devices. Instead of modelling each room in the building, we have modelled only a few room classes using the relevant attributes: size, orientation, floor location and types of inputs to control the rooms (valves, blinds). Our principal constraint was to have the same inputs and outputs for every room in the simulated model and in reality.

We have then trained a neural network to mimic the dynamics of the simulated building, and retrained the neural network with real data from the site (four months of data, sampled every ten minutes) to have a better fit to reality. We have used careful retraining techniques to keep as much as possible the physics learnt with the simulation and to avoid overfitting the model to the narrow band of real observed data and setpoints.

The main advantage of our approach is to remove the process of fine-tuning of parameters and architectural design. Instead this

part is automatically done by the neural network via retraining on real data. Moreover, we can produce different models by varying the length of the retraining episodes and the learning rates, fitting more or less closely the reality. These different models can be used to make the building controller robust.

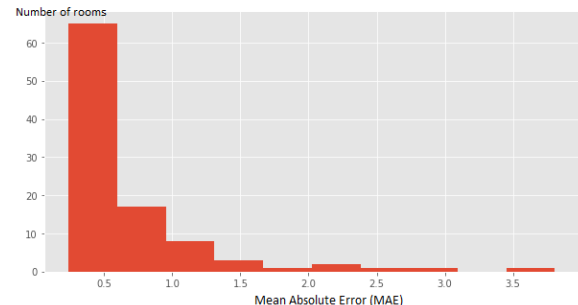


Figure 1: Distribution of mean absolute error in the room temperatures predicted by the model (trained on a separate range of dates) in June. Some errors are high ($>1.5^{\circ}\text{C}$) because of sensor problems in the rooms.

In a second step, we are developing a controller using state of the art techniques for continuous and discrete action space control. In every room, we have a local controller that controls the blinds (and/or the valves) and a global controller that controls ventilation and heating/cooling supply. The global controller works in continuous action space, whereas the local controllers have discrete action spaces.

Our controllers are modelled with neural networks and trained with the most recent reinforcement learning techniques (in particular DQN^[2], DDPG^[3] and PPO^[4]) on our offline models of the building. We are currently investigating which of these algorithms are the most robust and need less fine-tuning of hyper-parameters. One of these algorithm, PPO, has recently proven to be easily transferable to real situations for complex robotics control tasks and has been used to construct collaborative agents in video games. It can be used for continuous and/or discrete action spaces but is less data efficient than the other two algorithms. Work is ongoing to address these issues for the THERMOSS project.

This work was supported by the Swiss State Secretariat for Education, Research and Innovation (SERI) under contract number 16.0106.

[1] <http://www.bfe.admin.ch/themen/00507/00607/index.html?lang=en>

[2] V. Mnih, et al., “Playing Atari with Deep Reinforcement Learning,” presented at NIPS Deep Learning Workshop, 2013.

[3] T. P. Lillicrap, et al., “Continuous control with deep reinforcement learning,” arXiv:1509.02971 [cs, stat] (2015).

[4] J. Schulman, F. Wolski, P. Dhariwal, A. Radford, O. Klimov, “Proximal Policy Optimization Algorithms,” arXiv:1707.06347 [cs] (2017).

Model-based Online Estimation of the State of Charge in Lithium-ion Batteries

C. Brivio, R. E. Carrillo, P.-J. Alet

Everyone has seen the remaining charge on their mobile phone drop near instantly from 15% to zero. CSEM is developing a novel state of charge (SoC) estimator under the BESTIMATOR project. This algorithm improves the state of the art through: (i) a robust approach based on an electrical model developed at CSEM in the past few years; (ii) the mathematical processing to derive the SoC from the measurements at the battery terminals. First tests on real measurements show that our estimator achieves a maximum SoC estimation error of 3% and beats both the common Coulomb counting and advanced methods from industry leaders. The Bestimator™ algorithm can be implemented in battery management systems (BMS) for online SoC estimation in a broad range of applications including electric vehicles and grid services.

The Bestimator™ SoC estimation algorithm developed at CSEM comprises two main parts (see Figure 1). The first part is the physics-based lithium-ion model developed at CSEM^[1] that accounts for the nonlinearities of Li-ion cells with respect to current and SoC levels. The novelty of our approach lies in the clear link between the equations describing the electrochemical phenomena in the battery, and the impedance blocks in the model. Its development used electrochemical impedance spectroscopy (EIS) and open circuit voltage (OCV) measurements, and the model was validated on lithium nickel oxide cells. The accurate battery model makes Bestimator™ highly reliable in simulating the correct behavior of the cell.

The second part of the algorithm is an extended Kalman filter which estimates the SoC based on the voltage and current levels at the battery terminals. It operates in three stages: parts: (i) predicting OCV and the voltage drops across the impedance blocks of the battery model; (ii) correcting the OCV and voltage drops based on the error between the estimated and measured terminal voltage values; (iii) deriving the SoC from the estimated OCV with an OCV-SoC relationship derived from the cell model.

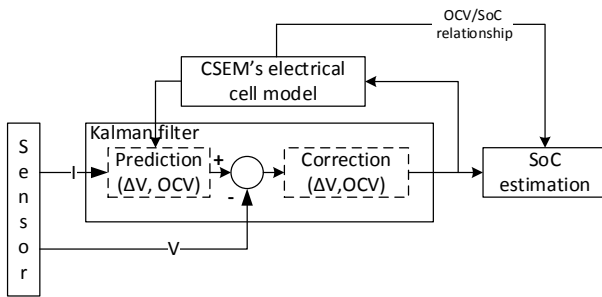


Figure 1: Block diagram of CSEM's Bestimator™ algorithm.

We have compared Bestimator™ with two other methodologies which represent the state of the art:

- Coulomb counting algorithm, which simply computes the integral of the current over time and updates the SoC with respect to the nominal capacity of the battery cell. Coulomb counting is very sensitive to initial conditions and prone to deviating over longer estimation time.
- Panasonic patent application EP 3115797 (A1)^[2], which uses a Kalman filter to correct the error from the Coulomb counting SoC estimation. It uses a simplified electrical

battery model to compare the measured voltage with the predicted one at the estimated SoC.

All methods struggle at extreme values of SoC (below 20% and above 80%, not shown here). While Bestimator™ is satisfactory above 80%, current efforts are focused on improving the method for the 0%-20% SoC region.

Figure 2 shows a comparison of the performance of the three algorithms in a demanding application: grid-connected battery storage for primary control reserve. The fluctuating current profile leads to periodic changes in the cell voltage. Both the Panasonic approach and Bestimator™ succeed in reproducing the measured voltage thanks to the Kalman filters corrections. Coulomb counting has the lowest estimation error of the three methods at the beginning due to the known initial condition however it drifts over time. Indeed, since it is an integral-based methods it accumulates the error if not re-initialized. After only 20 days its error level is the highest. The Panasonic approach starts with the highest error then gradually corrects the error and outperforms plain Coulomb counting after 15 days. Bestimator™ consistently outperforms both methods over the whole time range and achieves a maximum error of 3%.

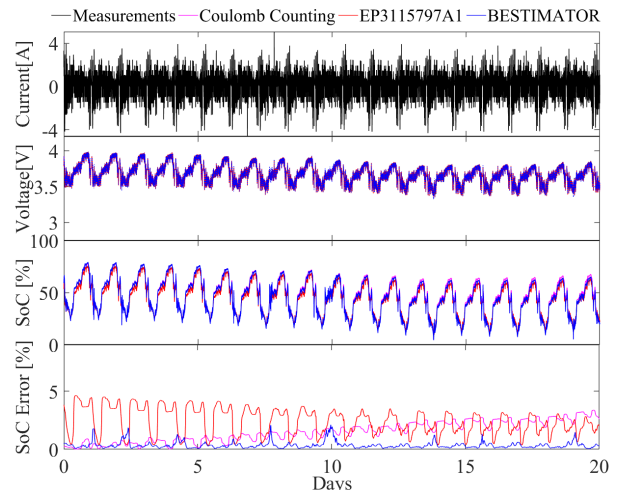


Figure 2: Comparison of estimates from the Bestimator™ algorithm, Coulomb counting, and the Panasonic method with measured values on a Boston Power Swing 5300 Li-ion cell for 20 days.

The BESTIMATOR project is co-funded by Innosuisse under project number 28008.1 PFNM-NM.

^[1] C. Brivio, V. Musolino, M. Merlo, C. Ballif, "A physically-based electrical model for lithium-ion cells", IEEE transactions on energy conversion, 2018 [Accepted].

^[2] T. Omi, K. Miura, S. Hiwa, T. Iida, K. Kakutani, "Battery state estimation device and method of estimating battery state", EP3115797 (A1), 11-Jan-2017.

Optimal Control Platform for Coupling Energy Vectors

W. Martin, E. Muntané Calvo, E. Olivero, A. Hutter, P.-J. Alet

CSEM is working in a consortium of European partners to develop a smart energy management platform. This platform provides tools to use the flexibility of existing controllable equipment and conversion systems between energy vectors (electricity, gas, heat). District operators using it will be able to integrate large shares of renewable energy at optimal costs and comfort.

Since power generation from centralized plants (combustible fuels, nuclear) is expensive to modulate, balancing power production and consumption in real time has always been a challenge. This challenge is only getting bigger with increased variability and uncertainty of electricity consumption (e.g., electric vehicles) and distributed power generation (solar and wind)^[1].

This issue can be addressed by increasing the flexibility of electric loads and storage equipment, or by using cross-vector conversion systems. However energy carriers (electricity, gas, heat) are usually considered separately in energy management solutions, resulting in an under-optimal use of the capabilities of energy systems. An optimal synergy between energy vectors would increase the flexibility at local level and contribute to grid stability and market operations.

The European project PENTAGON intends to provide such a solution by developing a smart energy management platform for eco-districts based on a model predictive control (MPC) approach. The control algorithm is executed every 15 minutes and consists of three main steps:

- Computing the 24-hour forecast of consumption and production profiles for loads and renewable generators respectively. This computation uses machine-learning algorithms and advanced physical models.
- Solving a mixed-integer linear program (MILP) where these profiles provide information on the future, operational limits of each equipment in the eco-district define the constraints, and the cost function considers discomfort of households, curtailment of renewable generators, and the cost of supplying a utility network. The results represent the optimal operation schedules over the next 24 hours.
- Dispatching the first time step of the optimization results through building management systems (BMS) to each device seen as a controlled actuator. Feedback from on-site smart meters help to improve the forecasting algorithms of step one.

A typical eco-district is depicted in Figure 1 with the aggregated consumption of households represented by a single dwelling. Controllable energy conversion systems allow the transformation of electricity to heat (heat pump) and gas to heat (gas boiler). External ties act as infinite sources of energy and determine the cost of supplying the eco-district by importing or exporting power.

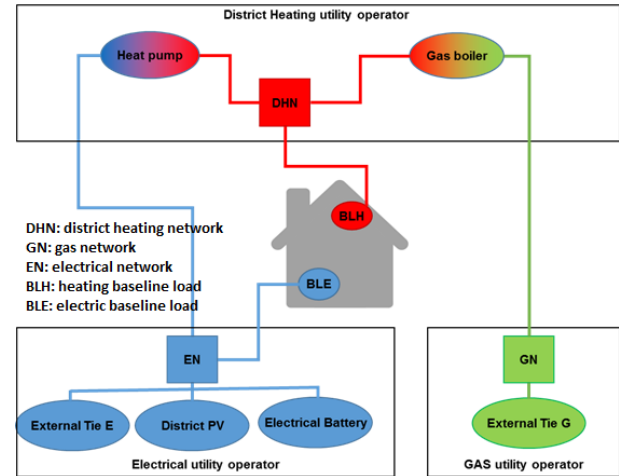


Figure 1: Component diagram of an eco-district with energy carriers interconnected through energy conversion systems (heat pump and gas boiler).

Prior to deployment on a demonstration site, we have validated the control platform by simulating its operations on the eco-district of Figure 1 over two weeks of forecast household consumption and solar production. The optimization problem was solved for every 15-minute time step. The resulting 24-hour profiles for each device are shown on Figure 2.

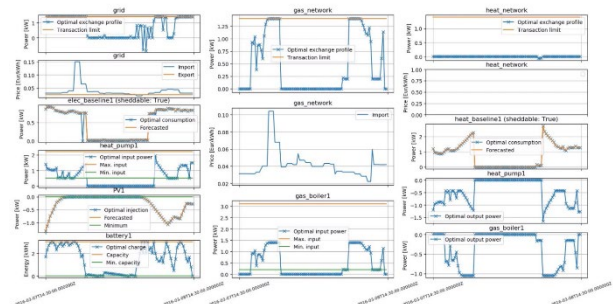


Figure 2: Optimized operation profiles each equipment of the eco-district (left: electrical devices; center: gas devices; right: heating devices).

The optimizer has efficiently managed to meet device constraints while minimizing the cost of supplying the three energy carriers. Curtailment of solar power was avoided and conversion systems were optimally operated with respect to power availability and cost.

This project has received funding from the European Union's Horizon 2020 research and innovation programme under grant agreement No 731125.

^[1] R. A. Verzijlbergh, L. J. De Vries, G. P. J. Dijkema, P. M. Herder, "Institutional challenges caused by the integration of renewable

energy sources in the European electricity sector", Renewable and Sustainable Energy Reviews, vol. 75, pp. 660–667, Aug. 2017.

Performance of Home Energy Management Systems: Insights from the Prosumer-Lab

Y. Stauffer, N. Koch, A. Hutter

The Prosumer-Lab aims at emulating the electric behavior of a building equipped with PV, batteries and a heat-pump in a controlled environment. It provides a test environment to precisely assess, with hardware in the loop, the impact of various energy management systems (EMS) on self-consumption of PV. In addition, control strategies involving different controllable elements can also be precisely benchmarked.

Prosumer-Lab allows to quantify under controlled conditions the impact of energy management systems (EMS) on the self-consumption ratio (SCR) of buildings equipped with PV and controllable electrical equipment. Since the internal time constants of the EMS affect the resulting SCR, tests have to run in real time. The full assessment therefore relies on a combination of live tests carried out on selected representative days coupled to one year simulations. Different hardware configurations (e.g., combination of controllable equipment) can be tested thanks to the modularity of the test bench to assess their impact on the SCR.

State-of-the-art commercial EMS are rule-based controller which are usually defined by the following parameters:

- Minimum turn-on power: the controllable system is turned on if the PV overproduction is above that value
- Turn-off power: the system is switched off if the overproduction drops below that value
- Minimum on time and off time of the controllable equipment.

To access these parameters, we defined a synthetic test profile. As shown on Figure 1, this profile consists in a constant (uncontrolled) load combined with linear ramps and step functions in PV power of variable length.

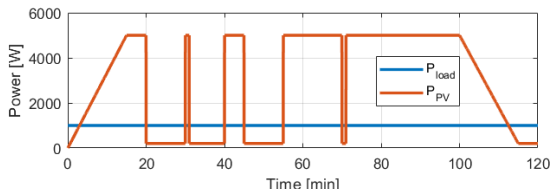


Figure 1: Synthetic test profile to access internal parameters of the EMS. Blue line: house electricity consumption; red line: PV production.

In addition, to evaluate the operation in realistic conditions, four representative simulation days were selected by clustering on weather data: one cold, sunny day; one cold, overcast day; one mid-season day with passing clouds; one warm, sunny day. These representative days thus cover periods of over and under production with specific consumption and production profiles to each seasonal meteorological condition in terms of temperature and sunshine.

Based on these two tests, the behavior of the studied EMS can be reproduced in a simulation program. Yearly simulations were run with the EMS output connected to a simulated smart-grid-ready heat pump. The internal controller of such a heat pump increases the set-point temperature of the domestic hot water and space heating water tanks if the EMS sends an activation

signal. In addition, features such as storage in the thermal mass of the building, batteries and combinations of these features were tested.

Thermal storage only increases the SCR by 8 percentage points on average over the year, with the highest potential in winter due to space heating. Adding batteries can increase the SCR. With a large electric-vehicle battery (100 kWh), this increase can be of 34 percentage points on average over the year. Finally, combining elements further raises the SCR.

From an economic perspective, different price configurations were applied to buying and selling electricity. In the case of net metering (same price for buying and selling electricity), the grid effectively behaves as an infinite, perfect battery. As a result, increasing the SCR with a local, imperfect storage is not desirable as it raises the net electricity bill (Figure 2). On the contrary, when the feed-in tariff is much lower than the purchase price of electricity, increasing the SCR is beneficial.^[1]

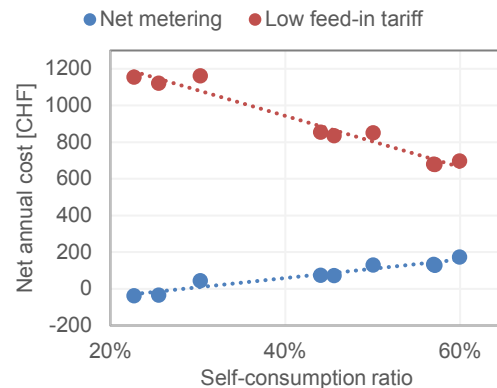


Figure 2: Net annual electricity bill as a function of self-consumption ratio and electricity price configuration. The different SCR values are obtained with different combinations of controllable equipment.

Work is now ongoing to:

- Implement and assess smarter control strategies such as model-predictive control
- Develop a more effective system sizing rule than the currently-applied 1 kW_p of PV and 1 kWh of battery for 1 MWh of annual electricity consumption
- Integrate capital expenditure, degradation and maintenance costs of equipment in the economic assessment of EMS.

This work is funded by the Swiss Federal Office of Energy under the grant n° SI/501431-01.

[1] Y. Stauffer, N. Koch, A. Hutter, N. D. Pflugradt, "Quantifying the potential of smart heat-pump control to increase the self-consumption of photovoltaic electricity in buildings," EuroSun

2018: 12th International conference on solar energy for buildings and industry, September 2018, Rapperswil, Switzerland.

SYSTEMS

Jens Krauss

The **Systems** research program is an interdisciplinary engineering field. We focus on innovations with system integration aspects of micro- and nano-subsystems as well as specific application demands such as resource limitation, miniaturization, precision, reliability, comfort, production cost, and environmental conditions. System integration requires significant coordination across disciplines and the development of new methods and modelling techniques as systems become smaller, interconnected, and more complex, approaching the physical limits. The **Systems** research program is application driven and our vision is to promote innovations and new product concepts along the three application domains of (1) *Scientific Instrumentation*, (2) *Automation*, and (3) *Medical Device Technology*. During the last reporting period we presented more than 60 scientific and journal papers for the different **Systems** application research domains, participated in roughly 30 conferences and workshops, and promoted our technologies at five exhibitions (CES, WT, Mobile Congress, Medica, and Photonics West and Lab Automation). Today we maintain an IP portfolio of more than 55 patents and during the last reporting period we filed four new patents.

Long-term objectives

Scientific Instrumentation: New precision manufacturing technologies together with CSEM's long-standing expertise in compliant mechanisms, MEMS, and MOEMS are transforming the capabilities and costs of high-end instruments and have game-changing advantages over traditional rigid alternatives. Rapid progress in material sciences and microtechnologies have led to rising ambitions in (scientific) instrumentation and a quest for ever-smaller and smarter multi-technology systems. Already today, system concepts integrate sensors, actuators, and mechanisms at the process level taking advantage of (metallic) additive manufacturing technologies to enable a new approach to complex instrument design. CSEM's *Scientific Instrumentation* activity aims to meet coming demands in the fields of space exploration and watchmaking, as well as meteorology and industrial and medical instrumentation. We design and implement complex, high-precision mechanisms for industrial applications and large science missions and strive for innovations in the domain of Si-based hybrid and compliant micro-mechanisms, laser sources and systems, and miniature atomic clocks. Our competencies in multi-physics simulations are key to our expertise in the design of such complex, miniature, and fully integrated systems, and thanks to our multidisciplinary expertise CSEM has become a European leader in the field of miniaturized flash imaging LiDAR.

Automation: Innovative Industry 4.0 solutions offer new, competitive production processes that can preserve Swiss manufacturing capabilities. Flexible and connected automation solutions with facilitated man-machine interaction enable an attractive total cost of ownership compared to a remote production site abroad, even for small to medium-sized production volume. In the framework of the *Automation* research activity we develop machine-learning techniques for automation and inspection tasks. We automate and interconnect complex manufacturing tasks, applying intelligent control and sensor

fusion techniques. We aim to further extend our Industry 4.0 application software framework in order to be able to easily deploy innovative solutions in different manufacturing and quality processes: drawing on the benefits of self-aware, smart components (software/hardware) and supportive robots (so-called work companions), we seek an optimum balance between flexibility, autonomy, and throughput. In coordination with the **Microsystems** and **Surface Engineering** research programs, we develop customized lab automation solutions, integrating smart sensors at the process level.

Medical Device Technology: The digital revolution is transforming the entire healthcare industry. Digitalization is entering the healthcare domain, improving efficiency and strengthening prevention, patient empowerment, and out-of-hospital care. CSEM's *Medical Device Technology* activity transfers human vital sensing and processing technologies into embedded, continuous on-body diagnostic systems, and drives global innovation toward new applications in the domains of rehabilitation, homecare, in particular for elderly, healthcare and promotion, security, and eHealth. It allows patients to be inconspicuously monitored during their daily activities, including work or sleep. And many more clinical and physiological studies in real conditions can now be envisaged thanks to systems that offer more comprehensive information. Digital (health) data aspects directly connected with wearables, in particular related to data reliability and privacy, as well as to low-power devices guaranteeing data security are also being addressed. CSEM's *Medical Device Technology* activity is certified according the standards of ISO-13485, and aims to outperform existing commercial medical products with regard to comfort, precision, cost, and maintenance, and to convince with a seamless integration into the digital healthcare system. CSEM provides innovative tools to manage pathologies and comorbidities, because the same embedded vital sign sensor can simultaneously measure bio-potential, impedance, temperature, pulse waves, sounds, and human kinetics parameters.

Highlights

With its multidisciplinary teams across CSEM's operational divisions, the **Systems** research program is one of the key drivers of CSEM's mission to transfer its (micro-) technologies, which is reflected in the program's increased industrial and licensing revenues. The slight increase in public funding has been allocated to new and additional digitalization activities across the program's three research activities, including for Industry 4.0 solutions in the *Automation* domain, additive manufacturing technologies within the *Scientific Instrumentation* domain, and privacy issues within the *Medical Device Technology* domain. Moreover, these additional funds have been used to support the preparation and spin-off of future start-ups in digital health (aktiia and MyStethos). Last but not least, we have further intensified our collaboration with other research programs in the framework of CSEM's Multidisciplinary Integrated Projects (MIP) initiative. In the following, last year's scientific highlights are summarized.

Scientific Instrumentation: Huge efforts have been deployed within the *Scientific Instrumentation* research activity to ensure timely flight model delivery in the framework of the following three

space missions: (1) the Corner Cube scanning Mechanism (CCM) for EUMETSAT's Third Generation satellite (MTG), (2) the Re-Focus Mechanism (RFM) for the close-up imager (CLUPI) of the Exomars rover, and (3) the LiDAR system for the international RemoveDebris mission. The last of these, the so-called Vision Based Navigation sensor (VBN), was delivered to the satellite provider SSTL (Surrey Space Technology Limited) at the beginning of 2018, was mounted successfully on the RemoveDebris satellite, and was sent on a Nanorack rocket to the ISS in April 2018. The mission highlight was the successful release of the RemoveDebris satellite from the ISS and into orbit in July 2018, and we have already received the first successful test data regarding our operational VBN system. The VBN is one of the key elements in the detection and removal of space debris and the experimental phase will continue until March 2019.

We would like to point to another highlight within the photonics domain, where CSEM has been awarded the prestigious European Quantum Flagship project *macQsimal*. CSEM will coordinate this flagship project together with a dozen recognized scientific partners with the aim of creating new commercial opportunities by leveraging quantum effects to achieve unprecedented sensitivity, accuracy, and resolution of devices for sensing and metrology applications. Last but not least, together with our colleagues from the **Microsystems** research program we would like to report the filing of two new patents re compliant and hybrid Si-based watch mechanisms.

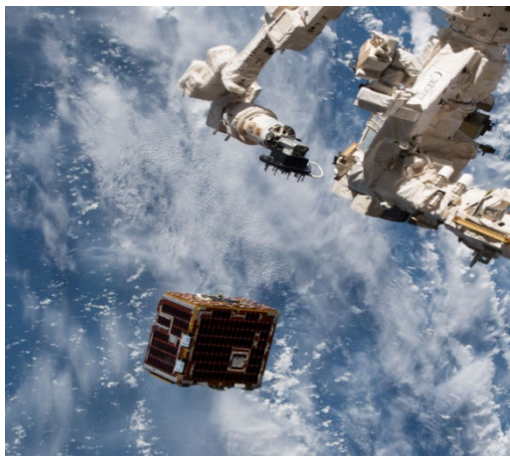


Figure 1: RemoveDebris satellite, integrating CSEM's LiDAR and 2D camera, during its release from the ISS.

Automation: During the last reporting period, within the *Automation* research activity we have increased our efforts toward the development of innovative Industry 4.0 solutions aiming at data collection and interpretation from several signal sources within an automation and/or manufacturing process in order to make decisions that optimize its overall performance. Our collaboration with our national railway company in the framework of the research focus machine learning has attracted international attention, and the whole predictive maintenance process, including data gathering, pre-processing, anomaly detection, and fault detection/ classification, has been developed, deployed, and is today operational. Moreover, we have further tightened the links to our *Scientific Instrumentation* activity regarding control strategies, real-time control, and embedded control systems.



Figure 2: Swiss railway experts during a railway integrity assessment session, relying on CSEM's deep learning tools.

Medical Device Technology: Our research activities in the field of medical device technology continue to gather awards and gain visibility. On the one hand, we would like to point to the start-up company AVA, the winner of the Swiss Medtech Award 2018 and elected "Best Swiss Startup" in 2017 and 2018. From its very inception AVA has collaborated with CSEM and it licenses our multi-signal monitoring technology IP background. With its sustainable funding, respected development timelines, and well-planned market entry, AVA is the role model with regard to a successful technology transfer from CSEM to Swiss industry.



Figure 3: AVA's fertility tracker relies on CSEM's vital sign monitoring technology and IP background.

On the other hand, we would like to highlight the creation of the CSEM start-up aktiia, which is the result of our 10-year research effort in the domain of cuffless, continuous blood pressure monitoring. Whereas aktiia will commercialize the use case of a medical wrist-worn device, CSEM continues to deploy its oBPM™ technology (and IP) portfolio within other form factors and for different body locations. We are about to transfer the technology of cuffless blood pressure monitoring to the swiss start-up Biospectral: by the end of 2019 a broad and worldwide clinical study shall be completed within a WHO program to validate Biospectral's smartphone optiBP™ solution for low-setting countries. Moreover, and related to the highlighted use cases of aktiia, Biospectral, and AVA, we have further increased our efforts in smart (rather than big) data research, with an emphasis on the privacy and security of health data. Following the recommendation of our Scientific Advisory Board, we intensified our collaboration with Swiss University Hospitals (such as CHUV, USZ, Inselspital, and HUG), and currently a dozen clinical studies are running according the ISO-13484 standards.

Recurrent Neural Network (RNN) Based Temporal Classification of Land Usage Using Satellite Imagery

P. Purwar, I. Kastanis, M. Hoechmer, P. A. E. Schmid

Recent advances in the field of deep neural networks makes them an ideal candidate for temporal data analysis. The use of satellite images as time series not only improves accuracy compared to purely spatial methods, but also opens the path for predictive assessment of crops in the future. This report focuses on the use of RNN for the purpose of data cleaning and classification of crop type.

Advances in the use of deep neural networks for temporal data have shown promising results in the field of natural language processing. Recurrent neural networks have demonstrated their capability to learn and infer from temporal behavior. This motivates the use of satellite images as temporal data. In addition, it compensates for the low spatial resolution of satellite images. Recent work by Rußwurm, et al.^[1] shows excellent results using RNN for land cover classification. Similarly, the aim of this project is to classify land usage using available satellite images from the Sentinel-2A satellite. The data consisted of multi-spectral images i.e., 4 bands, at a spatial resolution of 10 m and 16 dates from the year 2016 together with the location of parcels and crop type therein.

The initial inspection of the data showed that it is not consistent enough to directly train a new neural network. This required as a first step cleaning the data prior to training a classifier. The traditional approach is to use a statistical method to find the falsely labelled parcels and remove them. Typically this consists of manual analysis of the data and selection of features. The data-driven approach described below offers a convenient method of model generation avoiding some of the problems of standard statistical methods. The complete data was used to train a RNN based autoencoder which does not require labels for training. The idea was to represent the time series data of the parcels in a low dimensional space and apply clustering to find the outliers and falsely labelled parcels.

An autoencoder was trained using the crop type "Wheat", consisting of 1312 parcels. A variety of RNN architectures such as different number of layers, number of units, batch normalization etc. were tested and the best model was selected using a cross validation approach.

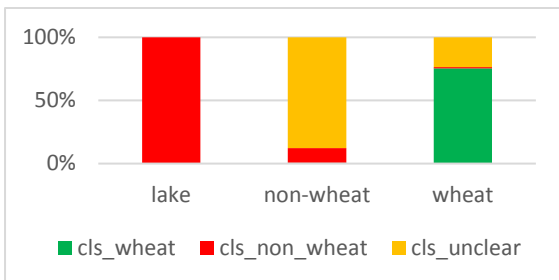


Figure 1: Plot showing percentage of pixels across 3 clusters.

Figure 1 shows the grouping of parcels into 3 clusters using k-means clustering. Some parcels were manually identified to indicate the meaning of the clusters. It can be seen that the parcels identified as "lake" mainly belong to "cls_non_wheat", while the parcels with a different temporal signature from wheat

(labeled as non-wheat) mainly belonged to "cls_unclear". The remaining parcels are mainly "cls_wheat" with a significant amount of pixels also belonging to "cls_unclear". In this manner consistent data can be selected. The features were projected in 2-D to visualize the clusters using Principal Component Analysis. The clusters show the variation in the pixels labelled as "Wheat" and clearly points to all pixels that are not "wheat".

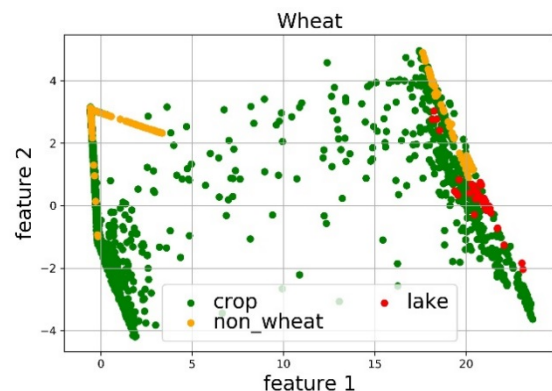


Figure 2: Projection of feature vectors for all pixels to 2D using PCA.

The parcels for which all pixels belonged to "cls_wheat" were labelled as "wheat" and the parcels from other crop types were labelled as "non-wheat". This collection of parcels was used to train a classifier using additional layers over the pre-trained encoder part. Figure 3 shows the results for the test samples. We can conclude that both the autoencoder and the classifier provide a convenient pipeline for land usage analysis from satellite images taking significant steps towards the automation of the process.

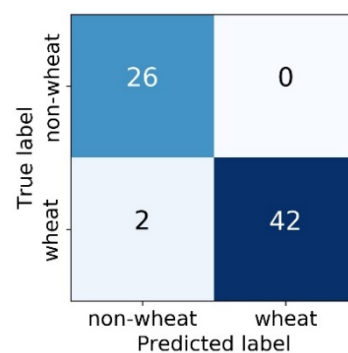


Figure 3: Confusion matrix on test data, accuracy = 0.9714.

This project has received funding from the European Union's Horizon 2020 research and innovation programme under grant agreement No 732064.

^[1] M. Rußwurm, M. Körner, "Multi-Temporal Land Cover Classification with Sequential Recurrent Encoders", IJGI, 2018.

A Wireless Solar Powered Pressure Pad for Sail Performance Monitoring

T. Burch, S. Bitterli, M. Fretz, E. Schaller

A wireless solar powered thin and flexible Pressure Pad for sail performance monitoring has been developed and tested on a sailing yacht on Lake Lucerne. The Pressure Pads continuously measure the pressure on the front region of the foresail and transmit the data to an associated software tool which helps the sailing crew to find the optimum sail trim.

Even if woolen telltales have been an efficient aid to good sail trim for decades, they have limitations. They are difficult to see on the leeward side and only give binary indication about laminar or turbulent flow without any trim optimization feedback. To overcome these limitations, CSEM has developed novel Pressure Pads, based on the Pressure Strip Technology^[1].

Nine self-adhesive Pressure Pads are attached on three different sections of the sail (Figure 1). Each Pad samples the differential pressure between leeward and windward and runs a data pre-processing cycle. The relevant information for indication of the sail trim is sent via Bluetooth low energy interface to the display in the cockpit. Hence the new sensor system allows the crew to anticipate the aerodynamics performance of the sail trim without actually seeing the sails.

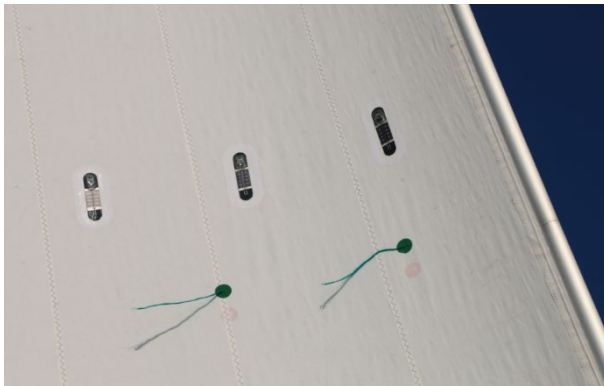


Figure 1: Pressure Pads attached above two original woolen telltales on the middle section of a foresail.

One of the key advantages of the sensor is its thin and flexible shape. The Pad thickness at the measurement location is only 0.6 mm, which ensures very low flow disturbance. CSEM's patented micro-channel technology is used to transmit the pressure from the measurement location to the electronics package located on the bottom of the Pad (Figure 2). To prevent blockage of the micro-channels due to moisture or dust, a micro-perforated membrane protects the pressure inlets.

The Pressure Pad performance has been evaluated in the laboratory and during a field test campaign on a 34 foot sailing yacht on Lake Lucerne. In the laboratory, both the specified sensitivity of 0.1 Pa and the accuracy of 1% FS could be confirmed (Figure 3). The field tests showed reliable pressure measurement starting already at very low wind speeds below 3 knots (or 1 Beaufort). The average power consumption in operation mode is below 1 mW and the integrated solar cell delivered this energy even in overcast weather conditions and

until after sunset. To use the system also during night, a small battery could be easily integrated in the electronics package.



Figure 2: Solar powered, self-adhesive Pressure Pad prototypes ready for simple attachment on the sail.

Besides high sensitivity and accuracy, ease of application and robustness are additional features of the Pressure Pads. The installation of the prototypes on the test sail took only a few minutes. During intensive testing the sensors withstood flogging and repeated furling of the foresail without degradation. Further miniaturization of the electronics package will result in increased robustness, which means sensor equipped sails can be handled as original sails without special care.

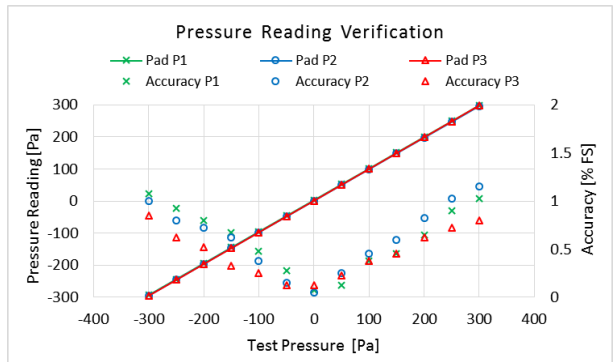


Figure 3: Pressure reading and accuracy of three Pressure Pads measured in the calibration laboratory.

In summary, the developed and tested Pressure Pad prototypes showed reliable and robust measurement performance and demonstrated great potential for industrialization. The current Pressure Pad design is clearly tailored to the sailing application, but has also potential for aerodynamics field-testing on any other object, for instance in the sports, automotive or aviation market.

CSEM would like to thank the Swiss Federation and the MCCS Micro Center Central Switzerland for their financial support.

[1] T. Burch, et al., "Novel System for Pressure Measurements on Yacht Sails", CSEM Scientific and Technical Report (2016) 97.

Controlling the End-Effector Absolute Pose of a Large Hybrid Manufacturing Robot based on Real-time Laser Tracking Technology

F. Crivelli, A. Steinecker, P. A. E. Schmid

An affordable and efficient solution for high quality hybrid manufacturing of large parts. Motion control and metrology based on absolute laser-tracking technology allow real-time compensation of positioning and motion errors, caused by inaccurate components and unmodeled disturbances. The result is an economically sustainable solution which combines both high accuracy and large workspace.

Important branches as automotive, aerospace, and energy industry demand production of large, high precision components. Production approaches based on 3D printing and hybrid processes (HM), which combines both additive (AM) and subtractive manufacturing (SM), are growing. These techniques allow making parts directly out of 3D models and present many advantages such as design freedom and complex enclosed structure, when compared with traditional machining or formative manufacturing. Additionally, in AM/HM manufacturing costs do not depend on the batch size, making prototyping and customer specific solutions economically sustainable^[1].

However, available AM/HM machines have a limited workspace and there is a lack of solutions for large parts manufacturing. The main challenge is combining a large workspace with high accuracy. Scaling up existing machines is often inapplicable due to the costs of large, high resolution mechatronical components. Moreover, in large structures the presence of small construction and modelling errors added to unpredictable and unmodeled disturbances, can considerably affect manufacturing accuracy^[1].



Figure 1: CSEM setup. 1) 6DOF robot 2) Laser tracker 3) 6D laser tracker module (T-Mac) 4) Resin dispenser 5) Spindle 6) Rails for reproducing displacement and oscillations due to the crane mounting.

To overcome these limitations, the European project KRAKEN^[2] proposes a novel approach based on laser tracking technology^[3]. The external laser tracker provides accurate measurement of absolute position and orientation of machine components and manufacturing tools. This feedback is acquired in real-time and used within a close-loop controller, to compensate deviations from the reference trajectories. This guarantees high accuracy, independently on workspace size and hardware characteristics. Thus, standard components can be used, limiting the price of the machine. The project involves 15 highly specialized partners.

^[1] F. Crivelli, V. Baumann, et al., "An all-in-one robotic platform for hybrid manufacturing of large volume parts," in Proceedings of the 8th IPAS, 2018, in press.

^[2] <https://krakenproject.eu>

CSEM plays a key role and is responsible for integrating the laser tracker into the control architecture of the system.

The KRAKEN prototype is composed by a 6 degrees-of-freedom (DOF) manipulator (NJ130, Comau S.p.A., Torino, I) mounted on a 3-axes crane. The crane guarantees a large workspace of 22x4x2 m, while the manipulator provides high flexibility. This design fits well the varying requirements of hybrid manufacturing and customized production. The current machine includes a spindle for SM (e.g., milling, polishing), a dispenser for resin AM, and an arc welding tool for metal AM. An absolute laser tracker AT960 from Leica (AT960, Leica/Hexagon Manufacturing Intelligence, Unterentfelden, CH) completes the system. Based on absolute interferometer technology (AIFM), the AT960 combined with a T-Mac reflector guarantees high-accuracy and high-speed tracking of a moving target. A development test-bench has been implemented at CSEM using a smaller robot (NS12-1.85). The rail system allows reproducing displacement and oscillations of the robot base, simulating desired and undesired effects due to crane mounting.

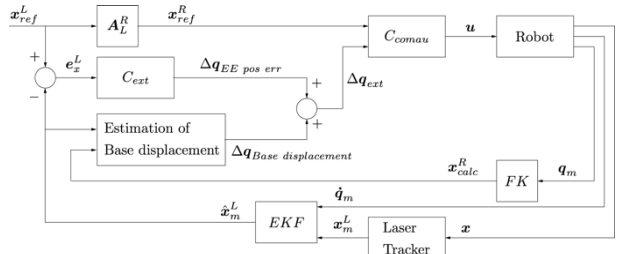


Figure 2: Flow chart summarizing the control architecture^[3].

The control strategy designed by CSEM is divided in two components: the standard robot controller from Comau (C4G Open) and an external controller implemented on a desktop PC. A Linux OS patched with RTAI extension guarantees real-time execution of the control algorithms (1kHz). The Comau controller moves the robot along pre-calculated reference trajectories, while the external controller integrates the end-effector pose measured by the laser and calculates a correction contribution (Figure 2). This strategy is being tested and optimized on the CSEM setup before being transferred to the full prototype.

This project has received funding from the EU Horizon 2020 research and innovation program (grant agreement No 723759). This support is gratefully acknowledged.

^[3] F. Crivelli, V. Baumann, et al., "Large volume hybrid manufacturing based on absolute laser tracking technology ", in Proc. of the 1st ICWNNDT, 2018, in press.

3D Lightfield Imaging for 100% Inspection in MEMS and Microsystems Manufacturing

J. Pierer, I. Kastanis, P. A. E. Schmid

State-of-the-art MEMS devices are found in many applications with various functionality. One thing all these MEMS devices have in common is their three-dimensional nature. In the IC industry many planar inspection tools have been developed. However there is a strong need for automated inspection tools that can inspect 3D micro structures. CSEM is working within the European funded project CITCOM together with partners on a potential solution implementing a 3D Lightfield camera. The system is based on a commercial wafer prober and therefore simple to implement into existing manufacturing environments.

The term micro-electro-mechanical systems (MEMS) was traditionally used for micro-fabricated devices that converted electrical signals in movement (micro-actuators) or movement into electronic signals. Presently the term MEMS is additionally being used for a much larger class of emerging devices and applications that are all being manufactured using micro-fabrication tools and equipment. These include miniaturized medical systems, micro-fluidic systems, Organ-on-Chip devices and implantable systems.

Shown in Figure 1 is an example of an intravascular ultra-sound transducer (IVUS) representing one of the most complex and highly integrated smart catheter products on the market. It is used to form a radial ultra-sound image of the coronary artery to establish the nature of the blocking and to assist in selecting the proper stent (diameter and length).

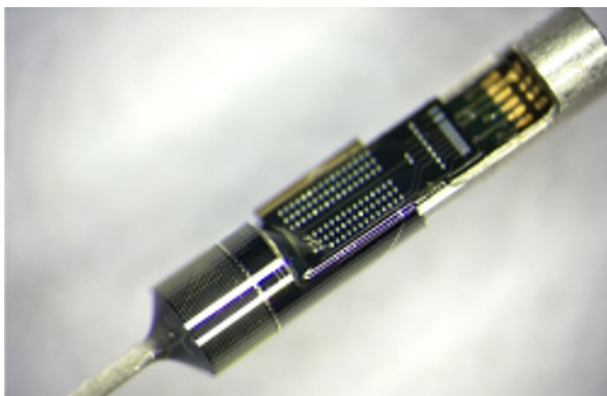


Figure 1: Example of an IVUS catheter tip [1].

Next generation products are based on capacitive micro-machined ultra-sound transducer (CMUT, see Figure 2) and will have a smaller diameter (0.8-1.0 mm) and a shorter rigid tip length.

This new class of MEMS devices has been enabled by advancements in micro-fabrication materials and processing. One thing all these MEMS devices have in common is that they are all (highly) three-dimensional in nature.

Whereas the IC industry has developed many planar inspections tools, there is a more or less urgent need for automated inspection tools that can structurally inspect 3D micro structures. Manual inspection is presently the only alternative, adding big part to the costs.

[1] Images in Figures 1 and 2 provided in courtesy by Philips Electronics Nederland B.V.

[2] www.citcom.eu This project has received funding from the European Union's HORIZON 2020 research and innovation program under Grant Agreement no. 768883.

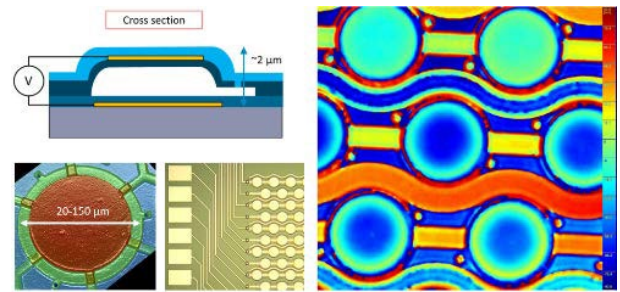


Figure 2: Schematic cross-section of a CMUT device (top-left), optical microphotographs in top view (lower-left) and a holographic microscope picture.

CSEM is working within the European project CITCOM^[2] to fill this gap in the manufacturing cycle by developing a fully automated 3D inspection instrument. One of the systems used is based upon the 3D Lightfield cameras provided by the company Raytrix^[3]. The 3D image depicted in Figure 2 was obtained during early tests and shows the CMUT structures after production on the silicon wafer.

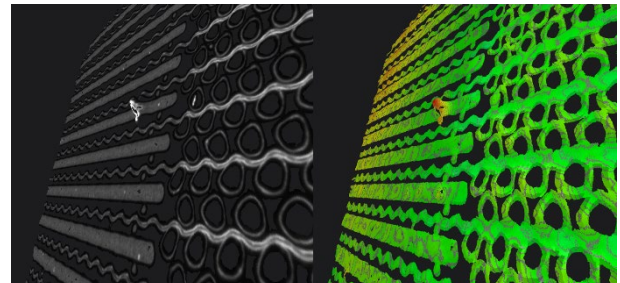


Figure 3: 3D and depth map lightfield images of CMUT device.

The inspection system is fully integrated into a commercial wafer prober system as provided by the company aixACCT^[4]. The proven hard- as well as software enables simple integration with existing manufacturing lines. Acquisition as well as processing of the 3D image data happens fully automated in the background with the CSEM VISARD^[5] (Vision Automation and Robotics Designer). Results such as defects and defect categories are stored and presented within standardized wafer map files. Especially during implementation of new processes for new products the operator has the option to show the image data. This might assist e.g., understanding and categorizing of new defects and finally to improve the overall production yield.

[3] Raytrix GmbH, Schauenburgerstraße 116, D-24118 Kiel, Germany.

[4] aixACCT Systems GmbH, Talbotstr. 25, 52068 Aachen, Germany.

[5] M. Höchmer, I. Kastanis, P. Schmid, "VISARD—Vision Automation Robotics Designer", CSEM Scientific and Technical Report (2016) 95.

Generic Condition-based Monitoring for CSEM VISARD Automation Platform

M. Höchemer, P. A. E. Schmid

CSEM's VISARD (*Vision Automation and Robotics Designer*) platform is the CSEM solution for Industry 4.0 and automation demands. With its modular approach, VISARD is used from subsystems over controlling special purpose machines to automation of whole production units. VISARD reduces the complexity of designing and implementing automated processes. The aim of this project is to integrate a new feature into VISARD, namely an automated method for identifying errors and aging components or more generally analyzing a systems' health status and finally even predicting this. The approach uses state of the art methods in Neural Networks and Deep Learning. VISARD will also be able to store the acquired data, visualize it live and generate status reports – on a regular basis, on critical situations or upon request. This fundamentally changes the way how to monitor the status of complex machines and systems and enables condition based and predictive maintenance.

VISARD is actively developed at CSEM for many years and widely used for image processing, quality control and process automation. CSEMs expertise in deep learning for image and time series processing now allows to use these technologies for reusable and automated System Health Monitoring.

Each VISARD module is able to provide so called Health Status Information with a convenient interface. Health status can be Hardware or Process related. Hardware modules (e.g., camera, robot, input/output) may add Information on timings, connection quality, power consumption, system resources (RAM, CPU load), illumination and lots more. Process related health data may contain information about the process, like dimension measurements, scores, surface quality, cycle times, temperatures, humidity.

VISARD gathers all this data asynchronously, computes some statistical means (average, standard deviation, trend, range, frequency) and stores all this information in regular time intervals into an INFLUX^[1] time series database. The database can be hosted on the VISARD machine itself, centralized to allow multiple machines to store its data or even inside the cloud. This allows long term condition based monitoring and report generation. By using these modules for a project, the solution is automatically collecting health data. This concept brings reusable condition based monitoring capabilities to every project that was realized with the CSEM VISARD. For further analytics and research, data can be exported to the scientific HDF5 data format and is easily available in Matlab or Python.

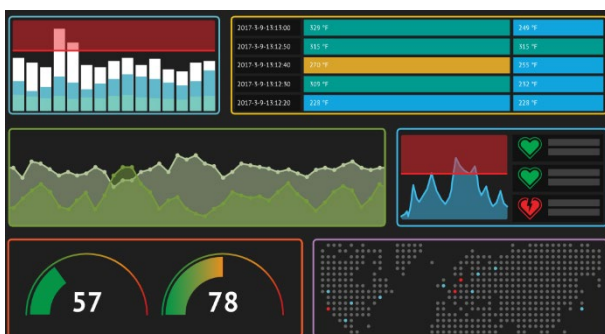


Figure 1: Online Health Data Visualization in Grafana web frontend.

For real time and historic Data Visualization, VISARD supports the open source visualization tool GRAFANA^[2], a graphical frontend for time series data. GRAFANA can be hosted locally, on a central local server or in the cloud. For an easy setup, the tool was integrated into the new VISARD CBM ribbon page.

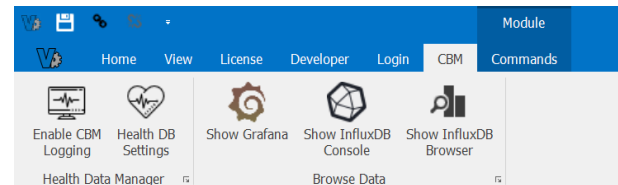


Figure 2: New VISARD ribbon page, condition-based monitoring.

GRAFANA provides an intuitive user interface and allows custom designs to visualize the health data and to generate alarms and send notifications in case of critical situations - by mail or to smart devices.

For many sensor signals it is not possible to monitor their status isolated with a simple threshold. Cross dependencies and different situations require a more sophisticated approach. Easy "If-Then-Threshold" conditions are currently state of the art in production industry. More complex ones use hand crafted features (e.g., FFT) and compare them to a threshold. In this project we are developing a generic CBM module based on deep learning technologies to monitor the actual "health condition" of the machine based on health data from the modules. This ultimately reduces complexity for the end user as there is no need for manual feature engineering and deep physical system understanding. After an unsupervised learning phase the module is able to identify anomalies – by taking into account different operation conditions and cross dependencies.



Figure 3: Production machine in the lab for demonstration.

As demonstration CSEM is building a small production machine in the lab with cameras, robot, conveyer-belt, sorter, feeder, IOs and illumination. The machine emulates the production of small SMD fuses with integrated quality control and condition based health monitoring. CSEM thanks Aurovis AG, Schurter AG and maxon motor AG for their valuable support.

[1] <https://www.influxdata.com>

[2] <https://grafana.com>

RailCheck—Deep Learning for Railway Track Inspection

N. Rauschmayr, M. Höchemer, P. A. E. Schmid

RailCheck is a joint development project between Swiss Federal Railways (SBB) and the Robotics and Automation team at CSEM. SBB operates several 'diagnosis' trains (DFZ: Diagnosefahrzeug, gDFZ: gezogenes Diagnosefahrzeug) that are equipped with multiple high-resolution cameras and other sensors that obtain images from railway tracks while traveling at speed of up to 160 km/h. The goal of RailCheck is to apply deep learning technologies to massively improve the detection and classification of faults on railway tracks and other relevant infrastructure.

The current software in place at SBB produces too many false positives/negatives to the extent that the system has not been of much use: e.g., when the DFZ went through the newly opened Gotthard base tunnel for the first time, the software recorded about 40'000 faults. It was clear that the new railways would not contain any faults at all. Such large number of false positives is a problem, since each of them has to be manually evaluated by an expert.



Figure 1: Diagnosis train (DFZ), Gotthard line, Lake of Uri.

Besides minimizing false positives, the project focuses on solving additional issues:

- Large amounts of data: image resolution is 1 pixel per mm (DFZ) and 0.75 pixel per mm (gDFZ). SBB is planning to inspect 3800 km per month by 2020
- Influence of changing weather conditions on images e.g., rain drops and snow should not be detected as faults
- Very little training data and certain fault categories require the judgment of well-trained railway experts who may not always agree.

In a preprocessing step regions of interests (railway, clamps and ties) are extracted from the images. In a second step a special Convolutional Neural Network (Faster RCNN^[1]) is applied in order to detect and classify faults. Given the small amount of training data, detected anomalies are often assigned to wrong categories. On top of that many faults need to be judged by railway experts, so the annotated images are uploaded to a webserver where each railway expert can give feedback. Having the feedback of multiple experts allows for different opinions to be taken into account. Based on the feedback, data is relabeled, added to the training set and then the Faster RCNN is retrained.

By doing these steps iteratively, the model accuracy improves over time (Lifelong Learning).

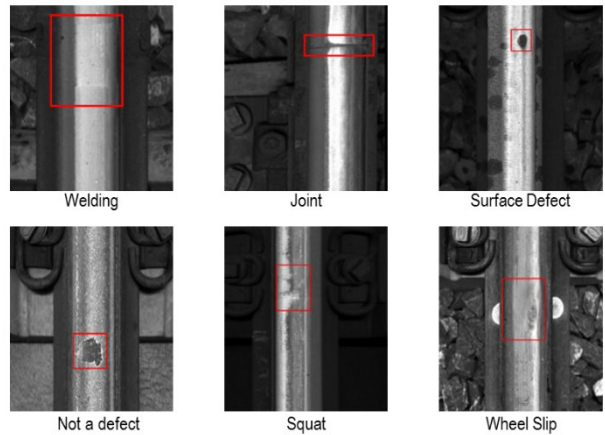


Figure 2: The 6 different fault types for railway surfaces.

The next step in the workflow is the so-called fingerprinting. The diagnosis trains travel the same routes multiple times a year. As such, the system has to identify which faults have been previously recorded and which ones are new. The challenge is that faults and weather conditions can change and the positioning data includes a high uncertainty. Given the position, faults within a range of (+/-5 m) are retrieved from a database. The fingerprinting algorithm computes a feature vector for each of the given images by inputting the image into a pretrained CNN model (Inception Resnet^[2]) and retrieving one of the early layers in this CNN.

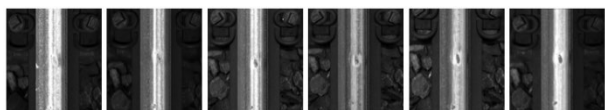


Figure 3: Fingerprinting: history of a defect (11.2016 - 08.2017).

The fingerprinting is an important step for two reasons. If a new fault is found, experts may have to go to the railway to do an onsite inspection and the number of such inspections shall be kept at a minimum. Secondly, it allows for evaluation of how faults develop and may in future help to prevent them altogether.

The above workflow is running within SBB on an NVIDIA DGX Station^[3] which consists of 4 GPUs, each with 16GB. This workstation is specifically optimized for leading edge AI development and therefore most suitable for our business case.

[1] S. Ren, K. He, R. Girshick, J. Sun, "Faster r-cnn: Towards real-time object detection with region proposal networks", In C. Cortes, N. D. Lawrence, D. D. Lee, M. Sugiyama, and R. Garnett, Eds, Advances in Neural Information.

[2] C. Szegedy, S. Ioffe, V. Vanhoucke, "Inception-v4, Inception-ResNet and the Impact of Residual Connections on Learning", In CoRR, abs/1602.07261, 2016.

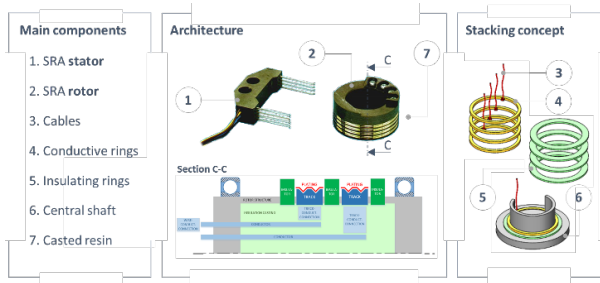
[3] NVIDIA DGX STATION, <https://www.nvidia.com/dgx-station>

Redesign, Manufacturing, and Testing of a Slip Ring Rotor for Space Applications based on Additive Manufacturing

H. Saudan, L. Kiener, F. Cochet•, S. Liberatoscioli•

Herewith we do present a novel design concept based on an Additive Manufacturing (AM) process, enabling the development of mechanical parts featuring built-in electrical wires and interfaces. The concept is successfully applied to re-design the rotor of a Slip Ring Assembly (SRA) intended for space applications. The implementation of the concept leads to a significant simplification of the product's physical architecture, with a subsequent reduction of the manufacturing and assembly operations. Funded by the SERI's Swiss Space Office (SSO), this project was carried out jointly by RUAG Slip Rings SA (RSSR) and CSEM, each partner bringing its own expertise, respectively the design of SRAs and the re-design of an existing product based on advanced manufacturing technologies.

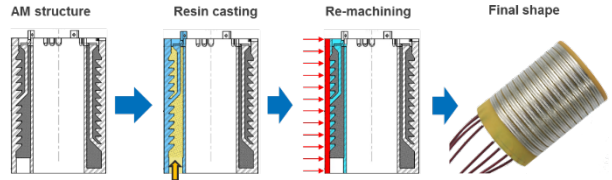
Slip Ring Assemblies (SRAs) are continuity devices whose function is to transfer electrical signals from a stationary member to a rotating member. In space, SRAs are part of many satellite sub-systems such as Solar Arrays Drive Mechanisms (SADM), Antenna Pointing Mechanisms, Control Momentum Gyroscopes and others. The physical architecture of SRA rotors relies on a delicate manufacturing and assembly sequence involving many operations. Notably, each conductive ring is manually soldered to a cable (see Figure 1.), itself manually routed and connected to a terminal block. Furthermore, stacking conductive and insulating rings implies a long tolerance chain which makes it mandatory to achieve high dimensional precision for each component. As an example, a 30 channels SRA rotor involves the stacking of 60 rings. Considering a ring thickness tolerance of $\pm 10 \mu\text{m}$, the overall track pitch deviation increases to $\pm 600 \mu\text{m}$, causing obvious design, machining and assembly issues.



To avoid the use of cables and to reduce the number of components, a novel design concept based on an AM process is proposed and applied to the SRA use-case. The concept enables the metallic structural parts design. Current alternatives are limited to insulating polymer structures combined with conductive inks or polymers offering lower power transmission capacities and reduced design flexibility for electrical interfaces.

The developed rotor consists of a monolithic structure made of aluminum and printed by Selective Laser Melting (SLM), which includes conductive rings and electrical wires (see Figure 2). The structure comprises a sacrificial shell, which allows to cast the inner volume with resin and therefore creating the insulating barriers between each ring. The shell is finally removed, giving the rotor its final shape.

- RUAG Slip Rings SA (RSSR)



The rotor was manufactured and validated by means of electrical performances and lifetime testing. The achieved performances are compatible with the requirements of SADM applications for low and geostationary orbits. The new concept allows significant mass reduction, since the central shaft can be removed or optimized. Considering a number of 30 channels, the new concept enables a reduction of the components from more than 90 parts to one. It induces therefore a drastic decrease of the manufacturing and assembly costs. A preliminary cost analysis indicates a gain of 40% as realistic. To consolidate the product concept, the development will be continued in order to fully define the design geometries and process parameters. The final prototype shall then be fully qualified with respect to the application requirements foreseen.



Figure 3: Two SLM-made SRA rotor prototype examples.

Thanks to the very close cooperation between RSSR and CSEM, the project outcome is considered as very successful by both partners. The project was also awarded in 2018 with the innovation prize of the AMX conference in Lucerne (CH).

A common development roadmap involving the whole SRA was elaborated, targeting future ESA development programs. Moreover, the original and patented concept was developed to avoid the use of cables in the SRA and can be advantageously applied to other electro-mechanical components and assemblies, with the same potential for cost reduction and reliability improvement.

Flight Model Acceptance Test Campaign of Two Corner Cube Mechanisms for MTG

P. Spanoudakis, J. Bennes, M. Gumi, L. Kiener, G. Perruchoud, Y.-J. Regamey, H. Saudan, P. Schwab, V. Teodoridis

The two Flight Model (FM) Corner Cube Mechanisms (CCM) completed their acceptance test campaign successfully. They are part of the interferometer assembly of the infra-red sounder (IRS) instrument for the Meteosat Third Generation (MTG) satellites.

The acceptance test campaign of the two Flight Model (FM) Corner Cube Mechanisms (CCM) started in mid-2017 following the successful qualification test campaign on the Engineering Qualification Model (EQM). The acceptance test campaign was comprised of a series of critical tests: performance tests, random vibration tests, thermal vacuum cycling (TVC), performance tests after environmental tests and micro-vibration tests. The test campaign was covered by successes and setbacks but, at the end, solutions were found and implemented.

The TVC part of the Proto-Flight Model (PFM) tests completed the qualification of the CCM since these tests were not performed on the EQM. A delta-QR (Qualification Review) was held successfully validating the overall test program for final delivery of the PFM to Thales Alenia Space (TAS-F) for integration of the CCM at interferometer level.

Prior to the start of the random vibration tests on the PFM, an inspection of the CCM was carried out. It was discovered that a number of critical bolts had loosened despite the fact that they were locked by adhesive. A six-month investigation was carried out to determine the source of this major non-conformity and to implement corrective actions. Even though the EQM utilized the same types of bolts and coating, the PFM bolts loosened due to the anti-friction coating stability. The corrective action implemented consisted of the replacement of all mechanism bolts with another coating and without disassembly of the two CCMs. The bolts were replaced sequentially without compromising the alignment and assembly tolerance of the mechanism.

Another setback to the test campaign was the discovery of the FM2 Optical Switch (OS) ruler broken inside the mechanism while the final sequence of the bolt replacement procedure was being carried out. A Non-conformance Review Board (NRB) was held and following the inspection and expertise of the glass ruler, a root cause analysis indicated a failure due to a flaw on the glass surface and possible contact with an endoscope during an inspection step. Corrective actions were implemented. The OS ruler was replaced and the hardware re-integrated in the CCM. The FM2 performance tests were executed in parallel to the PFM environmental test campaign.



Figure 1: FM2 Optical Switch broken ruler and its support.



Figure 2: PFM and FM2 following assembly.

Following the various corrective actions, the PFM and FM2 acceptance tests were performed during the first half of 2018.

The PFM and FM2 performance tests confirmed the previous EQM test results. The maximum lateral deviation (parabolic shift) for a stroke of 10 mm (± 5 mm) was measured at 0.4 μm in Z and 0.3 μm in Y compared to the 2 μm specification.

Following the EQM micro-vibration tests, improvements were identified to shift mechanism frequencies away from the input disturbances generated by the cryo-coolers which mainly affect speed stability and lateral shift. Local mass tuning implemented on the mobile stages of the CCM improved performance in these areas.

With the injected micro-vibration disturbance profile, two speed stability parameters were measured:

- the absolute value of speed error during dwell time measured at 0.54 mm/sec (EQM 0.73) (spec: 0.25 mm/sec)
- the standard deviation of speed error during dwell time measured at 0.12 mm/sec (EQM 0.29) (spec: 0.06 mm/sec)

Even though these values are out of specification, the results were expected and accepted by the client since they are directly proportional to the injected disturbance levels.



Figure 3: PFM during micro-vibration tests at TAS-F (Cannes).

Both models will be delivered to TAS-F in Cannes before end of 2018. This work is performed in partnership with TAS-F and is funded by the European Space Agency. CSEM thanks them for their support.

Close-Up Imager (CLUPI) for the EXOMARS Mission: Focus Mechanism Test Campaign

G. Perruchoud, A. Verhaeghe, P. Schwab, M. Gumy

Over the years CSEM has developed a track record and reputed expertise for compliant high-precision opto-mechatronics systems used for space missions or other applications under harsh environments. In the frame of the Exomars mission, CSEM designed, developed and tested the CLUPI Focus Mechanism with the resulting Qualification Model that has to sustain severe mechanical and environmental test conditions.

In the frame of the ESA Exomars mission, CSEM developed and built one EQM (Engineering Qualification Model) and one FM (Flight Model) of the CLUPI Focus Mechanism (CFM), based on flexure elements. The mechanism is part of the CLUPI imager mounted onto the drill of the Exomars Rover. The CLUPI imager development is under the responsibility of Thales Alenia Space (TAS) Switzerland whereas the Project Investigator activity is performed by the Space Exploration Institute in Neuchâtel (CH).



Figure 1: EXOMARS rover.

The CLUPI Focus Mechanism (CFM) will allow the frictionless adjustment of the focal distance of the imager. Its design accounts for the launch mechanical loads (high random vibration loads) and the harsh environment of Mars, especially the lower temperature. The main challenges of the CFM development were the low mass requirements (under 200 grams), together with the new development of a new launch lock device. The CFM is presented in the following figure.

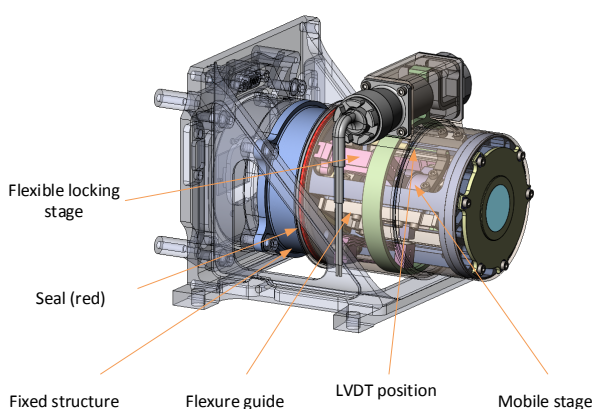


Figure 2: CFM (CLUPI Focus Mechanism) overview.

Mechanical tests

The mechanical tests, i.e., random vibration and shocks, were successfully passed at TAS-Toulouse premises. The main concern was the flexure resistance when submitted to the launch excitation spectrum. During the course of the development, this spectrum was increased from 11 grms up to 28 grms due to mission and implementation constraints. Nevertheless, CSEM succeeded in upgrading the CFM resistance without changing the overall design. Finally, no mechanical damages were observed and the nominal functioning performances were conserved.



Figure 3: CLUPI CFM mounted on the shaker, ready for tests.

Thermal tests

The CFM critical components, such as the Voice Coil actuator and the position sensor were successfully qualified, during the previous project phase, down to -130°C over 300 cycles. The complete assembled models (EQM and FM) were then tested inside a Thermal Vacuum Chamber at RUAG Space in Zürich.

A thermal cycle including non-operating temperature (-130°C) and Dry Heat Microbial Reduction temperature (DHMR @ +115°C) was successfully passed. The DHMR is a process to achieve acceptable microbial bioburden levels prior to launch and is mandatory in order not to contaminate the Mars environment with terrestrial organisms.

Finally, thermal cycling at operating temperature, -55°C to 40°C, with performance tests and Launch Lock Device release was performed to prove that the CFM can operate and perform accordingly when submitted to its environmental temperatures.

Based on the performed environmental tests, CSEM successfully verified the robustness of the design with respect to the harsh Martian environment and to the high mechanical load during the rocket launch. CSEM thanks ESA and the Swiss Space Office (SSO) for its support during the development.

RemoveDebris, in-orbit Experimentation of CSEM LiDAR

A. Pollini, C. Pache, M. Toimil, G. Perruchoud, L. Giriens, J.-L. Nagel, P.-A. Beuchat, L. Balet, A. Moreira De Sousa, Y. Chevallier, F. Droz

RemoveDebris aims at testing technologies for Active Debris Removal in-orbit. For this mission, CSEM provided a vision-based instrument to capture 2D and 3D images allowing to find, track, capture and de-orbit artificial targets that are going to be released by the main satellite. Space debris is a growing concern for the space community and in mid-term regular missions will be launched to dispose of space junks.

RemoveDebris is a European FP7 project aiming at testing technologies for Active Debris Removal (ADR) in space. It is a low-cost mission to perform several experiments in-orbit representative of operational scenarios with debris position acquisition and tracking, capture and de-orbiting.

The principle platform is the 100 kg main satellite that is capable of deploying two smaller satellites once in-orbit as artificial debris. They will serve as targets for debris capture demonstrations with a net and a harpoon as well as close fly-by. In addition to these two technologies for ADR, a vision-based navigation instrument (VBN) and a dragsail are also placed on-board. The VBN role is to capture 2D / 3D image bursts of the targets while the dragsail will be used to de-orbit the main satellite at the end of the mission. The VBN contains a color camera and a Light Detection and Ranging sensor (LiDAR).



Figure 1: Deployment of RemoveDebris (up right) from the ISS.

CSEM has developed LiDAR technologies for more than 20 years. At the beginning, aerosols and clouds were the targets. Since 10 years, CSEM has developed LiDAR targeting space navigation space. Recently, new applications for terrestrial applications are emerging, such as bathymetry, rock fall tracking or autonomous vehicles.

For space, the usual development line goes through the design and delivery of several models of an instrument. The instrument Technology Readiness Level (TRL) has been increased at each stage until the flight model (FM) is delivered. The FM represents TRL 9. This corresponds to the instrument version that can operate in space with the related environmental constraints (temperature, radiation, vibration, etc.). In general, the technology development process takes place through several project stages and may last more than 10 years.

For CSEM, RemoveDebris is a unique occasion to take a short-cut through this traditional approach. In the frame of the same project, we moved in no more than 5 years from the VBN paper concept to the in-orbit test. To achieve this challenge, CSEM, for the first time, followed a development philosophy inspired by the CubeSat community. The CubeSat standard was created in 1999 in first place to facilitate access to space for university students. Since then, it has got more and more popular as it was adopted

by hundreds of organizations worldwide including private companies. It is the root of many recent commercial initiatives which are revolutionizing the way we access and use space. In this dynamic, new launch services are now available for small satellites. For example, Nanoracks has access to a deployment platform on-board the International Space Station (ISS) that has been used for RemoveDebris after being sent into orbit with the SpaceX's re-usable launcher and cargo.

For CSEM, this context provides the possibility to procure some of VBN building-blocks in a reasonable budget envelop. This covers blocks such as the on-board computer board and some parts of the color camera. Other parts such as the communication interface with the main satellite and the LiDAR were designed from scratch entirely by CSEM with off-the-shelf commercial components. The whole system was also qualified for space re-temperature and in vibration by CSEM.

To date, the commissioning phase is ended. In September 2018, RemoveDebris will experiment the debris capture using the net. The next demonstrations will take place until March 2019 when the dragsail will be deployed to slow down the main satellite until it gets burned in the atmosphere.

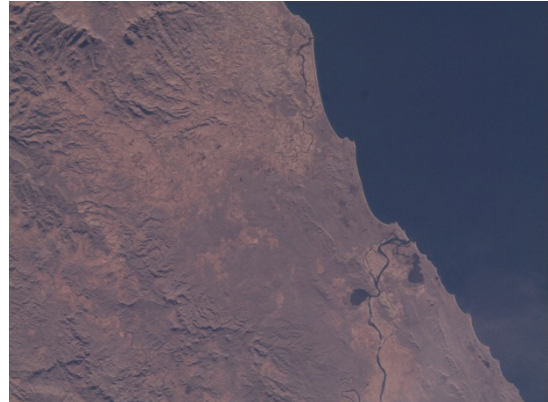


Figure 2: A 2D image of Perth's area taken during the commissioning.

The commissioning of the satellite and the payloads showed that the VBN (including CSEM LiDAR) is fully functional and ready to capture burst of 2D and 3D images for the net, the harpoon and the close fly-by main satellite-target experiments.

The present project is co-funded by the Seventh Framework Programme (FP7/2007-2013) of the European Commission under grant agreement No. 607099 and we do thank the European Commission and the SERI for its financial support. RemoveDebris is led by the Surrey University Space Centre (SSC). Project partners are: Airbus, Ariane Group, Inria, Innovative Solutions in Space, Stellenbosch University and CSEM.

Broadband Swept-Wavelength Infrared GaSb Laser for in-vivo Sensing Applications

N. Torcheboef, S. Droz, I. Šimonytė •, A. Miasojedovas •, A. Trinkūnas •, K. Vizbaras •, A. Vizbaras •, D. L. Boiko

We demonstrate a rapidly (3 ms) and widely (220 nm) tunable, compact external cavity GaSb-based diode laser with a MEMS mirror. It delivers from 6 to 25 mW power over the tuning range, showing a side-mode suppression ratio of >50 dB and controllable mode-hops of ~18 GHz.

We report on a simple and compact tunable GaSb laser in the short-wavelength infrared (SWIR) spectral range for a variety of sensing applications in medical and environmental sensing as well as for industrial applications. The prototype is built within the framework of the Eurostars project SWIRSENSE.

Targeting the spectroscopy applications in the aqueous solutions, we compromise a common spectroscopic requirement for a mode-hop-free tuning of the laser spectrum while providing a broadband tunability (~200 nm) to distinguish the molecules of interest from the background absorption of water. The laser implements an external Littman-Metcalf cavity with a diffraction grating, a light-weight tunable micro-electromechanical system (MEMS) mirror and a treated GaSb gain chip for spectral purity and selectivity (Figure 1). The wavelength tuning is achieved electronically by tilting the MEMS mirror about its pivot axis. High precision movement of the MEMS mirror enables continuous or step-wise wavelength tuning with high repeatability and fast speed.

The largest tunable range of 220 nm is obtained at the pump current of 230 mA [Figure 2a]. The output power exceeds 6 mW at the tails of the tuning range and reaches a maximum of 25 mW at 2220 nm. The mirror is rotated in steps of 0.01°, yielding frequency tuning of 17.7 GHz per step, fully controlled by the mirror tilt angle (Figure 2b). For comparison, the Free Spectral Range (FSR) of the free-running chip is 40 GHz and the FSR of the ECDL cavity is 1.7 GHz. The histogram of the frequency steps (Figure 2c) shows their distribution. The side-mode suppression ratio is larger than 50 dB and confirms the spectral purity of the laser. The mechanical resonance frequency of the MEMS mirror of roughly 195 Hz enables the wavelength sweeping rates in excess of 100 Hz across the entire spectral range.

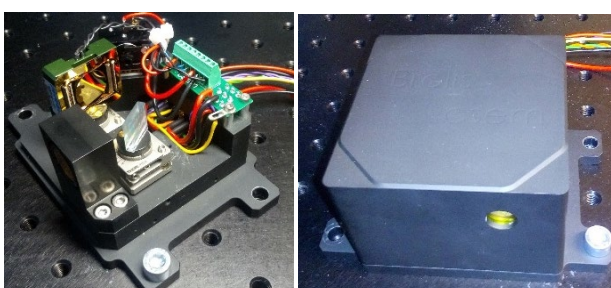


Figure 1: Photographic images of the integrated swept-wavelength GaSb laser prototype.

The swept wavelength source performance is validated in comparative spectroscopic measurements of lactate, glucose, urea and albumin in aqueous solutions as well as a non-invasive in-vivo sensing of human serum albumin through the skin. We obtain an excellent agreement of measured spectra with the corresponding references (Figure 3)^[1].

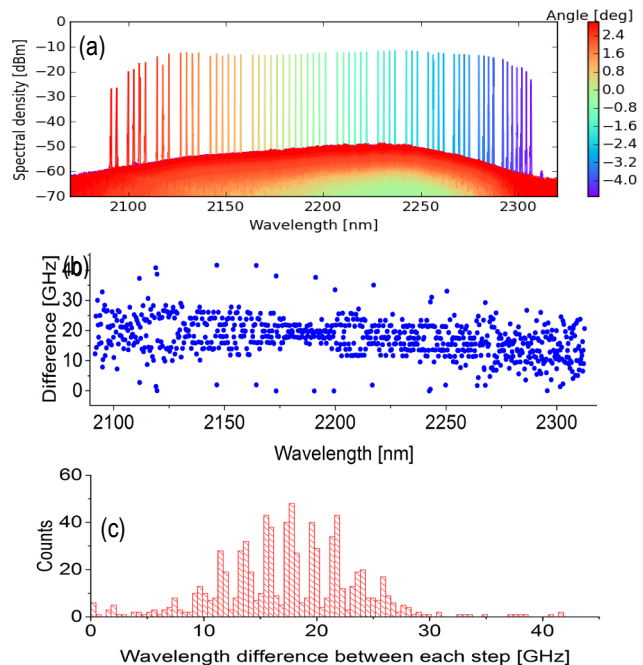


Figure 2: (a) Superimposed lasing spectra showing continuous tuning over 220 nm; (b) Distribution of the mode hop frequencies; (c) Histogram of the mode hop frequencies

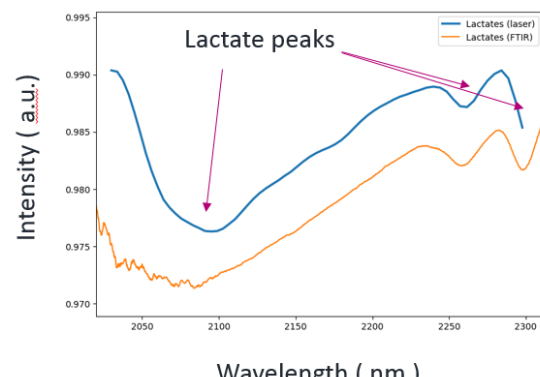


Figure 3: Spectroscopy of lactate solution (30 mmol/l) with our ECDL vs. FTIR spectrometer measurement.

The R&D project partner is Brolis Semiconductors (Vilnius, Lithuania). This work was partly funded by Eurostars program. CSEM thanks them for their support.

• Brolis Semiconductors, LT-14259 Vilnius, Lithuania

[1] A. Vizbaras, I. Šimonytė, A. Miasojedovas, A. Trinkūnas, T. Bučiūnas, M. Greibus, G. Naujokaitė, N. Torcheboef, S. Droz, D. Boiko, Ž. Dambrauskas, A. Gulbinas, K. Vizbaras,

“Swept-wavelength lasers based on GaSb gain chip technology for non-invasive biomedical sensing applications in the 1.7–2.5 μm wavelength range”, To appear in Biomed Opt Express 2018.

High-power Femtosecond Laser System for High-throughput Manufacturing

E. Portuondo-Campa, N. Torcheboeuf, E. Rutz, S. Lecomte

Short pulse lasers are becoming key precision manufacturing tools. In order to increase the manufacturing throughput, femtosecond lasers with high average power are necessary. The Innosuisse project Femtopower has just demonstrated the next generation of such industrial lasers which will find numerous applications on the production floor.

High-power femtosecond (fs) lasers are light sources with rapidly growing impact in modern industrial manufacturing. Unique processes applied to industries producing goods such as solar cells, large flat panel displays and cell-phone touch screens as well as micromachining of medical, automotive and consumer electronics products are key drivers for the widespread implementation of such lasers in manufacturing lines. In conjunction with this broad set of applications, the worldwide market for such lasers has demonstrated a growth of 20% over the last years. This is expected to continue in the future. In order to cope with the applicant's demands for increasing the production throughput and hence further decrease the production costs, femtosecond laser sources with more average output power and/or pulse energy together with sub-500 fs pulses are requested.

In the framework of a CTI (now Innosuisse) project, CSEM teamed up with the company NKT Photonics Switzerland GmbH (located in Zurich) and with the Berner Fachhochschule (BFH) to tackle the challenge of a high-power femtosecond laser. Equally important to the power increase, the source architecture has to be in-line with costs, reliability and dimension of the final industrial laser product. After 2 years of intense efforts, consisting of system simulations by the BFH, and prototype development by NKT and CSEM, the developed laboratory laser system successfully demonstrated cutting-edge performances.

- Average output power of 165 W
- 300 fs pulse duration
- Pulse repetition rate from 500 kHz to 40 MHz
- Beam quality: $M^2 < 1.4$
- Wavelength 1030 nm

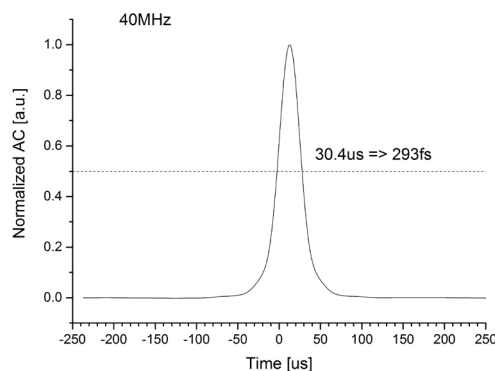


Figure 1: Typical autocorrelation trace at 40 MHz repetition rate.

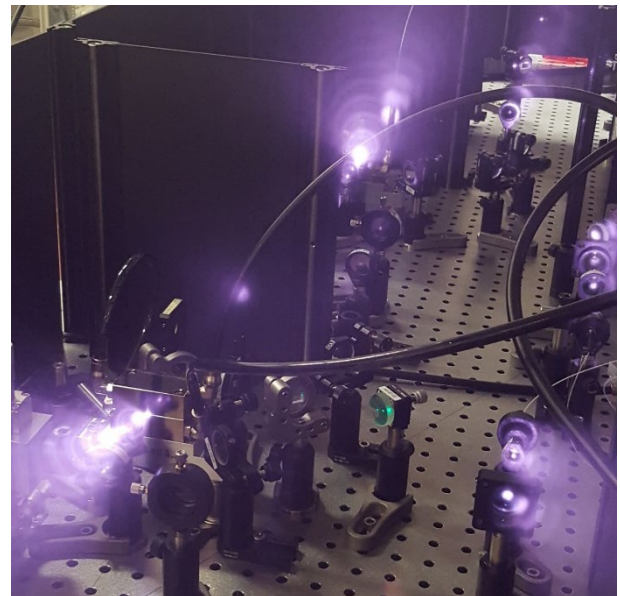


Figure 2: Femtopower system in action.

Figure 3 benchmarks the obtained results with respect to the project initial objectives and the competitive products on the market. A new parameters space has been reached. This achievement has now triggered an intense product development effort by NKT for near future product release

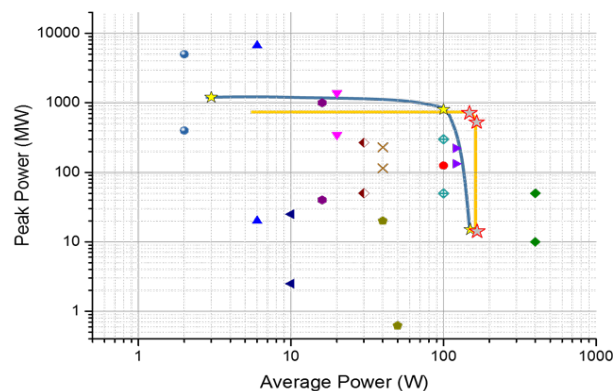


Figure 3: Benchmarking of the Femtopower results (red stars) against project objectives (yellow stars) and products available on the market (other symbols).

In addition, new technical perspectives on high-power femtosecond laser system design have been gained and will trigger further R&D efforts towards even higher power and shorter pulses sources. Future industrial and scientific applications will for sure benefit from these unique laser systems.

CSEM thanks Innosuisse for its support.

oBPM™—Location Independent Continuous Optical Blood Pressure Monitoring

M. Proen  a, G. Bonnier, D. Ferrario, P. Renevey, A. Lemkaddem, R. Delgado-Gonzalo, C. Verjus, M. Lemay

The clinical demand for technologies to monitor blood pressure (BP) in ambulatory scenarios with minimal use of inflation cuff is rising. To differentiate from an increasing number of worldwide actors claiming methods to measure BP, CSEM positions itself in terms of reliable and clinically-supported results. In this context, CSEM accelerated the transfer and validation of its Optical Blood Pressure Monitoring (oBPM™) technology to multiple form factors such as smart bracelets (aktiia), armpods (Biovation), and more recently smartphones (Biospectral, Riva Digital).

The need of medical solutions for continuous blood pressure (BP) monitoring combined with the development of cuffless solutions significantly increased the industrial demand to integrate BP measurement in embedded devices with medical validation. In this context, CSEM transferred its oBPM™ technology – which provides beat-by-beat BP estimates from photoplethysmographic (PPG) signals – to multiple form factors located at different body locations, and performed clinically-supported validations (Table 1). Clinical studies were conducted for each form factor using invasive and non-invasive reference systems, with experimental protocols designed to induce significant BP variations to validate and test the oBPM™ algorithms in real-case and challenging conditions.

Table 1: Summary of clinical studies performed to test the performance of the oBPM™ technology at multiple body locations: 1) Fingertip with smartphone camera; 2) Fingertip with PPG sensor; 3) Wrist with smart bracelet (PPG sensor); 4) Upper arm with armpod (PPG sensors).

Location	Form Factor	Population	Reference
1.		35	Brachial cuff
2.		8	Arterial line
3.		15	Brachial cuff
4.		17	Arterial line

The performance of the oBPM™ algorithms (Table 2) was assessed in terms of the following metrics:

- The average and standard deviation of the difference between the BP estimate and the reference, which allow evaluating the agreement between both quantities in actual pressure units (mmHg). The ISO81060-2 standard for non-

invasive sphygmomanometers sets a maximal error of ± 5 mmHg and a maximal standard deviation of 8 mmHg.

- The correlation between the BP estimate and the reference, which allow evaluating the sensitivity and capability of the algorithms to track BP trends or changes.

Table 2: Performance results of the clinical studies.

Form Factor	Error (mean \pm SD) (mmHg)	Correlation	Publication
	4.0 ± 8.2	0.63	[1]
	0.3 ± 7.7	0.94	[2]
	3.2 ± 4.3	0.75	[3]
	1.1 ± 4.2	0.80	[4]

The overall performances of the oBPM™ algorithms are compliant with the requirements of ISO81060-2 standard for all form factors except the smartphones which exhibit a slightly higher standard deviation than the required 8 mmHg ($SD = 8.2$ mmHg). Nevertheless, further developments are currently conducted to increase the accuracy on the smartphone. The high correlation suggests a strong ability of the algorithms to track changes in BP. Finally, the versatility of the technology to multiple body locations demonstrates its robustness in various contexts of use. On the strength of these results, CSEM collaborates with clinical and industrial partners to integrate the oBPM™ technology in different devices:

- Smartphones: Biospectral (<http://biospectral.com/>), Riva Digital (<https://www.rivadigital.ch/>)
- Smart bracelets: aktiia (<https://aktiia.com/>)
- Armpods: Biovation (<https://www.biovotion.com/>)

[1] J. Sol  , M. Proen  a, et al. (2018), "Blood Pressure Monitoring Using a Smartphone Camera: Performance of the OBPM Technology", Proc. IEEE BHI 2018 International Conference, Las Vegas, USA.

[2] J. Sol  , et al. (2018), "Tracking Blood Pressure Changes in Anesthetized Patients: the Optical Blood Pressure Monitoring (oBPM) Technology", Proc. IEEE EMBC 2018 Annual International Conference, Honolulu, USA.

[3] J. Sol  , M. Proen  a, F. Braun, et al., "Cuffless blood pressure monitoring: experimental evidences of a beat-to-beat PPG technique", IEEE EMBC 2016 Annual International Conference, Orlando, USA.

[4] T. Degen, et al. (2018), "Wearable multisensor for continuous physiological monitoring: a feasibility study of blood pressure", Swiss Medtech Day 2018, Bern, Switzerland.

Pediatric Respiratory Rate Estimation through Deep Neural Networks

P. Starkov, S. Manzano •, F. Hugon •, F. Braun, A. Lemkaddem, C. Verjus, R. Delgado-Gonzalo, J. Sola, A. Gervaix •, M.-R. Benissa •

We present results for respiratory rate determination using deep learning and classic machine learning and based on analysis of respiratory sounds recorded on 48 children less than 60 months old and presenting an acute lower respiratory infection (ALRI). The method has an overall rms error for determining respiratory rate of 0.02 (± 0.86) breaths per 10 seconds.

In low-resource settings, ALRI is diagnosed using children's respiratory rate^[1]. Breaths are counted manually by care givers with one-minute timers. Following our previous publication^[2], this study intends to illustrate determination of respiratory rate through respiratory sound analysis. More precisely, in this abstract, we do present the data acquisition and annotation protocol—a methodology combining deep learning and classic machine learning techniques as well as results regarding automatic respiratory rate counting.

Material

Using the Littmann 3200® electronic stethoscope, chest sounds were recorded from 48 children at the pediatric emergency department of the University Hospital of Geneva. All children were aged under 60 months and had clinical diagnosis of chest infection (fever $\geq 38^{\circ}\text{C}$, dyspnea, polypnea, tachypnea, respiratory distress, cough, or relevant auscultation), and had a parent or a legal representative signing an informed consent. Eight auscultation sites (anterior-posterior, right-left, superior-inferior) were recorded, on each patient, with an average of 10.76 (± 3.42) seconds per site. Recorded sounds were downloaded on a computer using Stethassist® software and annotated using Audacity® software. A board-certified pediatrician annotated inspirations and expirations contiguously.

Methods

Chest sound waveforms were transformed into Mel-spectrograms. An overlapping sliding window technique was used to create 2-second spectrogram patches with 0.0125 s displacement between windows. Each patch was assigned a label, either inspiration or expiration.

A pipeline containing a convolution neural network and hidden Markov model was used for spectrogram segmentation. The network was composed of 12 deep-learning layers, Convolution, Activation and Max Pooling, and 1 Dense layer. Dropout was used as a regularization technique. Automatic respiratory rate was determined by counting the number of inspiration-expiration predicted events.

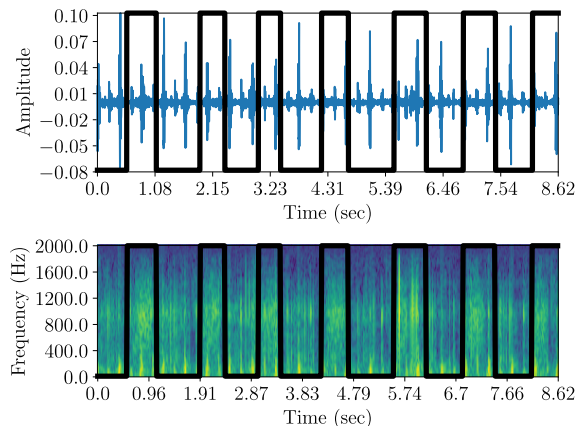


Figure 1: Contiguous inspiration and expiration annotation. Waveform on the top and Mel-spectrogram on the bottom. The black line represents segmentation of inspirations and expirations. When the black line is on the top of the plot, it represents inspiration. When the black line is at the bottom of the plot, it represents expiration.

Results

Automatic respiratory rate determination was performed using leave-one-out cross-validation, meaning that for each patient that is tested, 47 other patients are used for algorithm training from scratch.

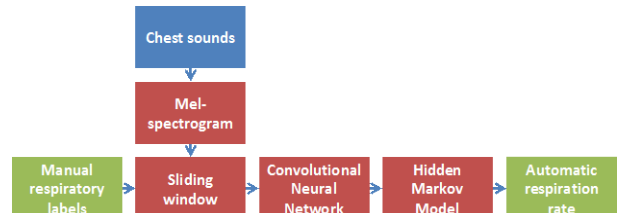


Figure 2: Automatic respiratory rate estimation methodology.

The system predicts chest sound spectrogram sliding window labels with a sensitivity of 85%, a specificity of 87.9% and an accuracy of 86.9%.

Due to limitations in duration of recorded auscultations, respiratory rate was calculated as the number of breaths per 10 seconds. Even though segmentation, through sliding window technique, does not perfectly match manually labeled respiratory events, respiratory rate determination is precise, with an overall root-mean-square error of only 0.02 (± 0.86) breaths per 10 seconds.

• HUG, Hôpitaux Universitaires de Genève

[1] WHO, "Integrated management of childhood illness by outpatient health workers: technical basis and overview. The WHO Working Group on Guidelines for Integrated Management of the Sick Child", Bulletin of the World Health Organization, p. 20, 1997.

[2] J. Solà, et al., "Towards an unsupervised device for the diagnosis of childhood pneumonia in low resource settings: Automatic segmentation of respiratory sounds", Conf Proc IEEE Eng Med Biol Soc., Aug. 2016.

Chest-based PPG for Pulse Oximetry and Non-occlusive Blood Pressure Monitoring

D. Ferrario, P. Theurillat, A. De Sousa, M. Frosio, M. Proen  a, C. Verjus, M. Rapin, P. Liechti, O. Ch  telat

With the global increase of healthcare cost a solution to continuously and inconspicuously monitor the main vital signs is needed to provide an early diagnosis, personalized medical care, and predictive insights. To this aim, CSEM has developed a proprietary chip for dry-electrode electrocardiograph (ECG) and transthoracic impedance measurements^[1]. To complement the monitoring capabilities of this solution, and obtain a unique wearable system, a reflective photoplethysmogram (PPG) sensor was added to allow the measurement of peripheral oxygen saturation (SpO_2) and blood pressure by oBPMTM (CSEM's proprietary technology). The present document depicts the prototype allowing multiple signal monitoring at the chest and the performance of SpO_2 estimation from corresponding PPG signals.

Acquiring PPG signal, from a reflective sensor, with sufficient quality to extract physiological parameters such as SpO_2 or blood pressure is recognised as challenging and in certain conditions, the origin of the pulsatile waveform is still discussed^[2]. To tackle this challenge CSEM has worked on the design of the sensor geometry and on dedicated algorithms to estimate these parameters.

The system shown in Figure 1 combines the advantages of CSEM's dry-electrode technology with the measurement of green, red, and infrared PPG channels, altogether providing a unique system for the monitoring of several vital signs, including ECG and transthoracic impedance, and parameters, such as heart rate, breathing rate, SpO_2 , and physical activity.

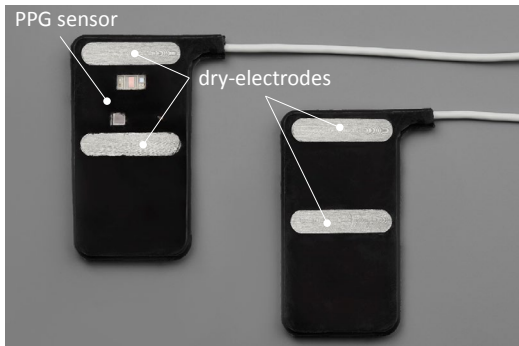


Figure 1: Illustration of the multi-parameter wearable device.

Both sensors contain an own electronics (including a proprietary ASIC) and a battery for 24 hours of autonomy. Data can be stored locally and transferred via Bluetooth for real-time streaming or for download.

Targeting medical application, the system was designed according to the applicable regulations. All materials in contact with the skin are biocompatible according to ISO 10993-1, the system is compliant with the electrical safety standards: IEC 60601-1, and the ECG complies with the medical standard for Holter devices: IEC 60601-2-47.

SpO_2 is estimated from the ratio between red and infrared lights: $R = (\text{AC}_{\text{red}}/\text{DC}_{\text{red}}) / (\text{AC}_{\text{IR}}/\text{DC}_{\text{IR}})$, with AC and DC being the magnitude at cardiac frequencies and non-modulating components of the PPG signals. SpO_2 is then obtained from the ration R using a calibration function. The performance metric recommended by the ISO 80601-2-61 standard is the accuracy

(A_{rms}), defined as the root-mean-square difference between the estimated and reference SpO_2 values.

By taking advantage of the information of the multiple signals acquired at the chest of adult volunteers and by introducing a specific quality index, in a recent study^[3], we were able to reduce the SpO_2 estimation accuracy (A_{rms}) from 6.7% to 3.1%. These performances were obtained after an automatic rejection of low-SNR signals by our dedicated quality index (see table below and Figure 2).

Performance metrics	
A_{rms} without data rejection	6.7%
A_{rms} after data rejection	3.1%
Data rejection rate	30%

These results highlight the challenge to acquire reliable PPG signals with a reflective sensor located at the chest – since 30% of the data were rejected – and the importance of our automatic rejection algorithm, as only the results after automatic rejection of noisy data comply with the requirements set by the ISO 80601-2-61 standard (A_{rms} to be $\leq 4\%$).

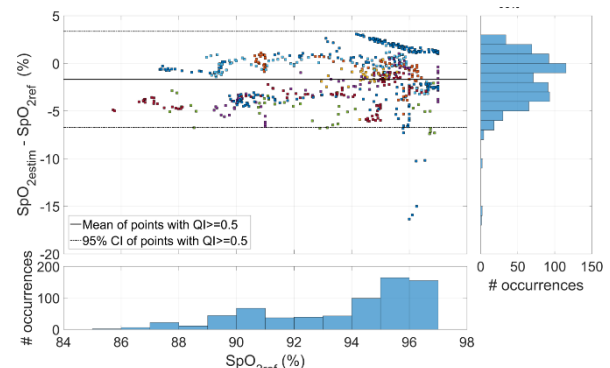


Figure 2: Bland-Altman analysis, each color represents a subject.

Future work should focus on validation under deeper hypoxia since our hypoxia were limited to values $>85\%$. However the promising results and in particular the capacity of the algorithm to rejected noisy PPG demonstrates the possibility to estimate SpO_2 from reflective PPG and pave the way towards oBPMTM estimation at the chest.

[1] P. Theurillat, et al., "Demonstration of a Proprietary Chip for Dry-electrode ECG and Impedance Measurements", CSEM scientific and Technical Report (2017), 118.

[2] A. Kamshilin, et al. (2017) "Origin of photoplethysmographic waveform at green light." Physics Procedia 86: 72-80.

[3] M. Proen  a, et al. (2018), "Performance Assessment of a Dedicated Reflectance Pulse Oximeter in a Neonatal Intensive Care Unit", IEEE EMBC 2018 Annual International Conference.

Wearable Vital Sign Monitoring System for Reinforced Speech Processing

G. Yilmaz, J.-A. Porchet, M. Crettaz, O. Grossenbacher, M. Frosio, O. Chételat, M. M. Doss •

Existing speech technologies largely focus on modeling the oral cavity information from the acquired acoustic signals. However, there are unexploited aspects such as changes in speaker's behavior or psychological state which could effectively be linked to the variations in the physiological signals. Additionally, it is, according to current trends, foreseen that the future of health care and rehabilitation will be shaped by an amalgamation of novel sensing methods, signal processing, and machine learning. Consequently, there is an increasing interest in reinforcing speech processing by means of multi-modal signal acquisition and this work serves to respond this interest.

Sensor solutions developed at CSEM readily provide high quality electro-physiological signal acquisition, such as electrocardiography (ECG) and impedance plethysmography (IPG). Equipping the available systems with acoustic information, such as cardiac or respiratory sounds, is envisaged to open new paths in body signal monitoring.

In this particular work, we collaborate with Idiap Research Institute (Martigny, Switzerland) to reinforce speech processing algorithms that use speech as a biomarker to detect onsets of diseases or behavioral changes such as Parkinson's disease, dementia, and depression^[1]. Moreover, application areas of such a system ranges from remote health care to rehabilitation of people with speech impairments resulting from accidents and medical conditions such as stroke or neuro-degenerative diseases. To this end, a system which can synchronously record speech along with ECG, IPG, and cardiac sounds, is developed. Synchronous recording of these signals enable us to investigate links between temporal changes in speech and physiological signals of interest.

The developed prototype (Figure 1) is built upon a modified version of SENSE, CSEM's proprietary system which can measure ECG, breathing rate, skin temperature and classify activities. The system can be worn by using either the belt or the vest designed for SENSE. Measuring sensor (M) of the SENSE module was modified so that it can create a signal for synchronization of new modules and receive external on/off commands. Data acquisition from SENSE modules is performed via Bluetooth.

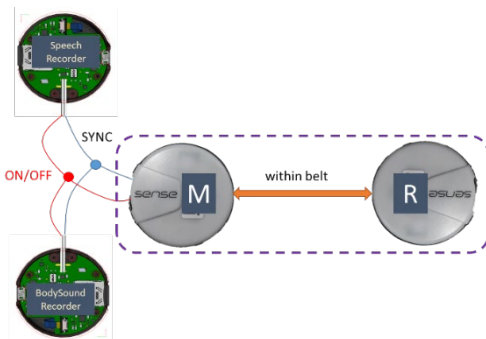


Figure 1: Illustration of the developed prototype composed for multi-modal signal acquisition for reinforced speech processing.

Firstly, a speech recording module is added to the modified SENSE system. This module can synchronously record ambient sound, thus voice of the user as well as others', while SENSE module synchronously records ECG, breathing rate, and skin temperature. It is possible to record for more than 4 hours on a micro SD card inserted into this module. Speech recording unit

employs an off-the-shelf bottom-port MEMS microphone interfaced with proprietary electronics developed at CSEM. Positioning of the microphone has been defined and refined with our collaborator to ensure that quality of the recording is suitable for post-processing.

Body sound recording module (stethoscope) incorporates a contact microphone designed and fabricated in-house. The sensing unit is realized by a piezoelectric material which is formed into a specific shape. The microphone has been tuned to capture particularly cardiac signals, in line with stethoscopes available to clinicians, by modifying its shape. Again it is interfaced with a signal-acquisition chain developed at CSEM. Apart from the sensor and frontend electronics, this module has the same capabilities as the speech recording module. Particular attention is paid to the housing design so that this module minimizes interference of external vibrations and common mode electrical signals, e.g., 50 Hz line signal. Both modules are powered by an internal lithium-polymer battery which can be recharged via USB.

In conclusion, the developed system enables synchronous recording of cardiac sound, ambient sound, ECG, and IPG which reveals breathing rate (Figure 2). For cardiac sound acquisition, it is observed that S1 and S2 heart sounds are clearly distinguishable. In the next phase, Idiap will use this system to collect multi-party conversation data and develop tools for non-verbal analysis of conversations integrating physiological signals.

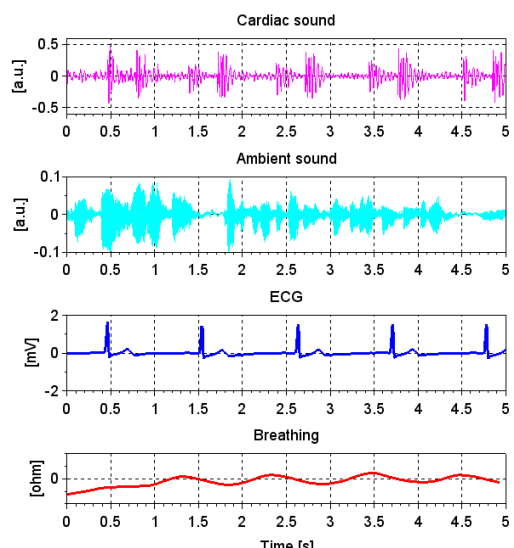


Figure 2: Synchronized waveforms acquired by SENSE and two additional modules designed for speech and body sound recording.

• Idiap Research Institute, Martigny, Switzerland

[1] <https://www.tapas-etn-eu.org>

Common-mode Rejection in the Measurement of Wearable ECG with Cooperative Sensors

M. Rapin, Y.-J. Regammey, O. Chételat

The electrocardiogram (ECG) is among the most frequently used vital sign monitoring. However, the integration of classical ECG Holter in wearables is problematic since shielded cables and gel electrodes are required to get high-quality signals. We have recently introduced a new type of active electrodes (so-called cooperative sensors) suitable for dry electrodes and significantly reducing the cabling complexity. This report details how cooperative sensors address the rejection of the common-mode voltage induced by electromagnetic disturbances. The proposed approach uses an auto-identification technique based on a continuous-time calibration of the system. Measurements on healthy volunteers showed that the signal quality obtained with our system (using dry electrodes) is equivalent to the one measured with a gold-standard medical device (using gel electrodes).

The cooperative-sensor architecture (Figure 1) is based on active electrodes connected by a bus of two unshielded wires (instead of the classical star arrangement and shielded cables). The system is made of one master, one reference (ref.), and at least one voltage-sensing (type V) sensor. The ref. wire sets the common reference potential required for ECG measurement. Any sensor-specific potential on the skin is measured with respect to this wire. The voltages u_1 to u_N are amplified, filtered, and digitized locally by the electronic circuit embedded in each sensor. Each sensor has its own power supply (a battery). The com. wire is used together with the ref. wire for duplex communication between the sensors in order to gather the measured data in the master sensor^[1].

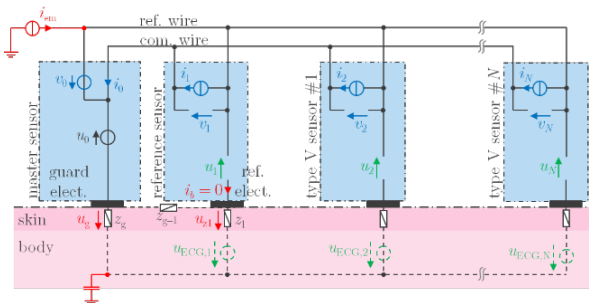


Figure 1: Architecture for common-mode rejection with cooperative sensors. The voltage u_1 measured by the reference sensor is sent to the master sensor and controlled to zero via the voltage source u_0 . The current induced by electromagnetic disturbances is represented by i_{em} .

In this architecture, the electrode potentials are measured with respect to the potential of the ref. wire. Therefore, the voltage u_g induced by the disturbance current i_{em} flowing through z_g sums up to the physiological signal to measure. In order to address this issue, the digitized value of voltage u_1 measured in the ref. sensor is sent to the master sensor where it is controlled to zero by a feedback loop acting on the voltage source u_0 . The sampling frequency of u_1 needs to be fast enough to allow a good rejection of the common-mode voltage. For example, for $f_s = 50$ kHz, one gets a rejection factor of 159 (44 dB) for mains disturbances ($f = 50$ Hz)^[2]. Such rejection prevents the saturation of the sensor amplifiers but is not perfect since the voltage u_1 is not exactly 0. Therefore, the ECG leads are digitally computed as the

difference of the measured signals u_i with the reference u_1 approximately equal to zero.

However, since the voltages u_i are amplified in each sensor, the matching between the gain of each sensor impacts the common-mode rejection. The gain of the sensors depends on the accuracy of resistances, capacitors, and voltage references. Our cooperative-sensor demonstrator reaches an overall common-mode rejection ratio (CMRR) of 78 dB with reasonable tolerance of components. This already comply with the international standard for ambulatory ECG (IEC 60601-2-47) which states that the minimal CMRR shall be at least 60 dB.

Nevertheless, when higher CMRR are required (e.g., for clinical ECG) or if we use lower precision components (e.g., in view of the integration of the system in an ASIC where gain mismatches between chips can reach $\pm 10\%$ at cut-off frequencies), we solve the problem of mismatch between sensors by identifying and compensating for the gains and transfer functions of all sensors^[3]. The identification and compensation process is performed online thanks to an identification signal (0.5 Hz square wave) added to the voltage source u_0 . Since this signal and the ECG are not correlated, averaging on a sufficient long time allows the system to get the sensor responses to the identification signal alone, hence providing the transfer functions (and gains) of all sensors. By signal processing, the transfer functions can then be 'rectified', bringing the total CMRR to very high values (Figure 2).

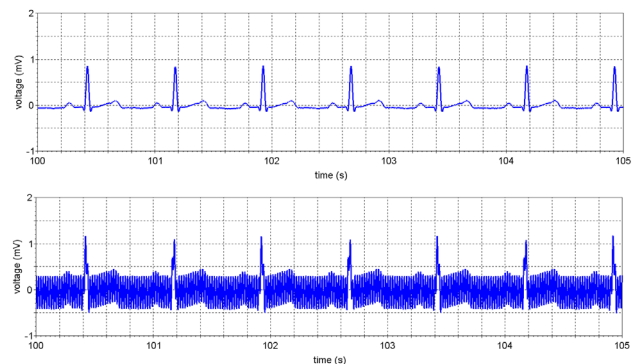


Figure 2: Signal obtained with (top) and without (bottom) the proposed identification and compensation method for a large common mode disturbance (± 50 mV, 50 Hz).

[1] M. Rapin, et al., "Two-wire bus combining full duplex body-sensor network and multilead biopotential measurements," *IEEE Trans. Biomed. Eng.*, vol. 65, no. 1, pp. 113–122, Jan. 2018.

[2] M. Rapin, et al., "Electromagnetic disturbances rejection with single skin contact in the context of ECG measurements with cooperative sensors," *EMBC*, pp. 4427–4430, Jul. 2017.

[3] M. Rapin, et al., "Common-mode rejection in the measurement of wearable ECG with cooperative sensors," www.degruyter.com, 2018, *in press*.

Enhanced Robotic Surgery with Multimodal Sensing

E. Muntané Calvo, D. Ferrario, G. Yilmaz, C. Meier, A. Adler, O. Chételat

Robots have been present in surgery rooms since the early 80's to help surgeons in their delicate procedures. This is what is currently known as Robot-assisted surgery. The tremendous progress made in robotics, computing, and visualization have enabled technology to prove itself of valuable help to the surgeon in operating procedures. This evolution of assistance robotics started as surgeon-based guidance, then evolved to image-guided surgery to be now in the intelligent sensor-guided surgery. In the frame of two collaborative project^[1,2], CSEM in collaboration with ARTORG and Inselspital are bringing sensing capabilities to robot for safer surgery during cochlear implantation and spine operations.

The aim of these projects performed in collaboration with ARTORG and Inselspital is to leverage the capabilities of sensor-guided surgery, introduce augmented robotic technology into the clinic, and begin the process of clinical adoption of the next generation of neurosurgical interventions. CSEM's impedance spectroscopy technology to detect a tissue change is combined with force-density correlation, and electromyography, to provide a multimodal approach to avoid unexpected tissue breach and potential nerve damage. These three sensing technologies provide key aspects to guide the robot and the surgeon in the procedure so as to avoid hurting irreversibly the patient.

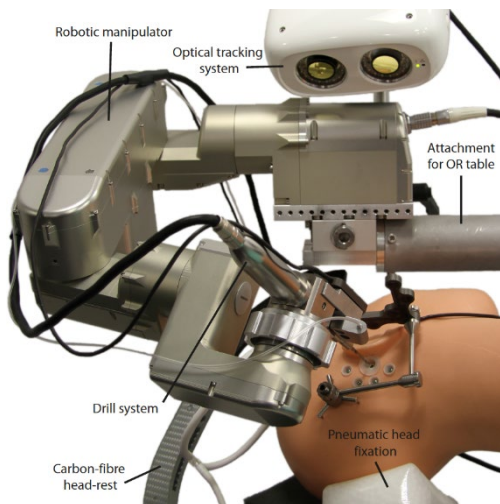


Figure 1: Robotic Aided Hearing Restoration Setup.

In the frame of hearing restoration via minimally invasive cochlear implantation (see Figure 1), these technologies allow a drastic reduction of invasiveness and improve the outcome of cochlear implant surgery. The patient recovery is faster and post-operative hospital stay is shorter. Initial clinical trials were carried out on sheep and the obtained results showed that a multimodal sensing approach enables safe and unsafe distance margins to be discriminated during robotic cochlear implantation to distances down to 0.4 mm^[3].

More recently, in the frame of a BRIDGE Discovery project, the same consortium is developing a new sensor-enabled surgical technology which provides a new level of safety for complicated spinal operations. In the case of spinal surgery procedures,

requirements are even more demanding (in the order of 0.1 mm). This entails developing new technology such as an instrumented drill bit (in collaboration with EMPA) to be able to simultaneously drill while measuring critical distances to the spinal nerves. This new drill bit together with improved multimodal sensing technologies should allow the clinician to differentiate bone from muscular tissue at a higher precision. This will be of extremely valuable help to the surgeon since drill bits will not have to be continuously swapped with probes during surgery in case that a dangerous situation arises.

To optimize the electrode configuration and impedance spectroscopy, several simulations are being carried via finite element analysis of the interactions between the electrical fields generated by the probe when applied to different tissues.

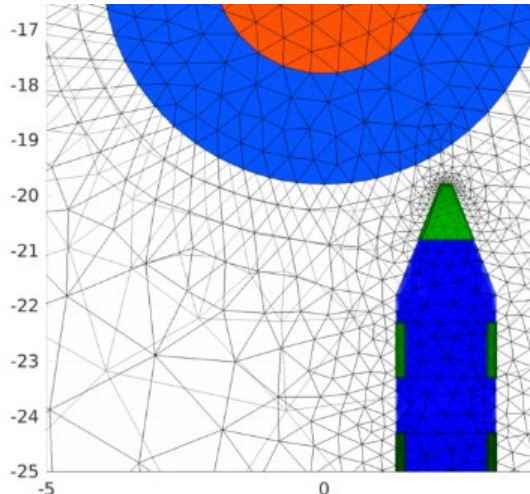


Figure 2: Simulating Interaction between Probe-Tissues Simulation.

Tissue spectroscopy or electromyography are suitable also for other use cases. One could envisage employing them in any situation where surgery procedures encounter tissues of different nature that need to be distinguished or where there exists the danger to damage a nerve.

The projects have been performed in the frame of the Nano-Tera initiative and the BRIDGE Discovery program and CSEM thanks them for their support during the development and the co-funding of the activities.

[1] Nano-tera, HearRestore: <http://www.nano-tera.ch/projects/362.php>

[2] Bridge, Sensor-enhanced surgical robot enables highly precise and safe spinal operations, <https://bridge.ch>

[3] J. Ansò, et al., "(2016). A neuromonitoring approach to facial nerve preservation during image-guided robotic cochlear implantation. Otology & neurotology, 37(1), 89-98.

Flexible, Hollow Organs with Inner Structures for Medical Validation and Training

T. Parkel, I. Stergiou, S. Cattaneo

CSEM developed a new process to fabricate hollow and flexible anatomical organs for validation purposes in various domains. By exploiting the advantages of CAD, 3D freeform modeling and additive manufacturing, complex organs with inner structures and inserts can now be realized in a fully digital fashion, replacing the complex and time consuming manual fabrication methods used so far. Cancer treatment experts are using these novel tools to study the radiation planning and radiation delivery under the influence of respiratory motion

Since several years, CSEM has been developing anthropomorphic breathing phantoms, which, in combination with a versatile phantom ventilator, were used to validate proton beam cancer therapies at Paul Scherrer Institute (PSI). In early prototypes, the complex flexible models were designed and manufactured by assembling discrete parts produced by molding and mechanical machining. As each phantom was essentially handcrafted, the reproducibility could not be guaranteed and the integration of more complex inner structures could not be achieved.

To solve these issues, we developed a new generation of validation organs based on the most recent developments in CAD and additive manufacturing techniques. The newly developed processes allow creating hollow and flexible anatomical organs for validation purposes in various domains, along with setting a digital foundation for further development.

Realistic inner structures were created by merging patient data from a bronchial tube and a lung cancer spot into a new generic lung that perfectly fits into the existing Luca Phantom ribcage. The diaphragm is the most flexible interface between the lung (on one side) and the liver and other digestive organs (on the other side), and should move in SI-plane (Superior Inferior) by approximately 20 mm with every breathing cycle. Other non-organ shapes were integrated as a cutout to place ionization chambers from the outside through the diaphragm into the lung (cylinder shape).

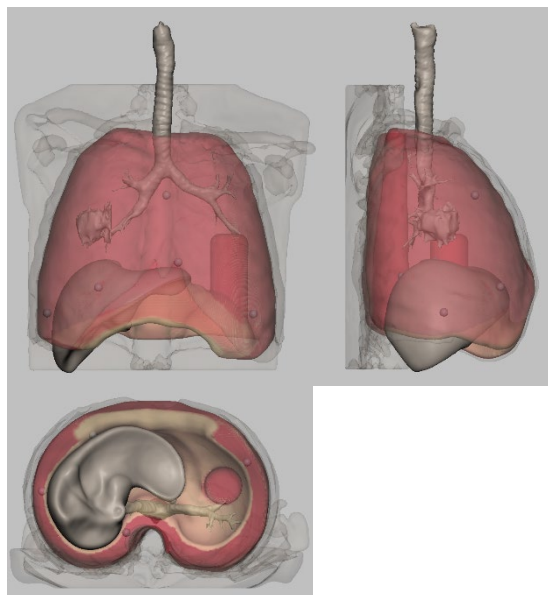


Figure 1: CAD design of generic lung with bronchial tree, tumor spot, CT-MR-markers, diaphragm with tube spacing and connected liver.

To enable the anthropomorphic breathing and motion of the entire lung, its inner open-celled structure with irregular patterns was digitally designed to include various sections with different structure designs and varying elastic properties in both contraction and expansion.

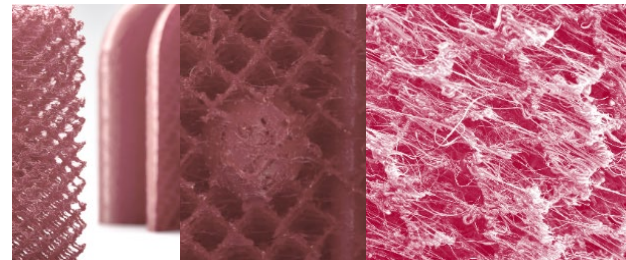


Figure 2: Printed open cell mesh structure with variations between generic tumor sphere and bronchial tube.

A fused deposition modeling (FDM) dual-head 3D printer was mechanically modified to enable printing of TPU soft materials of shore hardness A60. For the support structure a water soluble material (PVA) was chosen. During the printing process 6 CT-MR visual markers were inserted and encapsulated.

In order to make the elastomer materials visible with magnetic resonance imaging (MRI), the entire lung and its inner structure were surface-treated with MR visible material. Since 3D-printed thin flexible walls are known to be permeable to air, the outside of the lung was coated with a thin layer of PUR-skin to make the lung air-tight. The soft tissue displacement under breathing at different locations in the lung is currently being characterized.

With these newly developed processes, CSEM is able to design digital models that can be physically realized with 3D printing to produce various types of flexible, structured and MRI visible hollow anatomical organs. Even multi-organ sections including lung, diaphragm, stomach, liver, bowel with integrated visual markers can be realized, ultimately leading to an entire anatomical validation system. These flexible models will enable the exploration and simulation of soft tissue displacement in complex inner organ structures in a wide range of medical applications.

The future research effort will focus on the development of actuatable, life-like training or validation organs made of even softer material, and on the integration of sensors providing real-time feedback on various medically relevant parameters within the models.

ULTRA-LOW-POWER INTEGRATED SYSTEMS

Alain-Serge Porret

The **Ultra-Low-Power (ULP) Integrated Systems** program addresses the key challenges and technologies required to build very low power, (often) wirelessly interconnected, embedded smart systems or remote sensing nodes. The availability of such components is central to several global technological trends such as the Internet of Things (IoT) revolution, the advent of wearable technologies for wellness and medical applications (in line with the needs of an aging population), and the generalization of machine-to-machine (M2M) communications required by Industry 4.0.

It is generally recognized that the number of interconnected devices will continue to increase exponentially (as wearable items in our clothes or on our wrists, for implantable health monitors, at home in our appliances, to improve the security of our transport infrastructure, to track goods, etc.).

Many of the targeted applications demand packing extended functionalities into tiny, often cost-optimized, wireless nodes. Moreover, in many cases such nodes cannot benefit from wired power, either because the device is attached to a moving part, is mobile or worn, is implanted, or is not located near a suitable power source, or simply because the wiring required to connect large numbers of remote nodes is costly or impractical. Therefore, power consumption needs to be reduced in order to reach a battery life of years or ultimately to match the life of the device. Harvesting energy from its surroundings, when practical, can help in achieving this goal by trickle charging the battery.

Additionally, many types of sensors generate too large an amount of raw data to stream wirelessly. Local processing is therefore required to isolate the useful information from the noise. Embedded artificial intelligence (or so-called edge processing) will provide the tools to efficiently achieve this goal, enabling a paradigm shift from “big data” to “smart data”.

This ambitious vision requires significant advances in a number of fields, ranging from system architectures to hardware devices

and algorithms (see Figure 1). It covers in particular energy storage (not studied here), energy harvesting (covered by the **PV & Energy Management** program), energy management, wireless communications, sensor interfaces, advanced embedded data processing hardware, efficient machine learning algorithms, and resource-limited machine vision.

The program focuses on the “edge” of the Internet—the frontier between the real world and the collected data sent to servers or to the Cloud. The ultimate overarching goal is therefore to provide tools to measure any physical quantity, extract any meaningful information (processed, as opposed to raw data), and—more generally—interact remotely with everything, everywhere, whenever useful. This will be made increasingly possible by trending toward devices characterized by:

- Zero batteries—unlimited life and based on energy harvesting
- Zero cost—to allow data collection everywhere in ubiquitous ways
- Zero size—for miniature, invisible, pervasive sensing
- Zero failure—through robust design and redundancy
- Zero hassle—easy to install, self-configuring, no maintenance

This course is largely enabled by today's mature IC technologies—which allow the packing of an incredible number of interfaces and of remarkable amounts of computational power in an ever-smaller volume, with constantly shrinking costs and lower power consumption—and is also clearly aligned with the so-called More than Moore paradigm. Therefore, the development of ASICs (application-specific ICs) is a significant component of the program, although reliance on COTS (commercial, off-the-shelf) solutions is preferred when suitable devices are already available.

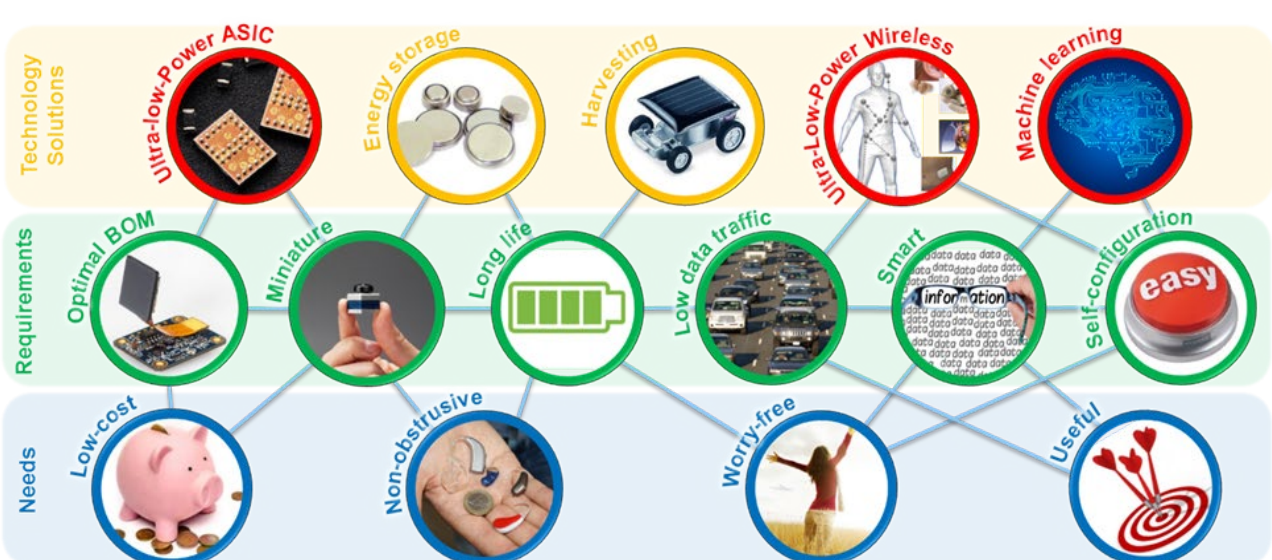


Figure 1: Needs, requirements, and solutions for modern IoT and wearable devices.
The circles highlighted in red are some of the key challenges covered by the program.

The markets covered by the program are very diverse, as the generic nature of Figure 1 suggests, and are growing in scope with the development of the Internet of Things (IoT), which is also aligned with the megatrends of “wireless everywhere” and “smart everything”. Applications covered by this research program include:

- Consumer electronics (Bluetooth Smart devices, GPS-enabled devices, home automation and security systems, and image processing for occupancy analysis)
- Industrial systems (high-performance sensor interfaces, sensor networks for harsh environments, and optical quality control)
- Metrology (integrated measurement microsystems or optical encoders for various purposes)
- Medical and wellness (implants, vital sign monitoring, and electronic prostheses)
- Automotive (smart sensors in harsh environments, tire monitoring, driver attention monitoring)
- Aeronautics (distributed sensors and touchless man-machine interfaces)

The **ULP Integrated Systems program** is subdivided into three research activities and the main areas of focus are summarized below for each.

Wireless Systems: (1) Reduction of the effective energy per bit required to send information through a realistic network, with stringent latency, security, robustness, or quality-of-service requirements. (2) Development of high-performance integrated transceivers. (3) Use of electromagnetic waves for ranging, localization, and remote sensing (for instance for vital sign monitoring).

Vision Systems: (1) Development of very low power imagers. (2) Development of machine learning algorithms with a special emphasis on embedded systems. (3) Design of specialized compact smart cameras, inside and outside of the visible spectrum, including with multi/hyper-spectral capabilities. (4) 1D to 6D accurate position measurement through optical means.

System-on-Chip: (1) Mastering of extremely low power (ELP) subthreshold logic design techniques. (2) Design of ELP mixed-signal sensing interfaces, with an emphasis on vital sign monitoring and timing devices. (3) Dedicated architectures suitable for ELP logic, including multi-core processors and dedicated accelerators, for example for artificial intelligence inference. (4) Design of the supporting power management circuits.

These efforts resulted in notable advances in 2018. A selection of topics covered subsequently is briefly highlighted below.

Regarding low-power wireless sensor networks, the upcoming 5G standard is discussed in the context of its use for Internet of Things applications in demanding environments in “5G Technologies for IoT and Low power Wireless Communications”.

Two additional papers describe solutions to real-life, demanding applications. “Interoperability of ULP Wireless Sensor Networks” proposes a solution to enhance a water supply monitoring network while guaranteeing backward-compatibility. “A Power Optimized Hybrid TDMA-WiseMAC Switchable Protocol for Hand

Prostheses” describes a multimode MAC protocol that adapts to strongly varying network traffic conditions.

The topic of “interfacing life” with electronic devices is addressed, for in vivo applications, in “Miniature Acquisition, Processing and Wireless Communication System on Chip for Prosthetic Applications based on Electromyography (EMG)” and “Switched capacitor Degeneration for PVT Robust and Power Efficient Biomedical AFEs”. In vitro stimulation and readout of the electrical response of a “brain slice” is explored in “High Density Microelectrode Array with 4096 Full-duplex Channels”.

The design and capabilities of generic low-power short distance communications are investigated in “An active Near Field Communication (NFC) System” and “Link Budget, Power Trade offs using Optimized Bluetooth 5 Transceiver IP”.

The opportunity to operate at much higher frequencies for radar applications, but within a similarly tight power consumption budget, is explored in “Comparison of 20 GHz Low power Wide range Oscillators in 28 nm CMOS” and a possible application is described in “Remote Vital Signs Monitoring using a FMCW Radar and Machine Learning”.

Power management is becoming more and more complex and central to the performance of a complex ULP SoC, especially since efficiency needs to be high for a wide operational range, from always-on mode to full-power computation or data transmission modes. A solution to this problem is proposed in “A Highly Efficient DC-DC Buck Converter for Load Currents from 1 μ A to 50 mA”.

Great efforts were committed to the development of low-cost, resource-limited smart cameras:

- Optimization of a CMOS imager toward the goal of VGA resolution below 1 mW of power consumption, in “An Ultra-low Power High Dynamic Range Image Sensor”
- Design of efficient hardware classification accelerators in “FastEye+: A High-speed Camera with Embedded Neural Networks for Smart Vision”
- Improvement of algorithms operating toward embedding in inexpensive hardware in “Efficient Deep Learning Algorithm for Person Detection from Ceiling Mount Cameras” and “Intelligent Multispectral Imaging System for Detecting Human Skin”

Finally, the all-important topic of data validation, often ignored and leading to the feeding of widely inaccurate data into complex information processing tools, is explored in “Data Validation using Machine Learning”, in the hope of avoiding “garbage in, garbage out” syndrome.

Interoperability of ULP Wireless Sensor Networks

D. Piguet

CSEM can improve the reliability and lifetime of legacy wireless networks through the development of tailor-made wireless communication protocols, a custom interoperability layer and the addition of backbone relays based on recent technology adapted to the legacy system. The development and successful deployment of a compatibility layer between two generations of the LORNO wireless sensor network for water supply monitoring serves as a showcase for CSEM's competences in this field.

Hinni AG is the Swiss market leader in the production, sales and maintenance of water hydrants and associated services. More than a decade ago, Hinni introduced the LORNO wireless monitoring system for the public water distribution network. The concept uses water hydrants as access points to the underground pipes. They are equipped with wireless sensors capable of measuring the status (opened / closed), temperature and pressure, as well as a hydrophone for leak detection and, for the most recent system generation, leak localization. The sensor measurements are transmitted to relays installed on street light posts and forwarded to a gateway connected to the internet.

CSEM was selected by Hinni as the developer of the communications system for the new generation of the LORNO wireless monitoring system. The solution developed by CSEM brought considerable improvements: time synchronization to support leak localization, self-organization of the network, latency reduction by two orders of magnitude.

Even though the new generation ("LORNO 3") is a success, it is not always feasible or desirable to replace hydrants equipped with the earlier generations ("LORNO 1" and "LORNO 2") with the new one due to mechanical compatibility issues on old hydrants, etc. Nevertheless, Hinni customers who wish to keep their LORNO 1 & 2 sensors still can benefit from some of the improvements brought by LORNO 3 by replacing relays in the street light posts by LORNO 3 relays that are able to communicate with LORNO 1 & LORNO 2 sensor nodes.

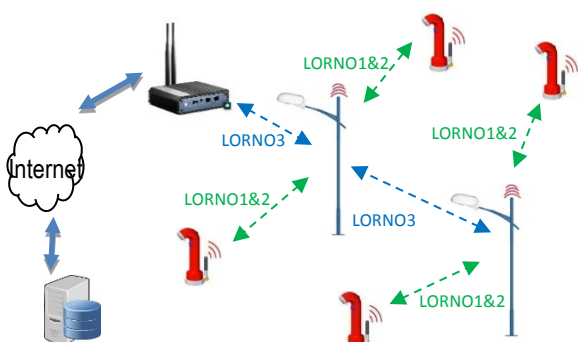


Figure 1: Older generation water supply monitoring network with an interoperable new generation backbone of relays.

The resulting hybrid network consists of a self-organized LORNO 3 relay backbone. The LORNO 3 relays communicate with earlier generations of the sensor nodes installed on hydrants thanks to a compatibility protocol layer implemented on the relays, which controls the transfer of messages between a LORNO 3 relay and a legacy wireless sensor.

The interoperability layer ensures the compatibility of the older and newer generations in spite of the inherent challenges due to the technical gaps and differences between the two generations of networks: the physical layer and the communication protocols are very different. Whereas the older LORNO generations rely on pre-configured network topologies and deterministic access (TDMA – Time Division Multiple Access), the new generation is

self-organized and uses WiseMAC, an adaptive wake-up preamble random access Medium Access Control. The physical layer characteristics are also different (waveform modulation, bitrate, coding). In such situations, early identification of (future) compatibility requirements is essential. In this case, Hinni identified them in the specification phase of the new generation system. This enabled selection of compatible hardware, meaning a radio that can be configured to operate with the waveform characteristics of both generations. Also important was the selection of a micro-controller with sufficient program memory to accommodate protocol extensions, such as a compatibility layer.

The compatibility layer itself was developed after a careful analysis of the previous generation protocol. An important constraint was the fact that it is not possible to modify the firmware of the previous generation modules due to physical access constraints. Also, on-site measurements and reverse-engineering were necessary in order to accommodate unexpected frequency variations due to the aging of the hardware in the older generations of modules. The ultra-accurate time synchronization protocol used for leak localization in the new system is employed in the compatibility layer to enforce the transmission schedule of the sensor nodes in the older modules. Additionally, smart exploitation of the limited similarities between the two systems results in an optimal implementation with reduced use of resources and minimal configuration.

Thanks to the development of the custom interoperability layer, networks equipped with LORNO 1 & LORNO 2 connected to LORNO 3 relays benefit from numerous advantages. The first one is extended lifetime because the procurement of older electronic boards from the previous generation is becoming increasingly difficult as many components are no longer available on the market. More importantly, the reliability is improved and the transmission delays are shortened thanks to more frequent transmission opportunities in the new generation backbone network. Given the multi hop nature of the networks, this is especially beneficial for long fragmented messages in presence of difficult propagation conditions.

The new compatibility extension is available since the beginning of 2018 and Hinni regularly installs interoperable LORNO 3 relays in cities and villages owning LORNO 1 and LORNO 2 equipped hydrants.

5G Technologies for IoT and Low-power Wireless Communications

D. Piguet, L. Bergamini, P. Dallemande

CSEM is exploring future cellular communications technologies and their applicability to Internet of Things (IoT) applications in demanding environments that require high reliability, low latency and low power solutions. In addition to broad-based hardware and software development expertise, CSEM is acquiring practical knowledge leveraging its extensive competence in testbeds, laboratory measurements and network simulations.

The Internet of things (IoT) refers to connected objects of all sorts. The objects can be simple (a temperature sensor) or complex (a train, an autonomous drone). Some are restricted to local or even personal communications (e.g., wearable devices such as heart-rate monitors), whilst other objects can be part of a more complex system involving long distance communications, for instance, in smart cities applications, transportation and environmental monitoring systems. Even when the object can communicate only locally, there is often an access point or base station which relays the information to the wider network. In most cases, the object has a direct wireless link to an access point or it is part of a more complex network where nodes are interconnected and can relay each other's data to a gateway. In some cases, the gateway is connected to the internet using a cellular network like 3G.

Some objects installed in remote locations, or which are mobile like vehicles, may access the cellular network directly, but they must have a large battery (or other power source) due to the potentially long distance to the base station, as well as to support potentially large data rates that may be required. For these reasons, cellular communications consume much more energy than the low power local connections such as Bluetooth (i.e., up to 100 times more). Another shortcoming of current cellular networks with respect to their use for IoT connectivity is that they are optimized for voice and broadband data services, less so for high concentrations of low data rate and low resource devices typical in the IoT.

Over the past few years, LPWAN technologies (Low Power Wide Area Network) have emerged which offer low power and long distance radio communication for low data rate devices. The most popular LPWAN solutions today are Sigfox® and LoRa®; two commercial products operating on the 868 MHz ISM band. Although on average such systems can support a range of 10 to 15 km, their capacity is limited to several bytes every 10 minutes in order to reduce energy consumption and to respect the emission rules of the ISM band.

Recently, the 3rd Generation Partnership Project (3GPP), which is the standardization body for cellular networks, began to show interest and has proposed solutions in the recent cellular network standards releases. 3GPP added a new branch of standards within 4G-LTE (Long Term Evolution) that introduces LPWAN in the cellular system. Diverging from the traditional "wider bandwidth, higher data rate" paradigm, the new 4G categories of NB-IoT (NB for Narrow Band) and LTE-M (M for Machine) offer narrower channels with increased link budget in order to address the needs of IoT devices. Typical applications include, for example, wireless meters (e.g., gas, water or electricity), which are often installed in the basement of buildings where the cellular network coverage is limited.

Thanks to the use of regulated spectrum and controlled resource allocation, NB-IoT and LTE-M support higher data rates and potentially large numbers of users. Furthermore, radio spectrum

resources has been allocated to LPWAN in the guard bands between regular LTE channels.

Beyond NB-IoT and LTE-M, 3GPP is currently working on 5G, the 5th generation of cellular networks. For the first time, connected objects and machine type communications are taken into account from the start in a new cellular generation. Indeed, 5G targets three families of use cases:

- eMBB – enhanced Mobile Broadband: wider bandwidth, ultra-fast data rate (ultra-high definition video, virtual reality)
- URLLC – Ultra Reliable and Low Latency Communications: support for mission critical and real-time applications such as vehicular communications and drone control
- mMTC – massive Machine Type Communications: high numbers of wireless sensors and actuators

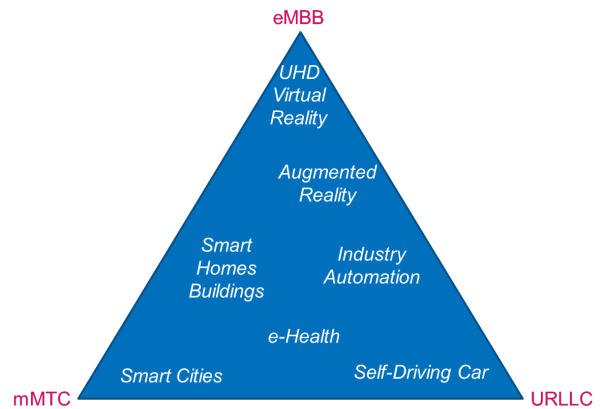


Figure 1: 5G use case families.

The standards for URLLC and mMTC will be published by the end of year 2019. CSEM is closely monitoring their evolution and uses its expertise in networking protocols, software and communications circuits in order to assess the relevance of 4G IoT technologies and future 5G solutions to meet the needs of its customers. Important questions to be considered include the spectrum regulations, network capacity, potential power reduction and the ability of the operators to optimally allocate the available spectrum across very diverse applications.

CSEM also has substantial competences and assets in the domain of radio propagation measurements and is in contact with telecommunication operators for the deployment of testbeds. Additionally, CSEM has extensive experience with network simulators and uses them to evaluate the suitability of new communication technologies for a specific application.

Data Validation using Machine Learning

E. Daskalaki, J.-D. Decotignie

Data validation and cleaning are challenging tasks which are crucial for the development of reliable machine learning algorithms and data-based applications. To date, these tasks are performed manually or with the use of hand-crafted algorithms, a procedure that is very time consuming and possibly sub-optimal. Our objective is to investigate, design and develop automated data validation and cleaning techniques via the use of machine learning and deep learning architectures.

Data validation refers to the assessment of the quality of data produced by a single sensor, a sensor network or a heterogeneous group of sensors. Sensor data may present outliers, out-of-range values, drifts, biases and frozen values (fail-dirty). On a wireless sensor network scenario, faulty data may result due to communication problems (e.g., missing/corrupted data, synchronization issues) even if the individual sensors are properly working. Data validation may also refer to the identification of redundancies, complementary information or duplicates in the data as well as to the case where data are influenced by external factors (e.g., multi-path). Finally, data validation aims to identify the source of errors in order to initiate the cleaning process.

An important aspect of data validation is anomaly detection. Anomalies are events in the data which present different statistical characteristics than the nominal dataset. An event may arise from a sensor(s) problem but it may also be attributed to the system under measurement (e.g., failure of the machine). The starting point most methods for anomaly detection is the development of a model which characterizes the nominal data distribution. Detection of an event is performed by measuring the statistical distance between the model's error during run time and the nominal model error distribution. To date, the state-of-the-art approach for anomaly detection using machine learning is based on an encoder-decoder model^[1]. Various distance metrics have been proposed such as the Mahalanobis distance and the Kullback-Leibler divergence. The general scheme of anomaly detection is shown in Figure 1.

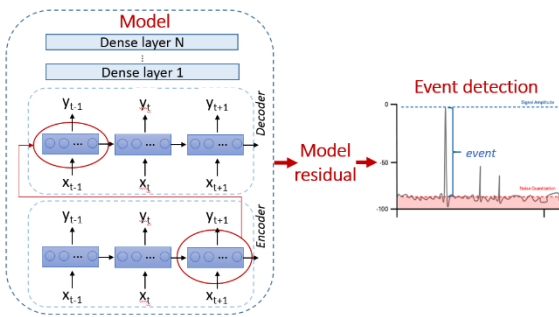


Figure 1: Anomaly detection architecture based on encoder-decoder.

In this work, an algorithm based on the encoder-decoder scheme has been developed for event detection in data. The algorithm was optimized and tested on different datasets. Results on two of these datasets are presented hereafter.

[1] P. Malhotra, et al., "LSTM-based encoder-decoder for multi-sensor anomaly detection." arXiv preprint arXiv:1607.00148 (2016).

The first dataset is related to fraud detection in oil transactions. The provided data are comprised of 29 measurable features related to the transaction as well as ground truth information with respect to "fraud" or "not fraud". Figure 2 presents the Mahalanobis distance between the model's run time error and the nominal error distribution obtained during training. It can be seen that the fraud period is denoted by increased distance values.

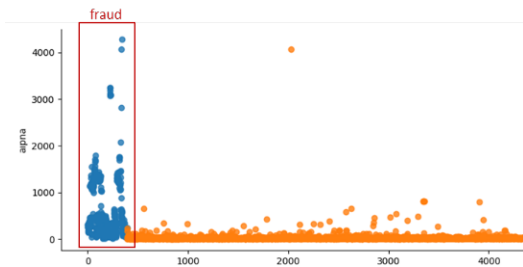


Figure 2: Model output for fraud detection.

The second dataset contains measurements from six sensors attached to a milling tool including AC/DC spindle motor current, table/spindle vibration and table/spindle acoustic emission^[2]. The flank measurement at the end of each run is the ground truth of the tool's "health" condition. The model is evaluated for each run over the tool's life cycle. Figure 3 shows an increasing model error through the life cycle of the tool which can be used as an indicator of the tool's life expectancy.

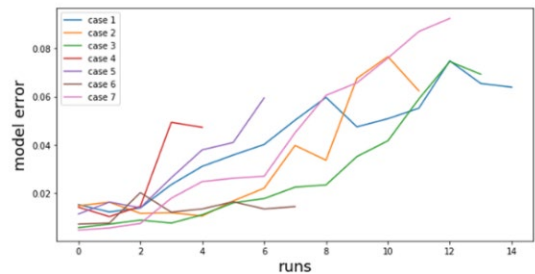


Figure 3: Model error during the milling tool lifecycle.

Our preliminary study demonstrates the feasibility of automatic data validation. Challenges remain with respect to the design of the algorithms and the definition of the distance metrics. Next steps include the assessment of the developed algorithms on different datasets, the exploration of further data validation strategies and the development of automatic data cleaning methods.

[2] A. Agogino, K. Goebel (2007), BEST lab, UC Berkeley, "Milling Data Set", NASA Ames Prognostics Data Repository (<http://ti.arc.nasa.gov/project/prognostic-data-repository>), NASA Ames Research Center, Moffett Field, CA.

Remote Vital Signs Monitoring using a FMCW Radar and Machine Learning

E. Daskalaki, N. Gonçalvez, O. Vorobyov, C. Hennemann, E. Le Roux

A remote vital signs monitoring system was designed and developed based on a frequency modulated continuous wave radar. Signal processing and machine learning-based techniques were explored for the detection of respiration and heart rate (HR) and the effect of the respiration pattern on the quality of HR estimation was investigated and demonstrated.

Radio-frequency (RF) sensing enables the remote and unobtrusive measurement of vital signs (VS) without the need to wear any special device or clothing and under any lighting conditions opening the door for applications from hospital care and assisted living to automotive. A RF VS sensing demonstrator, based on frequency modulated continuous wave (FMCW) radar, was designed and developed in the framework of the M3TERA H2020 project [1]. Previously, a continuous wave radar had been developed to demonstrate the principles of remote VS sensing [2]. The developed FMCW radar demonstrator operates at 110 GHz with bandwidth of 1 GHz. Ultimately, the target is to operate in either the 122.25 GHz ISM band or the 60 GHz ISM band. To achieve mm-wave frequency operation, a super-heterodyne architecture was implemented with a mix of commercially available and internally developed components.

Separation of the HR signal from the respiration harmonics is a crucial challenge with respect to reliable estimation of the HR remotely via RF. In order to investigate and better understand the effect of respiration on the HR estimation, and the potential to improve the reliability of the demonstrator further, a measurement protocol was defined. This protocol covers four cases of: i) normal breathing, ii) slow breathing, iii) rapid breathing and iv) periods during which the test subject held his or her breath. VS estimation was performed using the phase of the received signal. The reference HR and breath rate (BR) were monitored at the same time with an ECG device.

For the detection of BR, three algorithmic approaches were investigated: i) Fast Fourier Transform (FFT), ii) Hilbert transform and iii) adaptive instantaneous frequency detection. The standard FFT outperformed the other methods with an average estimation error of less than three breaths per minute.

For the case of HR detection, three standard techniques were first investigated including i) FFT, ii) Adaptive Harmonic Notching and iii) Principal Component Analysis. While FFT presented the best performance, its reliability depended strongly on the respiration pattern. To this end, as a next step, two advanced algorithmic techniques were explored based on Machine Learning (ML).

In the first approach, a Long-Short Term Memory (LSTM) neural network was developed for the separation of the HR spectrum from the mixed phase spectrum containing both HR and BR. The root mean square error (RMSE) between the reference and estimated HR was decreased by 50% compared to FFT for the case of rapid breathing, while the performance was improved for

all breathing patterns. The RMSE was 18, 10, 13 and 7 bpm for fast, normal, slow and no breathing respectively.

In the second approach, a model of the received signal's phase was developed for the prediction of future phase values based on a LSTM neural network. The difference between the actual and predicted phase signals maintained the HR information as part of the model's residual while removing the dominant respiration component. Figure 1 presents the actual and the predicted signal (left) along with the spectrum of the original and residual signal (right) where the suppression of the respiration peak can be observed.

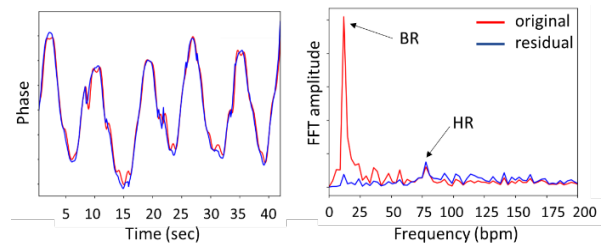


Figure 1: Actual and predicted phase (left) and spectrum of original signal and model's residual (right).

As a second step, the residual signal was used as an input to a FFT-based algorithm for the detection of the HR. Figure 2 depicts an example of HR detection using this approach during normal breathing. It can be seen that the estimated HR closely follows the reference HR monitored by the ECG.

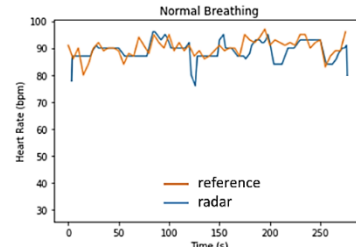


Figure 2: Reference and estimated HR with the predictive LSTM model.

The results demonstrate the effect of the respiration pattern on the HR detection and show that ML is a promising solution for improving the reliability of HR detection. The next steps include: i) exploration of additional ML strategies, as well as, their combined use for reliable HR detection under any breathing pattern ii) transition to a commercially available radar platform in order to realize an ultra-compact, lightweight remote VS demonstrator and 3) investigation of antenna polarization and angle position to help optimize signal quality.

[1] M3TERA (EU project under GA No 644039) <https://m3tera.eu>

[2] O. Vorobyov,,et al., "Feasibility of remote vital signs sensing with a mm-Wave CW reflectometer", IEEE 38th International Conference

A Power Optimized Hybrid TDMA-WiseMAC Switchable Protocol for Hand Prostheses

L. Bergamini, B. Perrin, P. Dallemande, J.-D. Decotignie

WiseTOP is a multimode Medium Access Control (MAC) protocol which adapts to strongly varying network traffic conditions, while enabling low power operation. WiseTOP is particularly efficient in applications exhibiting both sleep and active modes, e.g., arm prostheses for which periods of low duty-cycled operation alternate with periods of high throughput, intense activity.

Radio communication typically consumes the majority of the energy in a wireless sensor network (WSN). One way to reduce the power consumption is via duty cycling of the radio, thus allowing the sensor nodes to sleep as much as possible and transmitting only when needed. The result is lower power consumption, at the cost of higher latency and lower throughput and this can be acceptable for most scenarios. When dealing with a low-power wireless network in which the traffic may vary from periods of almost no traffic to high traffic intensity and strict latency requirements, however, a tradeoff is necessary: on the one hand, using a low power protocol does not guarantee the required performance when the traffic exceeds a given threshold, while on the other hand, the use of a high-performance protocol may waste precious energy when the network traffic load is very low.

WiseTOP is designed to quickly adapt to widely varying traffic conditions. It does so by combining two different MAC layer protocols, each of them best suited to a particular operating region with respect to the traffic load, and by defining the criteria that determine when to switch the whole network from one protocol to the other. For the specific application, a 2.4 GHz radio was used, so the protocol supports a channel hopping mechanism to protect the communications from external interference (e.g., Wi-Fi or Bluetooth).

The first and default protocol is WiseMAC, which addresses less demanding application requirements in terms of throughput and latency while guaranteeing very low energy consumption. The second protocol is based on Time Division Multiple Access (TDMA) which handles the high-throughput and bounded latency requirements of the application when the traffic load is high. In WiseTOP, one of the nodes takes the role of network coordinator and periodically transmits a beacon which contains the allocation of transmission slots for all the nodes in the network.

A Traffic Management Module (TMM) running at the application level at the sink, enables the WiseTOP solution to adapt to different types of applications. The TMM is responsible for analyzing the current traffic status of the network, for deciding which MAC protocol should run at a specific moment and for exchanging traffic status information with other nodes in the network, which it does by piggybacking the information in a data message. The switching criteria depends on the specific requirements of the application and may vary from one application to another.

The experiments performed at CSEM were aimed at measuring the energy consumption and communication performance of the two protocols. The overall consumption of a protocol results by the sum of the cost in terms of energy of all of the basic operations performed by each of the protocols: reception, transmission and baseline consumption (e.g., the minimum amount of energy needed to make the protocol work).

Figure 1 depicts the energy needed by the two protocols with respect to the number of transmitted packets. As we can see in

the picture, WiseMAC offers better energy efficiency when the traffic offered to the system is lower than about 20 packets/minute, while the TDMA protocol is more energy efficient above this threshold. The energy saving offered by WiseMAC over TDMA is particularly evident when the number of transmitted packets is extremely low (1-2 packets/minute): in this situation WiseMAC divides the power consumption by about 2 compared to TDMA. When the traffic increases, however, the overall consumption is lower for the TDMA protocol. The reason for this is that the overhead associated with a single packet transmission and reception is higher in WiseMAC than it is in the case of the TDMA protocol, while the overhead required to maintain TDMA operation is higher than it is in the case of WiseMAC. In both cases, the reliability of the communication system is close to 100%.

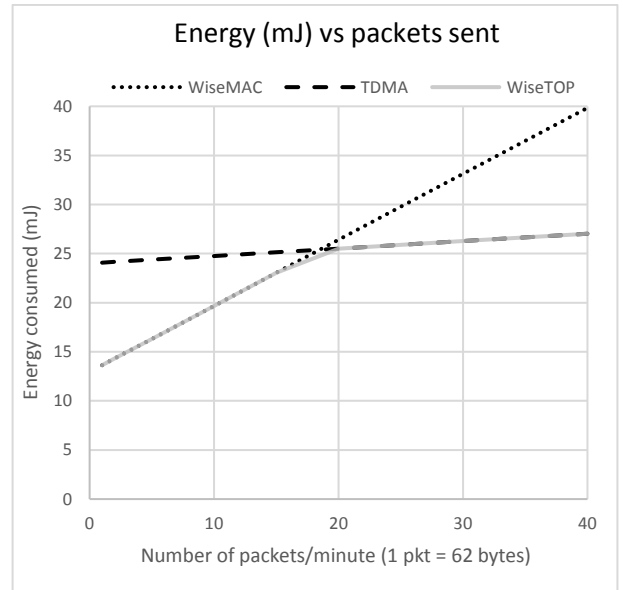


Figure 1: Energy consumption and transmitted packets.

The results obtained on a small yet real testbed in laboratory demonstrate the benefits in terms of power consumption and communication performance. The current implementation runs on the CSEM WiseNode platform and will be ported to custom ultra-low power CSEM hardware, optimized for the target prosthetics application. The switching mechanisms operate as expected from one MAC to the other. The proposed approach, designed for a prosthetics application, is also suited to other potential applications, such as wireless sensor and actuator networks in cars, planes, drones, etc.

This project is partly supported by the European Commission under the Horizon 2020 Framework Program for Research and Innovation (LEIT-ICT-24-2015, GA #687905).

Comparison of 20 GHz Low-power Wide-range Oscillators in 28 nm CMOS

F. Chicco, S. Cerida Rengifo, E. Le Roux

Two 20 GHz low-power and wide-range LC oscillators with different tuning approaches have been designed for a FMCW radar application. Integrated in TSMC 28 nm CMOS technology, one of the two oscillators relies on a purely digital tuning, while the other has a limited analog tuning extended by digitally controlled sub-bands. Measurements show that the DCO and VCO circuits have similar power consumption, however the DCO performs better in terms of phase noise because of a better quality factor.

The millimeter wave (mmW) frequency band has become increasingly attractive over the past decade because the spectrum is less heavily utilized than lower frequency bands and larger bandwidths are available. Increased bandwidth enables the conception of new communication standards supporting high data rate communications and offers the potential to enhance the performance of radar and sensing applications. Indeed, FMCW radars greatly benefit from the high carrier frequency and multi-GHz bandwidth available for improvement of angular and radial resolution respectively.

Designing integrated circuits at mmW poses challenges for CMOS IC design: the most advanced CMOS technologies are required to obtain an improved transit frequency at the cost of more complex design rules and constraints. Furthermore, in order to design a low-power oscillator with wide tuning range and good phase noise performance, the choice of the frequency synthesis approach is key. Setting the oscillator frequency equal to the output frequency leads to several disadvantages. Firstly, the quality factor of integrated capacitors and varactors is low at 60 GHz while for inductors it is limited to a few tens due to the skin effect and substrate losses. The parasitic capacitance represents also a significant fraction of the total tank capacitance, hence reducing the tuning range. Secondly, first stages of the associated frequency divider draw comparatively non-negligible power. Nevertheless, the choice of a lower oscillator frequency requires the use of a frequency multiplier, which is usually a power-hungry block. A possible alternative is the choice of 20 GHz as the carrier frequency with a convenient up-conversion strategy [1].

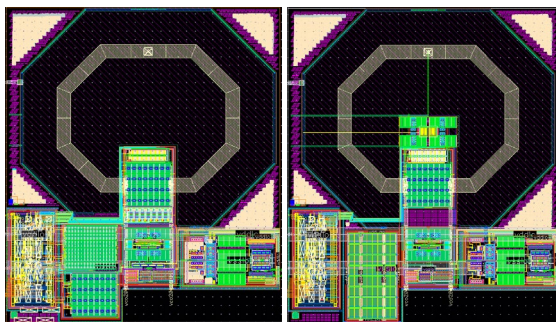


Figure 1: Oscillators layout: DCO (left) and VCO (right).

In this work, a comparison between two 20 GHz low-power and wide-range LC oscillators designed in TSMC 28 nm CMOS technology with different tuning approaches is proposed.

[1] A. H. M. Shirazi, et al., "On the design of mm-wave self-mixing-VCO architecture for high tuning-range and low phase noise," IEEE Journal of Solid-State Circuits, vol. 51, no. 5, (May 2016) 1210–1222.

One is a digitally controlled oscillator (DCO) and the other is a voltage controlled oscillator (VCO) whose varactors are assisted by capacitor banks to extend their tuning range. The goal is to show which one is the best suited with respect to the core of a 60 GHz frequency synthesizer for FMCW radar applications. In order to make a fair comparison, the two oscillators share the same topology and resonator their layout being largely identical, except for the tuning blocks (Figure 1).

A complementary cross-coupled pair oscillator topology is considered for current reuse and improved efficiency. The tail current source has been removed to increase the maximum voltage swing and the cross-coupled pairs are voltage-biased so to ensure class-C operation^[2]. The DCO has four tuning banks, each one with a different step, which enables us to achieve both a large tuning range and high resolution with a reasonable number of elements. The VCO shares with the DCO the two capacitor banks with larger steps and includes two varactors for differential analog tuning. The signal is output by a transformer-loaded power amplifier.

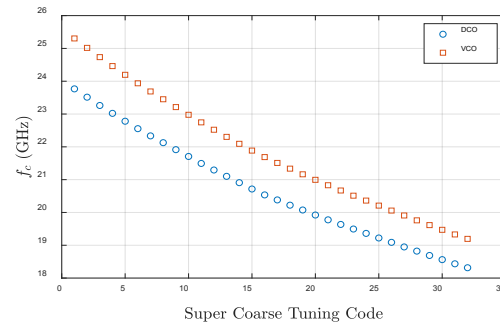


Figure 2: Oscillators tuning range with coarsest capacitor bank.

The measured power consumption close to the voltage-limited regime is 3.1 mW for the DCO and 3.2 mW for the VCO. Figure 2 shows the tuning range (TR) of the two oscillators, from 23.8 to 18.3 GHz for the DCO and from 25.3 to 19.4 GHz for the VCO (TR = 26%) The phase noise is -91 dBc/Hz at 1 MHz offset for the DCO at maximum carrier frequency, while it is -89 dBc/Hz for the VCO. The performance of the two oscillators is comparable in terms of power consumption and tuning range due to the many similarities in structure and components. Nevertheless, the analog tuning causes a higher phase noise due to the lower quality factor of varactors.

This research is part of EU H2020 M3TERA^[3] project.

[2] L. Fanori and P. Andreani, "A high-swing complementary class-C VCO," Proc. ESSCIRC, pp. 407-410, (Sept. 2013).

[3] M3TERA (EU project under GA No 644039) <https://m3tera.eu>

Link Budget, Power Trade-offs using Optimized Bluetooth 5 Transceiver IP

E. Le Roux, N. Scolari, N. Raemy

CSEM is continuously upgrading its icyTRX RF silicon IP [1] in accordance with the evolution of the Bluetooth Low Energy standard. For example, CSEM is currently implementing future direction-finding features. Bluetooth Low-Energy 5 introduced variable data rates for speed-range trade-off. Here, CSEM presents some figures, based on measurement and a propagation model, illustrating the potential impact of this trade-off on power consumption.

Bluetooth 5 introduced a variable data-rate to make a trade-off between communication range and speed^[2]: in addition to the 2 Mbit/s data rate, Long-Range 500 kbit/s and 125 kbit/s rates are also now possible with the use of coding on top of basic 1 Mbit/s rate. As the rate impacts the energy per bit, this is also a trade-off between distance and product lifetime or battery size. Based on icyTRX measurements, CSEM presents a quantitative example of this trade-off and its potential benefits. For simplicity, and without loss of generalization, CSEM considers a symmetric communication between two icyTRX transceivers with 0 dBi antenna gains. The received power can be evaluated based on the following equation:

$$P_{Rx\ dB} = P_{Tx\ dB} + G_{AntTx\ dBi} - PathLoss_{dB} + G_{AntRx\ dBi}$$

For the purposes of making a relative comparison and understanding the tradeoffs, a simple propagation model is considered for the Path Loss [3]:

$$20 \cdot \log_{10} \left(\frac{4\pi \cdot 1m}{\lambda} \right) + 10 \cdot \eta \cdot \log_{10} \left(\frac{\text{range}}{1m} \right) + \mathcal{N}(0, \sigma^2)$$

1st meter free-space *η is path loss exponent* *Normal distrib.*
σ² variance

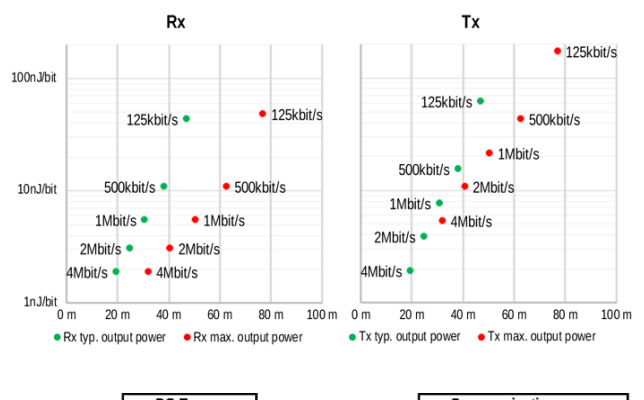
The η path loss exponent and σ standard deviation of Log-normal distribution are, respectively 2 and 0 for a free-space propagation context, 2.1 and 4.3 for a "corridor" Line-Of-Sight context, 2.9 and 6.1 for an "obstructed" Non-Line-Of-Sight context. Those parameters may vary quite a lot depending on real propagation context. The Log-Normal distribution is used to extract a $2.3 \cdot \sigma$ margin for a 99% connection probability.

Two different output powers are considered, with associated DC power consumption: the typical case is associated with the minimum 1.0 V supply voltage of the RF Power Amplifier (PA) and the maximum corresponds to the case of a 1.6 V PA supply voltage. The measured sensitivities associated with the selected data rates are also considered. In addition to the standard BLE cases, a proprietary 4 Mbit/s 4-FSK is considered for the purposes of comparison. A summary of the results for the various different cases is provided in Figure 1.

The best approach tends to be the maximization of data rate. When communication range is insufficient, the preferred

approach is to increase the output power before to reduce the data rate, if associated peak current can be supported.

Of course, additional considerations are associated with a specific application in which such a Bluetooth IP is implemented: possible asymmetry (typ. communication with cellular phone), packet overheads (including RF wake-up energy), antenna, interferer rejection, max. needed data rate, communication delay constrain or peak current that impacts the end-of-life voltage through battery internal impedance. A dynamic model of this impedance is preferred for simulations with currents profiles as battery-related time constants tends to be longer than packets duration.



Mode	DC Energy			Communication range			
	Rx	Tx	Output power	Sensitivity @PER = 10 ⁻³	Free-space	Corridor (LOS)	Obstructed (NLOS)
BLE 0.125Mbit/s	43nJ/bit	61nJ/bit	-0.7 dBm	-103.5 dBm	1345 m	327 m	47 m
BLE 0.5Mbit/s	11nJ/bit	15nJ/bit	-0.7 dBm	-100.9 dBm	997 m	246 m	38 m
BLE 1 Mbit/s	5nJ/bit	8nJ/bit	-0.7 dBm	-98.2 dBm	731 m	183 m	31 m
BLE 2 Mbit/s	3nJ/bit	4nJ/bit	-0.7 dBm	-95.5 dBm	535 m	136 m	25 m
4FSK 4Mbit/s	2nJ/bit	2nJ/bit	-0.7 dBm	-92.5 dBm	379 m	98 m	20 m
BLE 0.125Mbit/s	48nJ/bit	170nJ/bit	5.5 dBm	-103.5 dBm	2746 m	645 m	70 m
BLE 0.5Mbit/s	11nJ/bit	42nJ/bit	5.5 dBm	-100.9 dBm	2036 m	485 m	63 m
BLE 1 Mbit/s	5nJ/bit	21nJ/bit	5.5 dBm	-98.2 dBm	1492 m	361 m	51 m
BLE 2 Mbit/s	3nJ/bit	11nJ/bit	5.5 dBm	-95.5 dBm	1093 m	268 m	41 m
4FSK 4Mbit/s	2nJ/bit	5nJ/bit	5.5 dBm	-92.5 dBm	774 m	193 m	32 m

Figure 1: Energy-distance trade-off (only Obstructed Non-Line-Of-Sight case illustrated in graphic).

[1] CSEM Scientific and Technical Reports (2012-2017)

[2] M. Wooley, "Bluetooth 5 go faster. Go further", Bluetooth SIG, <https://www.bluetooth.com/bluetooth-technology/bluetooth5/bluetooth5-thankyou>

[3] T. S. Rappaport, "Wireless communications: principles and practice (2nd Edition)". (2001).

A Highly Efficient DC-DC Buck Converter for Load Currents from 1 μ A to 50 mA

V. Kopta, F. X. Pengg, E. Pérez Serna

High-efficiency, miniature DC-DC converters are needed in modern systems on chip in order to convert the battery voltage into a supply voltage that is compatible with the needs of deep sub-micron technology nodes. This work is focused on modifications to an existing DC-DC buck converter that enables lower output voltages and improved efficiency under low load current conditions.

Today's systems on chip (SoC) targeting applications such as the Internet of Things (IoT) consist of many different sub-blocks, such as BLE radio, ADC, DAC, sensor interfaces, processors, and memories. These blocks typically have different supply voltage requirements and may impose load currents varying from μ A to several mA. To minimize consumption, a DC-DC converter is needed that converts the battery voltage ranging from 1.7 V to 3.6 V into the required supply voltage, while maintaining a high efficiency for a wide range of load currents.

The existing buck DC-DC converter^[1] was optimized to supply power to CSEM's icyTRX BLE radio. It produces an output voltage ranging from 1.9 V to 1.2 V, and provides above 80% efficiency for load currents above 5 mA. However, most sensor nodes use the radio very rarely, and spend most of the time in a low power mode where the consumption drops to the μ A range. It is therefore the efficiency under these light load conditions that has a significant impact on the overall system efficiency.

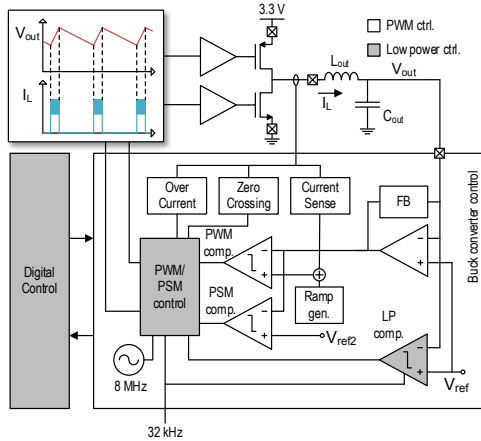


Figure 1: DC-DC buck converter block diagram.

The main obstacle with respect to improving efficiency under light load conditions is the power consumption of the control circuits, which consume around 300 μ A in the continuous pulse width modulation (PWM) mode. In this implementation, targeting the Fujitsu 55 nm DDS CMOS technology, duty cycling is combined with the pulse skip mode (PSM) in order to lower the consumption of the control circuits. Instead of operating in the standard PWM mode, the buck converter will provide short pulses of current that charge the output capacitor when the output current is low enough (typically below 1 mA). Between the pulses, the control circuits are switched off to minimize power consumption (non-shaded blocks in Figure 1). The converter stays in the off state as long as the output voltage is higher than

the reference voltage, once it drops below, the converter is activated and produces another pulse of current. The only circuits active during the off state are the comparator, references and low power logic. The implemented StrongARM^[2] clocked comparator consumes around 40 nA at 32 kHz. The overall consumption of the DC-DC converter in the off state is around 100 nA; mainly due to leakage of the logic gates and level shifters (voltage references not taken into account). The proposed duty-cycling technique increases the ripple of the output voltage. This ripple can be controlled via the amplitude of the current pulse. Lowering the pulse current results in a smaller ripple, but also increases the pulse rate and degrades efficiency. Owing to the low ripple frequency (on the order of kHz, and is inversely proportional to the load current) it can easily be suppressed by the LDO (low-dropout) regulator that typically follows the DCDC converter.

Efficiency enhancement of the buck converter, for typical conditions, is shown in Figure 2. In the continuous PWM mode, the efficiency drops to 40% for a load current of 1 mA. Once the low power PSM mode is introduced, the simulated efficiency increases to almost 85% and remains high all the way down to loads of 5 μ A. Below this current leakage starts to play an important role and effectively degrades the achievable results. Output voltage ripple is around 40 mV for the given simulation.

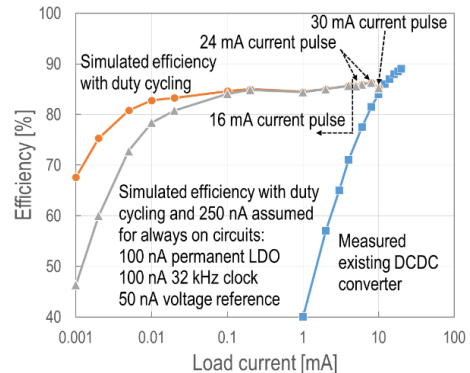


Figure 2: DC-DC converter efficiency with and without duty cycling.

The proposed modification extends the range of the DC-DC by another three decades of output current. To extend the range beyond 1 μ A, leakage should be minimized through reverse bulk biasing or power gating. Consumption of the comparator can be lowered by reducing the sampling clock frequency, an algorithm could be implemented that would adapt the sampling frequency and pulse amplitude to the load current. Finally, the consumption of voltage and current references and other service blocks must be minimized.

^[1] F. X. Pengg, et al., "A power management unit for ULP SoC including BLE radio" CSEM Scientific and Technical Report (2017) 134.

^[2] B. Razavi, "The strongARM latch," IEEE Solid-State Circuits Magazine, (Spring 2015).

Efficient Deep Learning Algorithm for Person Detection from Ceiling-mount Cameras

E. Türetken, L. A. Dunbar

Vision-based indoor positioning and occupancy analytics have applications in the healthcare, retail and hospitality industries. Current solutions require costly sensors and large computational resources, or lack localization accuracy. To overcome these limitations, CSEM developed an efficient deep learning model that can detect people from a standard overhead camera and can be run on inexpensive hardware with limited resources.

Indoor positioning technologies allow real-time detection, localization and tracking of people and objects in complex environments. According to Markets and Markets^[1] and Report Linker^[2], the indoor positioning market is expected to grow at a CAGR of 42% to over \$ 40 billion by 2022. The technology finds many applications from retail analytics and human-centric lighting to elderly care and assisted living.

In recent years, wireless wearable systems, such as RFID-based sensor networks, have served as the primary localization technology and have been successfully used in some of these application domains. However, their wide-scale adoption is impeded by several factors including high costs (mainly installation), poor localization accuracy, and the requirement that individuals must wear or carry a tag (i.e., receiver) to be localized. Vision-based person detection and tracking technologies provide a contactless alternative that emerged recently thanks to the abundance of public datasets, availability of performant computing hardware and the rise of deep learning algorithms. As a result, vision positioning market is expected to grow steadily and to reach \$ 9.25 billion by 2022^[3].

CSEM developed an efficient deep learning algorithm that can detect and locate people in indoor environments from low-cost ceiling-mount cameras. The system is designed to be reliable for smart building applications and to be integrated into low-cost microcontrollers with limited computational resources.

To train and validate the algorithm, CSEM acquired an indoor video dataset using various off-the-shelf cameras with high resolution sensors and wide-angle lenses. The cameras are mounted on ceilings at varying heights from 2.4 to 3 meters above the floor, and typically cover an area of around 20 square meters floor space. A total of 56 videos with durations varying from 5 to 15 minutes were acquired. A random selection of 40 videos was used for training the deep learning model, and the rest for testing. For labeling humans in the videos, CSEM developed a semi-automated annotation software, which significantly minimizes the labeling effort. Given manual bounding-box annotations of people in a video frame, the software performs identity preserving tracking of each person in the video within a certain temporal vicinity of the frame, which reduces the required labeling effort by more than an order of magnitude. All annotations are done by two annotators separately using the software and then cross-checked by them.

To achieve high computational efficiency, the developed deep learning network is comprised only of fully convolutional and max-pooling layers. The convolutional neural network (CNN) takes as input a small spatiotemporal cube of preprocessed

video data at a speed of 1 frame-per-second. It outputs, for the last frame, a probability map where each pixel signifies the likelihood that there is a human at the pixel location (Figure 1). For training, the ground truth probability maps are generated from the manual annotations of the human bounding boxes, and during prediction, they are estimated using a standard non-maxima suppression algorithm applied on the output probability maps from the CNN.

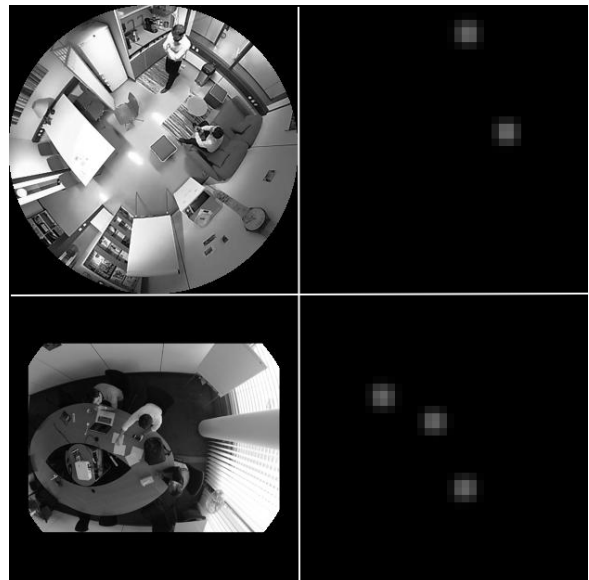


Figure 1: Sample results on two videos from the test dataset. Left: input normalized frames. Right: corresponding output probability maps.

Table 1: Algorithm performance results on the test dataset. The number of multiply-accumulate operations (MACs) and weights quantify the hardware resources needed to evaluate the deep network.

Precision	Recall	MACs	Weights
95%	94%	184 M	37 K

The system achieves a detection precision of 95% and a recall of 94% on the test dataset of about 100 minutes of video (Table 1). It can distinguish people with a spatial resolution of less than half a meter on the floor, which is sufficient for most applications. The trained model has 37 thousand weights, which takes less than 200 KB memory to store, and requires little computational resources to run in real-time.

Future work includes building a full demonstrator of the technology, requiring further optimizations of the deep architecture, and embedding on standard low-cost processors (e.g., ARM Cortex-M) and low-power hardware accelerators.

[1] MarketsandMarkets, "Indoor location market by component, deployment mode, application, vertical, and region", (2017).

[2] ReportLinker, "Global indoor location market analysis", (2017).

[3] MarketsandMarkets, "Vision positioning system market by component, location, solution, application, and region", (2017).

Intelligent Multispectral Imaging System for Detecting Human Skin

P. Nussbaum, L. A. Dunbar, J. P. Berti Ligabô, P. Pad

People detection and tracking is a field in computer vision with many applications. Applications such as smart buildings, smart cities, autonomous driving cars, security and sport analysis are just a few. Almost all image processing and machine learning methods today are based on the shape, color and movement of human body. To improve segmentation and therefore accuracy we add another property to this list, material composition. The reflection of different wavelengths of light is dependent on the material; by looking at these reflection signatures, we can distinguish human skin from its surroundings.

In computer vision, several methods have been developed for human detection [1-2]. Most of them are based on shape, color and movement. The main drawback of these methods are as follows: 1) they cannot differentiate between a real face and that of one on a computer display, a printed paper or a mannequin (false positive detection) and 2) in non-regular conditions, e.g., when a body is buried and only one part of the skin is visible, no human is detected (false negative detection).

One way to overcome these issues is by identifying the material of human skin versus other materials. Spectroscopy is a well-known technique suited to material identification based on their reflectance at different wavelengths. In this method, the reflectivity at different wavelengths (also known as spectral signature) act like fingerprints of each material. In conventional spectroscopy, we have only a single spectrum measurement giving no spatial information. Hyperspectral imaging has extended this idea to provide spectroscopic measurement of each position in a scene. Thus, the outcome of a hyperspectral camera is a hypercube, see Figure 1 (LHS), that at each pixel contains the samples of the spectrum of that pixel. Using this type of imaging, we can collect a spectral signature at each pixel which may be traced back to the material at this position in the scene.

However, there are some obstacles for the practical application of such a technique. First of all, hyperspectral imaging generates a huge amount of data which is problematic from both a data acquisition (long acquisition time) and data processing point of views (huge computational cost). Moreover, the hyperspectral cameras in today's market are bulky, relatively slow, costly, have high power-consumption and often need to be operated by an expert.

To overcome these problems, we propose an application-specific multispectral imaging system where instead of using a generic multi/hyperspectral camera, we collect only the relevant spectral bands avoiding collecting useless data, i.e., noise, that clogs up the system.

To demonstrate this, CSEM first performs a comprehensive data acquisition with a high resolution (both spectrally and spatially) hyperspectral camera. Afterwards, in the processing stage, we perform a compound machine learning algorithm that not only distinguishes the skin versus not-skin, but also learns the

wavelength bands that are important for the application. Using this knowledge, CSEM selects off-the-shelf filters to build a skin detecting imaging system using the patented multispectral camera architecture of CSEM [3]. Our demonstrator, shown in Figure 1 (RHS) is a 3 cm × 3 cm × 3 cm multispectral camera with 20 wide spectral bands for the application of real-time human skin detection.

Sample images after the application of machine learning algorithm is depicted in Figure 2. The results are produced by pixel-by-pixel processing, i.e., only using the spectral information of each pixel of the scene and there is no spatial pattern recognition involved. In this process the shape of human body or part in the scene does not influence the performance. Therefore, this creates the advantage that there is no lower limit on the number of pixels for the algorithm to work. This also suggests that by combining the spectral information with conventional people detection methods, we can improve performance or for an equivalent performance use less computational or optical complexity.

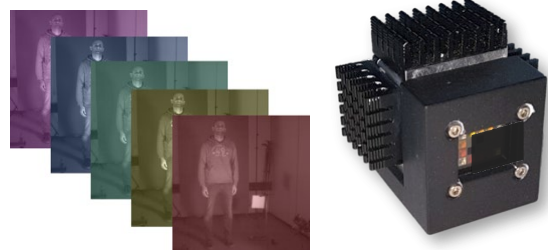


Figure 1: (LHS) Multispectral image-cube, (RHS) multispectral camera with 20 bands with 400×400 resolution.

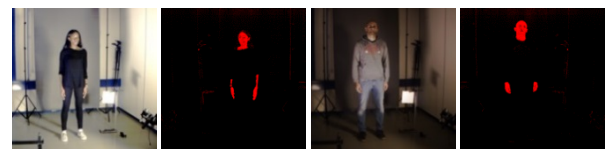


Figure 2: Detected skin based on 20 spectral bands.

Finally, although this project demonstrates this technique for human skin detection, it can be used in all computer vision application in which there exists relevant information in the spectral domain.

[1] M. Enzweiler, M. Dariu, "Monocular pedestrian detection: survey and experiments", IEEE Trans. on Pattern Analysis & Machine Intelligence, 12 (2008) 2179.

[2] E. Hjelmås, B. K. Low, "Face detection: a survey", Computer Vision and Image Understanding, 83.3 (2001) 236.

[3] P. Pad, N. Niketic, A. Chebira, E. Franzi, R. P. Stanley, L. A. Dunbar, "Versatile intelligent multispectral imaging camera made with off-the-shelf components", Proc. of SPIE, 10539 (2018) 10539.

An Ultra-low-power High Dynamic Range Image Sensor

P.-F. Ruedi, R. Quaglia, P. Heim, H.-R. Graf, C. Monneron, B. Schaffer

A $700 \mu\text{W}$ QVGA (320×320) 120 dB image sensor dedicated to IoT applications has been developed. Its on-chip frame memory, logarithmic data representation and ease of interface through a single 4-wire serial communication port will facilitate its integration in low cost and low power vision systems.

There is an increasing need for vision systems performing visual scene analysis (e.g., face detection, intrusion detection, object detection,...). Ideally these systems should be easy to install, have a small form factor and a long autonomy. These features can be helped by battery powered operation or by powering them with energy harvesting. The systems should, of course, remain robust and reliable and as such the imager should have a high dynamic range (DR), to cope with dramatically changing environmental conditions. Full autonomy can be created by limiting power consumption. This can be done by using imagers which deliver a data representation minimizes the processing power of subsequent stages. To achieve this goal, the image sensor presented in this paper offers the following features: 1) a 120 dB intra-scene dynamic range with a logarithmic representation of the luminance so that no adjustment to the environmental conditions (illumination) is needed, in addition the logarithmic encoding facilitates data processing, 2) the use of pixel-level A/D conversion and data storage to relax data transfer to the processing unit by storing a whole frame on chip, 3) image sensor control and data readout through a single 4-wire serial interface to facilitate interfacing with low-end microcontrollers, 4) a single 1.8 V supply voltage.

Figure 1 shows a block diagram of the image sensor. It is constituted of a 320×320 array of pixels with in-pixel A/D conversion and data storage, low drop-out regulators for on-chip supply voltage generation for the in-pixel memory, a quartz oscillator, a digital control unit and an SPI interface. The pixel is made up of an analog front-end and a digital 10 bit memory. Each pixel integrates the photocurrent delivered by its photodiode on a capacitor. The resulting voltage is constantly compared to a reference voltage. Once the reference voltage is reached, the pixel samples in its 10-bit memory a code delivered to all pixels in parallel. This code is proportional to the logarithm of the time elapsed since the beginning of the exposure. Using a logarithmic encoding enables to encode more than 6 decades of illumination on 10 bits, with 150 steps per decade.

Figure 2 shows a high dynamic range image acquired with the image sensor; both outside and inside details are clearly visible simultaneously. The image sensor achieves an intra-scene dynamic range of 120 dB , while the total power consumption is $700 \mu\text{W}$ at 10 frames per second. This high dynamic range enables to turn on the image sensor and acquire an image which will be correctly exposed, without needing to adapt to the illumination level.

The present image sensor benefits from an easy integration in a system through a simple 4-wire interface. Its high dynamic range and its low power consumption makes it an ideal candidate to be used in a series of connected sensor. It is an ideal component in a simple installation, autonomous, intelligent vision system. Indeed, CSEM believes it could make up one of the types of sensors needed amongst the 10's of billions of sensors necessary for the IoT revolution.

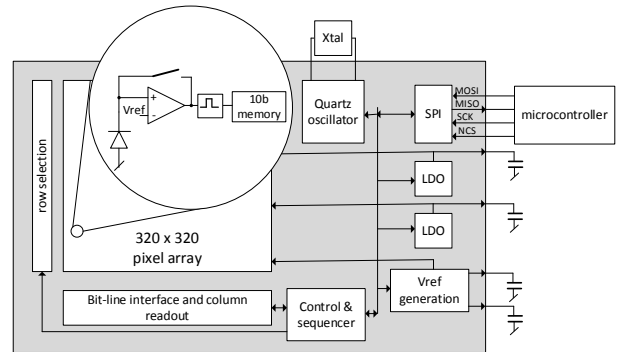


Figure 1: Block diagram of the chip.



Figure 2: High dynamic range image.

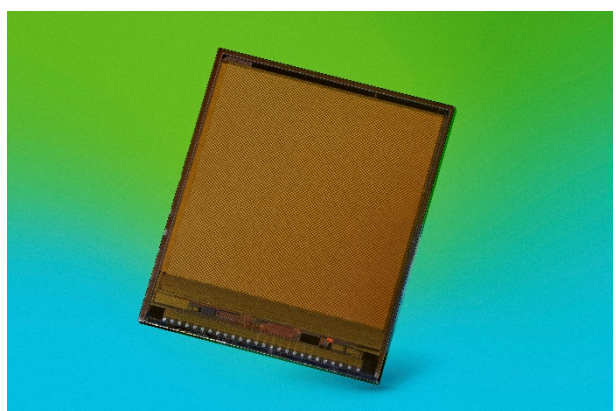


Figure 3: Microphotograph of the chip.

A Reticle-size X-ray Photon Counting Detector

R. Quaglia, P.-F. Ruedi, C. Monneron

A reticle-size chip embedding an array of 300 by 240 X-ray photon counting pixels with energy discrimination has been developed. Covalently bonded to a an X-ray absorber made of Germanium pillars it addresses a new generation of color X-ray imaging devices for medical imaging with better resolution and allowing lower X-ray doses than traditional X-ray detectors.

X-ray detectors are usually large as imaging optics at X-ray wavelengths are unpractical. Instead, the detector area is usually the same size as the area to be imaged. Previously we developed an X-ray color imager offering advantages in term of tissue or material discrimination^[1]. It consisted of a 16 by 16 array of photon counting and energy discrimination pixels, for direct detection, each of which was covalently bonded to a silicon absorber. Direct X-ray detection also provides sharper images, as well as reduced X-ray doses, compared to indirect detection based on a scintillator coupled to an image sensor. Building on these results, a detector having the size of the maximum reticle area which can be replicated on a wafer was developed. A block diagram of the chip is illustrated on Figure 1. It embeds an array of 300 by 240 pixels. Each pixel contains a charge amplifier, a shaper, 2 discriminators and 2 12-bit ripple counters and has an area of 100 μm by 100 μm . Sequencing of image acquisition and readout is performed by an external microcontroller to enable a high flexibility. Data read out is performed through a 12-bit parallel bus.

With centimeters long metal lines for control signals and data read out path, propagation delays become important and must be carefully considered. Additionally, as each photon counting pixel consumes 10 μA , thermal dissipation is critical with a DC current consumption of 720 mA corresponding to a power of 1.3 W which needs to be dissipated.

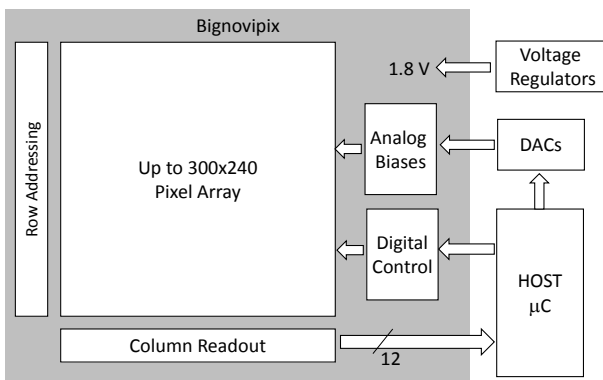


Figure 1: Block diagram of the chip and external components.

The chip was fabricated in a 150 nm process. Its area is 3.1 cm x 2.6 cm. Figure 2 shows a microphotograph of an 8" wafer which contains a total of 26 dies.

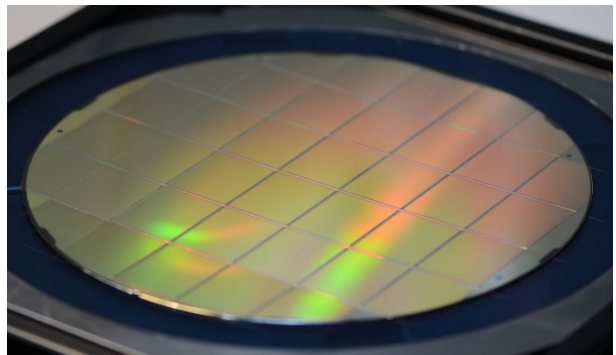


Figure 2: Microphotograph of the 8" wafer.

The post-processing of the wafer to bond together the CMOS wafer and the X-ray absorber was done by G-ray Medical. The CMOS wafer was first attached to a carrier wafer, then thinned down to a thickness of 12 μm . After low temperature covalent bonding of the absorber to the backside of the CMOS wafer, metallization is deposited on the absorber to enable to bias it up to a few hundred volts. Finally, the carrier wafer is removed and the passivation is opened over the pads of the CMOS chips.

Figure 3 shows the chip bonded on a PCB. Test of the chip is currently on-going.

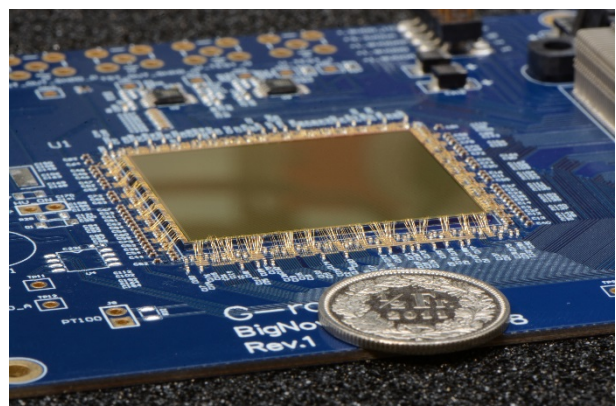


Figure 3: Microphotograph of the X-ray chip.

The project, realized in close collaboration with G-ray Medical, is a first step toward even larger detectors with smaller pixels to offer new imaging perspectives in the fields of medical X-ray imaging and non-destructive testing.

^[1] R. Quaglia, et al., "X-ray photon counting chip with backside detector", CSEM Scientific and Technical Report (2017) 137.

A Super High-performance Ultra-low-power Temperature Compensated Real Time Clock

D. Ruffieux, C. Arm, R. Godinho Caseiro, S. Dalla Piazza [•], O. Germann [•], Y. Godat ^{••}, R. Haeni [•], C. Monneron, D. Rihs ^{••}, C. A. Salazar Gutierrez, D. Séverac, N. Scolari, D. Sigg, S. Stanarevic

SuPeRTC focuses on the development of a 100 nA, 1 – 5.5 V TCXO RTC module with user-available temperature. It delivers on-demand or after any IRQ, a clock programmable between 8 kHz to 67 MHz. A versatile battery switchover/charger and user writable Flash further extend the use cases.

In a previous collaboration, CSEM and Micro Crystal have developed a temperature compensated Real Time Clock (RTC) module, the RV-8803-C7 [1], that has beaten three world records: lowest size ($3.2 \times 1.5 \times 0.8$ mm), lowest power (240 nA) and highest accuracy (± 3 ppm or ± 0.25 s/day over -40 to 85 °C). Such modules are likely to play an important role in the booming IoT and wearable markets where energy optimization via efficient scheduling, tighter synchronization is mandatory to extend autonomy and hence user comfort. The partners have thus paired up again to develop the next generation product targeting a threefold power reduction and incorporating many additional features while preserving both size and accuracy.

Figure 1 shows the architecture of the new circuit. The always-on part, identified by the dashed-box, corresponds to the functions of the RV-8803-C7. It consists of an ultra-low power voltage reference with built-in power-on-reset (POR) and brownout detection combined to a quartz oscillator (XO), a duty-cycled high resolution ring oscillator temperature sensor and the digital circuit implementing traditional RTC functions such as calendar, timer, and associated IRQs. Temperature readouts with a $0.1\text{ }^{\circ}\text{C}$ resolution are now available to the users coupled to two IRQs with programmable upper and lower thresholds. The threefold power reduction was obtained by lowering the reference voltage from 1.25 V to 1 V and the consumption from 240 nA to 100 nA. After a single point trim, the measured inaccuracy of the 1 V reference over -40 to $85\text{ }^{\circ}\text{C}$ is lower than $\pm 30\text{ mV}$ despite a consumption of only 20 nA. Technology scaling from 350 to 180 nm yields both significant dynamic power and area reduction. More aggressive clock gating and clock scaling techniques of the digital circuit and temperature sensor read out help reach the targeted figures. The LDO draws 15 nA, the XO 30 nA, the digital circuit 35 nA and the duty-cycled temperature sensor 10 nA.

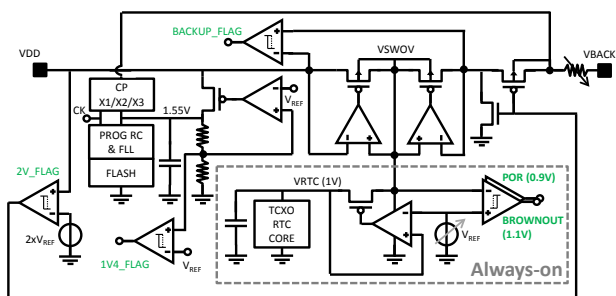


Figure 1: Block diagram of the newly developed RTC.

One of the added feature is a versatile battery charger and switchover that powers the RTC core from a backup source upon main supply failure. In the direct switching mode, the highest supply is automatically selected thanks to self-biased.

cross-connected, active MOS diodes. In the level switching mode, the main supply should first drop below a given threshold before direct comparison occurs. To prevent a POR, the corresponding 2 V comparator that controls the switch isolating the backup source must react in less than 1 μ s despite consuming a few tens of nA. The implemented solution relies on the trimmed 1 V reference, combines three detection circuits and draws 50x less power than competition while being robust to any type of power failure profile (rapid, slow and partial drop). Upon switching, the always-on part is fully isolated from the interface to prevent leakage until the power line is restored.

Charging of the backup source may be done directly at the main supply level (up to 5.5 V) or using a 1.55 V secondary power domain complemented with a x2 or x3 charge pump. SMT Li-ceramic and coin type ML batteries or supercapacitors may thus be charged at 1.55 V, 3.1 V or 4.6 V respectively using programmable resistors. In shelf mode, without V_{DD} , the power backed-up RTC module reaches sub-nA consumption thanks to an innovative isolation circuit minimizing self-discharge.

Also present on the 1.55 V domain, an RC oscillator running between 33 and 67 MHz is used on the one hand to drive the charge pump but also to provide, after proper division, a programmable clock source. The latter can run at any multiple of 8 kHz up to 67 MHz thanks to an all-digital frequency locked loop (FLL). A 64-bytes Flash with 0.9 V read and 1.4 V write minimum voltages, provided by EM Microelectronic-Marin, is used to store calibration, configuration and user parameters. The module can thus be completely configured in Flash such as to output a given clock frequency each time an IRQ is generated and be the sole timing source of the associated MCU further reducing the bill of material. Five comparators inhibit the different functions when the supply voltage is not sufficient.



Figure 2: Photograph of the RTC module (courtesy of Micro Crystal).

Funding from CTI/Innosuisse for the circuit development is acknowledged. The module pictured in Figure 2 is now ready for production. EM Microelectronic-Marin manufactures the circuit in ALP18 while Micro Crystal performs the assembly of the IC & quartz in a miniature package and module calibration.

- Micro Crystal AG, Switzerland

• EM Microelectronic Marin SA, Switzerland

[1] <http://www.microcrystal.com>

An Active Near-field Communication (NFC) System

J.-L. Nagel, A. Vouilloz, C. Arm, P. Persechini, E. Azarkish, C. Monneron, R. Cattenoz, J. Deng, M. Pons Solé, N. Scolari, E. Le Roux, D. Sigg

The CUBIC2 system-on-chip chip supports multiple modes (passive and active NFC, proprietary peer-to-peer) and opens new opportunities in ultra-low power and space-constrained contactless communication.

NFC is widely used in contactless communication e.g., the well-known smartcards used in payment, ticketing and access control, but it also offers opportunities in domains such as logistics, watches or IoT.

In classical NFC, the reader carrier is modulated by the card (or other device) by means of load modulation, i.e., by creating a resonance mismatch in the antenna circuit (in practice switching the load connected to the loop antenna). This approach is passive in the sense that no energy is emitted by the device to modulate the carrier. In many applications, this method can be implemented without a battery, since enough energy can be harvested from the carrier.

In a different way, the device can actively emit energy in counter phase of the expected load modulation to simulate a mismatch, or load, on the carrier. Although a battery is now needed because energy harvesting is no longer sufficient, the distance of the communication can be extended compared to passive communication, assuming the device receiver is sensitive enough to recover the carrier and its modulation. This gain in communication range can interestingly be traded off against reduced antenna size, a well-known limitation in NFC devices due to the 13.56 MHz carrier, or against packaging compromises, e.g., with the antenna close to metal surfaces or battery. Active NFC devices have the advantage of remaining compatible with NFC standards.

Synchronization of the device with the reader carrier is essential in active mode and is done by locking a PLL during non-modulated periods, e.g., using the non-modulated half bit of the Manchester coding in ISO 14443A lower bit rate.

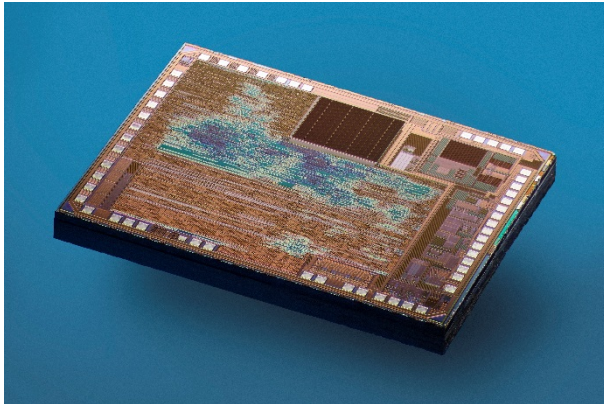


Figure 1: The CUBIC2 die (around 10 mm², integrated in TSMC 180 nm with embedded flash option).

The CUBIC2 system-on-chip (SoC) embedding the NFC IP was designed for the company Poken^[1] (now a subsidiary of GES

Event Intelligence) with the goal of reducing the power and the bill of material of the current solution. The SoC comprises a 32-bit icyflex2 processor, an embedded flash, ROM and RAM, standard interfaces (USB, I2C, SPI, UART, GPIO), timers (watchdog, real-time clock and performance counters) and on-chip debug (Figure 2).

The system can be supplied from a battery, from the energy harvested from the NFC field or from the USB. Two regulators (LDO) supply the 1.2 V (always-on) and 1.8 V used in the system, together with the primary supply. The passive NFC IP developed for this SoC supports ISO 14443 type A, at communication speeds up to 848 kbit/s. The active NFC IP is limited to the lower bit rates defined in the standard.

Several power modes are implemented, from a deep sleep mode consuming less than 1.5 µA, to full-on mode including flash access and active NFC communication, consuming over 10 mA on average. Duty-cycling between those modes enables proprietary peer-to-peer communication to run with an average current of 2 µA, i.e., 3 times less than the previous solution relying on many more off-the-shelf components.

The system comprises three clock sources: an optional 27 MHz crystal oscillator is used for active NFC communication; a 48 MHz RC oscillator is used by most of the digital and the USB interface; finally, an ultra-low power 32 kHz RC oscillator is used while in deep sleep mode. The RC oscillators can be calibrated using the crystal as a reference (if present) or using the NFC carrier.

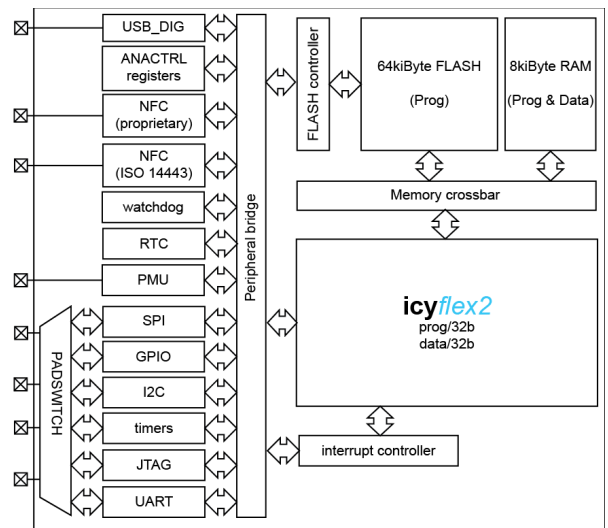


Figure 2: CUBIC2 block diagram.

[1] <https://www.poken.com>

Miniature Acquisition, Processing and Wireless Communication System-on-Chip for Prosthetic Applications based on Electromyography (EMG)

M. Pons Solé, E. Azarkhish, J.-L. Nagel, B. Schaffer, A. Bischof, Y. Zha, J. Deng, L. Zahnd, L. Bergamini, B. Perrin, C. Monneron, R. Caseiro, Y. Liechti, P.-A. Beuchat, J.-D. Decotignie, P. Dallemande, D. Manic, S. Emery

In the DeTOP H2020 European Project, CSEM has integrated a System-on-Chip for prosthetic applications based on EMG. It is a miniaturized design combining a 20 channel configurable analog frontend for EMG signals acquisition and an icyflex2 32-bit RISC processor system for data processing. The chip was produced in TSMC 55 nm LP technology.

DeTOP^[1] stands for Dexterous Transradial Osseointegrated Prosthesis with neural control and sensory feedback. The project addresses the recovery of hand function after amputation. Nowadays amputees continue to use prostheses developed over 40 years ago, namely myoelectric prostheses controlled via surface electrodes, which are known for their poor functionality, controllability and sensory feedback. The proposal of osseointegration for the direct skeletal attachment of limb prostheses, aside from providing an efficient mechanical coupling, which improves prosthesis functionality and the patient's quality of life, can also be used as a bidirectional communication interface between implanted electrodes and the prosthetic arm. This is today the most advanced technique for bidirectional neuromuscular interfacing.

The goal of the DeTOP project (Figure 1) is to make this technology clinically available to the largest population of upper limb amputees, namely transradial amputees, by developing a novel prosthetic hand with improved functionality, smart mechatronic devices for safe implantable technology, and by studying and assessing paradigms for natural control (action) and sensory feedback (perception) of the prosthesis through the implant.

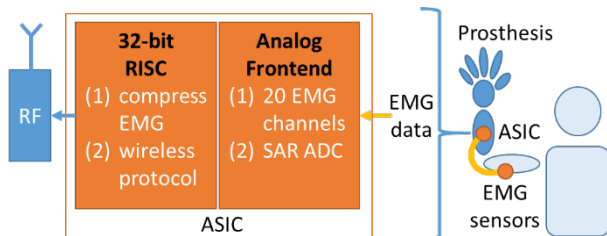


Figure 1: DeTOP application.

CSEM has developed the miniature acquisition, processing and wireless communication System-on-Chip for this application (Figure 2). The circuit collects EMG data, then compresses it in order to wirelessly send it to a central control unit, which then uses it to compute the movement of the prosthesis.

The 20 channel EMG acquisition analog frontend consists of an array of low-noise amplifiers with built-in programmable anti-aliasing filter followed by a 20 to 1 analog multiplexer that feeds the data to an ultra-low energy 12-bit scalable successive-approximation (SAR) ADC. Depending on the number of implanted electrodes available the number of

channels that are used can be configured. Programmable filters allow to also acquire other types of ExG signals (with voltage levels from μ V to mV, and with frequencies from Hz to kHz). The ADC can operate at up to 1 Msps. The power consumption is \sim 24 μ W/channel and \sim 100 μ W for the ADC.

The 32-bit RISC icyflex2 processor is used for lossless Huffman compression of the EMG signals to minimize the amount of data to be sent wirelessly, therefore reducing the power consumed in the transmission. For the prosthesis real-time application needs, the processor runs at 153 MHz and is able to compress the data in less than the required 100 ms (maximum delay from EMG sensing to prosthesis movement). Several interfaces and peripherals are available for maximum flexibility (UART, I2C, SPI, GPIO, Timers, JTAG). The RAM size is 256 kB. The ROM size is 64 kB. The consumption is \sim 25 μ W/MHz.

Power management, for the analog frontend and for the icyflex2 processor system, and a 153 MHz RC oscillator are also integrated on-chip.

A wireless protocol specially tailored for the prosthesis application has also been developed. The protocol is named WiseTOP^[2] and it implements the switching from CSEM low-power protocol (WiseMAC) to a standard high-throughput protocol (TDMA). Using a combination of both protocols, WiseTOP is able to adapt the power-throughput trade-off according to the EMG data to be transmitted. An external icyTRX chip is used for RF.

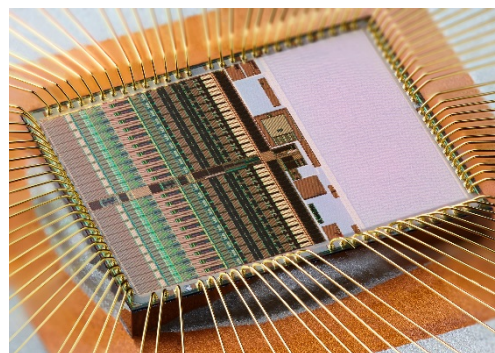


Figure 2: DeTOP System-on-Chip micro-photograph ($3 \times 3.7 \text{ mm}^2$).

The System-on-Chip will be integrated in the DeTOP project's prosthesis and the novel technologies and findings will be assessed by selected patients in clinical trials.

^[1] DeTOP project: European Commission under the Horizon 2020 Framework Programme for Research and Innovation (LEIT-ICT-24-2015, GA #687905). <http://www.detop-project.eu>

^[2] L. Bergamini, J.-D. Decotignie, P. Dallemande, "WiseTOP – a multimode MAC protocol for wireless implanted devices," ACM Real-Time Networks and Systems (RTNS), Poitiers, (Oct. 2018).

FastEye+, a High-speed Camera with Embedded Neural Networks for Smart Vision

P. Jokic, S. Emery

Streaming high-speed cameras are crucial components for visually inspecting fast processes and allowing systems to react to time-critical conditions with low latency. The vast amount of data produced by sampling images at multiple kfps puts communication interfaces and memories under considerable pressure, limiting the maximum streaming rate. To address this problem, the FastEye high-speed camera was extended to classify images on-board in real-time using binary neural networks, extracting relevant class information and thus reducing the communication load.

High-speed processes like mass production lines are often monitored using high-speed cameras to assess manufacturing quality in real time. This allows an early detection of faults and thus avoids costly production losses. Sampled images are usually transferred to an external computer for analysis. Using a 1 megapixel camera with 10 bit resolution at 2 kfps, this would continuously generate 26.2 Gbit/s of data, exceeding the maximum bandwidth of standard high-speed interfaces like USB 3.1 by a factor of more than 2x. Multiple cameras might have to be used for simultaneously monitoring different locations of a larger system, further increasing the required communication bandwidth. This work presents an extension to CSEM's FastEye high-speed camera, adding on-board image processing using binary neural networks (BNN): FastEye+ enables real time scene classification, making it possible to only send the recognized image class information instead of transmitting all pixel values. Figure 1 shows the camera, featuring a CSEM-made 1 MP image sensor (VIA1MP) and a powerful Kintex-7 FPGA module achieving frame rates of up to 2 kfps at full resolution.

BNNs are one of the many flavors of neural networks (NN), which are mostly used for machine learning. Their advantage over traditional NNs is a massively reduced computational complexity, due to reduced parameter and value precisions in hidden layers. The high connectivity between layers induces a large number of operations for computing the network, making computational simplifications highly beneficial. While NNs are normally computed with 32-bit floating point values, BNNs limit the weight and activation precisions to a single bit, reducing memory needs by 32x and simplifying the dominating floating point multiply-accumulate (MAC) operations to simple logic XNOR processing with appended bit-counting (popcount). Implementing BNNs on smart cameras is advantageous: On one hand, the reduced memory needs allow the network to entirely fit in fast internal SRAM, avoiding costly external DRAM access. On the other hand, XNOR multipliers with popcount adders are efficiently implementable in powerful FPGAs or custom ASICs, minimizing the computation latency.

FastEye+ implements the whole BNN on its FPGA module, making it an edge processing device. FPGAs can exploit the advantages of BNNs as they natively provide the required XNOR and popcount functions and provide large enough on-board memory for storing the network parameters. Because NNs are usually designed and trained in frameworks like Caffe, they first need to be mapped into a hardware description. As this is very time consuming, we developed a framework for automatically converting trained NNs into high-level C++ code compatible with the high level synthesis tool Vivado HLS. This allows customized

network architectures to be compiled into an IP block and instantiated in the camera FW (Figure 2).



Figure 1: The FastEye camera system with on-board FPGA.

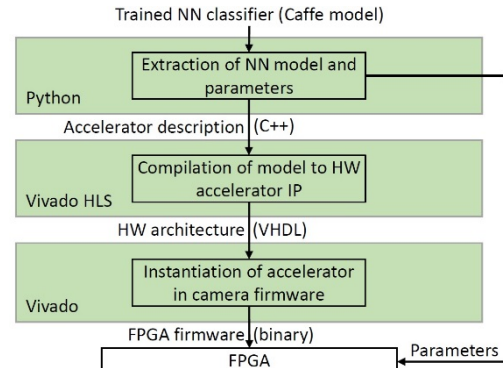


Figure 2: Design flow for mapping NNs onto the FPGA.

As a proof of concept, the presented system was configured to classify hand-written digits, e.g., for mail sorting systems. The real-time BNN classifier was fully embedded on the camera, achieving 19.28 us latency at 0.52 W power consumption and resulting in a 980x data reduction compared to raw data transmission^[1]. The advantages offered by embedding image processing directly onto the smart camera can be further exploited in applications of the following fields:

- Safety: detecting a hand in the movement zone of a robot
- Visual inspection: Self-triggering video acquisition without external triggering mechanisms by detecting a specified start condition (e.g., object of interest in the field of view)
- Production/Quality control: real-time quality assessment in high-speed production lines (e.g., sorting out faulty items)

^[1] P. Jokic, et al., "BinaryEye: a 20 kfps streaming camera system on FPGA with real-time on-device image recognition using binary neural networks," IEEE SIES, (2018) 1-7.

Switched-capacitor Degeneration for PVT Robust and Power Efficient Biomedical AFEs

K. Badami, T. Mavrogordatos, J. Deng, Y. Zha, A. Bischof, M. Pons Solé, S. Emery

ExG based bio-potential signals are crucial diagnostic monitors for the health of an individual. Yet, measuring these signals in a power efficient and PVT (Process-Voltage-Temperature) robust manner remains a challenge. This work introduces switched-capacitor degeneration assisted DC servo loop to improve the PVT robustness without sacrificing the power efficiency of these systems.

Portable bio-potential acquisition has a strong potential to improve the healthcare systems as it enables to reduce the time overhead between the diagnosis and the treatment. Yet, power efficient and PVT robust implementation of the analog frontend (AFE) for such a system faces a unique challenge. Typically the bio-potential signals (ExG) have a magnitude less than a few mVs, but are offset by large, up-to ± 300 mV, low-frequency signals commonly referred to as differential-electrode-offsets or DEO. Rejecting these DEOs in a PVT robust and power efficient manner is of paramount importance in a high-fidelity ExG acquisition AFE, the design of which is the target of this work.

Digital-intensive systems attempt to cancel the DEO after the ADC by using complex DEO estimation algorithms. This results in a power penalty in both the analog and the digital domain as the analog domain requires larger than necessary dynamic range in the AFE to accommodate the DEO only to be cancelled out by power hungry algorithms in the digital domain. On the other hand, early rejection of DEO in the analog domain requires to modify the transfer-function of the AFE from its traditional low-pass nature to a band-pass function. This bandpass transfer-function needs to have its lower-cutoff frequency (f_{-3dB}) in sub-hertz frequency range to be able to reject the DEO while not attenuating the ExG signal. This requires to establish time-constants larger than 1 s in a CMOS process which can be prohibitively area expensive.

State-of-the-art AFEs attempt to alleviate the above highlighted area/power penalty by using pseudo-resistors^[1] in the amplifier's feedback path as shown in Figure 1, to establish f_{-3dB} in the sub-hertz frequency range. Pseudo-resistors utilize switched-off MOSFETs to offer resistance as high as a few G Ω s without any area penalty. However, since this large resistance is based on the MOSFET's leakage current, these resistors show up-to 10 – 50X PVT variation thus affecting the design robustness.

This work overcomes the above highlighted drawback by a synergistic combination of a robust and precise current

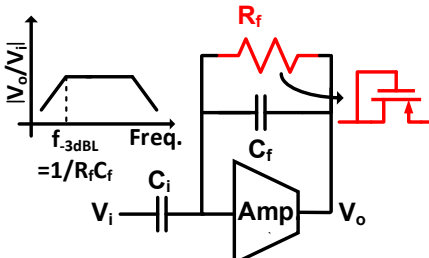


Figure 1: Commonly used AFE architecture. The feedback resistor is a pseudo-resistor and exhibits wide PVT variations.

feedback instrumentation amplifier (CFIA) and a switched-capacitor degeneration^[2] based DC servo loop. As

^[1] M. Konijnenburg, et al., *IEEE JSSC*, vol. 51, (2016) 2584–2595.

opposed to a traditional resistive degeneration, which linearizes the transconductance (g_m) with an area expensive resistor, a switched-capacitor degeneration combines the linearity benefit of degeneration without the area penalty of large on-chip resistors.

The architecture of the concept AFE is shown in the Figure (2). The f_{-3dB} for such an architecture is given by

$$f_{-3dB} = g_{m2,int}/2\pi g_{m,fb} R_{int} C_{int} \quad (1)$$

This frequency, however, is not as low as the one obtained by using pseudo resistors in the feedback path. Still, a comparably low value can be achieved for instance by modifying the integrator input as shown by the dashed-lines. This results in

$$f'_{-3dB} = (g_{m2,int}/2\pi g_{m,fb} R_{int} C_{int}) (R_1/R_2) \quad (2)$$

Further, as R_{int} is implemented as switched-capacitor degenerated g_m it can be expressed as $R_{int} \approx 1/f_{sw} C_{sw}$. This results in a highly precise and PVT robust f'_{-3dB} expressed as ratio of two identical components given as:

$$f'_{-3dB} = f_{sw}/2\pi (g_{m2,int}/g_{m,fb})(C_{sw}/C_{int}) (R_1/R_2) \quad (3)$$

The main challenge in this AFE is the mitigation of the offset of the feedback integrator when the inputs of the integrator are the attenuated signals shown by the dashed lines shown in the AFE in Figure 2. This attenuated feedback can be substituted by using alternative solutions such as g_m -scaling or switched- g_m to reduce the value of $g_{m2,int}$ to enable to reduce the transconductance of the feedback servo loop.

Switched-capacitor degeneration assisted DC servo loop as highlighted in Figure 2 can enable a pseudo-resistor free PVT robust AFE without the area/power penalty of the traditional implementations.

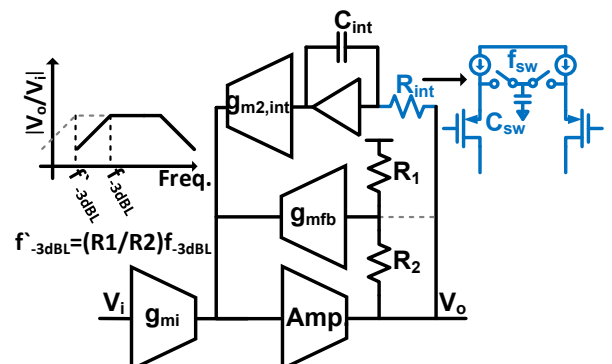


Figure 2: Switched-capacitor degeneration assisted DC servo loop for DEO attenuation.

^[2] K. Badami, et al., *IEEE ISCAS*, Montreal, (2016).

High-density Microelectrode Array with 4096 Full-duplex Channels

A. Bischof, Y. Zha, C. Monneron, J. Deng

A microelectrode array (MEA) with 4096 channels was integrated in a 0.35 μm CMOS process. The MEA is capable to read out all its channels at 20 kFrames/sec and simultaneously stimulate an arbitrary selection of electrodes.

In the pharmaceutical industry, in-vitro neurological models are widely used for pre-clinical tests of brain drugs. Having a reliable interface to the cultured neuronal tissue or brain slices that allows both stimulation and monitoring of the neuronal activity in high spatial and temporal resolution is of great importance. Conventional passive micro-electrode arrays (MEAs) cannot scale up the number of electrodes due to the increasing interconnection complexity. An alternative approach is the APS-MEA [1], which is inspired by the active pixel sensor concept of image sensors. Each electrode has its own low-noise amplifier. The read-out of the entire array is done by means of sequential multiplexing of the amplified electrode signals on a certain number of output channels. In this work, the low noise amplifier (LNA) of the original APS-MEA was redesigned, resulting in a much better input common mode suppression, better stability and less current consumption. In addition, the ability to stimulate each electrode individually was added. The basic structure of the electrode's LNA is shown in Figure 1.

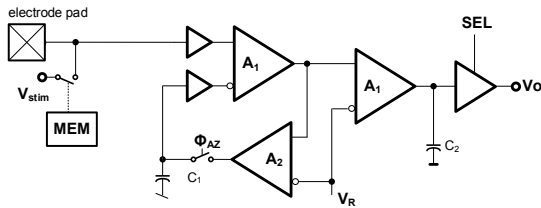


Figure 1: Simplified LNA schematic.

The electrophysiological signal is input to the LNA through a platinized aluminum pad. For stimulation purpose, the pad can be shorted to the external signal V_{stim} . The stimulation switch is controlled by a (local) memory cell, thus stimulation can be controlled individually for each electrode. In order to protect the 3.3 V amplifier circuitry from the 5 V stimulation signal, a buffer was added (implemented with 5 V transistors). The signal is then amplified using 2 gain stages (A_1). For noise reduction purpose, the output bandwidth is limited by the capacitor C_2 . As either the common mode drift of the electrode input signal or the offset of the amplifier stages (A_1) would lead to saturation, auto-zeroing was implemented. During auto-zeroing phase, the signal Φ_{AZ} is asserted. The output signal of the first gain stage (A_1) is fed back through the amplifier (A_2), and the offset is sampled on capacitor

C_1 . Auto-zeroing is performed periodically. The LNA acts as a band pass filter (see Figure 2 right). The lower cut-off frequency is around 100 Hz. The upper cut-off frequency is given by the filter capacitor of the low noise amplifier and is at 10 kHz.

The MEA was integrated in a 0.35 μm CMOS process and fully evaluated. Figure 2 (left) shows the output of one channel when the electrode pad is stimulated with a spike signal of 1 ms duration, an amplitude of 100 μV and a common mode drift of 300 mV. Auto zeroing (AZ) is performed every 75 ms. It can be observed that the spikes are amplified, while the input common mode is suppressed.

Table 1 summarizes the measured performance of the MEA.

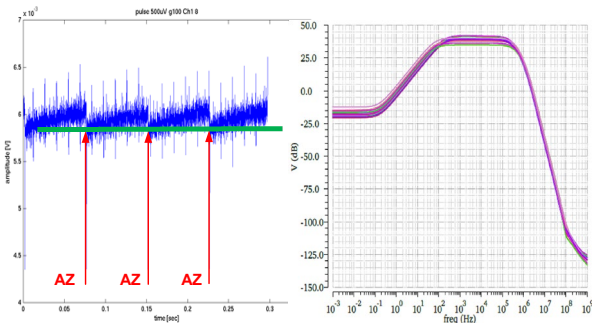


Figure 2: Frequency response of the low noise amplifier.

Table 1: Summary of MEA performance

Technology	0.35 μm 3.3 V CMOS
Number of electrodes	4096 (64 x 64)
Input common mode range	300 mV
Input referred noise	19.5 μV_{rms}
Overall gain	40/400
Stimulation voltage	5 V
Power consumption (LNA)	32 μW
Max frame rate	20 kFrames/sec
Area	64.2 mm^2

This work was done in collaboration with 3Brain under the CTI project name 18760.1 PFNM-NM. We would like to thank CTI for their funding.

[1] K. Imfeld, A. Garenne, S. Neukom, "High-resolution MEA platform for in-vitro electrogenic cell networks imaging", 3rd Int IEEE/EMBS Conference on Neural Engineering (2007).

ANNEXES

Publications

- [1] G. Abdellaoui, S. Abe, J. H. Adams, A. Ahriche, D. Allard, L. Allen, *et al.*, "EUSO-TA – First results from a ground-based EUSO telescope", *Astroparticle Physics*, vol. 102, pp. 98-111, Nov 2018.
- [2] G. Abdellaoui, S. Abe, J. H. Adams, A. Ahriche, D. Allard, L. Allen, *et al.*, "First observations of speed of light tracks by a fluorescence detector looking down on the atmosphere", *Journal of Instrumentation*, vol. 13, p. 18, May 2018.
- [3] S. Ardo, D. F. Rivas, M. A. Modestino, V. S. Greiving, F. F. Abdi, E. A. Llado, *et al.*, "Pathways to electrochemical solar-hydrogen technologies", *Energy & Environmental Science*, vol. 11 (10), pp. 2768-2783, Oct 2018.
- [4] A. Badin, F. Braun, L. J. S. Halloran, J. Maillard, D. Hunkeler, "Modelling of C/Cl isotopic behaviour during chloroethene biotic reductive dechlorination: Capabilities and limitations of simplified and comprehensive models", *Plos One*, vol. 13 (8), p. 16, Aug 2018.
- [5] A. Baghdasaryan, R. Grillo, S. R. Bhattacharya, M. Sharma, E. Reginato, H. Theraulaz, I. Dolamic, M. Dadras, S. Rudaz, E. Varesio, T. Burgi, "Facile Synthesis, Size-Separation, Characterization, and Antimicrobial Properties of Thiolated Copper Clusters", *ACS Applied Nano Materials*, 1 (8), 07 2018, 4258–4267.
- [6] C. Ballif, L. E. Perret-Aebi, S. Lufkin, E. Rey, "Integrated thinking for photovoltaics in buildings", *Nature Energy*, vol. 3 (6), pp. 438-442, Jun 2018.
- [7] S. Barcellona, L. Piegari, V. Musolino, C. Ballif, "Economic viability for residential battery storage systems in grid-connected PV plants", *Int. Renewable Power Generation*, vol. 12 (2), pp. 135-142, Feb 2018.
- [8] F. Braun, M. Proen  a, A. Adler, T. Riedel, J. P. Thiran, J. Sola, "Accuracy and reliability of noninvasive stroke volume monitoring via ECG-gated 3D electrical impedance tomography in healthy volunteers", *Plos One*, vol. 13 (1), p. 19, Jan 2018.
- [9] F. Braun, M. Proen  a, M. Lemay, M. Bertschi, A. Adler, J.-P. Thiran, *et al.*, "Limitations and challenges of EIT-based monitoring of stroke volume and pulmonary artery pressure", *Physiological Measurement*, vol. 39 (1), p. 16, Jan 2018.
- [10] C. Brivio, V. Musolino, P.-J. Alet, M. Merlo, A. Hutter, C. Ballif, "Application-independent protocol for predicting the efficiency of lithium-ion battery cells in operations", *Journal of Energy Storage*, vol. 15, pp. 415-422, Feb 2018.
- [11] G. Buchs, D. Bercoux, L. Mayrhofer, O. Gr  ning, "Confined electron and hole states in semiconducting carbon nanotube sub-10 nm artificial quantum dots", *Carbon*, vol. 132, pp. 304-311, Jun 2018.
- [12] G. Buchs, D. Bercoux, L. Mayrhofer, O. Gr  ning, "Confined electron and hole states in semiconducting carbon nanotube sub-10 nm artificial quantum dots", *Carbon*, 132, 02 2018, 304–311.
- [13] G. Buchs, S. Karlen, T. Overstolz, N. Torcheboeuf, E. Onillon, J. Haesler, and D. L. Boiko, "Nuclear spin decoherence time in MEMS atomic vapor cells for applications in quantum technologies", *AIP Conference Proceedings*, 1936 (1), March 2018, 020011.
- [14] A. Descoeuilles, C. Alleb  , N. Badel, L. Barraud, J. Champliaud, G. Christmann, *et al.*, "Low-temperature processes for passivation and metallization of high-efficiency crystalline silicon solar cells", *Solar Energy*, vol. 175, pp. 54-59, Nov 2018.
- [15] O. Dupre, B. Niesen, S. De Wolf, C. Ballif, "Field Performance versus Standard Test Condition Efficiency of Tandem Solar Cells and the Singular Case of Perovskites/Silicon Devices", *Journal of Physical Chemistry Letters*, vol. 9 (2), pp. 446-458, Jan 2018.
- [16] S. Essig, J. Dreon, E. Rucavado, M. Mews, T. Koida, M. Boccard, *et al.*, "Toward Annealing-Stable Molybdenum-Oxide-Based Hole-Selective Contacts For Silicon Photovoltaics", *Solar Rrl*, vol. 2 (4), p. 5, Apr 2018.
- [17] P. Glowacki, M. A. Pinheiro, A. Mosinska, E. Turetken, D. Lebrecht, R. Sznitman, *et al.*, "Reconstructing Evolving Tree Structures in Time Lapse Sequences by Enforcing Time-Consistency", *IEEE Transactions on Pattern Analysis and Machine Intelligence*, vol. 40 (3), pp. 755-761, Mar 2018.

- [18] I. Gyongy, A. Davies, B. Gallinet, N. A. W. Dutton, R. R. Duncan, C. Rickman, *et al.*, "Cylindrical microlensing for enhanced collection efficiency of small pixel SPAD arrays in single-molecule localisation microscopy", *Optics Express*, vol. 26 (3), pp. 2280-2291, Feb 2018.
- [19] T. H. Lin, T. Margossian, L. Q. Zheng, S. Kumar, I. Marozau, O. Sereda, *et al.*, "Conformal Deposition of Conductive Single-Crystalline Cobalt Silicide Layer on Si Wafer via a Molecular Approach", *Chemistry of Materials*, vol. 30 (6), pp. 2168-2173, Mar 2018.
- [20] R. I. Haque, O. Chandran, S. Lani, D. Briand, "Self-powered triboelectric touch sensor made of 3D printed materials", *Nano Energy*, vol. 52, pp. 54-62, Oct 2018.
- [21] S. J. Herr, V. Brasch, J. Szabados, E. Obrzud, Y. C. Jia, S. Lecomte, *et al.*, "Frequency comb up-and down-conversion in synchronously driven $\chi^{(2)}$ optical microresonators", *Optics Letters*, vol. 43 (23), pp. 5745-5748, Dec 2018.
- [22] J. L. Hodgkinson, H. M. Yates, A. Walter, D. Sacchetto, S. J. Moon, and S. Nicolay, "Roll to roll atmospheric pressure plasma enhanced CVD of titania as a step towards the realisation of large area perovskite solar cell technology", *Journal of Materials Chemistry C*, vol. 6 (8), pp. 1988-1995, Feb 2018.
- [23] S. Husein, M. Stuckelberger, B. West, L. Ding, F. Dauzou, M. Morales-Masis, *et al.*, "Carrier scattering mechanisms limiting mobility in hydrogen-doped indium oxide", *Journal of Applied Physics*, vol. 123 (24), p. 9, Jun 2018.
- [24] A. Ingenito, G. Nogay, Q. Jeangros, E. Rucavado, C. Allebe, S. Eswara, *et al.*, "A passivating contact for silicon solar cells formed during a single firing thermal annealing", *Nature Energy*, vol. 3 (9), pp. 800-808, Sep 2018.
- [25] M. Levivier, R. E. Carrillo, R. ChARRIER, A. Martin, J. P. Thiran, "A real-time optimal inverse planning for Gamma Knife radiosurgery by convex optimization: description of the system and first dosimetry data", *Journal of Neurosurgery*, vol. 129, pp. 111-117, Dec 2018.
- [26] I. Mack, J. Stuckelberger, P. Wyss, G. Nogay, Q. Jeangros, J. Horzel, *et al.*, "Properties of mixed phase silicon-oxide-based passivating contacts for silicon solar cells", *Solar Energy Materials and Solar Cells*, vol. 181, pp. 9-14, Jul 2018.
- [27] I. Marozau, M. Auchlin, V. Pejchal, F. Souchon, D. Vogel, M. Lahti, *et al.*, "Reliability assessment and failure mode analysis of MEMS accelerometers for space applications", *Microelectronics Reliability*, vol. 88-90, pp. 846-854, Sep 2018.
- [28] A. C. Martins, V. Chapuis, F. Sculati-Meillaud, A. Virtuani, C. Ballif, "Light and durable: Composite structures for building-integrated photovoltaic modules", *Progress in Photovoltaics*, vol. 26 (9), pp. 718-729, Sep 2018.
- [29] A. C. Martins, V. Chapuis, A. Virtuani, H. Y. Li, L. E. Perret-Aebi, C. Ballif, "Thermo-mechanical stability of lightweight glass-free photovoltaic modules based on a composite substrate", *Solar Energy Materials and Solar Cells*, vol. 187, pp. 82-90, Dec 2018.
- [30] J. A. Mayer, T. Offermans, M. Chrappa, M. Pfannmoller, S. Bals, R. Ferrini, *et al.*, "Optical enhancement of a printed organic tandem solar cell using diffractive nanostructures", *Optics Express*, vol. 26 (6), pp. A240-A250, Mar 2018.
- [31] M. M. McCarthy, A. Walter, S. J. Moon, N. K. Noel, S. O'Brien, M. E. Pemble, *et al.*, "Atomic Layer Deposited Electron Transport Layers in Efficient Organometallic Halide Perovskite Devices", *Mrs Advances*, vol. 3 (51), pp. 3075-3084, 2018.
- [32] S. Mertin, B. Heinz, O. Rattunde, G. Christmann, M. A. Dubois, S. Nicolay, *et al.*, "Piezoelectric and structural properties of c-axis textured aluminium scandium nitride thin films up to high scandium content", *Surface & Coatings Technology*, vol. 343, pp. 2-6, Jun 2018.
- [33] A. Mikhalychev, D. Mogilevtsev, G. Ya. Slepyan, I. Karuseichyk, G. Buchs, D. L. Boiko, A. Boag, "Synthesis of Quantum Antennas for Shaping Field Correlations", *Phys. Rev. Applied*, 9, February 2018, 024021.
- [34] B. Mohamed-Rida, P. Starkov, S. Manzano, F. Hugon, J. Solà, A. Gervaixl, "Diagnostic Performance of an Unsupervised Electronic Stethoscope for Community-acquired Childhood Pneumonia in a Paediatric Emergency Department: a Feasibility Case-control Study", *Swiss Medical Weekly*, vol. 148, pp. 2S-2S, May 2018.
- [35] D. Müller, M. Nogueira, S. Cattaneo, F. Meier, R. Drexel, C. Contado, A. Pagnoni, T. de Vries, D. Cohen, M. Portugal-Cohen, A. deMello, "Integration of Inverse Supercritical Fluid Extraction and Miniaturized Asymmetrical Flow Field-Flow Fractionation for the Rapid Analysis of Nanoparticles in Sunscreens", *Analytical Chemistry*, 90 (5), 02 2018, 3189-3195.
- [36] E. Obrzud, M. Rainer, A. Harutyunyan, B. Chazelas, M. Cecconi, A. Ghedina, *et al.*, "Broadband near-infrared astronomical spectrometer calibration and on-sky validation with an electro-optic laser frequency comb", *Optics Express*, vol. 26 (26), pp. 34830-34841, Dec 2018.

- [37] B. Paviet-Salomon, A. Tomasi, D. Lachenal, N. Badel, G. Christmann, L. Barraud, *et al.*, "Interdigitated back contact silicon heterojunction solar cells featuring an interband tunnel junction enabling simplified processing", *Solar Energy*, vol. 175, pp. 60-67, Nov 2018.
- [38] S. Perrin, H. Li, K. Badu, T. Comparon, G. Quaranta, N. Messaddeq, N. Lemercier, P. Montgomery, J.-L. Vonesch, S. Lecler, "Transmission Microsphere-Assisted Dark-Field Microscopy", *physica status solidi (RRL) – Rapid Research Letters*, Oct 2018.
- [39] A. Poulin, M. Imboden, F. Sorba, S. Grazioli, C. Martin-Olmos, S. Rosset, *et al.*, "An ultra-fast mechanically active cell culture substrate", *Scientific Reports*, vol. 8, p. 10, Jul 2018.
- [40] G. Quaranta, G. Basset, O.-J.-M. Martin, B. Gallinet, "Recent Advances in Resonant Waveguide Gratings", *Laser & Photonics Reviews*, 12 (9), 07 2018, 1800017.
- [41] G. Quaranta, G. Basset, B. Zdenek, O.-J.-M. Martin, B. Gallinet, "Light refocusing with up-scalable resonant waveguide gratings in confocal prolate spheroid arrangements", *Journal of Nanophotonics*, 12 (1), January 2018, 016004.
- [42] M. Rapin, F. Braun, A. Adler, J. Wacker, I. Frerichs, B. Vogt, and O. Chételat, "Wearable Sensors for Frequency-Multiplexed EIT and Multilead ECG Data Acquisition", *IEEE transactions on Biomedical Engineering*, August 2018.
- [43] M. Rapin, J. Wacker, O. Chételat, "Two-Wire Bus Combining Full Duplex Body-Sensor Network and Multilead Biopotential Measurements", *IEEE transactions on Biomedical Engineering*, 65 (1), Jan 2018, 113-122.
- [44] M. Rapin, Y.-J. Regamey, O. Chételat, "Common-mode rejection in the measurement of wearable ECG with cooperative sensors", *De Gruyter, at – Automatisierungstechnik*, 66 (12), Dec 2018, 1002-1013.
- [45] F. Sahli, B. A. Kamino, J. Werner, M. Brauninger, B. Paviet-Salomon, L. Barraud, *et al.*, "Improved Optics in Monolithic Perovskite/Silicon Tandem Solar Cells with a Nanocrystalline Silicon Recombination Junction", *Advanced Energy Materials*, vol. 8 (6), p. 8, Feb 2018.
- [46] F. Sahli, J. Werner, B. A. Kamino, M. Brauninger, R. Monnard, B. Paviet-Salomon, *et al.*, "Fully textured monolithic perovskite/silicon tandem solar cells with 25.2% power conversion efficiency", *Nature Materials*, vol. 17 (9), pp. 820+, Sep 2018.
- [47] S. Senck, M. Scheerer, V. Revol, B. Plank, C. Hannesschläger, C. Gusenbauer, J. Kastner, "Microcrack characterization in loaded CFRP laminates using quantitative two- and three-dimensional X-ray dark-field imaging", *Composites Part A*, 206-214 (115), Oct 2018, 206–214.
- [48] J. Solà, M. Bertschi, J. Krauss, "Measuring Pressure Introducing oBPM, the optical revolution for blood pressure monitoring", *IEEE Pulse*, vol. 9 (5), pp. 31-33, Sep-Oct 2018.
- [49] F. Sorba, C. Martin-Olmos, "High resolution polymer coated strain sensors for in-liquid operation", *Microelectronic Engineering*, vol. 191, pp. 38-41, May 2018.
- [50] P. M. Theiler, F. Lütfolf, R. Ferrini, "Non-contact printing of optical waveguides using capillary bridges", *Optics Express*, 26 (9), April 2018, 11934-11939.
- [51] C. Trompoukis, A. Abass, J. W. Schuttauf, T. Bosserez, J. Ronge, J. Lauwaert, *et al.*, "Porous multi junction thin-film silicon solar cells for splitting", *Solar Energy Materials and Solar Cells*, vol. 182, pp. 196-203, Aug 2018.
- [52] J. van den Boer, A. van der Lee, L. Zhou, V. Papapanagiotou, C. Diou, A. Delopoulos, M. Mars, "The SPLENDID Eating Detection Sensor: Development and Feasibility Study", *JMIR Mhealth Uhealth*, 6 (9), Sept 2018.
- [53] M. Villiger, R. Stoop, T. Vetsch, E. Hohenauer, M. Pini, P. Clarys, *et al.*, "Evaluation and review of body fluids saliva, sweat and tear compared to biochemical hydration assessment markers within blood and urine", *European Journal of Clinical Nutrition*, vol. 72 (1), pp. 69-76, Jan 2018.
- [54] A. Vizbaras, I. Šimonytė, A. Miasojedovas, A. Trinkūnas, T. Bučiūnas, M. Greibus, G. Naujokaitė, N. Torcheboeuf, S. Droz, D. L. Boiko, Ž. Dambrauskas, A. Gulbinas, K. Vizbaras, "Swept-wavelength lasers based on GaSb gain chip technology for non-invasive biomedical sensing applications in the 1.7–2.5 μm wavelength range", *Biomedical Optics Express*, 8 (10), Oct 2018, 4838-4849.
- [55] T. Volden, J. Goldowsky, N. Schmid, V. Revol, "Portable Systems for Metered Dispensing of Aggressive Liquids", *Slas Technology*, vol. 23 (5), pp. 470-475, Oct 2018.
- [56] A. Walter, S. J. Moon, B. A. Kamino, L. Lofgren, D. Sacchetto, F. Matteocci, *et al.*, "Closing the Cell-to-Module Efficiency Gap: A Fully Laser Scribed Perovskite Minimodule With 16% Steady-State Aperture Area Efficiency", *IEEE Journal of Photovoltaics*, vol. 8 (1), pp. 151-155, Jan 2018.

- [57] J. Werner, B. Niesen, C. Ballif, "Perovskite/Silicon Tandem Solar Cells: Marriage of Convenience or True Love Story? - An Overview", *Advanced Materials Interfaces*, vol. 5 (1), p. 19, Jan 2018.
- [58] J. Werner, F. Sahli, F. Fu, J. J. D. Leon, A. Walter, B. A. Kamino, et al., "Perovskite/Perovskite/Silicon Monolithic Triple-Junction Solar Cells with a Fully Textured Design", *Acs Energy Letters*, vol. 3 (9), pp. 2052-2058, Sep 2018.
- [59] J. Werner, G. Nogay, F. Sahli, T. C. J. Yang, M. Brauninger, G. Christmann, et al., "Complex Refractive Indices of Cesium-Formamidinium-Based Mixed-Halide Perovskites with Optical Band Gaps from 1.5 to 1.8 eV", *Acs Energy Letters*, vol. 3 (3), pp. 742-747, Mar 2018.
- [60] T. C. J. Yang, P. Fiala, Q. Jeangros, C. Ballif, "High-Bandgap Perovskite Materials for Multijunction Solar Cells", *Joule*, vol. 2 (8), pp. 1421-1436, Aug 2018.

Proceedings

- [1] T. Aderneuer, "Metameric Circadian Lighting: A Technology Analysis", *LED Professional Symposium (LpS 2018)*, Bregenz (AT), September 2018.
- [2] D. R. Andersson, H. Grönqvist, K. Mayora, M. Tijero, G. Voirin, A. Steinke, A. Albrecht, H. Wünscher, T. Frank, E. Moore, Y. Wang, "Smart access to small lot manufacturing for systems integration", *Pan Pacific Microelectronics Symposium (Pan Pacific)*, IEEE, Hawai (US), 5–8 February 2018, 1-9.
- [3] E. Annigoni, A. Virtuani, J. Levrat, A. Faes, M. Despeisse, C. Ballif, "Quantifying and Modeling the Impact of Interconnection Failures on the Electrical Performance of Crystalline Silicon Photovoltaic Modules", *IEEE 7th World Conference on Photovoltaic Energy Conversion (WCPEC)*, Waikoloa (USA), 10–15 June 2018, 3815–3818.
- [4] A. A. Antonov, D. I. Kuritsyn, A. Gajic, E. E. Orlova, N. Vukovic, J. Radovanovic, V. V. Vaks, D. L. Boiko, "Controlling the Quantum Cascade Laser Frequency Comb via Risken-Nummedal-Graham-Haken Instability", *IEEE International Semiconductor Laser Conference (ISLC)*, Santa Fe (USA), 16–19 September 2018, 1–2.
- [5] A. Arnaud, E. Romero, C. Remacha, D. Murer, D. Just, V. Revol, H. Proudhon, "Nondestructive testing of single crystal alloy by X-ray diffraction", *Nondestructive Evaluation of Aerospace Materials & Structures 2018*, Bridgeton (US), 5–6 June 2018.
- [6] M. Asgari, F. Lucci, B. Dunan, R. Smajda, G. Andreatta, S. Majeed, J. Bialek, S. Steiner, S. Frentzel, J. Hoeng, N. Blondiaux, J.-P. Schaller, A. K. Kuczaj, "Computational and experimental approaches to understand multispecies aerosol evolution and deposition in biologically relevant conditions", *Aerosol Technology 2018*, Bilbao (ES), 18–20 June 2018.
- [7] C. Ballif, M. Boccard, M. Despeisse, "The amazing improvement of silicon heterojunction technology: ready for a true mass market launch", *IEEE 7th World Conference on Photovoltaic Energy Conversion (WCPEC)*, Waikoloa (USA), 10–15 June 2018, 2104–2107.
- [8] G. Borque Gallego, L. Rossini, T. Achtnich, C. Zwyssig, D. Martins Araujo, Y. Perriard, "Force Analysis of a Slotless Lorentz-Type Active Magnetic Bearing Actuator", *21st International Conference on Electrical Machines and Systems - ICEMS 2018*, Jeju (KR), 7–10 October 2018.
- [9] G. Buchs, S. Karlen, T. Overstolz, N. Torcheboeuf, E. Onillon, J. Haesler, et al., "Nuclear spin decoherence time in MEMS atomic vapor cells for applications in quantum technologies", in *Fourth International Conference on Quantum Technologies*, vol. 1936, A. I. Lvovsky, M. L. Gorodetsky, and A. N. Rubtsov, Eds., ed Melville: Amer Inst Physics, 2018.
- [10] F. Crivelli, V. Baumann, M. Steiner, M. D'Urso, P. A. E. Schmid, A. Steinecker, "An all-in-one robotic platform for hybrid manufacturing of large volume parts", *8th International Precision Assembly Seminar (IPAS 2018)*, Chamonix (FR), 14–15 January 2018.
- [11] R. Delgado-Gonzalo, P. Renevey, A. Tarniceriu, J. Parak, M. Bertschi, "Learning a physical activity classifier for a low-power embedded wrist-located device", *IEEE EMBS International Conference on Biomedical & Health Informatics (BHI)*, Las Vegas (USA), 4–7 March 2018, 54–57.
- [12] M. Despeisse, L. Barraud, B. Paviet-Salomon, A. Descoeuadres, L.-L. Senaud, C. Allebé, J. Levrat, J. Horzel, A. Lachowicz, F. Debrot, J. Champliaud, A. Faes, N. Badel, J. Geissbühler, S. Martin de Nicolas, G. Christmann, J. Diaz, L. Ding, S. Nicolay, C. Ballif, "Engineering of Thin-Film Silicon Materials for High Efficiency Crystalline Silicon Solar Cells", *IEEE 7th World Conference on Photovoltaic Energy Conversion (WCPEC)*, Waikoloa (USA), 10-15 June 2018, 3888-3889.
- [13] O. Dupre, J. Levrat, J. Champliaud, M. Despeisse, M. Boccard, C. Ballif, "Reassessment of Cell to Module Gains and Losses: Accounting for the Current Boost Specific to Cells Located on the Edges", in *SiliconPV 2018: The 8th International Conference on Crystalline Silicon Photovoltaics*, vol. 1999, C. Ballif, R. Brendel, S. Glunz, G. Hahn, J. Poortmans, P. J. Ribeyron, et al., Eds., ed Melville: Amer Inst Physics, 2018.

- [14] O. Fernandez, "Semi-empirical characterization of freeform microlens arrays", LED Professional Symposium (LpS 2018), Bregenz (AT), September 2018.
- [15] Z. Halvorsen, H. F. Knapp, N. Schmid, V. Revol, S. Stavrakis, A. deMello, P. Ryser, "Miniaturization of fluid sample preparation platform for automated flow cytometry", International MicroNanoConference, Amsterdam (NL), 11-12 December 2018.
- [16] J. Haschke, R. Monnard, L. Antognini, J. Cattin, A. A. Abdallah, B. Aissa, et al., "Nanocrystalline Silicon Oxide Stacks for Silicon Heterojunction Solar Cells for Hot Climates", in Siliconpv 2018: The 8th International Conference on Crystalline Silicon Photovoltaics. vol. 1999, C. Ballif, R. Brendel, S. Glunz, G. Hahn, J. Poortmans, P. J. Ribeyron, et al., Eds., ed Melville: Amer Inst Physics, 2018.
- [17] M. Höchemer, "System Health Monitoring and Predictive Maintenance with Neural Networks", ILT Symposium on Lab Automation, Rapperswil (CH), 22 March 2018.
- [18] A. Ingenito, C. Allebe, G. Nogay, J. Horzel, P. Wyss, J. A. Stuckelberger, M. Despeisse, F.-J. Haug, C. Ballif, "A passivating contact concept compatible with a short thermal treatment", IEEE 7th World Conference on Photovoltaic Energy Conversion (WCPEC), Waikoloa (USA), 10-15 June 2018, 1524–1525.
- [19] P. Jokic, S. Emery, L. Benini, "BinaryEye: A 20 kfps Streaming Camera System on FPGA with Real-Time On-Device Image Recognition Using Binary Neural Networks", 13th International Symposium on Industrial Embedded Systems (SIES), Graz (AT), 6 June 2018.
- [20] S. Karlen, T. Overstolz, J. Gobet, J. Haesler, F. Droz, S. Lecomte, "Gold microdisks as alkali preferential condensation spots for cell clock long-term frequency improvement", EFTF 2018, Torino (IT), 16 April 2018.
- [21] I. Kastanis, P. Purwar, J. Sun, M. Höchemer, P. A. E. Schmid, A. Steinecker, "Machine Learning Using Satellite Imaging for Agriculture", EPoSS Annual Forum 2018, Thessaloniki (Gr), 2 October 2018.
- [22] I. Kastanis, P. Purwar, P. A. E. Schmid, A. Steinecker, "A Recurrent Neural Network (RNN) based approach for reliably classifying land usage from satellite imagery", Scientific Symposium FAIR Data Sciences for Green Life Sciences, Wageningen (NL), 12 December 2018.
- [23] L. Kiener, P. Spanoudakis, A. Verhaeghe, G. Perruchoud, P. Schwab, M. Gumy, "Development challenges of a focus mechanism for EXOMARS mission submitted to the harsh Martian environment", in Advances in Optical and Mechanical Technologies for Telescopes and Instrumentation iii. vol. 10706, R. Navarro and R. Geyl, Eds., ed Bellingham: Spie-Int Soc Optical Engineering, 2018.
- [24] L. Kiener, P. Spanoudakis, A. Verhaeghe, G. Perruchoud, P. Schwab, M. Gumy, "Development challenges of a focus mechanism for EXOMARS mission submitted to the harsh Martian environment", SPIE Astronomical Telescopes + Instrumentation, Austin (US), 12 June 2018.
- [25] C. Kirsch, R. Ferrini, T. Offermans, S. Altazin, M. Diethelm, R. Hiestand, L. Penninck, T. Beierlein, M. Regnat, B. Ruhstaller, "Electrothermal simulation of large-area semiconductor devices", SimOEP, Winterthur (CH), 4 September 2018.
- [26] M. Krakowski, P. Resneau, M. Garcia, E. Vinet, Y. Robert, M. Lecomte, O. Parillaud, B. Gerard, S. Kundermann, N. Torcheboeuf, D. L. Boiko, "High pulse energy stabilized passively mode-locked external cavity inverse bow-tie 980nm laser diode for space applications", Photonics West OPTO 2018, San Francisco (US), 1 February 2018, 10553–21.
- [27] M. Krakowski, P. Resneau, M. Garcia, E. Vinet, Y. Robert, C. Theveneau, M. Lecomte, O. Parillaud, B. Gerard, S. Kundermann, N. Torcheboeuf, D. L. Boiko, "Tapered Monolithic Mode-Locked Laser Diode with 200pJ Pulse Energy for Space Applications", IEEE International Semiconductor Laser Conference (ISLC), Santa Fe (USA), 16–19 September 2018, 227–228.
- [28] A. Lemkaddem, R. Delgado-Gonzalo, E. Türetken, S. Dasen, V. Moser, C. Gressum, J. Solà, D. Ferrario, C. Verjus, "Multi-modal driver drowsiness detection: A feasibility study", IEEE EMBS International Conference on Biomedical & Health Informatics (BHI), Las Vegas (USA), 4–7 March 2018, 9–12.
- [29] N. Marjanović, J. Disser, F. Zanella, J. Schleuniger, A. Mustaccio, R. Ferrini, M. Schnieper, E. Assaf, "Hybrid lightweight and flexible circuit boards for satellites", Electronic System-Integration Technology Conference (ESTC), Dresden (DE) 18–21 September 2018, DOI 10.1109/ESTC.2018.8546420.

- [30] W. Martin, Y. Stauffer, C. Ballif, A. Hutter, P.-J. Alet, and IEEE, "Automated quantification of PV hosting capacity in distribution networks under user-defined control and optimisation procedures", in 2018 IEEE Pes Innovative Smart Grid Technologies Conference Europe, ed New York: IEEE, 2018.
- [31] E. Obrzud, M. Rainer, A. Harutyunyan, M.H. Anderson, J. Liu, M. Geiselmann, B. Chazelas, S. Kundermann, S. Lecomte, M. Cecconi, A. Ghedina, E. Molinari, F. Pepe, F. Wildi, F. Bouchy, T. J. Kippenberg, T. Herr, "Synchronously-Driven Microresonator Solitons and Application in Astronomy", European Conference on Optical Communication (ECOC), Rome (IT), 23-27 September 2018, 1–3.
- [32] E. Obrzud, V. Brasch, S. Lecomte, T. Herr, "Temporal cavity solitons in synchronously-driven Fabry-Perot microresonators", in Laser Resonators, Microresonators, and Beam Control, vol. 10518, A. V. Kudryashov, A. H. Paxton, and V. S. Ilchenko, Eds., ed Bellingham: Spie-Int Soc Optical Engineering, 2018.
- [33] P. Pad, N. Niketic, A. Chebira, E. Franzi, L. A. Dunbar, "Versatile, intelligent multispectral imaging camera made with off-the-shelf components", Photonic Instrumentation Engineering V - Photonics West 2018, San Francisco (US), January 2018.
- [34] S. Paoletti, "Recent advances in non-invasive diagnostics, 3rd NanoBio Surfaces and Interfaces in Healthcare and Science Workshop", Recent advances in non-invasive diagnostics, 3rd NanoBio Surfaces and Interfaces in Healthcare and Science Workshop, Lausanne (CH), 8–9 May 2018.
- [35] A. Pollini, C. Pache, J. Haesler, et al., "CSEM Space Lidars for Imaging and Rangefinding", in Igasss 2018 – IEEE International Geoscience and Remote Sensing Symposium, ed New York: IEEE, 2018, pp. 1849–1852.
- [36] M. Proen  , O. Grossenbacher, S. Dasen, V. Moser, D. Ostojic, A. Lemkaddem, D. Ferrario, M. Lemay, M. Wolf, J.-C. Fauch  re, T. Karen, "Performance Assessment of a Dedicated Reflectance Pulse Oximeter in a Neonatal Intensive Care Unit", 40th Annual International Conference of the IEEE Engineering in Medicine and Biology Society (EMBC), Honolulu (USA), 18–21 July 2018, 1502–1505.
- [37] G. Quaranta, G. Basset, B. Gallinet, M. Schnieper, "Smartphone-based authentication with a new color-selective DOVID", Optical Document Security, San Francisco (US), January 2018, 162–168.
- [38] M. Rapin, F. Braun, J. Wacker, O. Ch  telat, "Performance Assessment of a Wearable EIT System", 19th International Conference on Biomedical Application of Electrical Impedance Tomography, Edinburgh (UK), June 2018.
- [39] P. Renevey, R. Delgado-Gonzalo, C. Verjus, S. Combertaldi, B. Rasch, B. Leeners, F. Dammeier, F. K  bler, "Respiratory and Cardiac Function Monitoring During Night Using a Wrist-worn Optical Device", IEEE Biomedical and Health Informatics (BHI), Las Vegas (US), 4–7 March 2018.
- [40] P. Renevey, R. Delgado-Gonzalo, A. Lemkaddem, C. Verjus, S. Combertaldi, B. Rasch, B. Leeners, F. Dammeier, F. K  bler, "Respiratory and cardiac monitoring at night using a wrist wearable optical system", 40th Annual International Conference of the IEEE Engineering in Medicine and Biology Society (EMBC2018), Honolulu (US), 17–21 July 2018.
- [41] P. Renevey, R. Delgado-Gonzalo, C. Verjus, S. Combertaldi, B. Rasch, B. Leeners, F. Dammeier, F. K  bler, "Sleep analysis using optical wrist-worn system", SSBE, Bern (CH), August 2018.
- [42] P. Renevey, R. Delgado-Gonzalo, A. Lemkaddem, C. Verjus, S. Combertaldi, B. Rasch, B. Leeners, F. Dammeier, F. K  bler, "Respiratory and cardiac monitoring at night using a wrist wearable optical system", 40th Annual International Conference of the IEEE Engineering in Medicine and Biology Society (EMBC), Honolulu (USA), 18–21 July 2018, 2861–2864.
- [43] C. Rojas, J.-D. Decotignie, et al., "Leveraging MAC Preambles for an Efficient Link Estimation", in 2018 14th International Conference on Wireless and Mobile Computing, Networking and Communications, ed New York: IEEE, 2018.
- [44] C. Rojas, J.-D. Decotignie, "Synchronous transmissions + channel sampling = energy efficient event-triggered wireless sensing systems", 14th IEEE International Workshop on Factory Communication Systems (WFCS), Imperia (IT), 13–15 June 2018, 1–10.
- [45] C. Rojas, J.-D. Decotignie, "Leveraging MAC Preambles for an Efficient Link Estimation", 14th International Conference on Wireless and Mobile Computing, Networking and Communications (WiMob), Limassol (Cyprus), 15–17 October 2018, 1–10.

- [46] H. Saudan, L. Kiener, G. Perruchoud, J. Kruis, K. Vaideeswaran, M. M. Dadras, *et al.*, "Compliant mechanisms and space grade product redesign based on Additive Manufacturing", in Advances in Optical and Mechanical Technologies for Telescopes and Instrumentation lii, vol. 10706, R. Navarro and R. Geyl, Eds., ed Bellingham: Spie-Int Soc Optical Engineering, 2018.
- [47] E. K. Schaller, "Sail Profile Performance Monitoring", Marine Equipment Trade Show / Conference - METS, E. Schaller, Amsterdam (NL), 14 November 2018.
- [48] P. A. E. Schmid, "Augmented working places, robot companions and bin picking", COMS 2018 - Commercialisation of Emerging Technologies, Montreux (CH), 25–26 September 2018.
- [49] J. Sola, M. Proençā, P. Schoettker, A. Lemkadem, F. Braun, C. Verjus, M. Bertschi, E. Jones, T. Kunz, "Blood Pressure Monitoring Using a Smartphone Camera: Performance of the OBPM Technology", IEEE Biomedical and Health Informatics (BHI), Las Vegas (US), 4–7 March 2018.
- [50] J. Sola, Y. Ghamri, M. Proençā, F. Braun, N. Pierrel, C. Verjus, M. Bertschi, P. Schoettker, "Tracking Blood Pressure Changes in Anesthetized Patients: the Optical Blood Pressure Monitoring (oBPM) Technology", 40th Annual International Conference of the IEEE Engineering in Medicine and Biology Society (EMBC2018), Honolulu (US), 17–21 July 2018.
- [51] P. Starkov, S. Manzano, F. Hugon, F. Braun, A. Lemkadem, C. Verjus, R. Delgado-Gonzalo, J. Sola, A. Gervaix, M.-R. Benissa, "Pediatric respiratory rate estimation through deep neural nets", 40th Annual International Conference of the IEEE Engineering in Medicine and Biology Society (EMBC2018), Honolulu (US), 17–21 July 2018.
- [52] A. Tarniceriu, J. Harju, A. Vehkaoja, J. Parak, R. Delgado-Gonzalo, P. Renevey, A. Yli-Hankala, I. Korhonen, "Detection of beat-to-beat intervals from wrist photoplethysmography in patients with sinus rhythm and atrial fibrillation after surgery", IEEE EMBS International Conference on Biomedical & Health Informatics (BHI), Las Vegas (USA), 4–7 March 2018, 133–136.
- [53] P. Theurillat, M. Rapin, M. Crettaz, P. Liechti, J. Wacker, E. Haenni, O. Chételat, "ASICSENSE: A Highly integrated thin and soft", World Congress on Medical Physics and Biomedical Engineering, Prague (CZ), 3–8 June 2018.
- [54] B. Timotijevic, L. A. Dunbar, A. Hoogerwerf, "Novel micro-fabricated Fabry-Perot filters in infrared", Photonics West, San Francisco (US), February 2018.
- [55] N. Torcheboeuf, S. Droz, I. Šimonytè, A. Miasojedovas, A. Trinkunas, K. Vizbaras, A. Vizbaras, D. L. Boiko, "MEMS Tunable Littman-Metcalf Diode Laser at 2.2µm for Rapid Broadband Spectroscopy in Aqueous Solutions", IEEE International Semiconductor Laser Conference (ISLC), Santa Fe (USA), 16–19 September 2018, 1–2.
- [56] T. Volden, S. Graf, S. Berchtold, V. Revol, "Microfluidic cartridge for liquid biopsy from whole blood with embedded reagents", International MicroNanoConference, Amsterdam (NL), 11–12 December 2018.
- [57] A. Vorobyov, E. Daskalaki, J. R. Farserotu, "Feasibility of Remote Vital Signs Sensing with a mm-Wave CW Reflectometer", 2018 IEEE 38th International Conference on Electronics and Nanotechnology (ELNANO), Kiev (UA), 24–26 April 2018, 417.
- [58] W. L. Wu, W. J. Lin, S. H. Zhong, B. Paviet-Salomon, M. Despeisse, Z. C. Liang, *et al.*, "22% Efficient Dopant-free Interdigitated Back Contact Silicon Solar Cells", in Siliconpv 2018: The 8th International Conference on Crystalline Silicon Photovoltaics, vol. 1999, C. Ballif, R. Brendel, S. Glunz, G. Hahn, J. Poortmans, P. J. Ribeyron, *et al.*, Eds., ed Melville: Amer Inst Physics, 2018.

Conferences and Workshops

N. Blondiaux, P.-F. Chauvy, M. Diserens, R. Pugin, "Surface structuring of 3D metal microparts and microstructured molds by means of nanosphere lithography", EUSPEN, Saclay (FR), 27–29 November 2018.

N. Blondiaux, R. Pugin, P.-F. Chauvy, M. Diserens, P. Vuillermoz, G. Vuillermoz, "Surface Nanostructuring of TiN Coated Microstructured Mold, Application to a Biodiagnostic Platform", World Congress on Micro and Nano Manufacturing, Portorož (SI), 18 September 2018.

- L. Burr, D. Schmid, S. Cattaneo, S. Generelli, "Characterization of nanomaterials for risk assessment – a tiered approach", Swiss Nanoconvention, Zürich (CH), 6–7 June 2018.
- F. Crivelli, V. Baumann, "Lasertracking in der Industrierobotik: EU Horizon 2020 Projekt KRAKEN", Geomatik-Frühlings-Kolloquium (FHNW), Muttenz (CH), 22 May 2018.
- M. Dadras, O. Sereda, K. Vaideeswaran, C. Yanahata, A. Bohlen, C. Spoerl, "Surface properties improvement of bio-compatible Ti6Al4V alloy by multi-charged ion implantation", 4th International Conference on Bio Tribology, Montreal (CA), 26–29 September 2018.
- M. Despont, "Additive Manufacturing meets Microsystems", NCEM-6, Barcelona (ES), 20–21 November 2018.
- S. Fricke, "Gedruckte Elektronik – Von der Forschung zur industriellen Anwendung", IVAM Systems Integration 2018, Alpnach (CH), 1 January 2018.
- L. Gasparini, M. Perenzoni, H. Xu, L. Parmesan, M. Moreno Garcia, D. Stoppa, B. Bessire, M. Unternährer, A. Stefanov, V. Mitev, D. L. Boiko, "Imaging with entangled photons", 1st International SPAD Sensor Workshop ISSW, Les Diablerets (CH), 28 February 2018.
- J. Haesler, S. Karlen, T. Overstolz, G. Buchs, D. L. Boiko, F. Droz, S. Lecomte, "MEMS atomic vapor cells at CSEM and their applications", Hot vapor workshop, Stuttgart (DE), 24 May 2018.
- M. Höchemer, "System Health Monitoring and Predictive Maintenance with Neural Networks", Swiss Symposium on Laboratory Automation, Rapperswil (CH), 22 March 2018.
- R. Jose James, G. Spinola Durante, M. Fretz, and A. Hoogerwerf, "Miniature, Hermetic Optical-Transparent Packages: from Active Implantable Medical Devices to Space Applications", Electronic Materials and Processes for Space Workshops EMPS-9, Yverdon-les-Bains (CH), 25–26 April 2018.
- S. Karlen, T. Overstolz, J. Gobet, J. Haesler, F. Droz, S. Lecomte, "MEMS atomic vapor cells fabrication and their performances in miniature atomic clocks", Hot vapor workshop, Stuttgart (DE), 24 May 2018.
- L. Kiener, H. Saudan, P. Spanoudakis, "AMAR - Additive Manufacturing of a SlipRing Assembly Rotor", ESA Mechanisms Final Presentation days, Noordwijk (NL), 16 March 2018.
- L. Kiener, P. Spanoudakis, A. Verhaeghe, Y.-J. Regamey, "High Accuracy, Flexure Guide Linear Scan Mechanisms for Space Applications", ESA Workshop on Optical Mechanisms & Mechanisms Final Presentation days, Noordwijk (NL), 14 March 2018.
- L. Kiener, "Tendances générales et exemples d'applications récentes en fabrication additive métallique", Comité Romand SWISSMEM, Delémont (CH), 23 March 2018.
- M. Krieger, "Sensors – Key Elements in the new world of Digitalization", Swissmem Delegation of Irish IoT companies in Switzerland, Zürich (CH), 12 June 2018.
- M. Krieger, "Technologies for Food Packaging", Swiss Food Research NTN Conference Food Packaging Workgroup, Brugg-Windisch (CH), 24 May 2018.
- S. Lani, "Additive Manufacturing: Moving to smaller and smarter components", MAM2018, Villars sur Ollon (CH), 4–6 February 2018.
- S. Lani, "Digital mirror array for harsh environment", Photonics West, San Francisco (US), 27 January–1 February 2018.
- F. Loizeau, "How Can MEMS Technologies Support SMEs' Innovation?", NEM2018, Singapore (SG), 22–26 April 2018.
- F. Lütolf, P. M. Theiler, L. Dümpelmann, J. Müller, S. Aghajani, A. Luu-Dinh, B. Gallinet, R. Ferrini, "Inkjet Printing for Photonics", LOPEC, Munich (DE), 15 March 2018.
- F. Lütolf, P. M. Theiler, L. Dümpelmann, J. Müller, S. Aghajani, M. Loretan, A. Luu-Dinh, B. Gallinet, R. Ferrini, "Inkjet Printing from waveguiding to plasmonics", Photonics Europe, Strasbourg (FR), 23 April 2018.
- N. Marjanovic, "Hybrid electronics systems by CSEM", EC Workshop on Flexible and Printed Electronics, Brussels (BE), 1 December 2018.
- I. Marozau, M. Auchlin, V. Pejchal, O. Sereda, "Reliability assessment and failure mode analysis of MEMS accelerometers for space applications", ESREF 2018 Conference, Aalborg (DK), 1–4 October 2018.
- I. Marozau, O. Sereda, M. Dadras, F. Souchon, D. Vogel, M. Lahti, N. Saillen, "MEMS reliability assessment for space applications", Electronics Materials & Processes for Space (EMPS) Workshops, Yverdon-les-Bains (CH), 25–26 April 2018.
- F. Meier, D. Müller, S. Cattaneo, C. Contado, T. de Vries, M. Portugal-Cohen, A. deMello, "Analysis of Nanoparticles in Sunscreens via Inverse Supercritical Fluid Extraction and Miniaturized Asymmetrical Flow FFF", Swiss NanoConvention 2018, Zürich (CH), 6–7 June 2018.
- C. Moufawad el Achkar, A. Lemkadem, E. Muntané Calvo, P. Renevey, R. Delgado-Gonzalo, S. Morton, S. Hughes, A. Bangash, Carlo Allocca, R. Ail, C. Verjus, "Real-time Fall Detection Using Smartwatches", EU Falls Festival, Manchester (UK), 2–3 July 2018.
- B. Niesen, J. Werner, F. Sahli, B. A. Kamino, M. Bräuninger, P. Fiala, T. Yang, A. Walter, S.-J. Moon, L. Barraud, B. Paviet-Salomon, C. Allebé, R. Monnard, O. Dupré, M. Boccard, M. Despeisse, Q. Jeangros, S. Nicolay, C. Ballif, "High-Efficiency 4-Terminal and Monolithic Perovskite / Silicon Tandem Solar Cells", Spring MRS, Phoenix, AZ (US), April 2018.
- J. Pierer, A. Steinecker, P. A. E. Schmid, "Visual Inspection Technologies", EPIC Meeting on Automation Tools for Packaging and Testing, Karlsruhe (DE), 22–23 May 2018.

- M. Proen  , M. Lemay, F. Braun, J. Sol  , S. F. Rimoldi, E. Rexhaj, "Towards non-invasive pulmonary artery pressure monitoring", Medtech & Pharma Platform Annual Meeting, Basel (CH), October 2018.
- R. Pugin, G. Andreatta, N. Blondiaux, X. Bulliard, A. Grivel, N. Hendricks, R. Smajda, G. Voirin, G. Weder, "Fabrication of nanostructured surfaces and components with enhanced performances or unique physical, chemical or biological properties", Nanotexnology conference NN18, Thessaloniki (GR), 2 July 2018.
- R. Pugin, G. Andreatta, N. Blondiaux, X. Bulliard, A. Grivel, N. Hendricks, R. Smajda, G. Voirin and G. Weder, "Surface Engineering at the micro/nanoscale", Infomat, Neuch  tel (CH), 8 November 2018.
- N. Rauschmayr, "Improving Passenger Safety with the Power of Deep Learning", NVIDIA Webinar Series, 29 August 2018.
- N. Rauschmayr, M. Hoechemer, "Deep Learning of Railway Track Faults using GPUs", GPU technology Conference (GTC), Silicon Valley (US), March 2018.
- V. Revol, "CSEM – Innovation Partner for the Life Sciences Industry", MIPTEC Stage, Alpnach (CH), 12 September 2018.
- V. Revol, "Der Doktor immer dabei – Science Fiction oder Realit  ?", SATW TecNight, Frauenfeld (CH), 22 October 2018.
- V. Revol, "Der Doktor immer dabei – Science Fiction oder Realit  ?", SATW TecNight, Sarnen (CH), 23 January 2018.
- V. Revol, "Digital Revolution in the Laboratory – Insights into CSEM technologies and LabTour", Precision Liquid Handling Workshop, Neuch  tel (CH), 23 October 2018.
- V. Revol, "How micro-technologies enable to capture the full potential of new micro-physiological systems – examples of technology transfer", Basel Life - Microfluidics and microenvironment workshop, Basel (CH), 14 September 2018.
- J. Schleuniger, "Smart implants by printed electronics", Bern-Spiessl-Symposium, Basel (CH), 14–16 June 2018.
- P. A. E. Schmid, A. Steinecker, "Data analysis / Application of neural networks in industry, automotive and medical applications for predictive maintenance and increased customer value", International Conference and Exhibition SIA CESA 5.0, Versailles (FR), 5–6 December 2018.
- P. A. E. Schmid, "Deep Learning to monitor and predict health-status of industrial machines.", Maintenance Pr  dictive - GESO, sensors.ch, fsrm, Neuch  tel (CH), 30 November 2018.
- P. A. E. Schmid, "Deep Learning: Revolution im Alltag", SATW TecNight, Frauenfeld (CH), 15 November 2018.
- P. A. E. Schmid, "Industrielle Revolution 4.0 - Chancen & Risiken f  r die Schweiz", Podiumsdiskussion by Zofingue Suisse, Luzern (CH), 28 July 2018.
- P. A. E. Schmid, J. Casutt, "Maintaining excellent passenger safety with the power of deep learning", CSEM Business Day - From Big Data to Smart Data, Neuch  tel (CH), 7 November 2018.
- P. A. E. Schmid, "LeafEye – Leaf Classification with Deep Learning", 3th Meeting of the Agro-Food Digitalization Innovation Group, Neuch  tel (CH), 15 November 2018.
- P. A. E. Schmid, M. H  chemer, I. Kastanis, A. Steinecker, "Mit Deep Learning von Big Data zu Smart Data – F  r industrielle Prozesse", Fachgruppensitzung Smart Systems - Robert Bosch GmbH, Renningen (DE), 12 October 2018.
- P. A. E. Schmid, M. Krieger, "Starten Sie Ihre Digitale Reise", Digital Summit f  r KMU, Z  rich (CH), 29 August 2018.
- P. A. E. Schmid, "Machine Learning im Dienste der Landwirtschaft", 5. Nationale Ackerbautagung, Murten (CH), 30 January 2018.
- P. A. E. Schmid, "Machine Learning im industriellen Umfeld", IVAM Systems Integration 2018, Alpnach (CH), 16 January 2018.
- P. A. E. Schmid, "Neuronale Netzwerke: Revolution im Alltag", SATW TecNight, Sarnen (CH), 23 January 2018.
- P. A. E. Schmid, "Predictive Maintenance mit Deep Learning f  r Robotik & Automation", 3. F&E-Konferenz zu Industrie 4.0, Brugg (CH), 15 January 2018.
- P. A. E. Schmid, "Von der Mikrorobotik zum gr  sstten Hybriden Industrieroboter der Welt - KRAKEN", Swissmem - Besichtigung zum Thema „Industrielle Revolution – Teil 2, Alpnach (CH), 7 September 2018.
- O. Sereda, M. Dadras, K. Vaideeswaran, A. B  hlen, C. Yamahata, C. Spoerl, "PEEK tribology properties improvement by helium multi-charged ion implantation", 4th International Conference on Bio Tribology, Montreal (CA), 26–29 September 2018.
- F. Sorba, C. Martin Olmos, "Fabrication of high resolution insulated strain sensors", Micro Nano Engineering MNE, Copenhagen (DK), 24–27 September 2018.
- R. Smajda, G. Voirin, G. Andreatta, A. Grivel, S. Heub, R. Pugin, "Miniaturized sensor fabrication using AerosolJet Technology for biological and chemical detection", SIWAN8, Szeged (HU), 7 October 2018.
- F. Sorba, A. Poulin, B. Dunan, M. Despont, H. Shea, C. Martin Olmos, "Miniaturized elastomer-based pneumatic actuator to measure mechanical properties of cell monolayers", ESMC 2018, Bologna (IT), 02–04 July 2018.
- F. Sorba, H. Shea, C. Martin Olmos, "Viscoelastic response of epithelial cell monolayers", MEMS 2018, Copenhagen (DK), 24–27 September 2018.
- F. Sorba, H. Shea, M. Despont, C. Martin-Olmos, "Tissue-scale mechanical properties measured on a pneumatically actuated microfluidic device", Proceedings of the Miniaturized Systems for Chemistry and Life Sciences (MicroTAS) Conference, Kaohsiung (TW), 11–15 November 2018.

F. Sorba, R. Ischer, C. Martin Olmos, "Single cell force measurements through high sensitive in-liquid strain sensors", Micro TAS 2018, Kaohsiung (TW), 11–15 November 2018.

P. Spanoudakis, "Large Angle Flexure Pivot Development for High Accuracy Positioning of Optical Payloads", ESA Workshop on Optical Mechanisms 2018, Noordwijk (NL), 14 March 2018.

G. Spinola Durante, P.-A. Clerc, M. Fretz, A. Hoogerwerf, R. Jose James, M. Despont, O. Dubochet, M.-A. Dubois, S. Mohrdiek, "Packaging technologies for harsh environments based on silicon-carbide (SiC) substrates ", Minapad 2018, Grenoble (FR), 16–17 May 2018.

G. Spinola Durante, et al., "Sensors Design & Simulation at CSEM", Workshop CSEM-Melexis, Neuchâtel (CH), 20 September 2018.

A. Steinecker, "Application of advanced data analysis in industrial environment", Smart Systems Integration 2018 – EpoSS Workshop, Dresden (DE), 11–12 April 2018.

A. Steinecker, "Datenanalyse mit neuronalen Netzwerken im industriellen Umfeld", microTEC Südwest Clusterkonferenz 2018, Freiburg (DE), 16–17 April 2018.

A. Steinecker, F. Crivelli, "Das Multitalent: Automated, Multimaterial, Additive & Subtractive Manufacturing", tfz Product&System Lunch Meeting, Steinhausen (CH), 25 September 2018.

A. Steinecker, "Packaging of active implants. Miniaturized light emitters and pressure sensors for various applications.", COMPAMED Frühjarsforum, Frankfurt am Main (DE), 3 May 2018.

A. Steinecker, "Technologies for the Medtech and Life Sciences Industry", COMPAMED High-Tech Forum 2018 by IVAM, Düsseldorf (DE), 12 November 2018.

B. Timotijevic, "Novel Fabry-Perrot Filters in the Infrared", EUROSENSORS' 18, Graz (AT), 9–12 September 2018.

F. Zamkotsian, I. Zhurminsky, P. Lanzoni, N. Tchoubaklian, Ch. Schneider, S. Fricke, M. Schnieper, F. Lütfolf, "Convex blazed gratings for high throughput spectrographs in space missions", October 2018.

Research Projects

Eurostars	ALIBERO – Low-power impulse-radio ultra-wideband module for remote control and keyless access
Eurostars	CIT-MSA – Disposable sensor array for bioprocess monitoring in disposable bioreactors
Eurostars	DEBORAH – Optimization of design and control of district level thermal energy systems
Eurostars	ENLIGHTENMENT – Enabling next-generation lighting manufacture in Europe
Eurostars	LAMMIC – Production of laminin-521™ coated microcarriers for stem cell expansion
Eurostars	MDFD – Medical device for measuring electro-mechanical properties of skeletal muscles
Eurostars	MINIHR – A wrist worn wearable device for women for stress detection and management
Eurostars	PERISCOPE – NILM for industrial and public buildings
Eurostars	POLYOMINO – All-in-one platform for the design and the production of customized free-form OPV modules
Eurostars	POLYOMINO – Preventing anastomotic leakage by developing an anastomotic perfusion measurement device (APM)
Eurostars	SensMotion – Patch-like sensor system for skeletal muscle and motion monitoring
Eurostars	SMARTBEAT -- ECG system for HRV lifestyle assessment
Eurostars	SWIRSENSE – Short-wavelength infrared tunable laser for sensing applications
Eurostars	WBPS – Wearable blood pressure system
Forschung Aargau	ANCHOR – Anchor guardian communication study
Interreg	HARISSA – Fabrication de pièces plastiques 3D microstructurées par injection plastiques : applications dentaires, médicales et horlogères
ITER	ITERBOLO – Bolometers prototyping for ITER

Nano-Tera	FLUSISAFE – Fluorescence lifetime encoding for anti-counterfeiting
Nano-Tera	FLUSITEX – Developing a wound dressing with an integrated sensing layer for non-invasive wound monitoring using fluorescence lifetime detection
Nano-Tera	HEARRESTORE – Image-guided micro surgery for hearing aid implantation
Nano-Tera	ICYSOC – Inexact sub-near-threshold systems for ultra-low power devices
Nano-Tera	NAMBPGATE – Transfer of NAMBP blood pressure technology into Ava product
Nano-Tera	NEWBORNCARE – Reducing the false alarms of neonate vital sign monitoring via a computer vision-based approach to accurately measure heart and respiratory rates in a contactless way
Nano-Tera	OBESENSEGATE – Improvement of commercial FieldWiz system with cardiac monitoring add-on
Nano-Tera	RASECAN – A new tool for rapid sensing of cancer by parallel AFM
Nano-Tera	SHINE – Solar to hydrogen integrated nano-electrolysis
Nano-Tera	SYNERGY – Systems for ultra-high performance photovoltaic energy harvesting
Nano-Tera	WISESKIN – Wise Skin for tactile prosthetics
NCCR PlanetS	SKY-RULER – EOM-based comb for spectrograph calibration: TRL increase and tests
SNI – Nanoargovia	DISP-BAT – Development of flow dispersion batteries
SNI – Nanoargovia	MegaNanoPower – Disruptive power storage technology applying electrolyte nano-dispersions and micro/nano structured electrodes
SNI – Nanoargovia	NFOPTICS – Uniaxially oriented anisotropic electrospun nano-fibrous layers for optical applications
SNI – Nanoargovia	PLASMORETARDER – Plasmonic nanoscale retarder controlled with liquid crystals
SNI – Nanoargovia	PLASPEC – PhD on Plasmonic enhanced photoelectro chemistry
SNSF	ACTIVE INTERFACES – Holistic strategy to simplify standards, assessments and certifications for building integrated photovoltaics
SNSF	AMELIZ – Advanced metallization strategies for heterojunction solar cells
SNSF	CELLSTRATES – Smart engineered substrates for high throughput mechanobiology
SNSF	EOCOMB – Broadband optical frequency comb source based on electro-optic modulation for resolved comb line precision spectroscopy
SNSF	EPISODE – Engineering of advanced hybrid perovskite for Integration with silicon photovoltaic optoelectronic devices
SNSF / BRIDGE	FILINE – Bridge proof of concept awarded to Victor Brasch
SNSF	MUSCLELAB – Silicon elastomer structures to measure mechanical properties of muscle models
SNSF	NOVIPIX – Novel integrated pixel X-ray detectors
SNSF	PERSI – Advanced functional perovskites for tandem solar cells
SNSF / BRIDGE Discovery	FEMTOCHIP – Research on pulsed lasers for ultraefficient microresonator frequency combs
SNSF / BRIDGE Discovery	POWER – Development of next generation solar cells and modules based on perovskite /silicon tandem architecture and perovskite/CIGS structure.
SNSF / BRIDGE Discovery	SMARTROBOT – Towards intelligent sensor-enhanced robotic neurosurgery
SNSF / Program NRP 70	PV2050 – Novel generation perovskite devices
SNSF / Program NRP 70	PV2050 – Photovoltaics into the built environment: from semi-transparent PV glazing to high efficiency roof integrated solutions

Swiss Federal Office of Energy (SFOE)	DCSMART – Distribution en courant continu dans les réseaux intelligents
Swiss Federal Office of Energy (SFOE)	ECUVILLENS – Demonstration d'une toiture PV terra-cotta sur une ferme traditionnelle
Swiss Federal Office of Energy (SFOE)	PAPERWALL – Test and demonstration of new solution for colored PV modules
Swiss Federal Office of Energy (SFOE)	PROSUMER-LAB – Einfluss neuartiger Strategien und Komponenten des Energiemanagements von netzintegrierten, intelligenten Gebäuden auf die Stabilität und Qualität des Haus- und Verteilnetzes
Swiss Federal Office of Energy (SFOE)	SKYCAM – Lokale Vorhersage der Sonneneinstrahlung
Swiss Federal Office of Energy (SFOE)	SODA – Solar data analytics for production forecasting and anomaly detection
Swiss Federal Office of Energy (SFOE)	SPET – Flexible Hochleistungskomponenten für die Elektrifizierung von zukünftigen aeronautischen Antriebssystemen basierend auf photoelektrischer Energieerzeugung
Swiss Space Center	GRATING-TRAP-SIM – Optical simulations for atomic trapping using diffraction gratings

Swiss Commission for Technology and Innovation

18101.1 PFNM-NM	3D NANOMET	Surface micro-nanostructuring of metallic surfaces for improved tribological performances
31952.1 INNO_ENG	AAOMVD	Couche MVD pour colmatage / Cheque Innovation InnoSuisse pour COLORAL
26245.1 PFLS-LS	AGAT	Automated Goldmann applanation tonometer
27751.1 PFLS.S	ALYVE	Artificial lymphoedema vessel
25701.1 PFNM-NM	AMTI	Additive Manufacturing of Ti based alloy for aerospace application
31080.1 INNO-EE	ATSTILE	In the frame of "Innosuisse Innovation cheque" (Innosuisse funding application no. 31080.1 INNO-EE), CSEM will support ATSHOME in the validation of the proposed high-performance and low-cost photovoltaic tile
25714.1 PFNM-NM	AUTOMIA	Automated bovine milk analysis by push-button identification and characterisation of somatic cells
27659.1 PFNM-NM	BASIMO	Backside replicated, folded (90-degree) micro-optical connectivity to wafer-scale arrays
28008.1 PFNM-NM	BESTIMATOR	Data-driven inline estimators of the state of charge and state of health of batteries
30120.1 IP-ENG	BIOASSAY	Wellplate bioassays based on highly sensitive resonant gratings
18623.1 PFNM-NM	BIOWAVE	Realisation of the BIOWAVE pre-product, a biometric watch activated by veins
27656.1 PFNM-NM	B-SOFT	Beam-shaping optical film technology for LED-based downlights
18473.2 PFNM-NM	BUBBLES	Fluid sensor with acoustical pattern analysis of physical properties and IoT integration
27049.1 PFES-ES	CBM	Deep learning for condition based monitoring on railway vehicles
26704.2 PFLS-LS	CERAMIC-TOOTH	Development of a manufacturing solution and surface topography for dental ceramic implant applications, using a novel two-piece implant design

26001.2 PFNM-NM	CLEAN-WAVE	Development of materials, processes and technologies for the manufacturing of cost effective self-cleaning solar reflectors
17863.2 PFLS-LS	COCO	Sustainable intensification of agricultural cropping systems supported by smart swiss ICT-AGRI solutions
27655.1 PFNM-NM	COMBI-NED	High field of view diffractive optical combiner for near-eye displays
28345.1 PFNM-NM	CONTACTS	Next generation industrial passivating contacts for high efficiency silicon solar cells manufacturing
18314.1 PFIW-IW	COTM	KU-KA frontend : Additive-manufactured Satcom user terminal front-end for connectivity on the move applications in Ku and Ka band
?? 18888.1 PFES-ES	CUBIC 2	The world's lowest-power platform to wirelessly exchange information peer-to-peer
16692.2 PFIW-IW	CUMAPRO	Massenproduktion von kundenspezifischen PV-Modulen für die Gebäudeintegration, Customised Mass Production
25600.1 PFNM-NM	DENSXO	Gas density sensors based on adaptive oscillators
32348.1 IP-EE	DIPPS	Development of integrated production processes for perovskite/silicon high efficiency photovoltaic
25726.2 PFNM-NM	DORES	Mirrored force resonance with double balance wheel for watches
25739.1 PFNM-NM	DSC-GLUE	Development of an adhesive formulation for durable dye-sensitive glass-modules for building integrated photovoltaic power generation
18633.1 PFNM-NM	DUALCOMB	Dual comb mid IR source technology
25374.1 PFNM-NM	ECHOPAD	Flexible pad-based ultrasound system for continuous heart monitoring
25790.1 PFIW-IW	EMAILLE	Oberflächeninspektion für grossflächige Emaillekörper
25365.1 PFNM-NM	EMIRS 2.1	Development of new infrared light sources for gas detection application
31942.1 INNO-ENG	ERGOTRACKING	Outil digital pour évaluation ergonomique de places de travail industrielles
18003.1 PFNM-NM	FASTOBS	Dynamic nanoindentation enabling fast observation, high stain rate, fatigue testing and multiaxial loading and force measurements
18481.1 PFNM-NM	FEMTOPOWER	Femtopower will develop ultrahigh power ultrashort pulse femtosecond laser source for highspeed industrial micromachining
30156.1 IP-ICT	FINGER-SENSE	Tactile fingertips for service robots
31563.1 INNO-ENG	FIREHUM	Physiologische Parameter, Sensoren und deren Integration in Schutzkleidung zur frühzeitigen Erkennung von Überhitzungsanzeichen bei Feuerwehrleuten
28478.1 PFIW-IW	FLASH	Advanced cell tester
28236.1PFNM-NM	GLAM	Glass micro-fluidics
25799.2 PFIW-IW	GMD	Predictive maintenance for mill drive power train systems
25839.2 PFLS-LS	GRAINVIEW	Flow speed measurement and morphological analysis of food grains
19288.1 PFNM-NM	HIFILL	Industrial fabrication of ultra-high fill factor microlenses
25138.1 PFNM-NM	HI-MU-LENS	Wafer-scale integration of high-refractive index microlenses on III-IV semiconductor photodiodes

18099.1 PFNM-NM	HIPERSTEER	High performance beam steering unit
18307.1 PFIW-IW	HOT-WINDOWS	Heated aircraft windshields- development of a transparent and more reliable heating for the production of aircraft windshiled series
25137.1 PFNM-NM	INDIFUSEHOLDER	Ultra-low energy voltage indicator for new type of fuses
27291.2 PFLS-LS	IN-SITU	Intelligent process control for 3D-bioprinting technology
27100.1 PFLS-LS	INTUBSENS	Development of a pressure sensor for medical applications
18737.1 PFNM-NM	LAOSS	Large area organic semiconductor software for photovoltaic and light emitting devices (LAOSS)
27435.1 PFNM-NM	MAGNETO	Inspection platform for magnetically oriented optical features
18959.1 PFIW-IW	MAXIMAL	Modular radial and axial active magnetic bearing for maxon motors
27513.1 PFNM-NM	MEMCELL	MEMS cells for miniature atomic clocks
18559.1 PFLS-LS	MEMO-MAB	Banking of human antibody repertoires for therapeutic use
26565.2 PFIW-IW	MODECORES	Speed-optimised simulation models for instant consulting on heating systems and energy management systems
18325.1 PFNM-NM	MULTISENSOR	Development of a module integrating an optical temperature sensor and two optical accelerometer
27901.1 PFLS-LS	MUSCLEANALYSER	Electrical stimulation & optical force measurement apparatus for 3Dprinted muscle tissues in multiwell plate
18760.1 PFNM-NM	NEURUG	Multi-well biosensor for drug screening applications
18808.2 PFIW-IW	OCTOPLUS	Development of a smart manufacturing Octopus cluster platform for thin film depositions on both sides of a substrate without breaking vacuum and without external substrate handling
18646.2 PFNM-NM	OPTINCLINO	Optical inclinometer: Development of a fully packaged MEMS inclinometer with remote optical readout for Structural Health Monitoring
18755.1PFNM-NM	OPTOGAS	CO ₂ /O ₂ gas mixing and sensing for life sciences
18327.1 PFNM-NM	OPTOREC	Development of high-end optical reference cavities for laser stabilization
31273.1 INNO-ENG	OPUPRE	Feasibility on optical processing unit (OPU) for smart sensor systems
25485.1 PFNM-NM	PERMUT	Investigation of feasibility of MEMS based ultrasonic air transducers for industrial applications
25701.1 PFNM-NM	PI3	Additive Manufacturing of Ti based alloy for aerospace application
18352.1 PFNM-NM	PIPPAF II	Pipetting system with flowsensor and microelement for passive flow control
28063.1 PFNM-NM	PRECISENSE	Development of a generic, high-performance, low-cost, absolute position sensor prototype
18926.2 PFNM-NM	PRINT-BAT	Feasibility study: Flexible printed batteries
18748.1 PFNM-NM	PRISM	High resolution multi-color detection system with adaptive algorithms for parallelized gene sequencing systems
18082.1 PFNM-NM	PROMISES	Perovskite photovoltaic material screening for enhanced stability
25422.2 PFIW-IW	PUMPOMAT	Robotergesteuerter Präzisionsmontagearbeitsplatz

26290.1 INNO-NM	PV TILES	Research and Development of a Terracotta coloured integrated solar roof tile
26116.1 PFES-ES	RAILCHECK	RailCheck with fingerprinting
33797.1 INNO-ENG	ROPESENS	Feasibility on the Kombination einer visuellen und magnetinduktiven Seilprüfeinrichtung zur Verbesserung der Fehleridentifikation
18465.1 PPNM-NM	SECUREFLIM	Fluorescence Lifetime Imaging Microscopy (FLIM) for the product and brand protection market
18462.1 PPNM-NM	SILICON EYE	Design of a vision for positioning systems
16584.1 PFEN-IW	SILVERLINE 2	Next generation production processes and quality controls for watch batteries
30363.1 INNO-ICT	SMARTPROFILE	Mobile Applikation zur Erkennung von komplexen Aluminiumprofilen in der Produktion
26824.1 PFIW-IW	SMINTEBI	Smart individual tenant billing (SMINTEBI) feasibility study
33395.1 IP-EE	SMINTEBI-MVP	Smart individual tenant billing minimal viable product
26845.1 PPNM-NM	SPYDERMAN	Indoor 2D and 3D device positioning system
16694.2 PFIW-IW	STABILITY	Dynamische Lageregelung für Hydraulikmodule demonstriert an einem Stelzentraktor im Rebberg
17518.1 PFEN-NM	SUPERTC	SuPeRTC, a super high performance temperature compensated miniature real time clock module
18679.2 PFIW-IW	SWISSHOLO	Security 1st and 2nd level features provide (hidden) unique identifying structures for trademark protection of titanium implants
18939.1 PPNM-NM	TEXAS	New casting tool for textured hydrogel surfaces for 3D cell culture
18130.1 PFIW-IW	TORS	Tribological optimization of spinning traveler and ring for spinning and twisting
18539.1 PFLS-LS	TRACTEUR	Development of an automated seed drill for the site-specific reseeding of grassland
18741.1 PPNM-NM	TRUEAIRSPEED	Pressure measurement system for paragliders
17324.1 PFLS-LS	U4P	Using physiological parameters measured with a wrist-worn device to predict ovulation, detect pregnancy, and monitor gestation
31512.1 IP-EE	UPpero	Development of deposition processes for future large scale production of perovskite based photovoltaic devices
18621.1 PFEN-NM	WATT.CH	Smart wristband powered by PV cells
25990.1 PPNM-NM	WAVEZ-F	Feasibility study for OBPM monitoring
18091.1 PFEN-NM	WISEROCK	Low-cost WSN with GNSS capability for long-term landslide monitoring
18394.1 PFLS-LS	ZEPTOTRACK	Real-time surgical instruments positioning with reference integrated in surgical lamp

European Commission Projects

H2020 – NMBP 2016	ACENANO	Analytical and Characterisation Excellence in nanomaterial risk assessment: A tiered approach
H2020 – IOT 2016	ACTIVAGE	Activating innovative IoT smart living environments for ageing well

FP7 – NMP	AMBASSADOR complement	Autonomous management system developed for building and district
H2020 – LCE 2016	AMPERE	Automated photovoltaic cell and module industrial production to regain and secure European renewable energy market
H2020 – Clean Sky	AMPWISE	Autonomous wireless current sensor for aircraft power lines
H2020 – ICT 2016	BIOCDX	A miniature bio-photonics companion diagnostics platform for reliable cancer diagnosis and treatment monitoring
FP7 – ICT	BIOFOS complement	Microring resonator-based biophotonic platform for food analysis
H2020 – LCE 2015	CHEOPS	Production technology to achieve low cost and highly efficient photovoltaic perovskite solar cells
H2020 – IND CE	CITCOM	Complimentary inspection technique based on computer tomography and plenoptic camera for MEMS components
H2020 – ICT 2016	DATABIO	Data-driven bioeconomy
H2020 – ICT 2015	DETOP	Dexterous transradial osseointegrated prosthesis with neural control and sensory feedback
H2020 – LCE 2016	DISC	Double-side contacted cells with innovative carrier-selective contacts
FP7 – SEC 2009	E-SPONDER complement	A holistic approach towards the development of the first responder of the future
H2020 – ICT 2016	FED4SAE	Federated CPS digital innovation hubs for the smart anything everywhere initiative
H2020 – ICT 2016	FLAIR	FLying ultra-broadband single-shot infra-red sensor
H2020 – MSCA-ITN 2016	FoodSmartPhone	Smartphone analyzers for on-site testing of food quality and safety
H2020 – MG 2014	FUTURESKY	Smart, green and integrated transport
H2020 – ICT 2014	GATEONE	Innovation service for European smartization by SMEs
FP7 – ENERGY	HERCULES complement	High efficiency rear contact solar cells and ultra-powerful modules
H2020 – EEB 2017	HYBUILD	Innovative compact hybrid electrical/thermal storage systems for low energy buildings
H2020 – EE 2015	INDIGO 2	New generation of intelligent and efficient district cooling systems
H2020 – SC5 2014	INREP	Towards Indium free TCOs
H2020 – ICT 2016	INSPEX	Integrated smart spatial exploration system
FP7 – ENVIRONMENT	INTASENSE complement	Integrated air quality sensor for energy efficient environment control
H2020 – FOF 2016	KRAKEN	Hybrid automated machine integrating concurrent manufacturing processes, increasing the production volume of functional on-demand using high multi-material deposition rates
FP7 – ICT	LASSIE-FP7 complement	Large area solid state intelligent efficient luminaires
H2020 – MG 2014	LYNCEUS2MARKET	Safer and more efficient waterborne operations through new technologies and smarter traffic management
H2020 – ICT 2014	M3TERA	Micromachined terahertz systems -a new heterogeneous integration platform enabling the commercialization of the THz frequency spectrum
H2020-FETFLAG-2018-2020	MACQSIMAL	Miniature hot atomic vapor cells based quantum devices for sensing and metrology applications

H2020-NMBP-FOF-2018	MANUELA	Additive Manufacturing Using Metal Pilot Line
H2020 – NMBP 2017	MANU-SQUARE	Manufacturing ecosystem of qualified resources exchange
H2020 – ICT 2014	MEDILIGHT	Miniatuerized smart system for light stimulation and monitoring of wound healin
H2020 – ICT 2015	MIRPHAB	Midinfrared photonics devices fabrication for chemical sensing and spectroscopic applications
H2020 – ICT 2017	MOLOKO	Multiplex photonic sensor for plasmonic-based detection of contaminants in milk
H2020 – SESAR 2015	NAVISAS	Navigation of airborne vehicle with integrated space and atomic signals
H2020 – LCE 2016	NEXTBASE	Next-generation interdigitated back-contacted silicon heterojunction solar cells and modules by design and process innovations
H2020 – SFS 2018	NutriShield	Fact-based personalized nutrition for the young
H2020 – NMBP-FOF 2018	OLEDSOLAR	Innovative manufacturing processes and in-line monitoring techniques for the OLED and thin film and organic photovoltaic industries (CIGS and OPV)
FP7 – ICT	PEGASO	Personalised guidance services for optimising lifestyle management in teen-agers through awareness, motivation and engagement
H2020 – LCE 2016	PENTAGON	Unlocking European grid local flexibility trough augmented energy conversion capabilities at district-level
H2020 – LCE 2017	PERTPV	Perovskite thin-film photovoltaics (PERTPV)
FP7 – SPACE	PHASER complement	High speed, high frequency electro-photonic ADC for space enabled routers
H2020 – FETFLAG 2018	PHOG	Sub-poissonian photon gun by coherent diffusive photonics
FP7 – NMP	PLIANT complement	Process line implementation for applied surface nanotechnologies
FP7 – KBBE	RADAR complement	Rationally designed aquatic receptors integrated in label-free biosensor platforms for remote surveillance of toxins and pollutants
H2020 – ICT 2014	RAWFIE	Road-, air- and water-based future internet experimentation
H2020-MSCA-RISE	RDC2MT	Research, demonstration and commercialization of DC microgrid technologies
FP7 – SPACE	REMOVE-DEBRIS	A low cost active debris removal demonstration mission
H2020 – SEC 2016/7	ROBORDER	Autonomous swarm of heterogeneous robots for border surveillance
H2020-LCE	SABINA	Smart bi-directional multi energy gateway
FP7 – SECURITY	SAVE-MED	Tackling counterfeit medicines and related criminal networks
FP7 – ICT	SEMIAH complement	Scalable multi-criteria energy management infrastructure for aggregation of households
H2020 – ICT 2014	SMARTER-SI	Smart access to manufacturing for systems integration
FP7 – NMP	SMARTNANO complement	Sensitive measurement, detection, and identification of engineered nano-particles in complex matrices
FP7 – NMP	SMARTRONICS COMPLEMENT	Development of smart machines, tools and processes for the precision synthesis of nanomaterials with tailored properties for organic electronics

FP7 – ICT	SPLENDID complement	Personalized guide for eating and activity behavior for the prevention of obesity and eating disorders
FP7 – ENVIRONMENT	STRATOCLIM	Stratospheric and upper tropospheric processes for better climate predictions
FP7 – ICT	SUNFLOWER complement	Sustainable novel flexible organic watts efficiently reliable
H2020 – FETOPEN 2014-2015	SUPERTWIN 3	All solid-state super-twinning photon microscope
H2020 – EE 2016/7	TABEDE	Towards building ready for demand response
H2020 – EEB 2016	THERMOSS	Building and district thermal retrofit and management solutions
FP7 – ICT	WELCOME	Wearable sensing and smart cloud computing for integrated care to COPD patients with comorbidities

European Space Agency, Swiss Space Office, and Swiss Space Center Projects

ESA Projects

CCM-MTG	Development and manufacture of corner cube mechanisms for MTG satellite
CECILE	LiDAR integrating compressive sensing
CLUPI	CLUPI instrument for Exomars
C-MAC	Ceramic miniature atomic clock physics package – C-MAC PP
COMAM	Development of a compliant mechanism based on additive manufacturing
CS4SPACE	Compressive sensing
DANOE	High-dynamic absolute nanometric optical encoder technology assessment for space phase II
DELIAN	Dextrous lightweight arm for exploration
ENRUM	Space and energy resources utilisation mapping (EnRUM)
EUSO-B2	Extreme Universe Space Observatory – Phase B2
FGU	Micro-optoelectronic frequency generation unit (FGU)
HIGHTS	Highly thermally conductive silver sintered die mounting
HOPP	Photodiode development
HOPWELL	Space validation of glass lid soldering techniques to hermetically seal small size optoelectronic parts
ISOL	Development of a high performance Microvibration isolation system
ITI-SIC	Silicon carbide sensors for harsh space environments
ITI-WHEEL	How to adapt Celerons wheel towards agility?
LAFF	Develop a large angle flex pivot for space applications
LIDISOR	LIDAR for inter-satellite optical ranging
MACAREW	Magnetic characterization of reaction wheels
MATMAT CCM	Matrix material for programmable flexure mechanism
MCC-X	Miniaturised motion controller customisation for exploration
MEMS GC-MS	MEMS-based gas chromatograph and mass spectrometer
MILA	Miniaturized imaging laser altimeter (miniature imaging LIDAR system, Phase 1)
MILEB	Miniaturized imaging LIDAR systems for the landing of spacecraft's
ML-BI-CIS	Microlenses deposition for backside illuminated imagers
MLSCL	Sub-picosecond model-locked semiconductor laser for space missions

MONALISA PHASE 1	Laser for LISA mission
MTS	Miniature timing source (mTS): miniature atomic clock, MEMS vapor cells, ASIC specifications
NIRS	NIR immersed grating in transmission for high resolution spectroscopy
NPI-BEARING	Miniature magnetic bearings for space actuators
NPI-CELL	PhD on fabrication of miniature atomic cells
OEO	Ultra-low phase noise reference oscillator
OSRC	Digital stabilisation electronics for lasers
REAC	Reliability evaluation of MEMS by accumulative tests for space application
STAR	Lidar for wavefront distortion
STIFS	Definition for optical atomic clock
SWIRS	New generation SWIR immersed grating (Phase1)
TOPCAM-CCM	Topologically optimised compliant mechanisms based on additive manufacturing
TRIPP	Verification of straylight rejection of optical science payloads using a pulsed laser source

Swiss Space Office Projects

AMAR	Additive Manufacturing of an SRA Rotor
printHeatApp	Fully printed heaters on CFRP structures for space applications

Swiss Space Center Projects

T-BEAR	Measurement method for Active magnetic bearing
--------	--

Industrial Property

Patent portfolio

In 2018, 32 invention reports were submitted internally for examination which have led to 35 patent applications filed in 2018 (33 regular applications and 2 provisional applications). The patent portfolio has been further enhanced by the extension of different countries of 11 patent files based on prior patent applications.

Collaboration with Research Institutes and Universities

University	Institute	Professor	Field of collaboration
AO Research Institute Davos	Biomaterials & Tissue Engineering program	M. Alini	Intervertebral disc biomechanics
Aristotle University of Thessaloniki	Laboratory of Medical Informatics	N. Maglaveras	Collection of large set of physiological signals
Bern University of Applied Sciences (BFH)	Micro- and Medicaltechnology	G. Gruener	WP4C – WorkPlace 4.0 Companion / Y-Delta
Bern University of Applied Sciences (BFH)	MSE	V. Koch	Sensory processing prosthetics
Berner Fachhochschule	Energy Storage Research Centre	A. Vezzini	Electrochemical battery storage
Brown University	School of Engineering	A. V. Nurmikko	Integrated circuits for brain implants
Chalmers University of Technology	Industrial and Materials Science	L. Nyborg	Additive Manufacturing
Christian-Albrechts-Universität zu Kiel	Klinik für Anästhesiologie und Operative Intensivmedizin	I. Frerichs	Electrical-impedance tomography
CHUV	Service de cardiologie	E. Pruvot	Cardiac arrhythmias

University	Institute	Professor	Field of collaboration
CHUV	Département Anesthésiologie	P. Schoettker	Blood pressure
Empa	Abteilung für Hochleistungskeramik	F. Clemens	Printed Electronics; printed ceramics
Empa	Laboratory for functional polymers	F. Nüesch	Transparent PV
Empa	Department of advanced materials and surfaces	P. Gröning	X-ray read out circuits
Empa	Swiss federal laboratories for materials science and technology	P. Hoffmann	Solid state lighting
EPF Lausanne	TCL Telecommunications Circuits Laboratory	A. P. Burg	Good enough circuits, Ultra-low power and sub-threshold design, bias control, library characterization
EPF Lausanne	ICLAB Integrated Circuits Laboratory	C. C. Enz	60GHz radar, Approximate arithmetic, ULP Radio and protocol for WiseSkin
EPF Lausanne	Automatic Control Laboratory	C. Jones	Model-predictive control of buildings
EPF Lausanne	Microtechnique	D. Briand	Printed electronics / Printed sensors
EPF Lausanne	STI - Materials Science and Engineering	D. Damjanovic	Printed electronics / Printed ceramics
EPF Lausanne	Medtronic Chair in Neuroengineering	D. Ghezzi	Printed Platinum electrodes
EPF Lausanne	Laboratoire de métallurgie thermomécanique	E. Boillat	Additive Manufacturing
EPF Lausanne	Advanced Quantum Architecture Laboratory	E. Charbon	Micro-optics
EPF Lausanne	Powder Technology Laboratory	H. Hofmann	Mesoporous Sol-Gel Films
EPF Lausanne	Microsystems Laboratory	J. Brugger	Printed Optics
EPF Lausanne	LESO	J.-L. Scartezzini	Human Centric Lighting
EPF Lausanne	SCI STI JMV Group	J.-M. Vesin	Newborn vital signs monitoring based on multiple vision sensors
EPF Lausanne	LIPID	M. Andersen	Human Centric Lighting
EPF Lausanne	Laboratory of advanced semiconductors for photonics and electronics	N. Grandjean	GaN-based semiconductor lasers / Solid-state lighting
EPF Lausanne	LAP Processor Architecture Laboratory	P. lenne	Embedded systems
EPF Lausanne	LTS2 Signal processing laboratory 2	P. Vandergheynst	Newborn vital signs monitoring based on multiple vision sensors
EPF Lausanne	Instant Lab Laboratory	S. Henein	Flexure guides
EPF Lausanne	LSBI Foundation Bertarelli Chair in Neuroprosthetic Technology	S. Lacour	Artificial skin, restore spinal connections
EPF Lausanne	Laboratory of Photonics and Quantum Measurements	T. J. Kippenberg	Optical microresonators and frequency combs

University	Institute	Professor	Field of collaboration
EPF Lausanne	Microtechnique	V. Subramanian	Printed Electronics; functional printing on 2D and 3D objects
ETH Zurich	deMello Group	A. deMello	Microfluidics
ETH Zurich	Biosystems Science and Engineering	A. Hierlemann	Spheroids
ETH Zurich	Laboratory for solid state physics	H. von Känel	X-ray read out circuits
ETH Zurich	Integrated Systems Laboratory	L. Benini	Sub-Near-Threshold Multicore, Neural Network
ETH Zurich	Department of Heal Sciences and Technology, Laboratory of Toxicology	S. Sturla	Aptamer-based assays for food safety
Hôpital neuchâtelois, HNE	Département de médecine	C. Pellaton	Multiple collaboration including a clinical investigation on non-invasive blood pressure
Idiap Research Institute	Speech and Audio Processing	M. Magimai Doss	Speech as biosignal
Imperial College of London	Faculty of Engineering, Department of Electrical and Electronic Engineering	E. M. Yeatman	Energy harvesting for wireless sensor networks in aerospace applications; smart materials
INAIL (National Workers' Compensation) Prosthetic Center, Bologna, Italy	Aids Area and Research and Training Area	R. Sacchetti	Clinical implantation and assessment
IPC-Oyonnax-France	Innovation Plasturgy Composites	L. Tenchine, S. Dessors	Injection Molding
Istituto Ortopedico Rizzoli (IOR), Bologna, Italy	2nd Orthopaedic and Traumatology Clinic	S. Zaffagnini	Clinical implantation and assessment
National Institute of Standards and Technology (NIST)	Optical Frequency Measurements group	S. A. Diddams	Optical frequency combs and their applications
ONERA-France	Modane-Avrieux Center	M. Lyonnet, Y. Michou	Pressure Sensitive Painting
ONERA-France	Meudon Center	M.-C. Mérienne	Pressure Sensitive Painting
Paul Scherrer Institute PSI	Laboratory for Micro- and Nanotechnology	Y. Ekinci	Plasmonic retarders for imaging
Scuola Superiore Sant'Anna, Pisa, Italy	The BioRobotics Institute	C. Cipriani	Artificial wrist, mechatronic couplers, artificial sensors for hand/wrist prosthesis, control algorithms, user assessment tools
Technical University of Kaiserslautern	Chair of real-time systems	G. Fohler	Real-time networking
Università Campus Bio-Medico, Roma, Italy	Department of Orthopaedics and Trauma Surgery	V. Denaro	Clinical implantation and assessment
Université de Bourgogne, France	LE2I	J. Dubois	Remote vital signal monitoring
University Hospital Inselspital Bern	Department of Cardiovascular Surgery	D. Reineke	Blood pressure

University	Institute	Professor	Field of collaboration
University Hospital Inselspital Bern	Cardiovascular Department	E. Rexhaj	Blood Pressure
University Hospital Inselspital Bern	Department of Pulmonary Disease	K. De Jaegere	Sleep
University Hospital Inselspital Bern	Department ENT Surgery	M. Caversaccio	Image-guided micro surgery for hearing aid implantation
University Hospital Zurich	Division of Neonatology	J.-C. Fauchère	Newborn vital signs monitoring based on multiple vision sensors
University Hospital Zurich	Biomedical optics research laboratory	M. Wolf	Newborn vital signs monitoring based on multiple vision sensors
University Neuchâtel	Institute of Biology	F. Kessler	Microstructural study
University of Applied Sciences and Arts (FHNW)	Institute for Medical and Analytical Technologies	M. de Wild	Imprint of nanostructures
University of Applied Sciences and Arts (FHNW)	Institut für Nanotechnische Kunststoffanwendungen	M. Kristiansen	Micro and nano structuring
University of Applied Sciences and Arts (FHNW)	Hochschule für Life Sciences	U. Pieles	Nano-dispersions
University of Applied Sciences and Arts of Southern Switzerland (SUPSI)	IDSIA Dalle Molle Institute for Artificial Intelligence	L. M. Gambardella	Machine Learning
University of Applied Sciences and Arts, Lucerne (HSLU)	CC Electronics	E. Niederberger	Solid state lighting
University of Applied Sciences and Arts, Lucerne (HSLU)	Medical Engineering	F. Ille	Bioreactor for microgravity environment
University of Applied Sciences and Arts, Lucerne (HSLU)	CC Aerospace biomedical science & technology / CC Mechanische Systeme / CC Electronics	M. Egli	Fluidic feeding system
University of Applied Sciences HTW Chur	Departement Angewandte Zukunftstechnologien, Institut für Photonics und ICT IPI	U. Hauser-Ehninger	Solid state lighting
University of Applied Sciences, Zurich (ZHAW)	Institute of Computational Physics	B. Ruhstaller	Electrode design for PV & Solid state lighting
University of Basel	Psychiatry Hospital / Center for Chronobiology	C. Cajochen	Human Centric Lighting / Chronobiology
University of Basel	Dept. of Physics	C. Schöneberger	Development of light management optics for solar cells
University of Basel	Department of Chemistry	E. Constable	Photo-Electrochemistry
University of Bern	Quantum Optics Lab	A. Stefanov	Entangled photons / quantum optics

University	Institute	Professor	Field of collaboration
University of Bern	ARTORG – Organ on chip	O. T. Guenat	Applications of cellulose-based materials to electrochemical sensing
University of Bern	ARTORG Center for Biomedical Engineering	S. Weber	Guided surgery / Image-guided micro surgery for hearing aid implantation
University of Essex, Colchester, United Kingdom	School of Computer Science and Electronic Engineering	L. Citi	Point-process and machine-learning-based neuro-muscular decoding/control algorithms
University of Geneva	Exoplanetary Systems	F. Pepe	Instrument for exoplanet search
University of Geneva	Physical Chemistry	T. Bürgi	Microstructural investigation
University of Geneva	Computer vision and multimedia laboratory	T. Pun	Obstacle detection for the elderly based on stereo vision
University of Gothenburg	Department of Orthopaedics	J. Wessberg	Sensory feedback
University of Lausanne	Earth Surface Dynamics	E. Verrecchia	Microstructural study
University of Lund	Department of Biomedical Engineering	C. Antfolk	Prosthetics, decoding of user intent, control, clinical assessment
University of Neuchâtel	Institute of Biology	J.-M. Neuhaus	Microstructural investigation
University of Neuchâtel	Laboratoire Temps-Fréquence	G. Miletí	Cell-based atomic clocks
University of Neuchâtel	Institute of Biology	P. Junoir	Ultrastructural investigation
Vienna University	Department of Physical Chemistry	P. Lieberzeit	Chemical Sensor
Wyss Center	Bio and Neuro Engineering	C. Clément	Integrated circuits for brain implants

Teaching

	Title of lecture	Context	Location
M. Dadras	Microscopy	Microscopy for ultrastructural investigation	University of Neuchatel
J.-D. Decotignie	Informatique du Temps Réel	Bachelor Informatique	EPF Lausanne
	Real Time Networks	Master Computer and Communication Systems	EPF Lausanne
M. Despont	Packaging and hybridization, the valorization of MEMS technologies	Micro- 534 Advanced MEMS 2018 (D. Briand)	EPF Lausanne
L. A. Dunbar	Innovation Management	Bachelor Management	EPF Lausanne
	Corporate Venturing and Open Innovation	eMBA	EPF Lausanne
J. R. Farserotu	Satellite Communication Systems and Networks	Master degree course under Communication systems and space technology	EPF Lausanne
I. Kjelberg	La Microtechnique et l'Astronomie	Cours EPFL Microtechnique 4e semestre	EPF Lausanne
	Optic 1 + 2	Formation en emploi	Haute Ecole d'Ingénierie et de Gestion du Canton de Vaud (HEIG-VD)

	Title of lecture	Context	Location
N. Marjanović and F. Zanella	MICRO-505 Organic and Printed Electronics	Master course with Dr. D. Briand	EPF Lausanne
S. Mohrdiek	Aufbau- und Verbindungstechnik (AVT) Technologieübersicht & Anwendung in Mikrosystemen (MEMS)	Seminar FS18 MIKROFAB	University of Applied Sciences and Arts, Lucerne (HSLU)
D. Ruffieux	Crystal Oscillator Design	MEAD postgraduate course	EPF Lausanne
G. Weder	Micro and Optical Technologies in Biomedical Science	EPFL summer school	EPF Lausanne

Theses

PhD Degrees Awarded in 2018

Name	University	Title
F. Braun	EPF Lausanne	Estimation of hemodynamics via electrical impedance
S. Karlen	University of Neuchâtel	Fabrication and characterization of MEMS alkali vapor cells used in chip-scale atomic clocks and other atomic devices
V. Kopta	EPF Lausanne	Ultra-low power FM-UWB transceiver for high-density wireless sensor networks
M. Rapin	ETH Zürich	Wearable EIT system
D. C. Rojas Quiros	EPF Lausanne	Routing for wireless sensor networks: from collection to event-triggered applications

CSEM Employees carrying out a PhD & PhD Funded by CSEM

Name	Professor / University	Theme / CSEM Unit	Start year
T. Aderneuer	C. Cajochen / University of Basel	Free form micro optics for human centric lighting / Center Muttenz	2017
M. Auchlin	V. Gass / EPF Lausanne	Electrical engineering topic / Micro&Nano Systems	2017
G. Borque Gallego	Y. Perriard / EPF Lausanne	Mignature magnetic bearing reaction wheel / Systems	2017
T. C. Müller	A. P. Burg / EPF Lausanne	Variation-aware digital design / Integrated and Wireless Systems	2016
S. Cerida Rengifo	C. C. Enz / EPF Lausanne	FMCW radar front-end / Integrated and Wireless Systems	2018
F. Chicco	C. C. Enz / EPF Lausanne	Frequency synthesis for FMCW radar. / Integrated and Wireless Systems	2017
L. Driencourt	E. Constable / University of Basel	Optical plasmonic nano-structures for enhanced / Center Muttenz	2017
T. Frei	EPF Lausanne	Thermal management of microsystem in harsh environment / Micro&Nano Systems	2017
Z. A. Halvorsen	A. deMello / ETH Zurich	Miniaturized fluid sample preparation for water quality monitoring / Center Alpnach	2017
D. Honzàtko	P. Fua / EPF Lausanne	Defect detection using deep learning / Integrated and Wireless Systems	2018
S. Jafari	S. Sturla / ETH Zurich	Aptamer-based assays for food safety / Centre Landquart	2017

Name	Professor / University	Theme / CSEM Unit	Start year
P. Jokic	L. Benini / ETH Zurich	Embedded Machine Learning / Integrated and Wireless Systems	2017
E. Obrzud	F. Pepe / University of Geneva	Optical frequency comb for spectrograph calibration / Systems	2016
G. Quaranta	O.J.F Martin / EPF Lausanne	Resonant waveguide gratings for spectrometry / Center Muttenz	2015
L.-L. Senaud	C. Ballif / EPF Lausanne	Photovoltaics	2017
F. Sorba	H. Shea / EPF Lausanne	Development of an integrated device for cell stiffness measurement / Micro&Nano Systems	2015
Y. Tang	O. Guenat / University of Bern	Applications of cellulose-based materials to electrochemical sensing / Centre Landquart	2017
A. M. Tuomiranta	C. Ballif / EPF Lausanne	Optimal design and operations of photovoltaic power plants / Photovoltaics	2015

Commissions and Committees

P.-J. Alet	Chairman, Intersolar Europe Conference Committee Executive committee of the European technology and innovation platform – Photovoltaics (ETIP PV) Governing board of the European technology and innovation platform – Smart networks for the energy transition (ETIP SNET) Jury, Intersolar Award Leader of the Digital solar PV and grid working group, ETIP PV
F. Amez-Droz	CSEM Representative, Swiss Association of Science Journalism
C. Bosshard	BaselArea.Swiss: Member of Advisory Board and Technology Field Leader Micro, Nano & Materials DayOne: Member of Core Team Managing Director of the Swissphotonics NTN Member of the University Council of the University of Basel
P. Dallemagne	Secretary and Swiss representative of Technical Committee 5 "Information Technology Applications", International Federation for Information Processing (IFIP)
J.-D. Decotignie	ISO TC 65 Swiss Committee ISO TC 65C, WG16 convenor, Wireless Industrial Communication Standardization Program Committee, Int. Conf. on Wireless For Space and Extreme Environments (WISEE), Huntsville, AL, USA Program Committee, Real-Time Networks and Systems, Poitiers, France Program Committee, Workshop on Factory Communication Systems, Imperia, Italy
M. Despont	Board Member of the International Micro and Nano Engineering Society – iMNEs Board member of the Swiss-MNT network Chairman of the IEEE International Conference on Micro ElectroMechanical Systems (MEMS), Belfast, UK, 2018 CSEM and HTA representative at the Micro- and Nano- Technology Workgroup, European Spatial Agency (ESA) Member of the editorial board of Microelectronic Engineering Journal (Elsevier) Member of the executive board of the Swiss research program NanoTera

M. Despont	Member of the Industrial Advisory Board, Nanotechnology Program, Prof H. Bahaskaran, Oxford University, UK Regional Program Chair of The 21st International Conference on Solid-State Sensors, Actuators and Microsystems (Transducers 202)
A. Di Iulio-Bassini	Member of the Association des journalistes scientifiques
M. El-Khoury	CNCI Chambre Neuchâteloise du Commerce et de l'Industrie, Neuchâtel Concours International de Chronométrie, Le Locle, Membre du Comité d'honneur Member of the Swiss Academy of Engineering Sciences SATW
S. Emery	Member of the Technical Committee of the IEEE SOI-3D-Subthreshold (S3S) Conference
J. R. Farserotu	Chair and Research Co-ordinator The Hermes Partnership Chair of ETSI Technical Committee Smart Body Area Networks (TC SmartBAN) Member of the Steering Committee, IEEE International Symposium on Medical Information and Communication Technology 2017 (ISMICT 2017)
R. Ferrini	Chair of the Swissphotonics Solid State Lighting - (SSSL) Swiss National Laboratory for Solid State Lighting Member of SciPiL (the Scientific Partnership in Lighting by Luger Research)
S. Generelli	Chair and member of the Jury, Graubunden Forscht, 2018
E. Györvary	Extended Board Member CSEM Brasil Extended Board Member of the Heterogeneous Technology Alliance (alliance federating the Fraunhofer (microelectronics), VTT, CEA-Tech, and CSEM) Member & CSEM representative of EARTO Working Group on Emerging Technologies for Healthcare Member of the Finnish Chamber of Commerce Member of the Latin American Chamber of Commerce Steering board member of Innovation Group Digitalization at Swiss Food Research
H. Heinzelmann	Expert, Austrian Bridge Initiative Expert, Austrian FTI Programme Member of the Begleitgruppe Aktionsplan synthetische Nanomaterialien 2018, Federal Office of Public Health FOPH Member of the Deutsche Physikalische Gesellschaft (DPG) Member of the Executive Board of EARTO Member of the Swiss Physical Society (SPS/SPG) Membre du Conseil d'Administration de Centredoc Program Committee, MNE Micro Nano Engineering 2018, Copenhagen Program Committee, SSI Smart Systems Integration 2018, Dresden Steering Committee, CCMX Competence Center for Materials Science and Technology VP Nanotechnology, Swiss Society for Optics and Microscopy SSOM
A. Hutter	Expert, Innosuisse
C. Julia-Schmutz	Communication Coordinator within the Heterogeneous Technology Alliance (HTA) CSEM Representative, BioAlps
H. F. Knapp	Board member for NTN INARTIS Board of Directors member for cluster initiative Toolpoint for Lab Science

H. F. Knapp	Executive Board member of biotechnet, Switzerland Jury member for Zinno Ideenscheck Pre-jury member for Swiss Technology Award
G. Kotrotsios	IEEE Subcommittee on Human-Machine in Manufacturing Environment Member of the Board of the Heterogeneous Technology Alliance (alliance federating the Fraunhofer (microelectronics), VTT, CEA-Tech and CSEM) Member of the Executive Board of EREA (the European Association of Aeronautics Research Centers) Member of the Steering Committee of the SATW Advanced Manufacturing Research Alliance Member of the Swiss Academy of Engineering Sciences SATW Micronarc, member of the Group of Experts Vice Chairman of the Board of Directors of CSEM Brasil
M. Krieger	CSEM Representative Greater Zurich Area (GZA) CSEM Representative Manufuture.ch association CSEM Representative SEMI global semiconductor industry association CSEM Representative Zürcher Handelskammer (ZHK) CSEM Representative, Advanced Factory Automation workgroup of Swissmem (AFA) International Advisory Board IPAS Precision Assembly Seminar Chamonix 2018
F. Kurth	Organizing Committee Member, 23rd International Conference on Miniaturized Systems for Chemistry and Life Sciences (μ TAS 2019, Basel, Switzerland) Technical Program Committee Member, 22nd International Conference on Miniaturized Systems for Chemistry and Life Sciences (μ TAS 2018, Taiwan)
A. Madrigal	Chair of the Advisory Board of the Space exhibition of the Museum of Transport of Lucerne Chair of the EARTO Working Group Space Research CSEM Representative, General Forum Clean Sky CSEM Representative, Swiss Aeronautics Security and Defense Division of Swissmem (Swiss ASD) CSEM Representative, Swiss Space Industries Group of Swissmem (SSIG) Expert for the evaluation of H2020 proposals in the Space Work Programme of the European Commission Member of the General Assembly of EREA (Association of European Establishments in Aeronautics) and CSEM Delegate in the Aviation and Security Research Groups of the Association Member of the Strategic Committee of the Swiss Aeropole
N. Marjanovic	Member of Technical Committee, ESTC2018 Conference (https://www.estc-conference.net/home), Sept. 18-21, 2018, Dresden Germany
S. Mohrdiek	Member of Phonotics21 Work Group 6 – Design and Manufacturing of Components and Systems Member of Swissmem Fachgruppe Photonics Swissphotonics, Head of Swiss Photonic Packaging Laboratory (SPPL)
J.-L. Nagel	Member of the Editorial Board of the Journal of Low Power Electronics (JOLPE)
R. Pugin	Member of the Expert Committee of the Association NTN Innovative Surfaces Member of the Scientific Committee of the 2017 World Congress on Micro and Nano Manufacturing Member of the Scientific Committee of the 4M Micro-Nano Manufacturing Association
D. Ruffieux	Member of the International Technical Program Committee of the European Solid State Circuit Conference (ESSCIRC) in the RF and mmWave Building Blocks

E. Schaller	Member of the Executive Board of sensors.ch, Switzerland
P. A. E. Schmid	CSEM Representative Swiss Mechatronics Cluster
P. Steiert	Advisory Board Member for Institute für Chemistry and Biological Chemistry at the ZHAW Advisory Council for cluster initiative Toolpoint for Lab Science Member of the Executive Board for microPark Pilatus
A. Steinecker	CSEM Representative EPoSS and Member of Working Group Robotics

Prizes and Awards

- March 2018 During the Swiss Additive Manufacturing Expo 2018 in Lucerne, CSEM and RUAG Space were awarded the AMX Innovation Award for their new design and manufacturing processes in slip ring assembly, which they developed through the AMAR project (Lucerne, CH).
- April 2018 Tobias Herr received the 2018 EFTF Young Scientist Award for his personal pioneering contributions to ultra-fast physics and soliton pulse generation in non-linear optical microresonators (Turin, IT).
- April 2018 One year after launching the bet to rally 100'000 people to prevent hypertension by maintaining a healthier lifestyle, CSEM's partner Riva Digital went on to win the Digital Switzerland Challenge (Zurich, CH).
- June 2018 The Swiss company AVA won the Swiss Medtech Award 2018. The jury based the win on the company's entrepreneurial performance, successful business model & considerable growth over a short period of time (Bern, CH).
- September 2018 The Swiss company AVA is awarded the title of best start-up 2018. The potential of this fertility wristband (developed through a technological partnership with CSEM) won over the experts who had the task of identifying the most promising and innovative companies in Switzerland (Zurich, CH).
- September 2018 Solaxess won the SUD Prize launched by Le Temps (Swiss newspaper) with the support of Romande Energie. This prize rewards a start-up active in the field of sustainable development, and in this case recognized the innovative white & colored PV panel technology developed by CSEM; a technology that is set to revolutionize the built environment (Geneva, CH).
- October 2018 Swiss Solar Prize 2018 in the 'Renovation' category was presented to CSEM and its partners (ISSOL, the Department of Energy and the Department of Cultural Property, the Swiss Federal Office of Energy and UserHuus) for the integration of photovoltaic solar sensors into protected sites (farmhouse at Ecuvillens, canton of Fribourg).

CSEM SA
Jaquet-Droz 1
CH-2002 Neuchâtel

CENTER ALPNACH
Untere Gründlistrasse 1
CH-6055 Alpnach

CENTER LANDQUART
Bahnhofstrasse 1
CH-7302 Landquart

CENTER MUTTENZ
Tramstrasse 99
CH-4132 Muttenz

ZÜRICH OFFICE
Technoparkstrasse 1
CH-8005 Zurich



CONTACT
www.csem.ch
info@csem.ch
jobs@csem.ch

